Food and Chemical Toxicology 100 (2017) 90–102

Contents lists available at ScienceDirect

Food and Chemical Toxicology

journal homepage: www.elsevier.com/locate/foodchemtox

Sulforaphane induces differential modulation of mitochondrial biogenesis and dynamics in normal cells and tumor cells

Mario Negrette-Guzmán [a], Sara Huerta-Yepez [b], Mario I. Vega [c], Juan Carlos León-Contreras [d], Rogelio Hernández-Pando [d], Omar Noel Medina-Campos [a], Esteban Rodríguez [b], Edilia Tapia [e], José Pedraza-Chaverri [a, *]

[a] Departamento de Biología, Facultad de Química, Universidad Nacional Autónoma de México, Mexico City 04510, Mexico
[b] Unidad de Investigación en Enfermedades Oncológicas, Hospital Infantil de México Federico Gómez, Mexico City 06720, Mexico
[c] Unidad de Investigación Médica en Enfermedades Oncológicas, Hospital de Oncología, Centro Médico Nacional Siglo XXI, Instituto Mexicano del Seguro Social (IMSS), Mexico City 06720, Mexico
[d] Sección de Patología Experimental, Instituto Nacional de Ciencias Médicas y Nutrición Salvador Zubirán, Mexico City 14000, Mexico
[e] Laboratorio de Fisiopatología Renal, Departamento de Nefrología, Instituto Nacional de Cardiología Ignacio Chavez, Mexico City 14080, Mexico

ARTICLE INFO

Article history:
Received 1 November 2016
Received in revised form
14 December 2016
Accepted 15 December 2016
Available online 18 December 2016

Keywords:
Sulforaphane
Mitochondrial biogenesis
Mitochondrial dynamics
Cell death
Cancer
Nuclear factor E2-related factor 2

ABSTRACT

Antioxidant-based chemotherapy has been intensely debated. Herein, we show that sulforaphane (SFN) induced mitochondrial biogenesis followed by mitochondrial fusion in a kidney cell line commonly used in nephroprotective models. At the same concentration and exposure time, SFN induced cell death in prostate cancer cells accompanied by mitochondrial biogenesis and fragmentation. Stabilization of the nuclear factor E2-related factor-2 (Nrf2) could be associated with these effects in the tumor cell line. An increase in the peroxisome proliferator-activated receptor-γ co-activator-1α (PGC1α) level and a decrease in the hypoxia-inducible factor-1α (HIF1α) level would suggest a possible metabolic shift. The knock-down in the nuclear respiratory factor-1 (NRF1) attenuated the SFN-induced effect on prostate cancer cells demonstrating that mitochondrial biogenesis plays an important role in cell death for this kind of tumor cells. This evidence supports SFN as a potential antineoplastic agent that could inhibit tumor development and could protect normal tissues by modulating common processes.

1. Introduction

In order to establish the best therapeutic strategy for each kind of tumor, a metabolic characterization should be done first in model cell lines. In some experimental cancer models it has been shown that mitochondrial-based metabolism is very important in the maintenance of cancer cell survival and malignancy (Zong et al., 2016). However, it is widely accepted that mitochondrial dysfunction contributes to cell growth and tumorigenesis. Many types of tumors rely on glycolytic metabolism to proliferate and invade (Boland et al., 2013). Like disturbing the redox status of cancer cells, shifting metabolism and promoting a mitochondria-dependent one could be an appropriate strategy for many types of cancer.

It is well known that preservation of mitochondrial function plays a major role in cytoprotection of non-cancer tissues (Guerrero-Beltrán et al., 2010; Sun et al., 2013). Recently, we found that curcumin, a bifunctional antioxidant, protected renal tubular cells against gentamicin toxicity through a mechanism that involved the nuclear factor E2-related factor-2 (Nrf2) and the regulator of mitochondrial biogenesis, the peroxisome proliferator-activated receptor-γ co-activator-1α (PGC1α) (Negrette-Guzmán et al., 2015). Likewise, it has been demonstrated that mitochondrial biogenesis is a crucial mechanism for proliferation, invasiveness, and metastasis control of several kinds of tumors (Liu et al., 2014; Onishi et al., 2014; Wang and Moraes, 2011), though others cancer types showed a noticeable adaptation when mitochondrial mass and function were increased (Alam et al., 2016; Zong et al., 2016). Mitochondrial dynamics have also been highlighted as a regulator of cell fate. In general, mitochondrial fusion has been associated with apoptosis resistance in cancer cells whereas mitochondrial fragmentation is a signal for apoptosis initiation. The GTPases mitofusin 1 (Mfn1), mitofusin 2 (Mfn2), and optic-nerve atrophy 1 (Opa1) are the main regulators of mitochondrial fusion

* Corresponding author.
E-mail address: pedraza@unam.mx (J. Pedraza-Chaverri).

http://dx.doi.org/10.1016/j.fct.2016.12.020
0278-6915/

and have been demonstrated to protect cells from mitochondrial outer membrane permeabilization and apoptosis (Jourdain and Martinou, 2009; Corrado et al., 2012; Thomas and Jacobson, 2012). The main protein in mitochondrial fission machinery, the dynamin-related protein-1 (Drp1), stimulates the oligomerization of Bcl-2-associated X protein (Bax) on the mitochondrial outer membrane, making it permeable, allowing the cytochrome *c* release and triggering intrinsic apoptosis (Montessuit et al., 2010). Mitochondrial hyperfusion has also been identified as a response to mild stress and could represent a pro-survival mechanism (Tondera et al., 2009).

Previously, mitochondrial modulation induced by the indirect antioxidant sulforaphane (SFN) on cancerous and non-cancerous cells was reviewed. SFN is an isothiocyanate derived from cruciferous vegetables and its best-known molecular target is Nrf2 (Negrette-Guzmán et al., 2013b). Nevertheless, the cytotoxicity and anti-proliferative effects of SFN on cancer cells have been linked to other mechanisms and targets, e.g., the activation of mitogen-activated protein kinases or the activation of the tumor suppressor protein p53, which can ultimately initiate an intrinsic apoptosis program (Rudolf and Cervinka, 2011; Rudolf et al., 2014). It has not been investigated if these pathways and proteins are associated to Nrf2. We proposed that both SFN-induced death in cancer cells and cytoprotection in non-cancer cells may be mediated by a differential regulation of mitochondrial biogenesis and dynamics that depends on the cell type. Mitochondrial biogenesis could be promoted by activation of Nrf2 (Negrette-Guzmán et al., 2013b). In this work, we used two characterized cell models in which SFN effects have been widely studied. It has been shown that SFN protects kidney tubular cells LLCPK1 against nephrotoxicants by means of nuclear accumulation of Nrf2, induction of an antioxidant response, preservation in mitochondrial functions, and finally, inhibition of mitochondrial apoptosis (Guerrero-Beltrán et al., 2010; Negrette-Guzmán et al., 2013a). However, SFN induces mitochondrial apoptosis in prostate cancer cells PC3 (Singh et al., 2004). Herein, we did not intend to compare redox and metabolic SFN-induced responses between tumor and non-tumor cells although this must be performed; we aimed to describe two known opposite SFN-induced effects in both (i) a non-transformed cell type which is a co-lateral target of antineoplastic agents and (ii) a tumor cell line used as a model for chemotherapy investigation. Our experiments were focused on the modulation of mitochondrial biogenesis and dynamics. Our results would boost SFN as an excellent agent in some cancer treatments. Further studies are still required.

2. Materials and methods

2.1. Reagents

SFN (S8044, a racemic mixture, R,S-sulforaphane) was purchased from LKT Laboratories (St. Paul, MN, USA); Dulbecco's Modified Eagle Medium (DMEM), Advanced Roswell Park Memorial Institute (RPMI) 1640 medium, fetal bovine serum (FBS), trypsin, and other supplements were obtained from Gibco-Thermo Fisher Scientific (Waltham, MA, USA). 3-(4,5-dimethyltiazol-2-yl)-2,5-diphenyltetrazolium bromide (MTT) and crystal violet were purchased from Sigma-Aldrich (St. Louis, MO, USA). The probes Mito-Tracker Green FM and 5,5',6,6'-tetrachloro- 1,1'3,3'-tetraethylbenzimidazolyl-carbocyanine iodide (JC-1), and Lipofectamine 2000 were acquired from Invitrogen-Thermo Fisher Scientific (Eugene, OR, USA). Mammalian Protein Extraction Reagent (M-PER) was purchased from Thermo Scientific-Thermo Fisher Scientific (Eugene, OR, USA). All buffers and reagents for Western blotting were obtained from Bio-Rad Laboratories (Hercules, CA, USA). The following antibodies were purchased from Santa Cruz Biotechnology (Dallas, TX, USA): anti-nuclear respiratory factor-1 (NRF1, sc-33771), anti-Bax (sc-493), anti-mitochondrial fission-1 (Fis1, sc-98900), anti-Drp1 (sc-32898), and anti-Nrf2 (sc-722). Anti-mitochondrial transcription factor-A (TFAM, 7495) and anti-β-actin (12262) were purchased from Cell Signaling Technology (Danvers, MA, USA). Anti-mitochondrially-encoded NADH dehydrogenase-1 (MT-ND1, ab74257) and anti-PGC1α (ab54481) were provided by Abcam (Cambridge, MA, USA). Novus Biologicals (Littleton, CO, USA) provided the anti-hypoxia-inducible factor-1α (HIF1α, NB100-479) antibody. Anti-voltage-dependent anion channel (VDAC, V2139) antibody was purchased by Sigma-Aldrich (St. Louis, MO, USA). *In Situ* Cell Death Detection Kit, POD (Cat. No. 11684817 910), was acquired from Roche Applied Science (Mannheim, Germany). Dicer-substrate small interfering RNA (DsiRNA) for silencing NRF1 and control DsiRNA were obtained from IDT Technologies (Coralville, IA, USA). Universal biotinylated link, streptavidin conjugated to horseradish peroxidase (HRP), and 3,3'-diaminobenzidine (DAB) were purchased from Dako (Carpinteria, CA, USA). All other chemical and compounds used were reagent grade and commercially available.

2.2. Cell culture, treatments and cell assays

Porcine renal epithelial cells LLCPK1 (CL-101, American Type Culture Collection, Rockville, MD, USA) were grown in DMEM supplemented with 10% FBS and 1% antibiotic under permissive conditions: 37 °C and 5% CO_2 (Guerrero-Beltrán et al., 2010). Androgen-independent human prostate cancer cells PC3 (CRL-1435, American Type Culture Collection, Rockville, MD, USA) were cultured in Advanced RPMI 1640 supplemented with 3% FBS, 1% antibiotic, 1% non-essential amino acids, 1% pyruvate and 1% glutamine. Both cell lines were seeded onto 96-well plates at a density of 5×10^3 cells/well and used for experiments the next day. Cells were incubated in medium containing 1–20 μM SFN for 24–96 h in order to evaluate the effect of SFN on MTT reduction. Every 24 h, culture medium was replaced by fresh medium with SFN. MTT reduction was assessed as was done previously (Negrette-Guzmán et al., 2015). Briefly, cells were incubated in medium containing MTT (0.125 mg/mL) at 37 °C for 1 h in humidified air supplemented with 5% CO_2. Medium was then discarded and the formazan crystals deposited in each well bottom were dissolved in 100 μL of 0.1 N HCl in isopropanol. Absorbance was determined at 570 nm using a Synergy HT multimode microplate reader (Biotek Instruments Inc., Winooski, VT, USA). Based on the results from MTT assays and other previous studies (Guerrero-Beltrán et al., 2010; Negrette-Guzmán et al., 2013a), following experiments were carried out with 5 μM SFN. 5-bromo-2-deoxy-uridine (BrdU) incorporation as a measurement of cell proliferation was assessed in LLCPK1 cells using the Cell Proliferation ELISA, BrdU kit (Roche, Mannheim, Germany) and following the manufacturer instructions. For crystal violet assay, the medium was discarded at the end of treatment, cells were washed with phosphate-buffered saline (PBS) pH 7.4, then fixed with 4% paraformaldehyde pH 7.4 for 30 min and stained with 0.2% crystal violet in 6% methanol for 30 min at room temperature. Finally, each well in the plate was carefully washed with distilled water until wastewater was not colored by crystal violet. The plate was left to dry and the crystal violet staining nuclei was dissolved using 100 μL/well of 0.5% sodium dodecyl sulfate (SDS) in a solution containing 0.1 M sodium citrate in 50% ethanol. The plate was read at 570 nm in a microplate reader.

2.3. Apoptosis detection

DNA fragmentation, as a late apoptosis marker, was evaluated by terminal-deoxynucleotidyltransferase mediated dUTP-digoxigenin

nick end labeling (TUNEL) and immunocytochemistry in PC3 cells after 72 h of SFN treatment. The immunocytochemical part was conducted as previously described (Negrette-Guzmán et al., 2015). Following the treatment, PC3 cells were detached, washed and fixed with 4% formaldehyde pH 7.4 on slides. Antigenic retrieval was performed by boiling in 0.01% sodium citrate solution pH 6.0 and reduction of background was done by blocking with 3% H_2O_2 solution in methanol and then with 2% normal swine serum in PBS. After, cells were incubated for 50 min at 37 °C in the dark with the enzyme terminal transferase (Tdt), added in a 1:200 mixture in buffer solution including fluorescein-conjugated oligonucleotides. Then, cells were washed in 1 × PBS and incubated for 30 min with the anti-fluorescein antibody at 37 °C. Finally, brown color on immunopositive regions was developed through incubation in DAB and counterstaining with hematoxylin. Images were acquired using an Olympus BX40 microscope (Olympus, Center Valley, PA, USA) and TUNEL-positive cells were counted manually.

2.4. Mitochondrial relative mass and mitochondrial membrane potential

Cells were seeded at a density of 1.5×10^5 cells/well in 6-well plates and treated with 5 μM SFN for 24, 48 and 72 h. At the end of treatment, cells were detached, centrifuged and re-suspended in basal medium containing 50 nM MitoTracker Green FM or 2 μM JC-1 Dye and incubated in darkness for 15 min at 37 °C. Then, cells were centrifuged, re-suspended in 1 × PBS and analyzed in a BD FACSCalibur flux cytometer (BD Biosciences, San Jose, CA, USA) at the proper channels.

2.5. Western blotting and subcellular fractionation

Levels of protein markers for mitochondrial biogenesis and dynamics and other proteins were obtained by Western blot as has been described (Vega et al., 2015) before with few modifications. Protein extracts were obtained from total or mitochondrial fractions at the end of treatments using M-PER containing protease inhibitor cocktail. A Bradford-based commercial kit assessed protein in samples. Then, samples were boiled with Laemmli buffer containing 5% β-mercaptoethanol for 7 min, separated on 12% SDS-polyacrylamide mini-gels, and transferred to nitrocellulose membranes using the *Trans*-Blot Turbo Blotting System (Bio-Rad, Hercules, CA, USA). Afterwards, membranes were incubated for 18 h at 4 °C in the following primary antibody solutions: anti-TFAM, anti-MT-ND1, anti-NRF1, or anti-Bax in total lysates; anti-Fis1 or anti-Drp1 in mitochondrial fractions. Anti-β-actin or anti-VDAC antibodies were used as loading controls in whole cell lysate or mitochondrial fraction, respectively. After incubation in proper secondary antibodies, membranes were revealed using the Odissey CLx Infrared Imaging System (LI-COR, Lincoln, NE, USA). Changes in protein levels were evaluated by densitometry in the immunoreactive bands and corrected against the respective loading control, then each obtained value was normalized to the respective untreated control value at each time point. This analysis was performed with the Image Studio Lite Ver 5.2 software (LI-COR, Lincoln, NE, USA).

For obtaining mitochondrial fractions, cells were seeded in 150 mm dishes at a density of 1.5×10^4 cells/cm^2 and incubated in medium with 5 μM SFN during 48 h. At the end of this period, cells were detached with a cell lifter and the Mitochondria Isolation Kit for Cultured Cells (Abcam, Cambridge, MA, USA) was used according to manufacturer instructions. Mitochondrial protein was quantified and samples were treated the same way as total cell lysates.

2.6. Knockdown

A DsiRNA was used to silence NRF1 expression and thus to evaluate its role in PC3 cell viability decrease induced by SFN. Transfections were performed using Lipofectamine 2000 and SFN treatments were started 48 h after transfection. Cells were harvested for Western blot analysis at 48 h of incubation with SFN or analyzed by crystal violet assay after 72 h of treatment.

2.7. Transmission electronic microscopy and mitochondrial morphology

In order to study changes in mitochondrial morphology induced by SFN, LLCPK1 and PC3 cells were detached at the end of treatments and fixed with 2.5% glutaraldehyde in 0.15 M cacodylate buffer, pH 7.2. After, cells were post-fixed with 1% osmium tetroxide, then dehydrated with ethyl alcohol in ascending concentrations and with propylene oxide. Following this, infiltration was performed with resin (Embed-812) diluted in propylene oxide (2:1, 1:1 and 1:2) and pure resin for 8 h. Sections were observed under electron microscopy 80 nm contrasted with uranyl acetate and lead citrate. Images were obtained with the electron microscope Tecnai Spirit BioTwin (FEI, Hillsboro, OR, USA) at 80 kV and quantification of mitochondrial area and circularity was carried out by using ImageJ 1.50g software (NIH, USA). Circularity is defined as $4\pi \times (\text{area}/\text{perimeter}^2)$ and is a value ranging from 0, meaning an infinitely elongated polygon, to 1, which indicates a perfect circle; this parameter intends to provide an idea of the shape of mitochondria.

2.8. Immunocytochemical detection of PGC1α, HIF1α and Nrf2

Immunocytochemistry was performed as previously described in the apoptosis detection procedure (Section 2.3.) but the slides were incubated overnight at room temperature with anti-PGC1α, anti-HIF1α or anti-Nrf2 primary antibodies instead of Tdt. The next day, slides were washed five times with 1 × PBS and incubated with universal biotinylated link and later with streptavidin-HRP. Please see Section 2.3. for color development and image acquirement procedures.

2.9. Statistical analysis

Most parameters were assessed as three independent experiments (n = 3, namely three different cell passages cultured in different dates). Experimental groups were analyzed by triplicated into independent experiments of some parameters (e. g. MTT reduction, BrdU incorporation, crystal violet, MitoTracker Green FM, and JC-1). Results were expressed as mean ± SEM. Data were analyzed by paired *t*-test or one-way ANOVA followed by multiple comparisons according to Dunnett or Bonferroni, as appropriate. The software Prism 5.0, GraphPad (San Diego, CA, USA) was used for this purpose. A *p*-value less than 0.05 was considered statistically significant.

3. Results

3.1. SFN induces mitochondrial activation in LLCPK1 cells

In a previous work, we observed that a 96 h treatment with 5 μM SFN on LLCPK1 cells induced an increase in MTT reduction without an increase in cell number (Negrette-Guzmán et al., 2013a). Evaluating this effect in a broader range of times and concentrations was required, as well as discarding a possible effect on the cell proliferation rate. Fig. 1A shows profiles of MTT reduction from LLCPK1 cells treated with 1–20 μM SFN at 24, 48, 72 and 96 h.

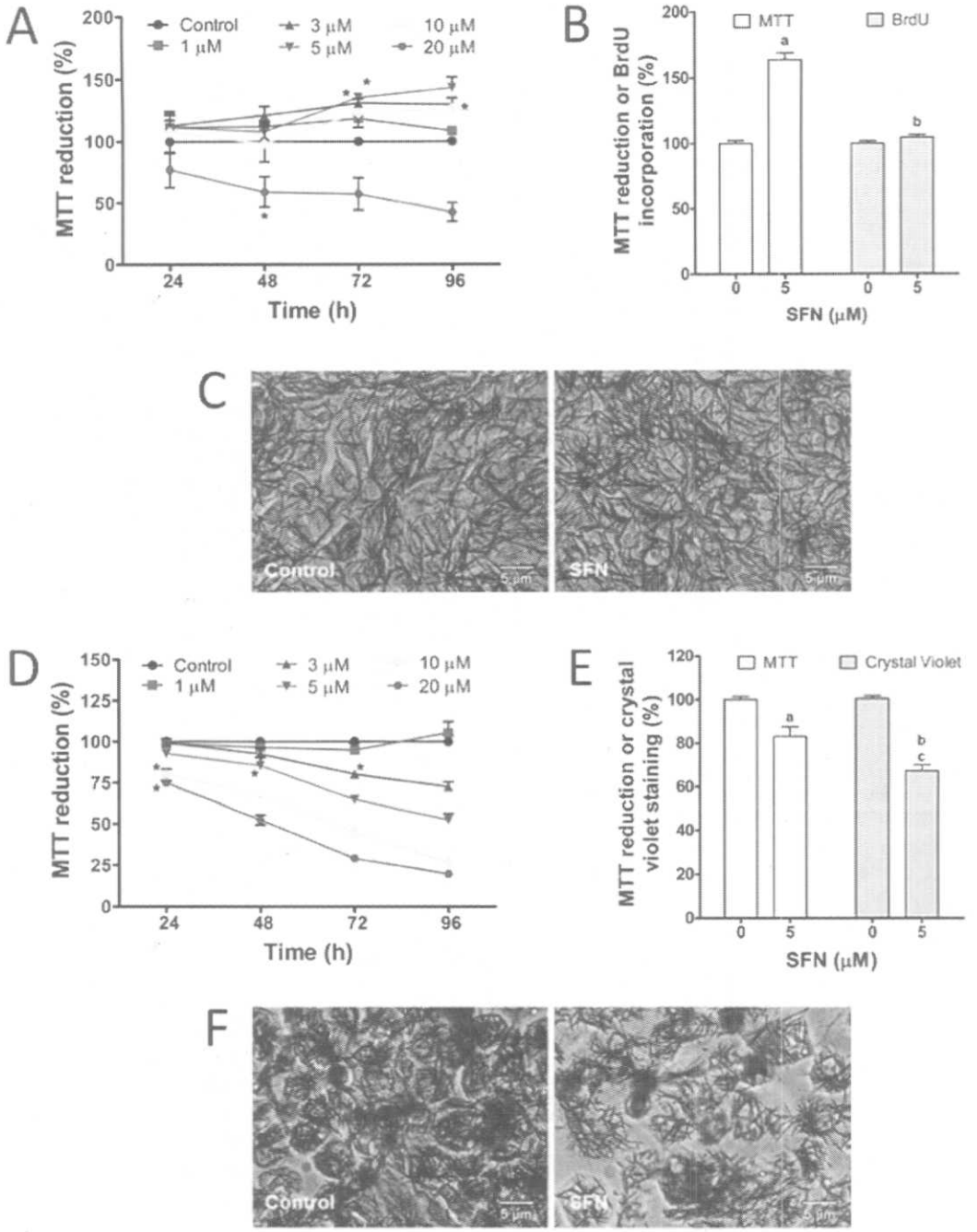

Fig. 1. Effect of sulforaphane (SFN) on mitochondrial activity, cell proliferation and cell viability in LLCPK1 and PC3 cells. **A**, MTT reduction profiles in LLCPK1 cells treated with 1, 3, 5, 10 and 20 μM SFN at 24, 48, 72 and 96 h. **B**, Comparison between MTT reduction and BrdU incorporation in LLCPK1 cells incubated 72 h with 5 μM SFN. **C**, Micrographs showing the formazan produced by MTT reduction in LLCPK1 cells after 72 h without treatment (left) and treated with 5 μM SFN (right). Chosen fields in each group have similar cell densities. 40×. **D**, MTT reduction profiles in PC3 cells treated with 1, 3, 5, 10 and 20 μM SFN at 24, 48, 72, and 96 h. **E**, Comparison between MTT reduction and crystal violet staining in PC3 cells incubated 72 h with 5 μM SFN. **F**, Micrographs showing the formazan produced by MTT reduction in PC3 cells after 72 h without treatment (left) and treated with 5 μM SFN (right). 40×. Percentages were calculated with respect to controls. Data are mean ± SEM, n = 3. $^{*}P < 0.05$ vs. Control, $^{a}P<0.05$ vs. MTT control (0), $^{b}P < 0.05$ vs. MTT SFN treated (5), $^{c}P < 0.05$ vs. Crystal violet control (0).

Positive slopes can be noticed at SFN concentrations of 3 μM (blue line) and 5 μM (green line) with significance at 72 h compared to untreated cells (black line). The treatment with 20 μM SFN (brown line) induced a decrease in cell viability also visible when cells were examined under the microscope after 24 h. The level of formazan produced by MTT reduction is directly proportional to the number of cells. However, this reduction happens in metabolically active cells and the changes in metabolic activity will result in changes in MTT reduction though the number of cells does not change. The major catalysts that convert MTT in formazan are mitochondrial dehydrogenases, so this metabolic activation could be considered a mitochondrial activation (Sumantran, 2011; Vega-Avila and Pugsley, 2011). Fig. 1B demonstrates that while MTT reduction was increased at 72 h of treatment with 5 μM SFN, BrdU incorporation

was not. These data suggest an SFN-induced mitochondrial activation rather than a promotion in cell proliferation of LLCPK1 cells. Fig. 1C shows greater formation of formazan crystals in LLCPK1 cells treated with SFN for 72 h compared to untreated cells.

3.2. SFN induces a fall in PC3 cell viability accompanied by mitochondrial activation and apoptosis

As for LLCPK1 cells, a similar MTT reduction profile was obtained for PC3 cells and the behavior was entirely different (Fig. 1D). 10 and 20 μM SFN (yellow and brown lines, respectively) induced a drop in cell viability after the first 24 h. 5 μM SFN (green line), the concentration that gave the best MTT reduction increase in LLCPK1 cells, induced a decline in cell viability after 48 h. As SFN-induced cell death in PC3 is well-known (Choi et al., 2007; Shankar et al., 2008; Xiao et al., 2009), it can be assumed that the decrease in MTT reduction corresponds to a decrease in cell viability. Nevertheless, a similar comparison as that for LLCPK1 cells was made. In Fig. 1E, it can be observed that viability measured as crystal violet staining was lower than that measured as MTT reduction for SFN-treated groups. It is worth mentioning that crystal violet assay relies on the nuclei staining of cells available in a microplate well and the color intensity is proportional to the number of viable cells. Together with the MTT assay, a mitochondrial activation effect can be distinguished (Vega-Avila and Pugsley, 2011); SFN induced a decrease in cell viability while inducing a mitochondrial activation in PC3 cells. Fig. 1F shows the formazan crystals formed after 72 h of treatment with SFN in PC3 cells and in untreated cells.

The mechanism by which SFN decreases cell viability in PC3 cells seems to be associated with mitochondrial apoptosis as shown in Fig. 2. Parallel to mitochondrial activation, disruption of mitochondrial membrane potential was observed after 48 h of treatment with 5 μM SFN (Fig. 2A). Accordingly, an increase in Bax levels was observed at 48 h (Fig. 2B) and late apoptosis was detected by TUNEL assay at 72 h of SFN treatment (Fig. 2C and D).

3.3. SFN induces mitochondrial biogenesis in LLCPK1 and PC3 cells

In order to explore the mechanisms that could be mediating the effects in LLCPK1 and PC3 cells observed above, some mitochondrial biogenesis markers were measured. Cells were treated with 5 μM SFN, a concentration which showed noticeably opposite cell-specific MTT patterns between LLCPK1 and PC3 cells (Supplementary Fig. S1); and which falls into a concentration range with pharmacokinetic pertinence (Negrette-Guzmán et al., 2013b). Relative mitochondrial mass was augmented by the first 24 h of SFN treatment in LLCPK1 cells but that effect was not observed by 48 h–72 h (Fig. 3A). This outcome was striking considering the MTT profile and BrdU incorporation obtained for LLCPK1 cells treated with SFN (Fig. 1B). Levels of proteins that have typically been used as mitochondrial biogenesis markers TFAM, MT-ND1, and NRF1 were evaluated (Fig. 3B). The behavior over time was very similar to that observed in relative mitochondrial mass with increases in protein levels at 24 h and a subsequent normalization compared to controls (Fig. 3C).

The effect of SFN in PC3 cells seemed to be temporarily different from that observed in LLCPK1 cells although the mitochondrial biogenesis markers also increased. A positive slope was observed in relative mitochondrial mass reaching significance at 48 h of treatment ($P < 0.05$, Fig. 4A). At 72 h there was a lot of dispersion, which would explain the loss in significance; however, none of the values measured in SFN-treated cells were lower than those for control cells. Protein levels did not clarify this much. In Fig. 4B and C, it can be observed that while TFAM reached a maximum at 48 h with normalization at 72 h, MT-ND1 seems to increase over time to become significant at 72 h after SFN treatment. A similar trend was observed for NRF1 level. Interestingly, hallmarks of apoptosis via-mitochondria were accompanied by mitochondrial biogenesis in this tumor cell line under SFN-treatment.

In addition, we wanted to take advantage of the information offered by JC1. JC-1 is a probe that diffuses to mitochondria and

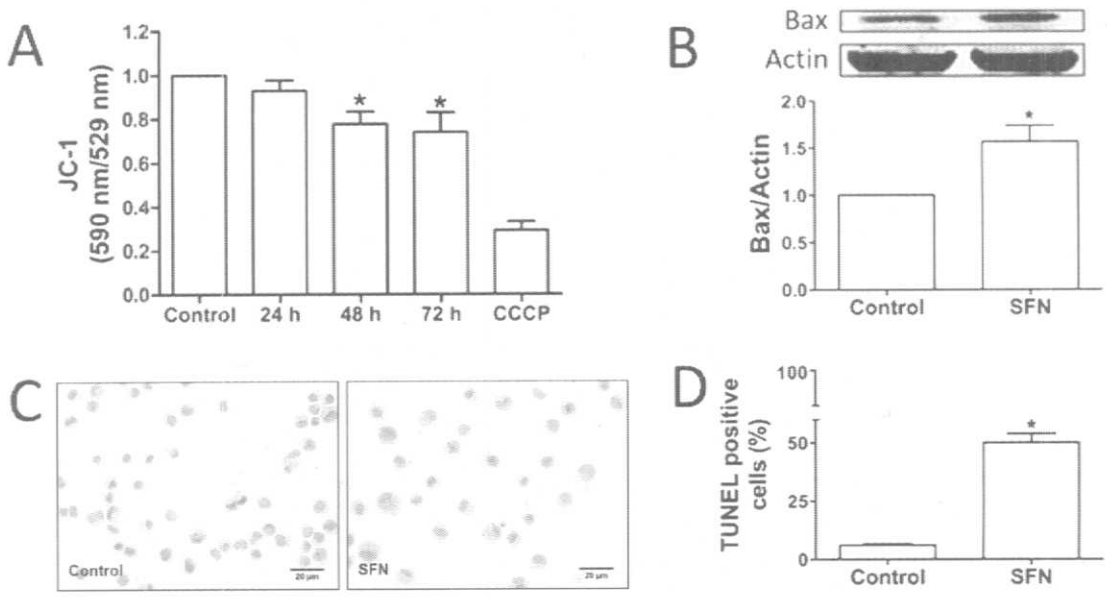

Fig. 2. Mitochondria-associated apoptosis induced by SFN in PC3 cells. **A**, Effect of 24, 48, and 72 h of incubation with 5 μM SFN on mitochondrial membrane potential of PC3 cells, measured as the ratio 590 nm/525 nm of fluorescence of JC-1 probe. Data shown are from normalizing raw values with respect to the control raw value in each experiment and time. **B**, Bax cell levels measured by Western blot in whole lysate of PC3 cells untreated (Control) and treated with 5 μM SFN for 48 h. Data shown are from normalizing raw values with respect to the control raw value in each experiment. **C**, Chromatin fragmentation assessed by terminal-deoxynucleotidyltransferase mediated dUTP-digoxigenin nick end labeling (TUNEL) in PC3 cells untreated (Control) and at 72 h of SFN treatment. 40×. **D**, TUNEL-positive cells counting. Data are mean ± SEM, n = 3. *$P < 0.05$ vs. Control. CCCP: carbonyl cyanide *m*-chlorophenylhydrazone.

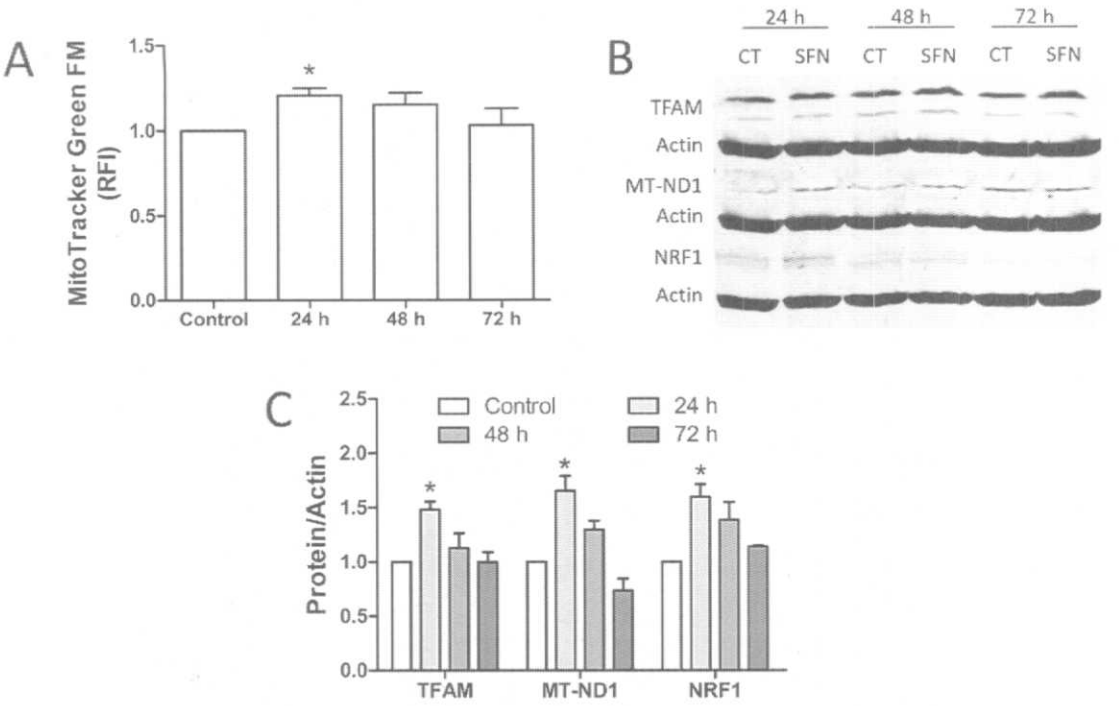

Fig. 3. Sulforaphane (SFN) induces mitochondrial biogenesis in LLCPK1 cells. **A**, Relative mitochondrial mass measured as relative fluorescence intensity (RFI) of MitoTracker Green FM in LLCPK1 cells treated with 5 μM SFN for 24, 48, and 72 h. **B**, Western blot for the mitochondrial transcription factor-A (TFAM), the mitochondrially-encoded NADH dehydrogenase-1 (MT-ND1), and the nuclear respiratory factor-1 (NRF1) in whole lysate of LLCPK1 cells treated with 5 μM SFN for 24, 48, and 72 h. **C**, Densitometry showing protein levels of TFAM, MT-ND1, and NRF1 at 24, 48, and 72 h. Data shown are from normalizing raw values with respect to the control raw value in each experiment and time. Data are mean ± SEM, n = 3 except for NRF1 (n = 2). *P < 0.05 vs. Control.

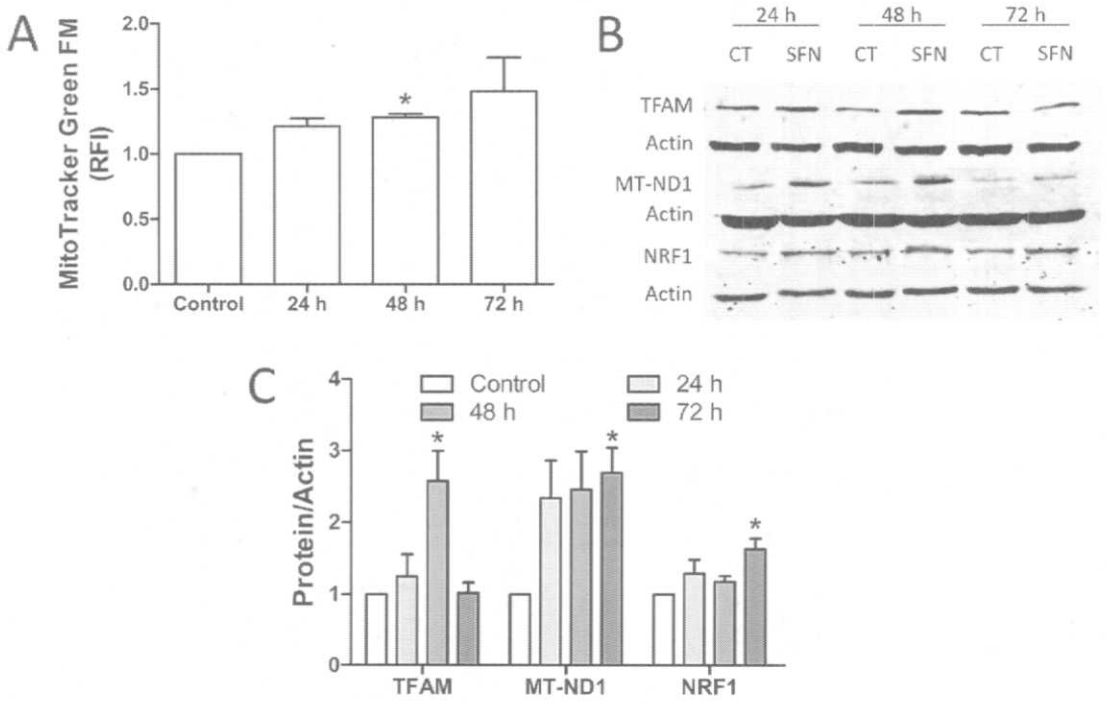

Fig. 4. Sulforaphane (SFN) induces mitochondrial biogenesis in PC3 cells. **A**, Relative mitochondrial mass measured as RFI of MitoTracker Green FM in PC3 cells treated with 5 μM SFN for 24, 48 and 72 h. **B**, Western blot for the mitochondrial transcription factor-A (TFAM), the mitochondrially-encoded NADH dehydrogenase-1 (MT-ND1), and the nuclear respiratory factor-1 (NRF1) in whole lysate of PC3 cells treated with 5 μM SFN for 24, 48, and 72 h. **C**, Densitometry showing protein levels of TFAM, MT-ND1, and NRF1 at 24, 48, and 72 h. Data shown are from normalizing raw values with respect to the control raw value in each experiment and time. Data are mean ± SEM, n = 3. *P < 0.05 vs. Control.

oligomerizes when the membrane potential is over −140 mV, giving a fluorescence signal at 590 nm (red). When mitochondrial membrane is depolarized, JC-1 remains monomeric and emits a fluorescence signal at 529 nm (green). The ratio 590 nm/529 nm is used as a measurement of how polarized mitochondria are (Cottet-Rousselle et al., 2011). Therefore, signals at 590 and 529 nm are originated by polarized and depolarized mitochondria, respectively, namely all mitochondrial mass. In this study, it was noted that whereas the ratio 590 nm/529 nm of fluorescence emission for JC-1 was getting lower in treated PC3 cells, the sum of these signals (590 nm + 529 nm) into a same assay was increasing (Supplementary Fig. S2). Because this pattern was repeated in all tests, it was decided to show these results without trying to introduce a new method. If this sum was taken as a relative mitochondrial mass marker, it would be found that the outcome is similar to that obtained by MitoTracker Green FM. This JC-1 approach had not been reported before and could become a good complementary tool for mitochondria research after an appropriate standardization. Supplementary Fig. S3 strengthens the observations above: mitochondrial and total protein were measured at 48 h of SFN treatment in LLCPK1 and PC3 cells for getting mitochondrial extracts. Outcomes were similar to those obtained by MitoTracker Green FM at 48 h (Figs. 3A and 4A).

3.4. SFN-induced NRF1 upregulation is required for a decrease in cell viability of PC3 cells

To establish the role of SFN-induced mitochondrial biogenesis in PC3 cell death, NRF1 was targeted for knockdown. In Fig. 5, it can be noted how NRF1 knock-down attenuated the effect of SFN on PC3 cell viability at 72 h. SFN induced a drop in cell viability of approximately 33% related to control cells when treated with the scrambled oligonucleotide. When NRF1 was silenced, the drop in cell viability induced by SFN was just 3–4%.

3.5. SFN induces mitochondrial fusion in LLCPK1 cells and mitochondrial fission in PC3 cells

After the findings about mitochondrial biogenesis induced by SFN in different cell types with different cell fates, we wanted to know how SFN affects mitochondrial morphology. The changes in LLCPK1 cell mitochondria after 48 h-treatment were very clear (Fig. 6A and B). Interestingly, when mitochondrial biogenesis markers were normalized in SFN-treated LLCPK1 cells (48 h and 72 h, Fig. 3B and C), an increase in the mitochondrial area was observed, compared to untreated cells (Fig. 6A and B). Together with the diminishment in mitochondrial circularity at 72 h of SFN treatment (Supplementary Fig. S4), it can be said that LLCPK1 mitochondria become larger and longer along SFN treatment. But mitochondrial fusion could be a result of an inhibition in mitochondrial fission. Fig. 6C shows how protein levels from the mitochondrial fission machinery are decreased by the SFN treatment. Fis1 was significantly decreased after 48 h of incubation with 5 μM SFN. The 60 kDa isoform of Drp1 showed a tendency to decrease but there was no statistical significance (Fig. 6D). The protein belonging to the mitochondrial fusion machinery Mfn1 did not show significant changes in LLCPK1 cells treated with SFN compared to untreated cells (Supplementary Fig. S5).

On the other hand, SFN induced a reduction in the size of mitochondria in PC3 cells after 24 h and 48 h of incubation (Fig. 7A and B). Micrographs in Fig. 7A show more individual mitochondria but with smaller areas at 24 and 48 h of SFN treatment. Mitochondria in control cells were significantly smaller at 48 h compared to 24 h. At 72 h, the size of mitochondrial area of SFN-treated cells was similar to that of control cells. Mitochondrial fractions of SFN-treated and control PC3 cells were obtained after 48 h; examination of mitochondrial fission protein levels by Western blot showed an elevation in the 60 kDa isoform of Drp1 and in Fis1 (Fig. 7C and D). This increase in mitochondrial fragmentation mediated by Drp1 and Fis1 was associated with the increase in Bax levels measured at 48 h (Fig. 2B) as well as the late apoptosis at 72 h of SFN treatment (Fig. 2C and D). Bax increase is a marker of intrinsic apoptosis that has been reported to be elevated in PC3 cells treated with SFN.

3.6. A seemingly SFN-induced metabolic shift was observed in PC3 cells with an early activation of Nrf2

Cell death in PC3 cells treated with SFN accompanied by mitochondrial biogenesis suggests a metabolic shift that would make tumor cells more competent to lead apoptosis via mitochondria. Fig. 8 shows micrographs of immunocytochemistry against PGC1α and HIF1α at 72 h of treatment with 5 μM SFN. Immunostaining is increased for PGC1α and diminished for HIF1α in SFN group compared to control group. Even though multiple molecular responses associated with PGC1α and HIF1α exist, they are well known as promoters of mitochondrial and glycolytic metabolism, respectively. Interestingly, those effects in PGC1α and HIF1α

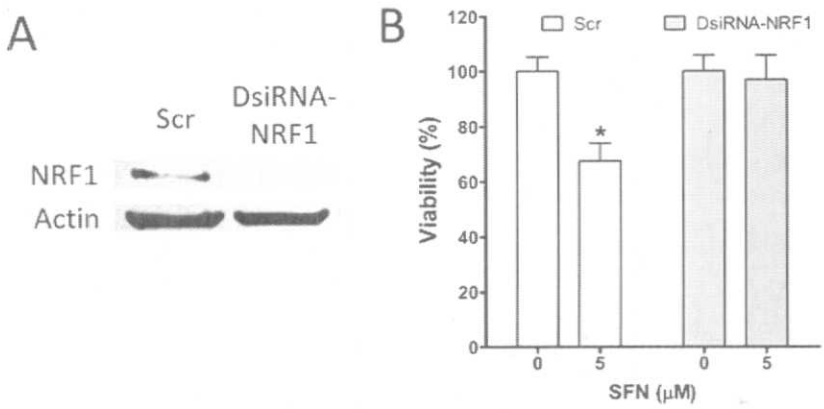

Fig. 5. Role of the nuclear respiratory factor-1 (NRF1) in sulforaphane (SFN)-induced viability decrease in PC3 cells. **A**, Knock-down of NRF1 confirmed by Western blot 72 h after transfecting PC3 cells with either control (Scr) or Dicer-substrate small interfering RNA (DsiRNA) targeted to knock-down NRF1 (DsiRNA-NRF1). **B**, Cell viability was measured by crystal violet assay after 72 h of incubation with 5 μM SFN (24 h after transfection). Data are mean ± SEM, n = 3, *P < 0.05 vs. Control.

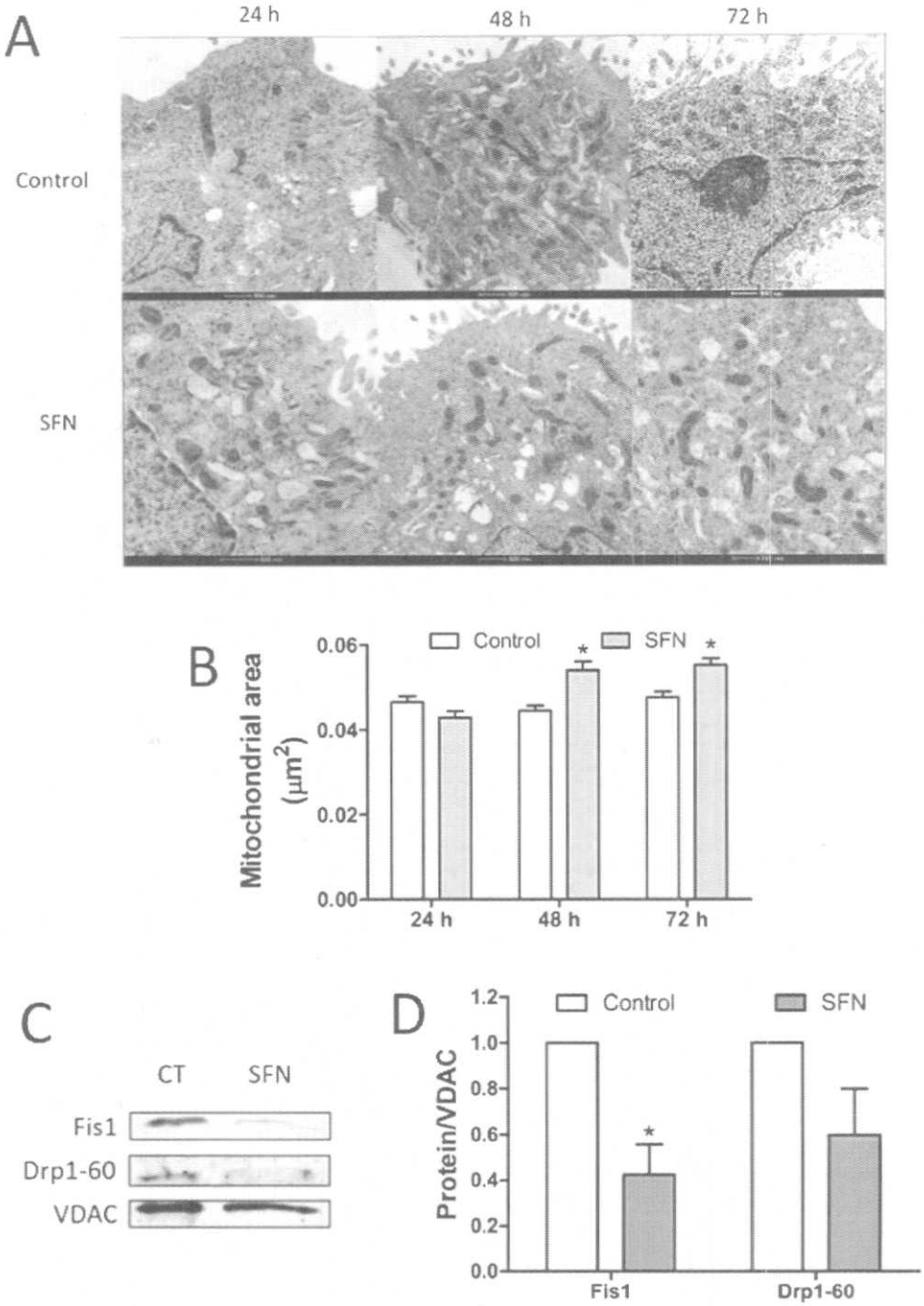

Fig. 6. Effects of sulforaphane (SFN) on mitochondrial dynamics in LLCPK1 cells. **A**, Representative electronic micrographs showing mitochondrial morphology of LLCPK1 cells treated with 5 μM SFN over 24, 48, and 72 h and controls. Magnification 9300×. **B**, Mean mitochondrial area for LLCPK1 cells treated with 5 μM SFN for 24, 48, and 72 h. 400–736 mitochondria per group. **C**, Western blot for mitochondrial fission 1 (Fis1) and dynamin-related protein-1 (Drp1, 60 kDa isoform) in mitochondrial fractions of LLCPK1 cells treated with 5 μM SFN for 48 h. **D**, Densitometry showing mitochondrial protein levels of Fis1 and Drp1 (60 kDa isoform). Values were normalized with respect to controls. Data are mean ± SEM, n = 3, *P < 0.05 vs. Control.

expression and stabilization were preceded by a strong nuclear localization of Nrf2.

4. Discussion

An interesting debate could be had from the first results of this study. Concentration-dependent hormetic effects were seen in a same cell type: while concentrations of SFN under 10 μM showed apparent benefits in mitochondrial activity and no effect in cell viability of LLCPK1 cells, 20 μM SFN started killing them since 48 h of incubation (Fig. 1A). This raises the questions: is it valid to test antiproliferative effects of SFN on cancer cells at concentrations as high as 20 μM or higher? Why not use the lower concentration with pro-apoptotic activity? This is even more important in the case of molecules which reportedly induce cytoprotective responses in other non-cancer tissues. Reductionist models of antitumor

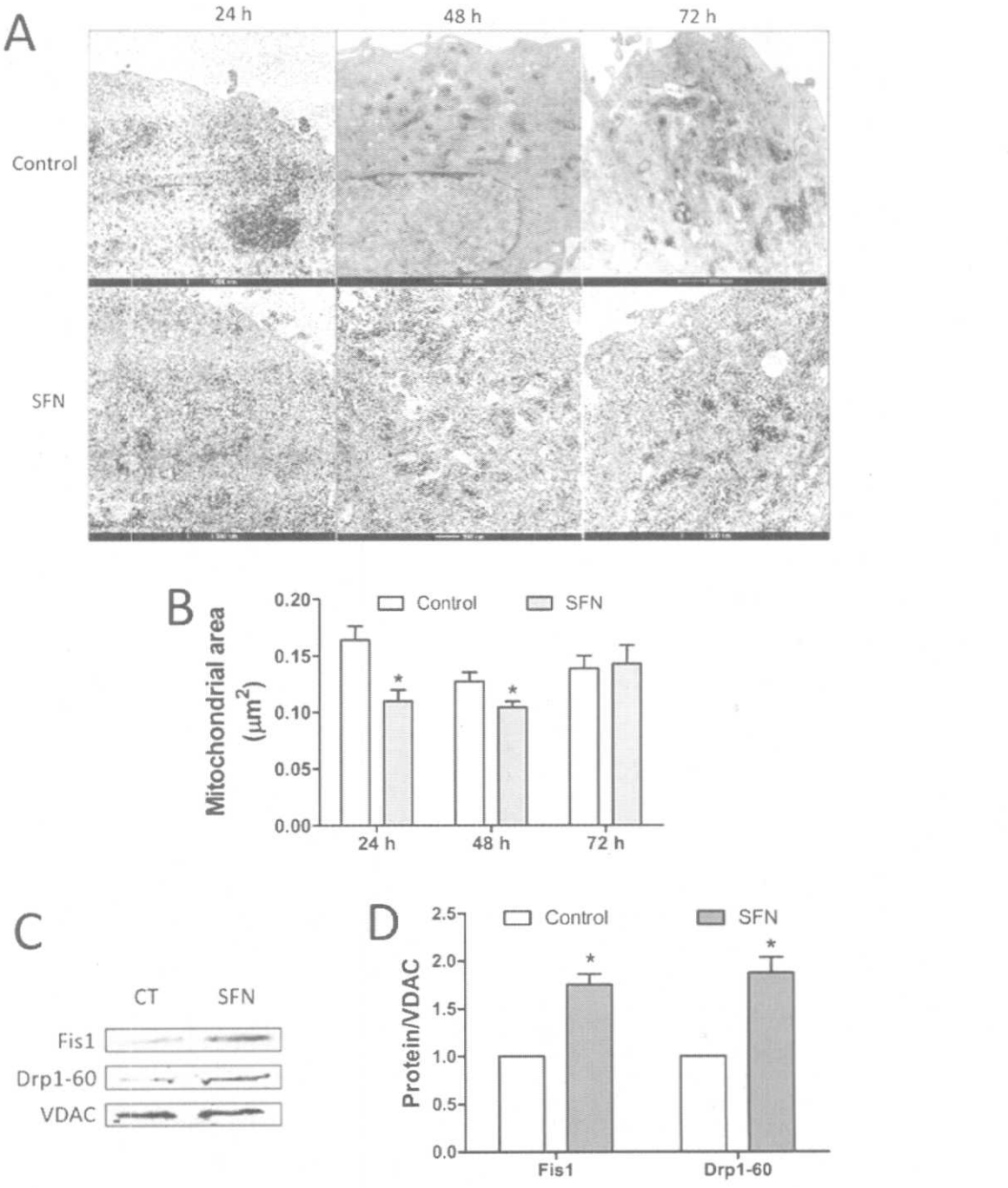

Fig. 7. Effects of sulforaphane (SFN) on mitochondrial dynamics in PC3 cells. **A.** Representative electronic micrographs showing mitochondrial morphology of PC3 cells treated with 5 μM SFN over 24, 48, and 72 h and controls. Magnification 9300×. **B**, Mean mitochondrial area for PC3 cells treated with 5 μM SFN for 24, 48, and 72 h. 48–330 mitochondria per group. $^{\#}P < 0.05$ vs. Control 24 h. **C**, Western blot for mitochondrial fission 1 (Fis1) and dynamin-related protein-1 (Drp1, 60 kDa isoform) in mitochondrial fractions of PC3 cells treated with 5 μM SFN for 48 h. **D**, Densitometry showing mitochondrial protein levels of Fis1 and Drp1 (60 kDa isoform). Values were normalized with respect to controls. Data are mean ± SEM, n = 3, $^{*}P < 0.05$ vs. Control.

therapies should be re-thought including side effects of the agents used, interactions with other molecules in other organs, and appropriates doses and concentrations. In the case of SFN, models have been found where concentrations into the range of 20–100 μM were used (Negrette-Guzmán et al., 2013b). In this study, a concentration applicable from the viewpoint of bioavailability and pharmacokinetics of SFN was chosen to lead the experiments. In clinical trials, peak concentrations of SFN between 2.9 and 7.8 μM after 1.5–3 h of consumption of broccoli sprouts or broccoli preparations enriched with isothiocyanates have been found (Negrette-Guzmán et al., 2013b). It is important to emphasize that 5 μM SFN allowed for observation of a cell-specific response that could become very helpful for establishing proper use of similar molecules in chemotherapy. Effects of concentration of

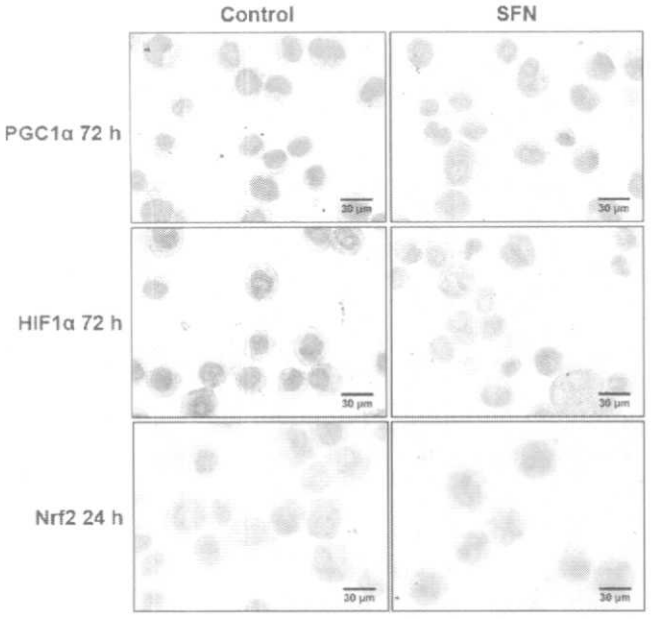

Fig. 8. Immunocytochemistry for the peroxisome proliferator-activated receptor γ co-activator-1α (PGC1α), the hypoxia-inducible factor-1α (HIF1α) and the nuclear factor E2-related factor-2 (Nrf2) in PC3 cells treated with 5 μM SFN at the indicated times. Magnification 40×. n = 3.

other bioactive small molecules on cell fates have also been reviewed considering both cancer and non-cancer cells (de Oliveira et al., 2016a,b).

Mitochondrial biogenesis is a cellular event linked to other global processes or stimuli, such as the cell cycle, exercise, heat shock, hypoxia, or oxidative stress (Díaz and Moraes, 2008). It has been also identified as a cytoprotective mechanism in several models that include the use of antioxidants (Kuo et al., 2012; Negrette-Guzmán et al., 2015; Yeh et al., 2014). In fact, SFN has been even found as an inducer of PGC1α (Brose et al., 2012; Fernandes et al., 2014; Whitman et al., 2013). Interestingly, Fernandes et al. (2014). found that MTT reduction was elevated in cardiac myoblasts after a 24 h-incubation with 5 μM SFN and this could be linked to mitochondrial biogenesis. Based upon these and our results, SFN-induced mitochondrial biogenesis would be an important cytoprotective mechanism only in short treatments. It was found that SFN increased MTT reduction along a treatment of several days in LLCPK1 cells (Fig. 1A), but the absence of cell proliferation at 72 h (Fig. 1B) would indicate that such effect is a result of mitochondrial activation (See section 3.1). However, mitochondrial biogenesis signals were only detected at 24 h of treatment (Fig. 3A, B and 3C). Therefore, understanding how SFN protects mitochondrial function and promotes mitochondrial activity in longer treatments was an intriguing question. Addressing this question around a mitochondrial dynamics modulation was a reasonable choice. It was found that SFN induced larger mitochondria at 48 and 72 h of treatment in LLCPK1 cells (Fig. 6A and B). Recently, mitochondrial fusion has been proposed as a mechanism of cell survival against mitochondrial stress. This response would involve a fine tuning in the levels of Mfn1, a protein belonging to mitochondrial fusion machinery (Park et al., 2014). It has also been shown that cells increase their oxidative metabolism and ATP production when mitochondria have a hyperfused morphology (Mitra et al., 2009; Rossignol et al., 2004). Mitochondrial fusion would explain why SFN-treated LLCPK1 cells increase their mitochondrial activity without increasing their mitochondrial biogenesis markers at 48 and 72 h (Fig. 1A and B, and 3). However, Mfn1 was not found to have increased in this study (Supplementary Fig. S5). Mitochondrial fusion can be induced by downregulation of proteins involved in mitochondrial fission. Lee and co-workers found (Lee et al., 2004) that silencing Fis1 in HeLa cells promoted mitochondrial fusion and apoptosis resistance without a role of Opa1, another GTPase that controls mitochondrial fusion in mammal cells. In this study, SFN induced mitochondrial fusion by downregulation of Fis1 in LLCPK1 cells (Fig. 6C and D), which could become a novel mechanism of cytoprotection attributed to this antioxidant. 60 kDa isoform of Drp1 also showed a bias toward downregulation in SFN-treated LLCPK1 cells. Alternative splicing gives rise to several isoforms of Drp1, of which the long form (~80 kDa) is the least functional (Macdonald et al., 2016). We observed several bands corresponding to Drp1 in the immunoblots but only a band close to 60 kDa was visible in the mitochondrial fraction and only this showed differences due the treatment (data not shown). How SFN down-regulates Fis1 and Drp1 inducing mitochondrial fusion in LLCPK1 cells is not clarified by this study but what gives rise to such a response can be hypothesized. Supported in previous reports from other groups, we had suggested that SFN would induce a mild oxidative stress in the cell when it is conjugated to glutathione and decreases its level within the first hours inside the cell (Negrette-Guzmán et al., 2013b). This transient oxidative stress could be responsible for some known effects of SFN as Nrf2 stabilization, and perhaps, mitochondrial fusion.

In the case of PC3 cells, it seems there was a time-dependent trend of the increase of mitochondrial biogenesis markers except for TFAM which was reduced back at 72 h (Fig. 4). Interestingly, this promotion in mitochondrial biogenesis happens simultaneously with a drop in cell viability (Fig. 1D and E). The mechanism for this SFN-induced cell death could be intrinsic apoptosis preceding by mitochondrial fragmentation, Bax oligomerization and cytochrome *c* release, according to how it has been described (Jourdain and Martinou, 2009). After the first 24 h of treatment with SFN, a fragmented morphology was observed in PC3 mitochondria (Fig. 7A and B and Supplementary Fig. S6). This diminishing in mitochondrial area (Fig. 7B) was accompanied by an increase in Bax cell level (Fig. 2B) as had been already reported for PC3 cells incubated with SFN (Xiao et al., 2009). However, this marker of intrinsic apoptosis as well as the mitochondrial membrane potential disruption (Fig. 2A) was obtained before with SFN concentrations equal or higher to 20 μM, an issue discussed above. The increase in Drp1 60 kDa has been reported before in cholangiocarcinoma cells treated with a combination of cisplatin and the Bcl-2 inhibitor ABT737 (Fan et al., 2015b). In this study, Drp1 60 kDa, but not Drp1 80 kDa isoform, was associated with pro-fission activity. As in LLCPK1 cells, Fis1 was also modulated by SFN in PC3 cells (Fig. 7C and D). Fis1 is a mitochondria-anchored protein that recruits Drp1 during mitochondrial fission and has shown to be crucial for apoptosis in a Drp1-independent way (Fan et al., 2015a; Lee et al., 2004). The mechanisms by which SFN modulates mitochondrial fission machinery need to be investigated as well as if these depend on the mitochondrial biogenesis.

Another interesting finding was done in PC3 cells at 72 h of SFN treatment: while SFN treatment abated cell viability (Fig. 1D and E), there was no difference in mitochondrial area between groups (Fig. 7B). This was seen as a possible clone selection in cells treated with SFN; it is feasible that at 72 h of treatment with SFN a population major formed by more resistant cells remain in the plate, this is, cells with a phenotype of fused mitochondria, and more resistant to the treatment. Alternatively, another cell death mechanism could be more important in this point of time, e.g. reactive oxygen species generation. More experiments would be required for driving this issue.

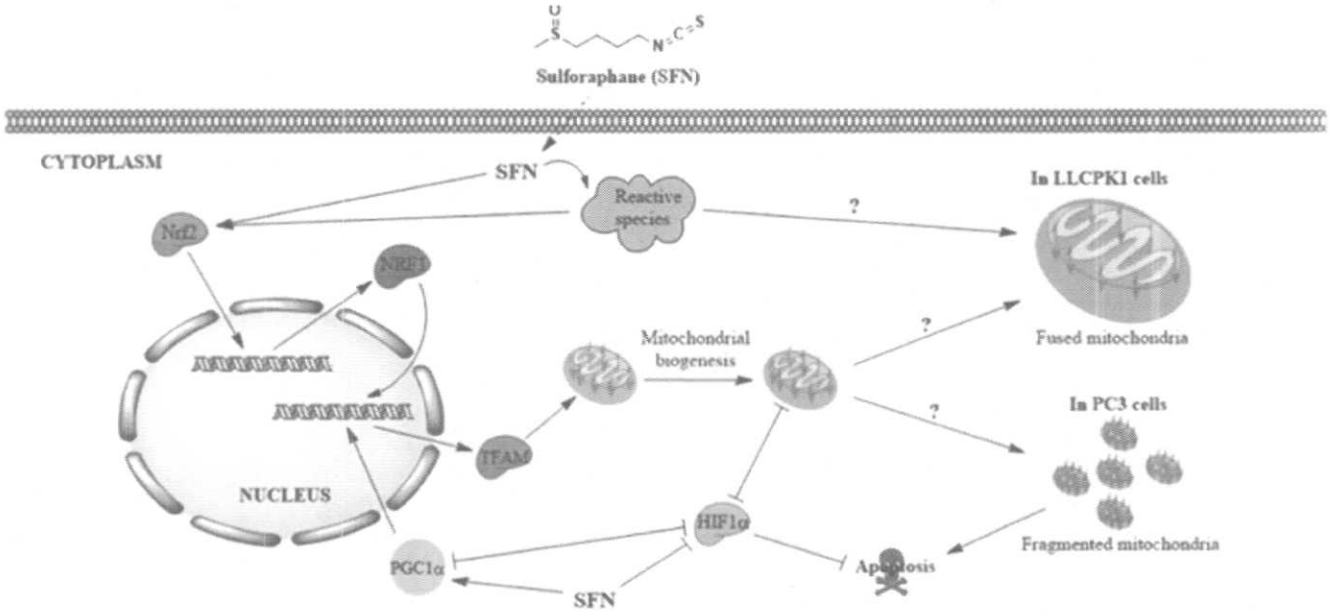

Fig. 9. Sulforaphane (SFN) is an isothiocyanate, a small molecule that can pass through the cell membrane by simple diffusion. Once inside, SFN can induce nuclear translocation of the nuclear factor E2-related factor-2 (Nrf2) either directly or by a transient augmenting in reactive species. Nrf2 induces transcriptionally the nuclear respiratory factor-1 (NRF1) expression and in turn it over-regulates proteins involved in mitochondrial biogenesis like the mitochondrial transcription factor-A (TFAM). How SFN induces both mitochondrial fusion in LLCPK1 cells and mitochondrial fission in PC3 cells is not clear, nor even if those events depend on a previous mitochondrial biogenesis activation. It is known that a moderate stress could induce mitochondrial fusion as a mechanism of cytoprotection; it is possible that such mild stress may be induced by SFN given its feature of reduction of glutathione levels at the first hours inside the cell. On the other hand, it is also known that the hypoxia-inducible factor-1α (HIF1α) promotes survival by apoptosis resistance in PC3 cells. This effect could be associated with other reported biological activities of HIF1α as the inhibition in mitochondrial biogenesis. The described PC3 responses to SFN could also be linked to its reported effects on HIF1α and the peroxisome proliferator-activated receptor γ co-activator-1α (PGC1α). SFN inhibits HIF1α and thus might be sensitizing PC3 cells to apoptosis. Even though it has not been elucidated how, SFN increases PGC1α levels which would also result in mitochondrial biogenesis. Both PGC1α and mitochondrial biogenesis have been demonstrated that inhibit HIF1α. (?) indicates issues that have to be further investigated.

When NRF1 was silenced in PC3 cells, the SFN-induced viability decrease was attenuated. Corresponding with the observed elevation in mitochondrial mass and protein markers of mitochondrial biogenesis, this result indicates that mitochondrial biogenesis plays a necessary role in the death of prostate cancer cells (Fig. 5). It has been reported that PC3 cell viability and invasion are highly dependent on HIF1α (Jeong et al., 2013) and PC3 cell line has been used as a model for studying aspects of the "Warburg Effect" in cancer (Lynch et al., 2012). In a simplified way, the "Warburg Effect" can be defined as the occurrence of glycolysis even in presence of oxygen (Johnson and Perkins, 2012). The transcriptional factor HIF1α is known as a potent inducer of enzymes involved in the use of glucose in numerous types of cancer. HIF1α can also inhibit mitochondrial metabolism; a possible interaction between the HIF1 system and PGC1α could explain this metabolic divergence (Smolková et al., 2011). SFN seems to shift this condition in PC3 cells as can be observed in Fig. 8. This redirection in the metabolism would explain the outcomes shown above in regards to SFN-induced death in prostate cancer cells. HIF1α sub-regulation and PGC1α over-regulation by SFN have been already reported separately in a number of works although the last had not been seen in cancer cells before (Fernandes et al., 2014; Jeon et al., 2011; Pastorek et al., 2015; Yao et al., 2008; Zhang et al., 2014). The present study has not rigorously compared two metabolic conditions of cells with a same origin or evaluated enough metabolic parameters nor included proper control cell lines to form a conclusion about this metabolic shift, but the results are a good starting point. This study was intended for describing two different effects of the same treatment in two different cell types.

Interestingly, all of these effects in PC3 cells may be triggered by the Nrf2 activation induced by SFN (Fig. 8). The axis Nrf2-NRF1 that launches the mitochondrial biogenesis program was demonstrated some time ago (Piantadosi et al., 2008). Therefore, Nrf2 induction can be recognized as an important target for some kinds of tumors. Fig. 9 serves for explaining and summarizing the main observations from this study together with facts known previously and others that required further investigation.

In conclusion, SFN -at controlled doses-can activate both a cytoprotective response in normal cells and a pro-apoptotic response in some cancer cells by promoting mitochondrial metabolism and modulating differentially mitochondrial morphology. These points favor the use of SFN in chemotherapy since target organs such as kidneys would be protected at the same time that the tumor is sensitized. There is a lot to learn in order to reach that goal and prostate cancer is a convenient model to continue the research.

Declaration of interest

The authors report no conflict of interest related to the content of this manuscript.

Acknowledgments

This work was supported by PAPIIT (Grant IN210316) and CONACYT (Grants 167949, 252008 and 220046).

Appendix A. Supplementary data

Supplementary data related to this article can be found at http dx.doi.org/10.1016/j.fct.2016.12.020.

Transparency document

Transparency document related to this article can be found online at http://dx.doi.org/10.1016/j.fct.2016.12.020.

References

Arnm, M.M., Lal, S., FitzGerald, K.E., Zhang, L., 2016. A holistic view of cancer bioenergetics: mitochondrial function and respiration play fundamental roles in the development and progression of diverse tumors. Clin. Transl. Med. 5 (1), 3.

Bland, M.L., Chourasia, A.H., Macleod, K.F., 2013. Mitochondrial dysfunction in cancer. Front. Oncol. 3, 292.

Brose, R.D., Shin, G., McGuinness, M.C., Schneidereith, T., Purvis, S., Dong, G.X., Keefer, J., Spencer, F., Smith, K.D., 2012. Activation of the stress proteome as a mechanism for small molecule therapeutics. Hum. Mol. Genet. 21 (19), 4237–4252.

Choi, S., Lew, K.L., Xiao, H., Herman-Antosiewicz, A., Xiao, D., Brown, C.K., Singh, S.V., 2007. D,L-Sulforaphane-induced cell death in human prostate cancer cells is regulated by inhibitor of apoptosis family proteins and Apaf-1. Carcinogenesis 28 (1), 151–162.

Collado, M., Scorrano, L., Campello, S., 2012. Mitochondrial dynamics in cancer and neurodegenerative and neuroinflammatory diseases. Int. J. Cell Biol. 2012, 729290.

Cottet-Rousselle, C., Ronot, X., Leverve, X., Mayol, J.F., 2011. Cytometric assessment of mitochondria using fluorescent probes. Cytom. A 79 (6), 405–425.

de Oliveira, M.R., Nabavi, S.F., Daglia, M., Rastrelli, L., Nabavi, S.M., 2016a. Epigallocatechin gallate and mitochondria – a story of life and death. Pharmacol. Res. 104, 70–85.

de Oliveira, M.R., Nabavi, S.F., Manayi, A., Daglia, M., Hajheydari, Z., Nabavi, S.M., 2016b. Resveratrol and the mitochondria: from triggering the intrinsic apoptosis pathway to inducing mitochondrial biogenesis, a mechanistic view. Biochimica Biophysica Acta 1860, 727–745.

Diaz, F., Moraes, C.T., 2008. Mitochondrial biogenesis and turnover. Cell Calcium 44 (1), 24–35.

Fan, S., Chen, W.X., Lv, X.B., Tang, Q.L., Sun, L.J., Liu, B.D., Zhong, J.L., Lin, Z.Y., Wang, Y.Y., Li, Q.X., Yu, X., Zhang, H.Q., Li, Y.L., Wen, B., Zhang, Z., Chen, W., Li, J.S., 2015a. MiR-483-5p determines mitochondrial fission and cisplatin sensitivity in tongue squamous cell carcinoma by targeting FIS1. Cancer Lett. 362 (2), 183–191.

Fan, Z., Yu, H., Cui, N., Kong, X., Liu, X., Chang, Y., Wu, Y., Sun, L., Wang, G., 2015b. ABT737 enhances cholangiocarcinoma sensitivity to cisplatin through regulation of mitochondrial dynamics. Exp. Cell Res. 335 (1), 68–81.

Fernandes, R.O., Bonetto, J.H., Baregzay, B., de Castro, A.L., Puukila, S., Forsyth, H., Schenkel, P.C., Ilesuy, S.F., Brum, I.S., Araujo, A.S., Khaper, N., Bello-Klein, A., 2014. Modulation of apoptosis by sulforaphane is associated with PGC-1α stimulation and decreased oxidative stress in cardiac myoblasts. Mol. Cell. Biochem. 401 (1–2), 61–70.

Guerrero-Beltran, C.E., Calderón-Oliver, M., Martínez-Abundis, E., Tapia, E., Zarco-Márquez, G., Zazueta, C., Pedraza-Chaverri, J., 2010. Protective effect of sulforaphane against cisplatin-induced mitochondrial alterations and impairment in the activity of NAD(P)H: quinone oxidoreductase 1 and γ glutamyl cysteine ligase: studies in mitochondria isolated from rat kidney and in LLC-PK1 cells. Toxicol. Lett. 199 (1), 80–92.

Jeon, Y.K., Yoo, D.R., Jang, Y.H., Jang, S.Y., Nam, M.J., 2011. Sulforaphane induces apoptosis in human hepatic cancer cells through inhibition of 6-phosphofructo-2-kinase/fructose-2,6-biphosphatase4, mediated by hypoxia inducible factor-1-dependent pathway. Biochimica Biophysica Acta 1814 (10), 1340–1348.

Jeong, C.W., Yoon, C.Y., Jeong, S.J., Hong, S.K., Byun, S.S., Kwak, C., Lee, S.E., 2013. The role of hypoxia-inducible factor-1α and -2α in androgen insensitive prostate cancer cells. Urologic Oncol. Seminars Orig. Invest. 31 (8), 1448–1456.

Johnson, R.F., Perkins, N.D., 2012. Nuclear factor-κB, p53, and mitochondria: regulation of cellular metabolism and the Warburg effect. Trends Biochem. Sci. 37 (8), 317–324.

Jourdain, A., Martinou, J.C., 2009. Mitochondrial outer-membrane permeabilization and remodelling in apoptosis. Int. J. Biochem. Cell Biol. 41 (10), 1884–1889.

Kuo, J.J., Chang, H.H., Tsai, T.H., Lee, T.Y., 2012. Curcumin ameliorates mitochondrial dysfunction associated with inhibition of gluconeogenesis in free fatty acid-mediated hepatic lipoapoptosis. Int. J. Mol. Med. 30 (3), 643–649.

Lee, Y., Jeong, S., Karbowski, M., Smith, C.L., Youle, R.J., 2004. Roles of the mammalian mitochondrial fission and fusion mediators Fis1, Drp1, and Opa1 in apoptosis. Mol. Biol. Cell 15 (11), 5001–5011.

Lin, W., Beck, B.H., Vaidya, K.S., Nash, K.T., Feeley, K.P., Ballinger, S.W., Pounds, K.M., Denning, W.L., Diers, A.R., Landar, A., Dhar, A., Iwakuma, T., Welch, D.R., 2014. Metastasis suppressor KISS1 seems to reverse the Warburg effect by enhancing mitochondrial biogenesis. Cancer Res. 74 (3), 954–963.

Lynch, T.P., Ferrer, C.M., Jackson, S.R., Shahriari, K.S., Vosseller, K., Reginato, M.J., 2012. Critical role of O-linked β-N-acetylglucosamine transferase in prostate cancer invasion, angiogenesis, and metastasis. J. Biol. Chem. 287 (14), 11070–11081.

Macdonald, P.J., Francy, C.A., Stepanyants, N., Lehman, L., Baglio, A., Mears, J.A., Qi, X., Ramachandran, R., 2016. Distinct splice variants of dynamin-related protein 1 differentially utilize mitochondrial fission factor as an effector of cooperative GTPase activity. J. Biol. Chem. 291 (1), 493–507.

Mitra, K., Wunder, C., Roysam, B., Lin, G., Lippincott-Schwartz, J., 2009. A hyperfused mitochondrial state achieved at G1-S regulates cyclin E buildup and entry into S phase. Proc. Natl. Acad. Sci. U. S. A. 106 (29), 11960–11965.

Montessuit, S., Somasekharan, S.P., Terrones, O., Lucken-Ardjomande, S., Herzig, S., Schwarzenbacher, R., Manstein, D.J., Bossy-Wetzel, E., Basanez, G., Meda, P., Martinou, J.C., 2010. Membrane remodeling induced by the dynamin-related protein Drp1 stimulates Bax oligomerization. Cell 142 (6), 889–901.

Negrette-Guzmán, M., García-Niño, W.R., Tapia, E., Zazueta, C., Huerta-Yepez, S., Leon-Contreras, J.C., Hernández-Pando, R., Aparicio-Trejo, O.E., Madero, M., Pedraza-Chaverri, J., 2015. Curcumin attenuates gentamicin-induced kidney mitochondrial alterations: possible role of a mitochondrial biogenesis mechanism. Evidence-Based Complementary Altern. Med. 2015, 917435.

Negrette-Guzman, M., Huerta-Yepez, S., Medina-Campos, O.N., Zatarain-Barrón, Z.L., Hernández-Pando, R., Torres, I., Tapia, E., Pedraza-Chaverri, J., 2013a. Sulforaphane attenuates gentamicin-induced nephrotoxicity: role of mitochondrial protection. Evidence-Based Complementary Altern. Med. 2013, 135314.

Negrette-Guzman, M., Huerta-Yepez, S., Tapia, E., Pedraza-Chaverri, J., 2013b. Modulation of mitochondrial functions by the indirect antioxidant sulforaphane: a seemingly contradictory dual role and an integrative hypothesis. Free Radic. Biol. Med. 65, 1078–1089.

Onishi, Y., Ueha, T., Kawamoto, T., Hara, H., Toda, M., Harada, R., Minoda, M., Kurosaka, M., Akisue, T., 2014. Regulation of mitochondrial proliferation by PGC-1α induces cellular apoptosis in musculoskeletal malignancies. Sci. Rep. 4, 3916.

Park, Y.Y., Nguyen, O.T.K., Kang, H., Cho, H., 2014. MARCH5-mediated quality control on acetylated Mfn1 facilitates mitochondrial homeostasis and cell survival. Cell Death Dis. 5 (4), e1172.

Pastorek, M., Simko, V., Takacova, M., Barathova, M., Bartosova, M., Hunakova, L., Sedlakova, O., Hudekova, S., Krizanova, O., Dequiedt, F., Pastorekova, S., Sedlak, J., 2015. Sulforaphane reduces molecular response to hypoxia in ovarian tumor cells independently of their resistance to chemotherapy. Int. J. Oncol. 47 (1), 51–60.

Piantadosi, C.A., Carraway, M.S., Babiker, A., Suliman, H.B., 2008. Heme oxygenase-1 regulates cardiac mitochondrial biogenesis via Nrf2-mediated transcriptional control of nuclear respiratory factor-1. Circul. Res. 103 (11), 1232–1240.

Rossignol, R., Gilkerson, R., Aggeler, R., Yamagata, K., Remington, S.J., Capaldi, R.A., 2004. Energy substrate modulates mitochondrial structures and oxidative capacityin cancer cells. Cancer Res. 64, 985–993.

Rudolf, E., Cervinka, M., 2011. Sulforaphane induces cytotoxicity and lysosome- and mitochondria-dependent cell death in colon cancer cells with deleted p53. Toxicol. Vitro 25 (7), 1302–1309.

Rudolf, K., Cervinka, M., Rudolf, E., 2014. Sulforaphane-induced apoptosis involves p53 and p38 in melanoma cells. Apoptosis 19 (4), 734–747.

Shankar, S., Ganapathy, S., Srivastava, R.K., 2008. Sulforaphane enhances the therapeutic potential of TRAIL in prostate cancer orthotopic model through regulation of apoptosis, metastasis, and angiogenesis. Clin. Cancer Res. 14 (21), 6855–6866.

Singh, A.V., Xiao, D., Lew, K.L., Dhir, R., Singh, S.V., 2004. Sulforaphane induces caspase-mediated apoptosis in cultured PC-3 human prostate cancer cells and retards growth of PC-3 xenografts in vivo. Carcinogenesis 25 (1), 83–90.

Smolková, K., Plecitá-Hlavata, L., Bellance, N., Benard, G., Rossignol, R., Ježek, P., 2011. Waves of gene regulation suppress and then restore oxidative phosphorylation in cancer cells. Int. J. Biochem. Cell Biol. 43 (7), 950–968.

Sumantran, V.N., 2011. Cellular chemosensitivity assays: an overview. Methods Mol. Biol. 731, 219–236.

Sun, L., Zhao, M., Yu, X.J., Wang, H., He, X., Liu, J.K., Zang, W.J., 2013. Cardioprotection by acetylcholine: a novel mechanism via mitochondrial biogenesis and function involving the PGC-1α pathway. J. Cell. Physiol. 228 (6), 1238–1248.

Thomas, K.J., Jacobson, M.R., 2012. Defects in mitochondrial fission protein dynamin-related protein 1 are linked to apoptotic resistance and autophagy in a lung cancer model. PLoS ONE 7 (9), e45319.

Tondera, D., Grandemange, S., Jourdain, A., Karbowski, M., Mattenberger, Y., Herzig, S., Da Cruz, S., Clerc, P., Raschke, I., Merkwirth, C., Ehses, S., Krause, F., Chan, D.C., Alexander, C., Bauer, C., Youle, R., Langer, T., Martinou, J.C., 2009. SLP-2 is required for stress-induced mitochondrial hyperfusion. EMBO J. 28 (11), 1589–1600.

Vega, G.G., Franco-Cea, L.A., Huerta-Yepez, S., Mayani, H., Morrison, S.L., Bonavida, B., Vega, M.I., 2015. Overcoming rituximab drug-resistance by the genetically engineered anti-CD20-hIFN-α fusion protein: direct cytotoxicity and synergy with chemotherapy. Int. J. Oncol. 47 (5), 1735–1748.

Vega-Avila, E., Pugsley, M.K., 2011. An overview of colorimetric assay methods used to assess survival or proliferation of mammalian cells. Proc. West. Pharmacol. Soc. 54, 10–14.

Wang, X., Moraes, C.T., 2011. Increases in mitochondrial biogenesis impair carcinogenesis at multiple levels. Mol. Oncol. 5 (5), 399–409.

Whitman, S.A., Long, M., Wondrak, G.T., Zheng, H., Zhang, D.D., 2013. Nrf2 modulates contractile and metabolic properties of skeletal muscle in streptozotocin-induced diabetic atrophy. Exp. Cell Res. 319 (17), 2673–2683.

Xiao, D., Powolny, A.A., Antosiewicz, J., Hahm, E.-R., Bommareddy, A., Zeng, Y., Desai, D., Amin, S., Herman-Antosiewicz, A., Singh, S.V., 2009. Cellular responses to cancer chemopreventive agent D,L-sulforaphane in human prostate cancer cells are initiated by mitochondrial reactive oxygen species. Pharm. Res. 26 (7), 1729–1738.

Yao, H., Wang, H., Zhang, Z., Jiang, B.H., Luo, J., Shi, X., 2008. Sulforaphane inhibited expression of hypoxia-inducible factor-1alpha in human tongue squamous

(.111•'.1 cell •• .In!! 1'1)~t,lI(' ,.Inc!') ,£'11<. Jrt.J. [,IIlft>1 1~1'6:. 12,'i-l::';1.
Yell, [) Y. hI. Y.H. Y,ln~ ye. 'v\'Jllg. J.l. 201<1, f(t'~\'t'r,l!r(j Jllt'vl<lles 1Ul1~'~d1t'fTI)d .md Tt'perfusI01Hnduct'd pulm('I1,}fV (Jpiil,ll)' ll1.1U1Y Ihroll:?h nl(Jdl)l.llln~ 11(1"- lllUI 11";I1llt","h(>ndriid nwtah-. k;lll. Transpl,1I11. Pro.:, 46 (4), 1131---11 4.
IhJng. Z. \.•m:. S., Z lOU. S., Y,ln. X. W,m::;. Y., Chell, 1" ~h'lkn. '" I(lln;<:. I.. (;11.1
T,m, Y., 711<'n;.;.'y. .l!. }I 14 SldIBl<lph.lIW P!Vt 1\h tlw c1(vl'!, d ol11Y0paLl1~'11 '\ pe ? dhlb('lic mice p 'obdbl~ b~' 1l".('I"'Jni. (OX Il1duced mhibllio I 01 •.••1 ll,\-H'K pillhwd\'. I. r>.lo1.Ctr lard 01. 1)
Zo ' \','.x .. R.lbirl'Nv Ii. p'. ~\:I\l1\ F. lOlr,. Mll{ldHlllldl l ,111j 111<",'1 '116,7" b7h.

JPP JOURNAL OF Pharmacy and Pharmacology
ROYAL PHARMACEUTICAL SOCIETY
JPP
Journal of Pharmacy
And Pharmacology
Research Paper

Curcumin prevents paracetamol-induced liver mitochondrial alterations

Luis Fernando Granados-Castro[a], Daniela Sarai Rodríguez-Rangel[a], Berenice Fernández-Rojas[a], Juan Carlos León-Contreras[b], Rogelio Hernández-Pando[b], Omar Noel Medina-Campos[a], Dianelena Eugenio-Pérez[a], Enrique Pinzón[c] and José Pedraza-Chaverri[a]

[a]Department of Biology, Faculty of Chemistry, National Autonomous University of Mexico (UNAM), University City, [b]Experimental Pathology Section, Instituto Nacional de Ciencias Médicas y Nutrición "Salvador Zubirán", México and [c]Animal Care Unit, Faculty of Medicine, National Autonomous University of Mexico (UNAM), University City, Mexico

Keywords
aconitase; adenosine triphosphate synthesis; mitochondrial dysfunction; mitochondrial membrane potential; respiratory complexes

Correspondence
José Pedraza-Chaverri, Laboratory 209, Building F, Faculty of Chemistry, Department of Biology, National Autonomous University of Mexico (UNAM), University City, 04510, D.F., México.
E-mail: pedraza@unam.mx

Received August 13, 2015
Accepted November 1, 2015

doi: 10.1111/jphp.12501

Abstract

Objective In the present study was evaluated if curcumin is able to attenuate paracetamol (PCM)-induced mitochondrial alterations in liver of mice.

Methods Mice (n = 5–6/group) received curcumin (35, 50 or 100 mg/kg bw) 90 min before PCM injection (350 mg/kg bw). Plasma activity of alanine aminotransferase (ALT) and aspartate aminotransferase (AST) was measured; histological analyses were done; and measurement of mitochondrial oxygen consumption, mitochondrial membrane potential, ATP synthesis, aconitase activity and activity of respiratory complexes was carried out.

Key findings Curcumin prevented in a dose-dependent manner PCM-induced liver damage. Curcumin (100 mg/kg) attenuated PCM-induced liver histological damage (damaged hepatocytes from 28.3 ± 7.7 to 8.3 ± 0.7%) and increment in plasma ALT (from 2300 ± 150 to 690 ± 28 U/l) and AST (from 1603 ± 43 to 379 ± 22 U/l) activity. Moreover, curcumin attenuated the decrease in oxygen consumption using either succinate or malate/glutamate as substrates (evaluated by state 3, respiratory control ratio, uncoupled respiration and adenosine diphosphate/oxygen ratio), in membrane potential, in ATP synthesis, in aconitase activity and in the activity of respiratory complexes I, III and IV.

Conclusions These results indicate that the protective effect of curcumin in PCM-induced hepatotoxicity is associated with attenuation of mitochondrial dysfunction.

Introduction

Paracetamol (PCM), also known as N-acetyl p-aminophenol, has been one of the widespread most frequently used drugs for analgesic and antipyretic purposes for the last 30 years.[1] PCM is a safe and effective drug at recommended doses: for adults 325–650 mg orally every 4–6 h with a maximum of 4 g per day and for children 10–15 mg/kg every 4–5 h with a maximum of 50–75 mg/kg per day.[2] PCM overdose is able to induce hepatotoxicity and acute liver failure. As a matter of fact, in 2006 alone, the American Association of Poison Control Centers implicated PCM in nearly 140 000 poisoning cases, in which more than 100 patients died.[3] It is responsible for more emergency room visits than any other drug on the market.[2]

In this context, several compounds have been used to attenuate PCM-induced hepatotoxicity, including N-acetylcysteine,[4,5] sulforaphane,[6] S-adenosylmethionine,[7] green tea polyphenols,[7] (RS)-n-propylthiazolidine-4(R)-carboxylic acid,[7] α-lipoic acid,[8] tymoquinone,[9] diphenyl diselenide,[10] methylene blue[11] and curcumin[12–15] among others.

Curcumin prevents PCM-induced increase in plasma alanine aminotransferase (ALT),[13,14] liver necrosis[12–15] and apoptosis,[13,14] malondialdehyde (MDA) content,[12,13,15] inflammatory cytokines[12] and liver deoxyribonucleic acid (DNA) fragmentation[14] among others.

The reactive toxic metabolite of PCM is N-acetyl-p-benzoquinoneimine (NAPQI).[11] The PCM toxicity was found to consist of two phases: the initial glutathione (GSH) depletion and covalent binding of NAPQI to target proteins and the subsequent increase in the mitochondrial permeability transition and nitration of proteins.[16] The impairment of GSH antioxidant system has been noticed to enhance the susceptibility to mitochondrial dysfunction from oxidative stress, resulting in the collapse of mitochondrial membrane potential and adenosine triphosphate (ATP) depletion.[16]

The mitochondrial alterations associated to PCM-induced liver toxicity include decrease in mitochondrial oxygen consumption,[5,16–19] ATP synthesis,[16,17,19] mitochondrial membrane potential,[16] and activity of mitochondrial complexes I (NADH dehydrogenase), II (succinate dehydrogenase) and IV (cytochrome c oxidase).[20] PCM inhibits complex II.[11] It has been shown that N-acetylcysteine,[5] diphenyl diselenide[16] and methylene blue[11] protect against mitochondrial dysfunction in PCM-induced liver toxicity. Interestingly, it has not been established whether curcumin may attenuate the following PCM-induced liver mitochondrial alterations: oxygen consumption, membrane potential, ATP synthesis, and activity of aconitase and respiratory complexes I, II, III and IV. In this context, it has been found that curcumin is able to attenuate mitochondrial alterations in the following experimental models: potassium dichromate-induced hepatotoxicity[21,22] and nephrotoxicity,[23] cardiac damage-induced by chronic renal failure[24] and maleate-induced nephrotoxicity.[25] By the above mentioned reasons it was hypothesized that curcumin may ameliorate PCM-induced mitochondrial alterations. The present study aimed to evaluate if the protective effect of curcumin in PCM-induced hepatotoxicity is associated with attenuation of mitochondrial dysfunction. This is the first work that aimed to address these points.

Materials and Methods

Reagents

The following reagents were from Sigma-Aldrich (St. Louis, Missouri, USA): Curcumin (catalogue number C7727, purity ≥80%), D-mannitol, sodium succinate dibasic, 4-(2-hydroxyethyl)-1-piperazineethanesulfonic acid (HEPES), safranin-O, glucose, glucose-6-phosphate dehydrogenase (G6PDH), bovine serum albumin fat free (BSA), β-nicotinamide adenine dinucleotide phosphate hydrate, carboxymethylcellulose sodium salt (CMC), hexokinase, adenosine 5′-diphosphate sodium salt (ADP), carbonyl cyanide 4-(trifluoromethoxy)phenylhydrazone (FCCP), ethylenediaminetetraacetic acid (EDTA), percoll, rotenone, sucrose, 2,6-dichlorophenolindophenol sodium salt hydrate (DCPIP), antimycin A, β-nicotinamide adenine dinucleotide hydrogen (NADH), decylubiquinone (DuB), malonic acid, cytochrome c and sodium borohydride. Sodium phosphate dibasic, sodium phosphate monobasic, potassium cyanide (KCN), Tween 20 detergent, magnesium chloride ($MgCl_2$) and sodium dithionite were from Merck (HES, Darmstadt, Germany). Potassium phosphate dibasic (K_2HPO_4) and potassium chloride (KCl) were from Mallinckrodt (Paris, Kentucky, USA). ALSL-0430 and ASSL-0430 kits to measure the plasma activity of ALT and aspartate aminotransferase (AST) were obtained from ELITechGroup (Princeton, New Jersey, USA). BIO-RAD Protein Assay (BIO-RAD Laboratories, Hercules, California, USA) was used for protein quantification. As sedative, Sedalphorte MR Reg. SAGARPA Q-7503-003 (Sodium pentobarbital, Mexico city) was used. Other compounds and reagents used were of high purity and were obtained commercially.

Animals

Male CD1 mice with an initial body weight of 35–40 g were used. Animals were housed on a 12-h light/dark cycle with *ad libitum* access to purified water and food (Teklad Global 2018S; Harlan Laboratories, Indianapolis, Indiana, USA). The Local Committee for the Care and use of Laboratory Animals (CICUAL) approved the project (FQ/CICUAL/044/12) and the experiments were conducted in accordance with the Guide for the Care and Use of Laboratory Animals.

Model of PCM hepatotoxicity

All animals were withdrawn from food 4 h before any manipulation. Six groups of animals were studied (n = 5–6): Control group (CT): Animals received 0.05% CMC (curcumin's vehicle) 90 min before an ip saline solution (PCM's vehicle) injection. Paracetamol group (PCM): animals received 0.05% CMC 90 min before an ip PCM injection (350 mg/kg bw). Curcumin + paracetamol (PCM + CUR): mice received 35, 50 or 100 mg/kg bw of curcumin 90 min before an ip PCM injection. The doses of curcumin were chosen based in previous pilot experiments. Curcumin (CUR): mice received curcumin (100 mg/kg bw) 90 min before an ip saline solution injection. Mice were sacrificed 14 h after the last administration. Animals were anaesthetized with sodium pentobarbital (80 mg/kg). Blood was obtained from the axillary vein in heparinized Eppendorf tubes and plasma was separated by centrifugation. Liver was immediately removed and prepared for histological and ultrastructural study.

Markers of liver injury

Hepatic injury was determined by measuring in plasma the activity of ALT and AST with commercial kits.

Histological analysis

Transverse slices of approximately 1 mm were obtained from freshly extracted liver. The slices were immersed in 10% formaldehyde diluted in phosphate buffered saline (PBS) for a week to fix the tissue. Then, the fixed tissue was immersed in different concentrations of ethylic alcohol and subsequently in xylol for later inclusion in paraffin wax; sections of 4 μm thickness were made and mounted on glass slide. After dewaxing, sections were stained with haematoxylin-eosin staining. The histological analysis was circumscribed to the hepatocytes located around the portal areas (150–200 μm width) because hepatocytes in this zone are the first to metabolize PCM.

Ultrastructural studies

To study the mitochondrial ultrastructural morphology, immediately after animal sacrifice, small liver tissue fragments were obtained and fixed by immersion into 10% glutaraldehyde dissolved in cacodylates buffer pH 7.2 during 24 h at 4°C. Then, tissue fragments were post-fixed with osmium tetraoxide, dehydrated in graded ethylic alcohol solutions and embedded in Epon resin (London Resin Company, London, UK). Thin sections from 70 to 90 nm were placed on cooper grids, contrasted with lead and uranium salts and examined with a FEI Technei electron microscope. The histological and ultrastructural studies were performed only with the curcumin dose of 100 mg/kg.

Isolation of liver mitochondria

Liver mitochondria were isolated from the whole liver using differential centrifugation with two different Percoll gradients according to Ratner *et al.*[26] The mitochondrial protein content was measured according to Bradford,[27] adapted to a 96 well plate, to assure the use of equal protein quantity among all subsequent determinations.

Determination of oxygen consumption

Measurement of mitochondrial oxygen consumption was carried out using a Clark-type electrode attached to a micro-chamber with a constant temperature of 37°C (Strathkelvin instruments, ML, Scotland, UK) according to previous studies of our group.[23,25]

Mitochondrial membrane potential (MMP)

A method based on a previous work[28] was used to determine the MMP. In brief, 2 μM safranin-O was used to measure fluorometrically the MMP at excitation and emission wavelengths of 530 and 590 nm, respectively, in a black 96 well plate.

ATP synthesis assay

Thirty μg of freshly isolated mitochondria were loaded in a well containing cold ATP-buffer (9 U/ml hexokinase, 220 mM glucose, 140 mM sodium succinate, 1.9 U/ml G6PDH and 2.6 mg $NADP^+$; pH 7.2). A basal ATP production was measured indirectly for 3 min at 340 nm, the ATP production was initiated with the addition of 1.2 mM ADP and it was monitored each 30 s for 5 min at 340 nm.

Activity of mitochondrial complexes

The enzymatic activities of all complexes were determined spectrophotometrically at 37°C with 5 μg of isolated liver mitochondria. For the activity assays of complexes I and II, mitochondria were broken with four freezing and thawing cycles. For complexes III and IV, Tween 20 was added to the solution as the freezing process has shown a decrease in these complexes enzymatic activities.[29] The activity of mitochondrial complexes was carried out independently in a 96 well plate in presence of the respective complex inhibitor. The specific activity of all complexes was determined by the subtraction of the activity in the presence of the specific inhibitor from the total activity. The final volume of each well was 300 μl.

Complex I activity

In each well, 5 μg of broken mitochondria were added to a mix solution containing 41 mM potassium phosphate buffer, 3.5 mg/ml BSA, 67 μM DCPIP, 1 μM antimycin A, 0.2 mM NADH and 0.2 mM KCN, pH 7.4. To inhibit complex I and to determine the non-enzymatic activity, 13 μM rotenone were added in an identic parallel well. The mix was incubated for 5 min at 37°C and the baseline was monitored by a kinetic reading for 2 min at 600 nm. The reaction was started by the addition of 3.12 mM DuB and the subsequent decrease in absorbance was followed for 3 min.

Complex II activity

In each well, 5 μg of broken mitochondria were added to a solution containing 30 mM potassium phosphate buffer, 0.4 mg/ml BSA, 67 μM DCPIP, 1 μM antimycin A, sodium 15 mM succinate and 0.2 mM KCN, pH 7.4. To inhibit

complex II and to determine the non-enzymatic activity, 10 mM malonic acid was added in an identic parallel well. The plate was incubated inside the spectrophotometer at 37°C for 10 min and the baseline activity was read at 600 nm for 2 min. The reaction was started by the addition of 3.12 mM DuB and the subsequent decrease in absorbance was followed for 3 min.

Complex III activity

In each well, 5 μg of hepatic mitochondria were added to a mix solution containing 30 mM potassium phosphate buffer, 0.4 mg/ml BSA, 220 μM Tween 20, 1 μM rotenone, 0.4 mM KCN, 0.6 mM $MgCl_2$, 0.1 mM EDTA and 17 μM oxidized cytochrome c, pH 7.4. To inhibit complex III and to determine the non-enzymatic activity, 1.8 mM antimycin A was added in an identic parallel well. The mix was incubated for 10 min at 37°C and the baseline was monitored by a kinetic reading at 550 nm for 2 min. The reaction was started by the addition of 3.12 mM decylubiquinol and the increase in absorbance at 550 nm was followed for 3 min.

Complex IV activity

In each well, a freshly prepared solution containing 37 mM potassium phosphate buffer, 0.4 mg/ml BSA, 220 μM Tween 20 and 17 μM reduced cytochrome c, pH 7.0, was placed. To inhibit the complex IV and to determine the non-enzymatic activity, 0.25 mM KCN was added to a similar parallel well. The plate was incubated inside the spectrophotometer at 37°C for 10 min and the baseline activity was read at 500 nm for 2 min. The reaction was started by the addition of 5 μg of hepatic mitochondria and the decrease in the absorbance at 550 nm was followed for 3 min.

Aconitase activity

Mitochondria were broken by sonication for 2 min in aconitase buffer (20 mM isocitrate, 0.6 mM $MnCl_2$, 50 mM Tris-HCl; pH 7.4). Fifteen μg of mitochondrial protein were used for each well, the mixture was incubated for 2 min at 25°C and then the production cis-aconitate was followed for 3 min at 240 nm.[25]

Statistical analysis

Results were expressed as means ± standard error of the mean (SEM). Data were analysed by one-way analysis of variance followed by multiple-comparisons according to Turkey test using Prism 6.0 software (GraphPad, San Diego, California, USA). The comparisons with a $P < 0.05$ were considered significant.

Results

Curcumin was able to attenuate, in a dose-dependent way, the PCM-induced increase in the plasma activity of ALT and AST (Figure 1). The increase in ALT activity was prevented with 50 and 100 mg/kg of curcumin and the increase in AST activity was prevented with the three doses of curcumin. Curcumin alone was unable to induce changes in the activity of these enzymes (Figure 1).

Moreover, curcumin (100 mg/kg) attenuated the PCM-induced liver histological damage (Figure 2). Four

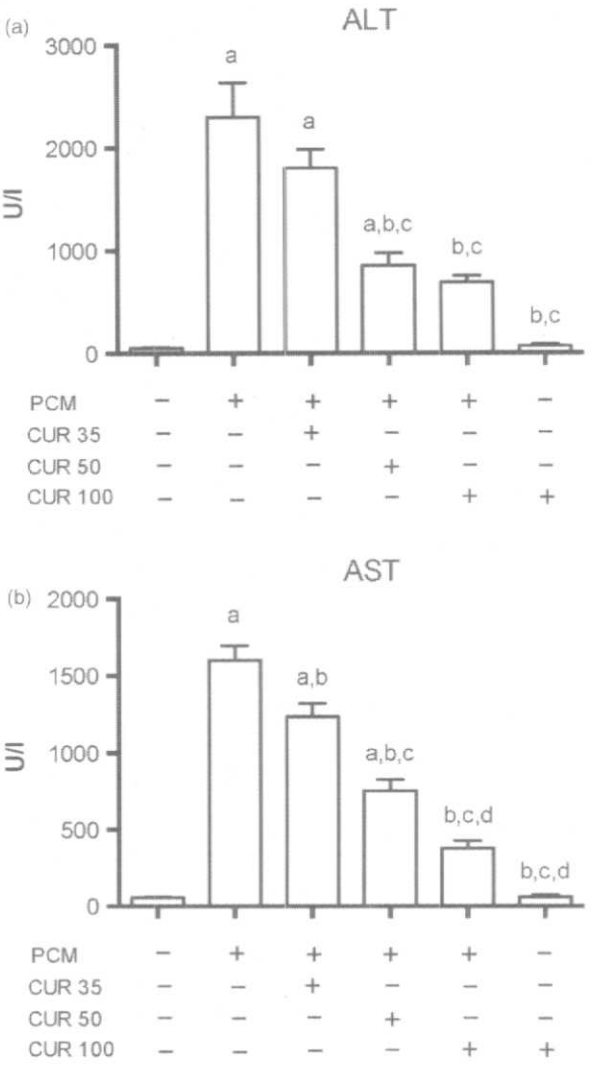

Figure 1 Curcumin (CUR) prevents, in a dose-response way, the paracetamol (PCM)-induced increase in the activity of alanine aminotransferase (ALT) and aspartate aminotransferase (AST). Data are presented as mean ± SEM, $n = 5$–6. $^{a}P < 0.05$ vs Control, $^{b}P < 0.05$ vs PCM, $^{c}P < 0.05$ vs PCM + CUR 35, $^{d}P < 0.05$ vs PCM + CUR 50.

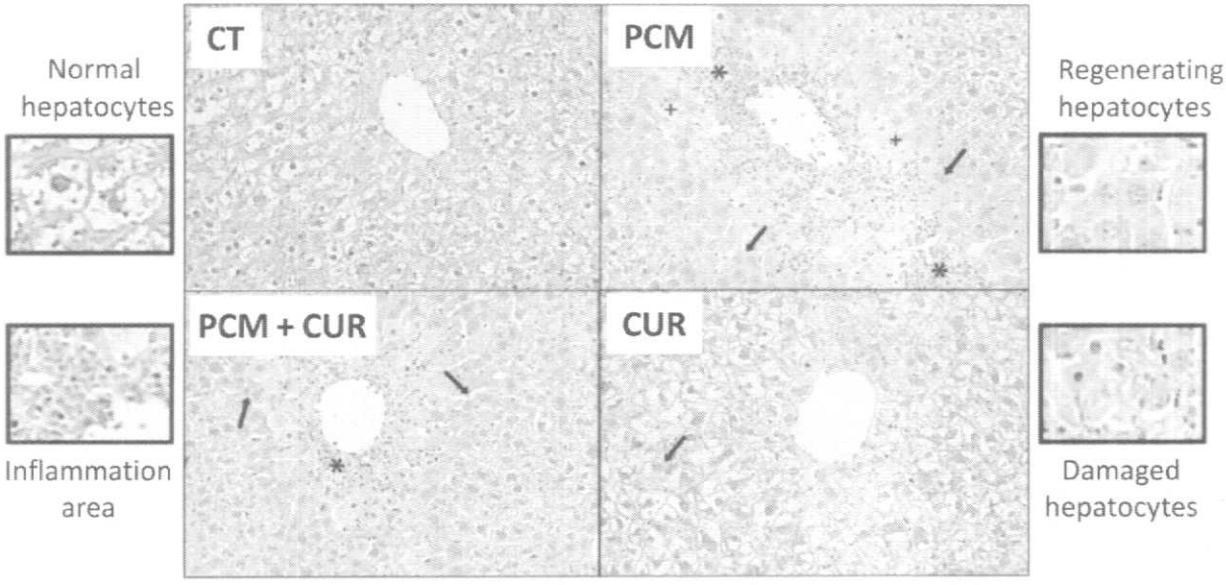

	CT	PCM	PCM+CUR	CUR
Inflammation area (%)	0.2 ± 0.1	23.5 ± 6.3 [a]	8.1 ± 2.7 [b]	0.0 ± 0 [b]
Normal hepatocytes (%)	95.0 ± 0.6	39.9 ± 2.4	61.8 ± 8.7 [a,b]	87.4 ± 2.0 [b,e]
Damaged hepatocytes (%)	0.0 ± 0.0	28.3 ± 7.7 [a]	8.3 ± 0.7	0.0 ± 0 [b]
Regenerating hepatocytes (%)	5.0 ± 0.6	30.4 ± 7.4 [a]	25.8 ± 5.2 [a]	12.5 ± 2.0

Figure 2 Curcumin (CUR, 100 mg/kg) prevents the paracetamol (PCM)-induced histological liver injury. Samples were stained with hematoxylin and eosin (H&E). The analysis was carried out only with the 100 mg/kg curcumin dose, as it was the most effective one. *Shows inflammation area, +shows damaged hepatocytes and arrows show regenerating hepatocytes. Quantification of all parameters measured; inflammation area was obtained from a total of 150 000 μm^2 and all cellular counts were made from a total of 50 000 μm^2. Data are presented as mean ± SEM, n = 5–6. [a]$P < 0.05$ vs Control (CT), [b]$P < 0.05$ vs PCM, [e]$P < 0.05$ vs PCM + CUR 100.

parameters were determined as tissue damage markers: (1) the percentage of the area occupied by inflammatory cells into and around portal zones based in a total area of 150 000 μm^2; (2) percentage of periportal normal hepatocytes in an area of 50 000 μm^2; (3) percentage of necrotic or apoptotic hepatocytes in the same areas; and (4) percentage of regenerative liver cells (binucleated hepatocytes or with very large nucleus, mitotic figures). Figure 2 shows that PCM-induced increase in the percentage of damaged hepatocytes and inflammation area was prevented by curcumin pretreatment. Animals treated with curcumin alone showed normal liver histology. These changes showed good correlation with the ultrastructural analysis, liver cells from PCM-treated animals showed numerous cytoplasmic vacuoles and swollen mitochondria with fragmented or effacement cristae and numerous electrondense amorphous deposits in the matrix, while these changes were seen occasionally in mice treated with PCM and curcumin (Figure 3). There were not ultrastructural abnormalities in animals treated only with curcumin.

Paracetamol induced decrease in oxygen consumption (Figures 4 and 5). Curcumin was able to attenuate the decrease in state 3, respiratory control ratio (State 3/State 4), uncoupled respiration, ADP/O (mol of ADP/mol of oxygen consumed during State 3) and increase in state 4 using either succinate (Figure 4) or malate/glutamate (Figure 5) as substrates of the electron chain

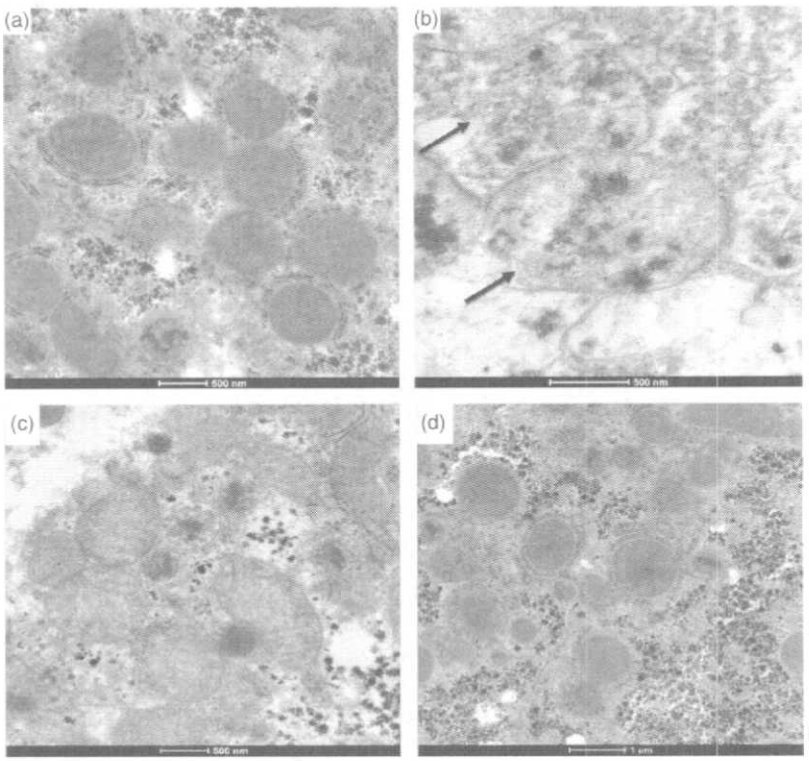

Figure 3 Representative electromicroscopy micrographs of mitochondria from the different experimental groups. (a) Normal mitochondria structure in hepatocyte from control mouse that received only the vehicle solution. (b) Swollen mitochondria with rupture of external membrane (arrows), effacement of cristae and electrondense deposits in the matrix induced by paracetamol (PCM) administration. (c) Curcumin (100 mg/kg) prevents the mitochondrial damage induced by PCM, only some mitochondria show electrondense material deposited in the matrix. (d) Administration of curcumin alone did not induce mitochondrial damage.

transport. Protective effect was observed with 50 and 100 mg/kg of curcumin.

Curcumin (100 mg/kg) prevented the PCM-induced decrease in membrane potential (Figure 6), ATP synthesis (Figure 7) and aconitase activity (Figure 7).

Paracetamol induced decrease in the activity of the respiratory complexes I, II, III and IV. Curcumin was able to prevent the decrease in the activity of respiratory complexes I, III and IV (Figure 7).

Curcumin alone increased the activity of respiratory complex III (Figure 7) and membrane potential. ATP synthesis, aconitase activity and activity of complex I, II and IV remained unchanged in the curcumin treated group.

Discussion

Paracetamol-induced hepatotoxicity has been a significant issue for several years because PCM is a widespread used drug for analgesic and antipyretic purposes[1] and it is responsible for more emergency room visits than any other drug on the market.[2] During overdose, PCM is mainly metabolized by cytochrome P450 into NAPQI, which reacts directly with GSH causing its depletion[16] (Figure 8). Consequently, NAPQI reacts with mitochondrial membrane proteins which causes reactive oxygen species (ROS) production,[30] mitochondrial DNA damage[31] mitochondrial transition pore (MTP) opening and decrease of ATP production[16,17,19] (Figure 8).

Moreover, it has been found translocation of the membrane protein B-cell lymphoma-2 (Bcl-2)-associated-X protein (BAX), which combines with Bcl-2 antagonist killer 1 (Bak) in the outer mitochondrial membrane to form pores and allow the release of intermembrane proteins such as cytochrome c[32] (Figure 8). Consistently, previous studies have shown that PCM and NAPQI inhibit mitochondrial respiration.[5,19,33,34] Furthermore, in an earlier study, the interaction between NAPQI and the respiratory chain was investigated using submitochondrial particles. Succinate dehydrogenase (associated with respiratory complex II) was found to be very sensitive to NAPQI, while NADH dehydrogenase (respiratory complex I) was inhibited to a lesser extent.[19] The well-documented PCM-induced alterations in mitochondrial function may also be related to the fact that PCM affects the expression of mitochondrial

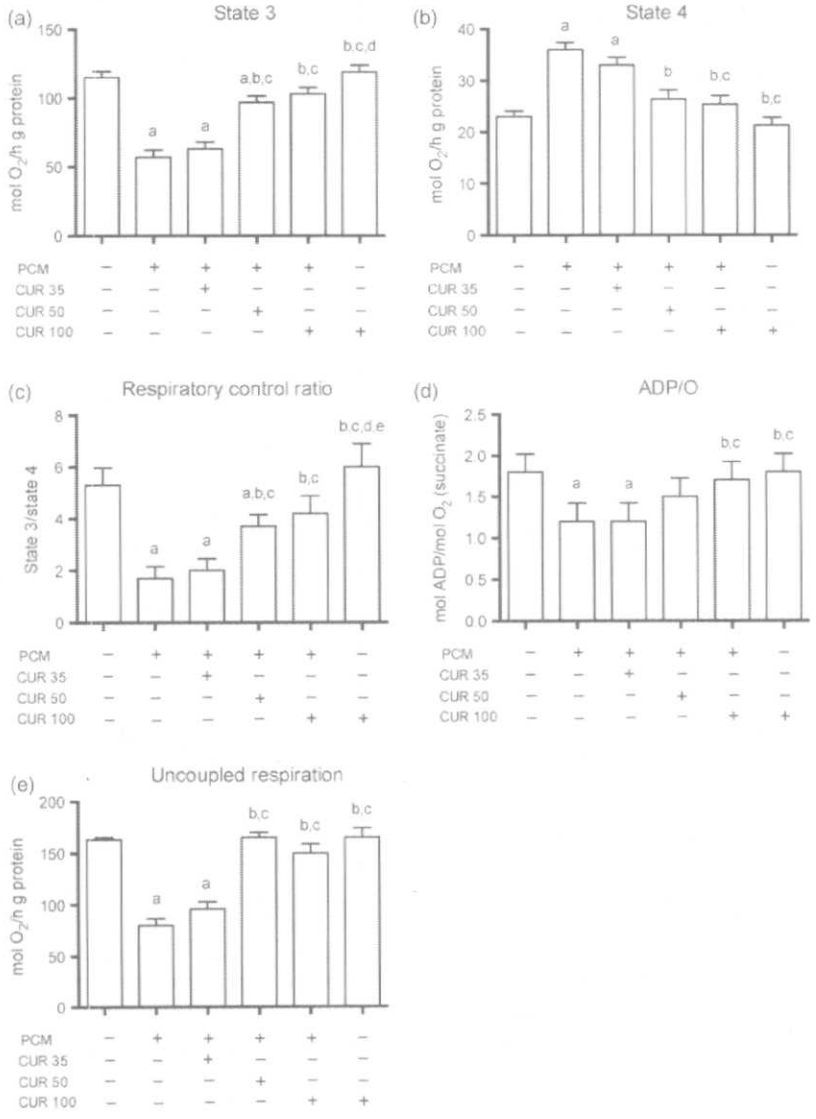

Figure 4 Curcumin (CUR) prevents paracetamol (PCM)-induced alterations in mitochondrial respiration using succinate as substrate of the electron transport chain. (a) state 3, initiated with adenosine diphosphate (ADP) addition in the chamber of respiration, (b) state 4, reached when the ADP is depleted, (c) Respiratory control ratio (RCR), (d) ADP/oxygen (O) ratio, (e) uncoupled respiration, initiated with carbonyl cyanide 4-(trifluoromethoxy)phenylhydrazone (FCCP) addition. Data are presented as mean ± SEM, $n = 5$–6. $^{a}P < 0.05$ vs Control, $^{b}P < 0.05$ vs PCM, $^{c}P < 0.05$ vs PCM + CUR 35, $^{d}P < 0.05$ vs PCM + CUR 50, $^{e}P < 0.005$ vs PCM + CUR 100.

protein-encoding genes related to the subunits of electron transport chain (ETC.) complexes.[31] These abnormalities may affect the assembly, stability and structure of ETC complexes.[31]

From the above described alterations it is clear that mitochondrial damage plays a critical role in the PCM-induced hepatotoxicity. Therefore, compounds with the potential protective effects on mitochondrial dysfunction may be useful to prevent PCM-induced hepatotoxicity. The antioxidant curcumin has been found to protect against mitochondrial dysfunction in several experimental models.[21–25 reviewed in 35] In potassium dichromate-induced nephrotoxicity model, curcumin was able to prevent the following mitochondrial alterations[23]: decrease in oxygen consumption, in oxidative stress, in ATP content, in calcium retention, and in mitochondrial membrane potential as well as in the activity of complexes I, II, II-III and V. In potassium dichromate-induced hepatotoxicity model, curcumin was able to prevent the decrease in the aconitase activity, in ATP content, in oxygen con-

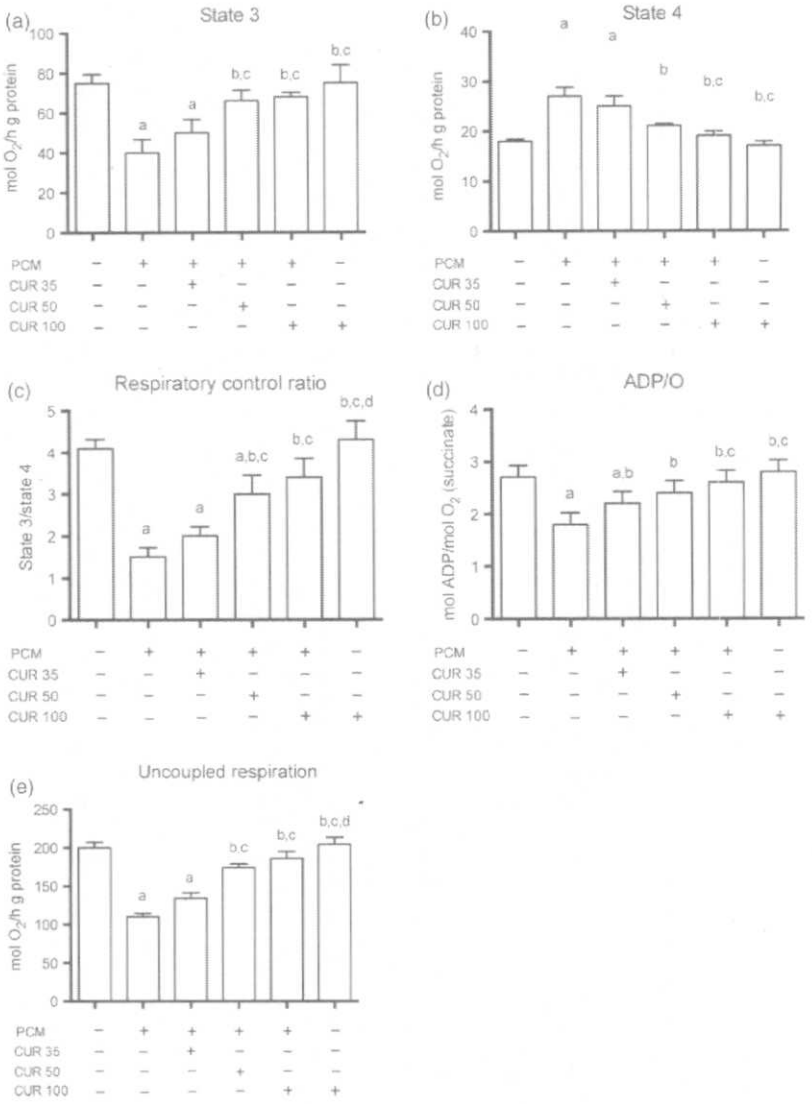

Figure 5 Curcumin prevents paracetamol (PCM)-induced alterations in mitochondrial respiration with glutamate/malate as substrate of the electron transport chain. (a) state 3, initiated with adenosine diphosphate (ADP) addition in the chamber of respiration, (b) state 4, reached when the ADP is depleted, (c) Respiratory control ratio (RCR), (d) ADP/oxygen (O) ratio, (e) uncoupled respiration, initiated with carbonyl cyanide 4-(trifluoromethoxy)phenylhydrazone (FCCP) addition. Data are presented as mean ± SEM, $n = 5–6$. $^{a}P < 0.05$ vs Control, $^{b}P < 0.05$ vs PCM, $^{c}P < 0.05$ vs PCM + CUR 35, $^{d}P < 0.05$ vs PCM + CUR 50.

sumption, and in the activity of respiratory complex I as well as the increase in oxidative stress and in permeability transition pore opening.[21,22] In maleate-induced nephrotoxicity model, it was able to prevent reduced oxygen consumption and activities of complex I and aconitase.[25] In addition, curcumin was also able to prevent the decrease in aconitase activity and in oxygen consumption in hearts of rats with chronic renal failure.[24] In addition, Subudhi *et al.*[36] found effects of curcumin on oxygen consumption. They reported that curcumin administration ameliorates hyperthyroidism-induced increase in state 3 and state 4 as well as in respiration in complex I in mitochondria from rat liver.

In the present study was found that curcumin indeed exerts a hepatoprotective effect against PCM-induced damage. Curcumin attenuated PCM-induced increment in ALT and AST plasma activity, which are sensitive indicators for the hepatic function; their excessive leakage into the blood shows the disruption of integrity of hepatic cell membranes. The hepatoprotective effect of curcumin was also

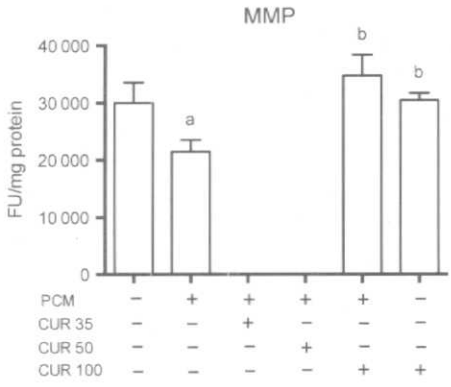

Figure 6 Curcumin (CUR, 100 mg/kg) prevents paracetamol (PCM)-induced decrease in mitochondrial membrane potential (MMP) that was obtained with the fluorescence of safranin-O. ΔFU = Change in fluorescent units. Data are presented as mean ± SEM, $n = 5–6$. $^{a}P < 0.05$ vs Control, $^{b}P < 0.05$ vs PCM.

confirmed by histological observations. The protective effect observed was consistent with the findings of Somanawat *et al.*[12] Li *et al.*,[13] Bulku *et al.*,[14] and Yousef *et al.*[15] Remarkably, the hepatoprotection observed in our study was associated with prevention of PCM-induced mitochondrial alterations. In fact, curcumin prevented the PCM-induced decrease in oxygen consumption (State 3, RCR, uncoupled respiration and ADP/O), in membrane potential, in ATP synthesis, in the aconitase activity and in respiratory complexes I, II and IV (Figures 4–8). These mitochondrial functional data obtained in isolated mitochondria were supported by ultrastructural observations seen in the liver of these animals. Figure 3 illustrates swollen mitochondria and disruption of external membrane, effacement of cristae and electrondense deposits in the matrix induced by PCM treatment (Figure 3b). Curcumin prevents these PCM-

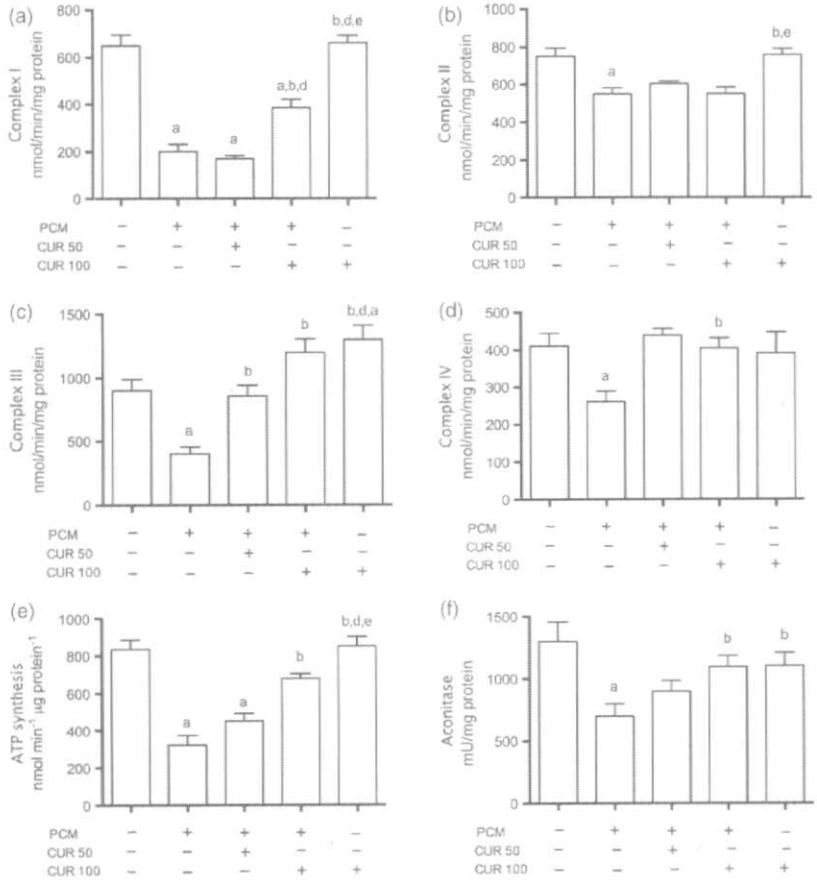

Figure 7 Effect of curcumin on paracetamol (PCM)-induced alterations in enzymatic activity of mitochondrial complexes (a) I, (b) II, (c) III and (d) IV, (e) ATP synthesis and (f) aconitase activity. ATP synthesis by the mitochondria was measured using glutamate/malate as substrate of the electron transport chain. Aconitase activity was determined as it is a mitochondrial marker of oxidative stress. The PCM + CUR 35 group was no longer determined as it showed no significant difference vs the Control group in various previous determinations. Data are presented as mean ± SEM, $n = 5–6$. $^{a}P < 0.05$ vs Control, $^{b}P < 0.05$ vs PCM, $^{d}P < 0.05$ vs PCM + CUR 50, $^{e}P < 0.05$ vs PCM + CUR 100.

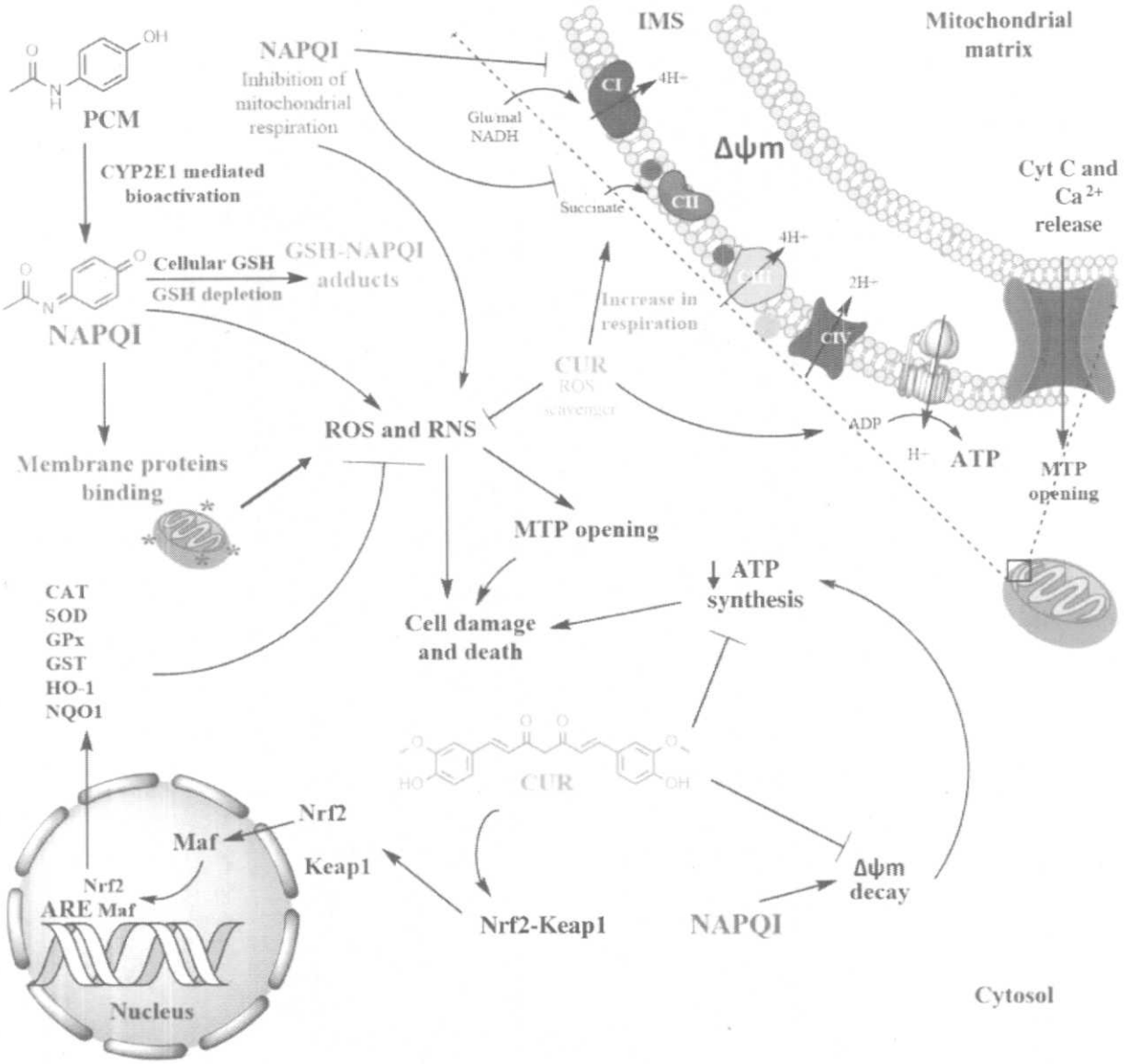

Figure 8 Graphical representation of the paracetamol (PCM), N-acetyl-p-benzoquinoneimine (NAPQ1) and curcumin interaction in mice hepatocytes. Curcumin is able to induce diverse cellular responses to decrease the PCM overdose alteration. ADP, Adenosine diphosphate; PCM or N-acetyl-p-aminophenol; ARE, Antioxidant response elements; ATP, Adenosine triphosphate; Ca^{2+}, Calcium cation; CAT, Catalase; CI, NADH:ubiquinone oxidoreductase; CII, Succinate dehydrogenase; CIII, Coenzyme Q: cytochrome c-oxidoreductase; CIV, cytochrome c oxidase; CUR, Curcumin (Diferuloylmethane); CYP2E1, Cytochrome P450 2E1; Cyt c, Cytochrome c; Glu/mal, Glutamate and malate; GPx, Glutathione peroxidase; GSH, Glutathione; GST, Glutathione-S-transferase; HO-1, Heme oxygenase 1; IMS, Intermembrane space; Keap 1, Kelch-like ECH-associated protein 1; Maf, Small maf proteins; MTP, Mitochondrial transition pore; NADH, Nicotinamide adenine dinucleotide hydrogen; NAPQI, N-acetyl-p-benzoquinone imine; NQO1, NAD(P)H dehydrogenase [quinone] 1; Nrf2, nuclear factor (erythroid-derived 2)-like 2; RNS, Reactive nitrogen species; ROS, Reactive oxygen species; SOD, Superoxide dismutase; Δψm, Mitochondrial membrane potential.

induced mitochondrial alterations since only some mitochondria show electrondense material accumulated in the matrix (Figure 3c).

To our knowledge, this is the first demonstration that curcumin prevents mitochondrial alteration in the PCM-induced hepatotoxicity. These data are consistent with the findings in other experimental models.[21–25] Interestingly, in all cases, the improvement of mitochondrial function was associated with the prevention of the decrease in the activity of aconitase, a marker of oxidative stress.[37] This

suggests that the antioxidant effect of curcumin is key in the protective effect of mitochondrial function. In fact, it has been well-established that curcumin is a direct antioxidant[38] that may be responsible of the protection against mitochondrial dysfunction in this experimental model (Figure 8). In addition, curcumin may also exert its antioxidant effect through an indirect mechanism via the transcription factor nuclear factor (erythroid-derived 2)-like 2 (Nrf2) (Figure 8). We have no enough data in this work to support the indirect antioxidant effect of curcumin in this experimental model. It is unknown if curcumin may be able to interfere with the direct inhibition of mitochondrial proteins by NAPQI. This deserves to be further analysed.

Our data suggest that curcumin may be useful to attenuate the PCM-induced liver damage in humans. Studies should be conducted in the future to evaluate this potential effect of curcumin in human beings.

Together, these mechanisms might explain, at least in part, some of the cytoprotective effects of curcumin on the PCM-induced hepatic damage.

Conclusion

These results indicate that the protective effect of curcumin in PCM-induced hepatotoxicity is associated with attenuation of mitochondrial dysfunction.

Declarations

Acknowledgements

This work was partially supported by PAPIIT IN210713 and CONACYT (220046 and 252008).

References

1. Toussaint K *et al.* What do we (not) know about how paracetamol (acetaminophen) works? *J Clin Pharm Ther* 2010; 35: 617–638.
2. Schilling A *et al.* Acetaminophen: old drug, new warnings. *Cleve Clin J Med* 2010; 77: 19–27.
3. Bronstein AC *et al.* 2006 Annual Report of the American Association of Poison Control Centers' National Poison Data System (NPDS). *Clin Toxicol (Phila)* 2007; 45: 815–917.
4. Lyons L *et al.* Treatment of acetaminophen overdosage with N-acetylcysteine. *N Engl J Med* 1977; 296: 174–175.
5. Donnelly PJ *et al.* Inhibition of mitochondrial respiration in vivo is an early event in acetaminophen-induced hepatotoxicity. *Arch Toxicol* 1994; 68: 110–118.
6. Noh JR *et al.* Sulforaphane protects against acetaminophen-induced hepatotoxicity. *Food Chem Toxicol* 2015; 80: 193–200.
7. Oz HS *et al.* Diverse antioxidants protect against acetaminophen hepatotoxicity. *J Biochem Mol Toxicol* 2004; 18: 361–368.
8. Elshazly SM *et al.* Insights in the mechanism underlying the protective effect of α-lipoic acid against acetaminophen-hepatotoxicity. *Eur J Pharmacol* 2014; 726: 116–123.
9. Aycan IÖ *et al.* Thymoquinone treatment against acetaminophen-induced hepatotoxicity in rats. *Int J Surg* 2014; 12: 213–218.
10. Wilhelm EA *et al.* Studies on preventive effects of diphenyl diselenide on acetaminophen-induced hepatotoxicity in rats. *Pathophysiology* 2009; 16: 31–37.
11. Lee KK *et al.* Targeting mitochondria with methylene blue protects mice against acetaminophen-induced liver injury. *Hepatology* 2015; 61: 326–336.
12. Somanawat K *et al.* Curcumin attenuated paracetamol overdose induced hepatitis. *World J Gastroenterol* 2013; 19: 1962–1967.
13. Li G *et al.* Curcumin protects against acetaminophen-induced apoptosis in hepatic injury. *World J Gastroenterol* 2013; 19: 7440–7446.
14. Bulku E *et al.* Curcumin exposure modulates multiple pro-apoptotic and anti-apoptotic signaling pathways to antagonize acetaminophen-induced toxicity. *Curr Neurovasc Res* 2012; 9: 58–71.
15. Yousef MI *et al.* Potential protective effects of quercetin and curcumin on paracetamol-induced histological changes, oxidative stress, impaired liver and kidney functions and haematotoxicity in rat. *Food Chem Toxicol* 2010; 48: 3246–3261.
16. Carvalho NR *et al.* New therapeutic approach: diphenyl diselenide reduces mitochondrial dysfunction in acetaminophen-induced acute liver failure. *PLoS ONE* 2013; 8: e81961.
17. Katyare SS, Satav JG. Impaired mitochondrial oxidative energy metabolism following paracetamol-induced hepatotoxicity in the rat. *Br J Pharmacol* 1989; 96: 51–58.
18. Meyers LL *et al.* Acetaminophen-induced inhibition of hepatic mitochondrial respiration in mice. *Toxicol Appl Pharmacol* 1988; 93: 378–387.
19. Burcham PC, Harman AW. Acetaminophen toxicity results in site-specific mitochondrial damage in isolated mouse hepatocytes. *J Biol Chem* 1991; 266: 5049–5054.
20. Devi KP *et al.* Protective effect of Premna tomentosa extract (L. verbanacae) on acetaminophen-induced mitochondrial dysfunction in rats. *Mol Cell Biochem* 2005; 272: 171–177.
21. García-Niño WR *et al.* Curcumin pretreatment prevents potassium dichromate-induced hepatotoxicity, oxidative stress, decreased respiratory complex I activity, and membrane permeability transition pore opening. *Evid Based Complement Alternat Med* 2013; 2013: 424692.

22. García-Niño WR *et al.* Curcumin attenuates Cr(VI)-induced ascites and changes in the activity of aconitase and F(1)F(0) ATPase and the ATP content in rat liver mitochondria. *J Biochem Mol Toxicol* 2014; 28: 522–527.
23. Molina-Jijón E *et al.* Curcumin prevents Cr(VI)-induced renal oxidant damage by a mitochondrial pathway. *Free Radic Biol Med* 2011; 51: 1543–1557.
24. Correa F *et al.* Curcumin maintains cardiac and mitochondrial function in chronic kidney disease. *Free Radic Biol Med* 2013; 61: 119–129.
25. Tapia E *et al.* Curcumin prevents maleate-induced nephrotoxicity: relation to hemodynamic alterations, oxidative stress, mitochondrial oxygen consumption and activity of respiratory complex I. *Free Radic Res* 2014; 48: 1342–1354.
26. Ratner V *et al.* Mitochondrial dysfunction contributes to alveolar developmental arrest in hyperoxia-exposed mice. *Am J Respir Cell Mol Biol* 2009; 40: 511–518.
27. Bradford MM. A rapid and sensitive method for the quantitation of microgram quantities of protein utilizing the principle of protein-dye binding. *Anal Biochem* 1976; 72: 248–254.
28. Pham T *et al.* Mitochondrial inefficiencies and anoxic ATP hydrolysis capacities in diabetic rat heart. *Am J Physiol Cell Physiol* 2014; 307: C499–C507.
29. Spinazzi M *et al.* Assessment of mitochondrial respiratory chain enzymatic activities on tissues and cultured cells. *Nat Protoc* 2012; 7: 1235–1246.
30. Gunawan BK, Kaplowitz N. Mechanisms of drug-induced liver disease. *Clin Liver Dis* 2007; 11: 459–475.
31. Jiang J *et al.* Increased mitochondrial ROS formation by acetaminophen in human hepatic cells is associated with gene expression changes suggesting disruption of the mitochondrial electron transport chain. *Toxicol Lett* 2015; 234: 139–150.
32. Lancaster EM *et al.* Acetaminophen hepatotoxicity: an updated review. *Arch Toxicol* 2015; 89: 193–199.
33. Ramsay RR *et al.* In vitro effects of acetaminophen metabolites and analogs on the respiration of mouse liver mitochondria. *Arch Biochem Biophys* 1998; 273: 449–457.
34. Landin JS *et al.* Identification of a 54-kDa mitochondrial acetaminophen-binding protein as aldehyde dehydrogenase. *Toxicol Appl Pharmacol* 1996; 141: 299–307.
35. Trujillo J *et al.* Mitochondria as a target in the therapeutic properties of curcumin. *Arch Pharm (Weinheim)* 2014; 347: 873–884.
36. Subudhi U *et al.* Alleviation of enhanced oxidative stress and oxygen consumption of l-thyroxine induced hyperthyroid rat liver mitochondria by vitamin E and curcumin. *Chem Biol Interact* 2008; 173: 105–114.
37. Gardner PR. Superoxide-driven aconitase Fe–S center cycling. *Biosci Rep* 1997; 17: 33–42.
38. Trujillo J *et al.* Curcumin prevents cisplatin-induced decrease in the tight and adherens junctions: relation to oxidative stress. *Food Funct* 2016; doi: 10.1039/C5FO00624D.

European Journal of Pharmacology 765 (2015) 472–481

Contents lists available at ScienceDirect

European Journal of Pharmacology

journal homepage: www.elsevier.com/locate/ejphar

Cardiovascular pharmacology

Inhibition of the nitric oxide/cyclic guanosine monophosphate pathway limited the cardioprotective effect of post-conditioning in hearts with apical myocardial infarction

Francisco Correa [a,*], Mabel Buelna-Chontal [a], Victoria Chagoya [b], Gerardo García-Rivas [c], Rosa María Vigueras [d], José Pedraza-Chaverri [e], Wylly Ramsés García-Niño [a], Rogelio Hernández-Pando [f], Juan Carlos León-Contreras [f], Cecilia Zazueta [a]

[a] Departamento de Biomedicina Cardiovascular, Instituto Nacional de Cardiología, I. Ch., Juan Badiano No. 1., Col. Sección XVI, México D.F. 14080, Mexico
[b] Departamento de Biología Celular, Instituto de Fisiología Celular, Universidad Nacional Autónoma de México, México, D.F., Mexico
[c] Centro de Innovación y Transferencia en Salud de la Escuela de Medicina del Tecnológico de Monterrey, Cátedra de Cardiología y Medicina Vascular, Instituto de Cardiología y Medicina Vascular del Tecnológico de Monterrey, Monterrey, N.L. 64710, Mexico
[d] Laboratorio de Histomorfología, Torre de Investigación, Instituto Nacional de Pediatría, SS, México D.F. 04530, Mexico
[e] Departamento de Biología, Facultad de Química, Universidad Nacional Autónoma de México, 04510 México DF, Mexico
[f] Sección de Patología Experimental, Departamento de Patología, Instituto Nacional de Ciencias Médicas y Nutrición Salvador Zubirán, Av. Vasco De Quiroga 15, Tlalpan, México D.F., Mexico

ARTICLE INFO

Article history:
Received 15 April 2015
Received in revised form
9 September 2015
Accepted 14 September 2015
Available online 18 September 2015

Keywords:
Post-conditioning
Isoproterenol
Reperfusion injury
cGMP

ABSTRACT

Reperfusion damage involves opening of the mitochondrial permeability transition pore (mPTP) and loss of ATP synthesis. Several cardioprotective pathways are activated by ischemic or pharmacological post-conditioning (PC). The mechanisms that are activated by PC in no co-morbidity murine models include: activation of rescue kinases, oxidative stress reduction, glycolytic flux regulation and preservation of ATP synthesis. However, relatively scarce efforts have been made to define whether the efficacy of PC signaling is blunted by risk factors or systemic diseases associated with ischemic heart pathology. Experimental evidence has shown that the nitric oxide (NO)/cyclic guanosine monophosphate (cGMP) signaling is a main mechanism activated by PC in hearts without pathological history. In this work we evaluated the participation of the NO pathway, through downstream kinase activation and inhibition of mPTP in hearts with previous infarct.

Myocardial infarction was induced with a single dose of isoproterenol (85 mg/kg i.p.) to male Wistar rats. After 24 h, the hearts were mounted into the Langendorff system and subjected to 30 min of ischemia and 60 min of reperfusion. PC consisted of 5 cycles of 30 s of reperfusion/30 s of ischemia, then the hearts were reperfused with or without inhibitors of the NO/cGMP pathway.

PC activates the NO/cGMP pathway, as increased cGMP and NO levels were detected in isoproterenol-treated hearts. The cardioprotective effect of PC was abolished with both L-NAME (inhibitor of constitutive NO synthase) and ODQ (inhibitor of soluble guanylate cyclase), whereas the NO donor (DETA-NO) restored cardioprotection even in the presence of L-NAME or ODQ. We also found that mitochondrial structure and function was preserved in PC hearts.

We conclude that PC exerts cardioprotection in hearts with previous infarct by maintaining mitochondrial structure and function through NO-dependent pathway.

1. Introduction

Cardiovascular ischemic diseases affect a high proportion of world population, being the leading cause of mortality and disability in adults. Timely reperfusion promotes cardiomyocyte survival, decreasing morbidity and mortality. Paradoxically, reperfusion of ischemic tissue by thrombolysis, percutaneous coronary intervention, coronary artery bypass grafting or cardiac transplantation, may result in additional cardiomyocyte dysfunction, a phenomenon termed "reperfusion injury". In this sense, post-conditioning (PC) has emerged as a powerful strategy to contend against reperfusion injury in animals models, as well as in some clinical studies (Zhao et al., 2003). It consists of the application of brief cycles of ischemia–reperfusion, after ischemia and

* Corresponding author. Fax: +52 55 5573 0926.
E-mail address: glicoproteico@gmail.com (F. Correa).

http://dx.doi.org/10.1016/j.ejphar.2015.09.018
0014-2999/

before prolonged reperfusion. PC has re-attracted scientific and clinical interest on reperfusion injury, particularly due to the acquired knowledge of the cellular and molecular events activated during the early phase of reperfusion (Costa et al., 2008; Zhao et al., 2003). However, most of PC studies had been performed in health and young animals. The application of experimental knowledge on the clinical practice requires demonstration of PC effectiveness in heart diseases resulting from co-morbidities.

In this sense, it has been described that patients with non ST-elevation acute coronary syndrome are at high risk for recurrent ischemic events due to complex coronary artery disease (CAD), and had lesser possibilities to be completely revascularized. Also, a percentage of patients ≥ 70 years of age with unstable angina discharged after myocardial infarction (PREVESE Study) and followed during three months, presented a second ischemic event (2.2%); whereas 11.2% developed angina (Kumbhani et al., 2013; de Velasco et al., 1997).

Isoproterenol (ISO) hydrochloride, a synthetic catecholamine and β-adrenergic agonist causes severe stress in the myocardium resulting in infarct-like necrosis damage in animal's models (Díaz-Muñoz et al., 2006). The pathophysiological changes produced by ISO in rat hearts are comparable to those observed in human myocardial infarction. Particularly cardiac apoptosis and/or necrosis, increase the incidence of cardiac arrhythmias (Tappia et al., 2001; Stelzner et al., 1987). ISO generates free radicals leading to lipid peroxidation and membrane permeability alterations (Sushamakumari et al., 1989; Tood et al., 1980). Augmented oxidative stress depresses sarcolemmal Ca^{2+} transport, promoting intracellular Ca^{2+} overload and ventricular dysfunction (Prabhu et al., 2006). It has also been reported that ISO decreases the antioxidant defense mechanisms (Chien et al., 1978) and that β-adrenergic receptors stimulates apoptosis in myocytes through reactive oxygen species (ROS) dependent activation of the mitochondrial pathway (Remondino et al., 2003).

As it is known that the nitric oxide/cyclic guanosine monophosphate (ON/cGMP) pathway is involved in PC protection in isolated rat hearts (without co-morbidity) (Penna et al., 2006) and, that ROS attenuation depends on the antioxidant action of NO (Todd et al., 1980), the aim of the present investigation was to demonstrate the effectiveness of PC in a heart model with previous infarct induced by ISO, to evaluate the robustness of the NO/cGMP pathway to confer cardioprotection and its impact on mitochondrial structure and function.

2. Materials and methods

This investigation was performed in accordance with the Guide for the Care and Use of Laboratory Animals, published by the United States National Institutes of Health (US-NIH).

2.1. Cardiac function in post-conditioned hearts from isoproterenol-treated rats

Male Wistar rats, weighing 250–300 g and provided with food and water *ad libitum*, were injected subcutaneously with a single dose of ISO (85 mg/kg/day) between 08:00 and 09:00 a.m.. Control animals received a subcutaneous injection of saline solution.

After 24 h the animals were anesthesized with sodium pentobarbital (60 mg/kg) and sodium heparine (100 U/kg). Five min after heparin injection, a midsternal thoracotomy was performed and the heart was rapidly excised and placed in ice-cold Krebs–Henseleit buffer solution of pH 7.4, consisting of 118 mM NaCl, 4.75 mM KCl, 1.18 mM KH_2PO_4, 1.18 mM $MgSO_4 \cdot 7H_2O$, 5 mM $CaCl_2$, 25 mM $NaHCO_3$, 5 mM glucose, and 100 μM sodium octanoate. Within 45 s, the heart was mounted onto a Langendorff heart perfusion system. The hearts were perfused retrogradely via the aorta at a constant flux of 12 ml/min with Krebs–Henseleit solution, which was continuously bubbled with 95% O_2 and 5% CO_2 at 37 °C.

Cardiac performance was measured at left ventricular end-diastolic pressure (LVEDP) of 10 mm Hg using a latex balloon inserted into the left ventricle and connected to a pressure transducer (Correa et al., 2008). Throughout the experiment, left ventricular developed pressure (LVDP) was continuously recorded using a computer acquisition data system designed by the Instrumentation and Technical Development Department of the National Institute of Cardiology (México, D.F., México). Heart rate (HR) expresses beat number/min. Cardiac contractile function was calculated by subtracting LVEDP from left ventricular peak systolic pressure, yielding LVDP. The double product (DP) was calculated by multiplying HR by LVDP. All variables were recorded using a computer acquisition data system designed by the Instrumentation and Technical Development Department of the National Institute of Cardiology (México, D.F., México).

The heart was perfused till stabilization with Krebs buffer for 20 min. The ISO hearts were subjected to global ischemia for 30 min by turning off the pumping system and then to 60 min of reperfusion (ISO+I/R). The post-conditioning maneuver consisted of five cycles of ischemia-reperfusion (30 s reperfusion and 30 s ischemia per cycle), followed by 60 min of reperfusion (ISO+I/R+PC). Hearts from the control group were also evaluated to compare functional and biochemical changes induced by isoproterenol, but were not subjected neither to I/R or PC.

2.2. Measurement of infarct size

At the end of the experiments the hearts to be used for infarct size calculations were frozen at −20 °C. Heart slices of ~3 mm were obtained and immersed in 1% triphenyltetrazolium chloride solution in phosphate buffer (8.8 mM Na_2HPO_4, 1.8 mM NaH_2PO_4, pH 7.4) for 10 min at 37 °C; the slices were incubated in a solution of formalin for 5 min, and digitalized on a Hewlett-Packard Scanjet 3800 scanner (Hewlett-Packard, Palo Alto, CA, USA). In each image the risk and the infarct zones were traced and the respective areas were calculated in terms of pixels using the software Image J®. Other group of hearts was assigned for histological analysis with the haematoxylin/eosin technique and electron microscopy. To study the mitochondrial ultrastructural morphology, small cardiac tissue fragments were obtained and immersed into 10% glutaraldehyde dissolved in cacodylate buffer pH 7.2. Then, the fragments were deposited into glass tubes and fixed by immersion in the same solution during 24 h at 4 °C. After extensive washing with cacodylate buffer, tissue fragments were post-fixed with osmium tetraoxide, dehydrated in graded ethyl alcohol solutions and embedded in Epon resin (London Resin Company, London, UK). Thin sections from 70 to 90 nm were placed on cooper grids, contrasted with lead and uranium salts and examined with a FEI Technei electron microscope.

2.3. Echocardiography analysis

Echocardiographic images were obtained using a Sonos 5500 echocardiographer (Koninlijke Philips Electronics, Eindhoven, NL) with a 12 MHz transducer. Parasternal long and short axis views were analyzed in the anesthetized rats. Two-dimensional-guided (2D) M-mode echocardiography was performed and determinations were made from at least 3 beats in each rat. Left ventricular (LV) cavity and wall thickness were measured to calculate the ejection fraction (EF) as follows: $\%EF = [(EDV - ESV/EDV) \times 100]$ where EDV is end-diastolic volume and ESV is end-systolic volume.

2.4. Preparation of cytosolic and mitochondrial fractions

At the end of the ischemia/reperfusion protocol, a group of hearts was placed in cold isolation buffer containing 250 mM sucrose, 10 mM Tris–HCl, and 1 mM EDTA, pH 7.3. Mitochondrial and cytosolic fractions were obtained by differential centrifugation, as previously described, by using the protease subtilisin A (Correa et al., 2008). Protein was measured by the Lowry method (Lowry et al., 1951).

2.5. Mitochondrial function in post-conditioned ISO hearts.

Mitochondrial oxygen consumption was measured using a Clark-type oxygen electrode (Yellow Springs Instruments, OH, USA). The experiments were carried out in 1.5 ml of basic medium containing 125 mM KCl, 3 mM Pi, pH 7.3. State 4 respiration was evaluated in the presence of 10 mM succinate plus 1 μg/ml rotenone, and 1 mg of mitochondrial protein. State 3 respiration was measured after addition of 200 μM Adenosine diphosphate (ADP). Respiratory control index (RC) was calculated as the ratio between state 3 and state 4 rates. Uncoupled respiration was measured by adding 1 μM carbonyl cyanide m-chlorophenylhydrazone (CCCP).

Aconitase activity was evaluated by measuring cis-aconitate formation at 240 nm, in a medium containing 25 mM KH_2PO_4 buffer pH 7.4 and 50 μg of mitochondrial protein as described by Hausladen and Fridovich (1994).

2.6. SOD and catalase levels in post-conditioned ISO hearts

Equivalent amounts of heart tissue were homogenized in phosphate buffer 50 mM pH 7.4, containing 0.1% triton X-100 and protease inhibitors: leupeptin (5 μg/ml), pepstatin A (7 μg/ml) and aprotonin (5 μg/ml) for ~15 s. After centrifugation at 21,000 × g for 20 min, supernatant samples (100 μg) were separated on 13% acrylamide gels, using TRIS–glycine running buffer at 100 V and 12 °C. The proteins were transferred to PVDF membranes for 1 h at 135 mV and subjected to western blot analysis. Immunodetection was performed using anti-SOD (1:500) or anti-catalase (1:1000) antibodies in PBS, pH 7.4. Alkaline phosphatase (AP)-conjugated secondary antibodies (1:25,000) and a chemiluminiscent reagent were used for signal detection. Control loading was determined by incubating the membranes against anti-GAPDH polyclonal antibodies (1:2500).

2.7. Activity of antioxidant enzymes in post-conditioned ISO hearts

SOD activity in heart homogenates was determined by a competitive inhibition assay. NBT reduction to formazan was achieved using the xanthine–xanthine oxidase system. The mixture reaction contained in final concentration: 0.122 mM EDTA, 30.6 μM NBT, 0.122 mM xanthine, 0.006% bovine serum albumin, and 49 mM sodium carbonate. 500 μl of tissue homogenates, were added to 1.66 ml of the mixture described above; then 50 μl xanthine oxidase (final concentration of 2.8 U/L) were added and incubated in a water bath at 37 °C for 30 min. The reaction was stopped with 66 μl of 0.8 mM cupric chloride and the optical density was read at 560 nm. 100% of NBT reduction was obtained in a tube in which the sample was replaced by distilled water. The amount of protein that inhibited NBT reduction to 50% of maximum was defined as one unit of SOD activity. Results were expressed as U/mg protein. The amount of protein that inhibits NBT reduction to 50% of maximum was defined as 1 unit of SOD activity. Results are expressed as units per milligram of protein (Fernández-Checa and Kaplowitz, 1990).

Cardiac catalase activity was assayed at 25 °C by a method based on the disappearance of H_2O_2 from a solution containing

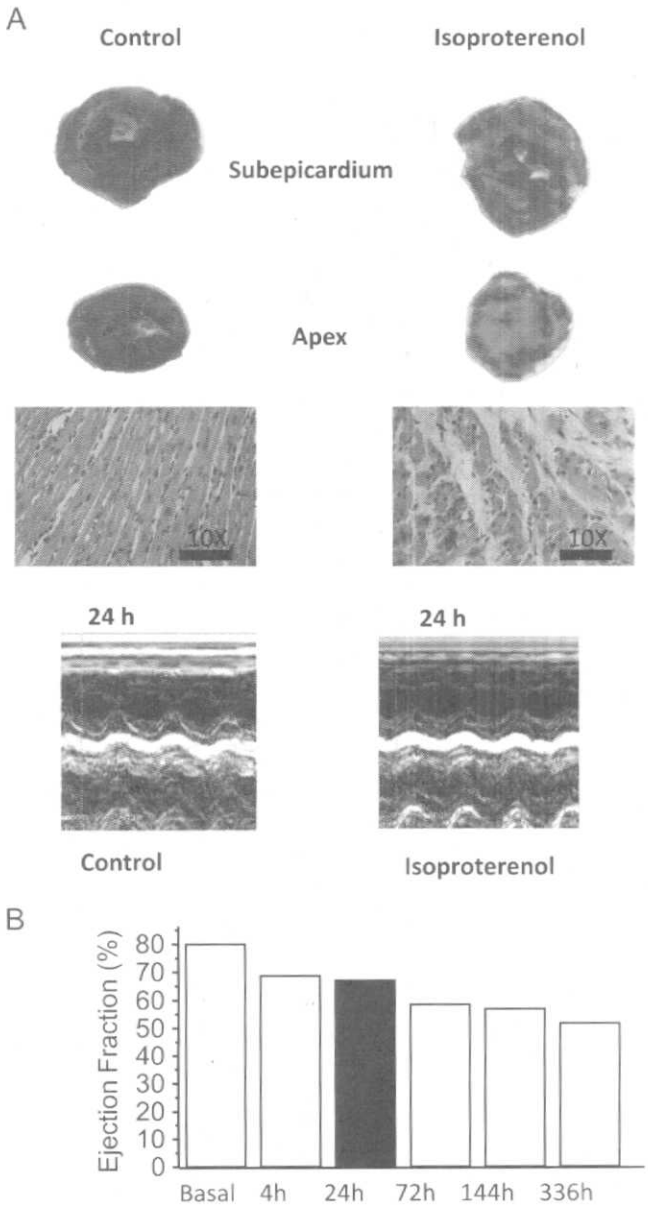

Fig. 1. (A) Apical infarct induced by a single dose of isoproterenol (85 mg/kg). Necrotic zones were determined by tetrazolium blue staining after 24 h (upper panel). The bottom panel shows cardiac tissue slices stained with hematoxilin–eosin. (B) Representative images of echocardiographic registers and ejection fraction data obtained from different animals at different times after isoproterenol administration.

30 mM H_2O_2 in 10 mM potassium phosphate buffer pH 7.0 at 240 nm. The reaction was started by the addition of 25 μl of the sample to 725 μl of H_2O_2. Under the described conditions, the decomposition of H_2O_2 by catalase contained in the samples follows a first order kinetic as given by the equation $k = 2.3/t \log A_o/A$ where k is the first-order reaction rate constant, t is the time over which the decrease of H_2O_2, due to catalase activity, was measured (15 s) and A_o/A is the optical density at times 0 and 15 s, respectively. The results were expressed as nmol/mg of protein (Pedraza-Chaverri et al., 1999).

2.8. Assay for total glutathione content in post-conditioned ISO hearts

At the end of the ischemia/reperfusion protocols, some hearts

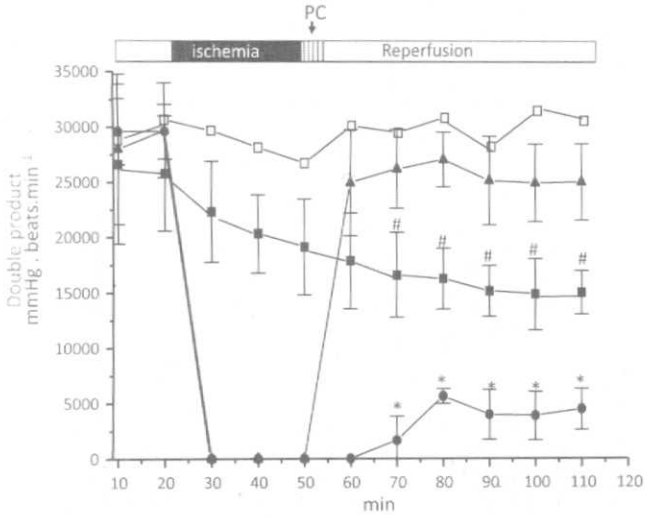

Fig. 2. Heart function in post-conditioned hearts from ISO-treated rats. Hearts were stabilized for 20 min, then subjected to 30 min ischemia and 60 min of reperfusion. (□) control hearts; (■) ISO hearts; (●) ISO+I/R and (▲) ISO+I/R+PC, $n=5$. $^{*}P \leq 0.05$ vs. all groups and $^{\#}P \leq 0.05$ vs. ISO+I/R+PC.

were frozen with liquid nitrogen, powdered with a pre-chilled pestle in a frozen mortar and stored until determination. Powdered tissue was homogenized during 15 s with a polytron in phosphate buffer 50 mM (1:3 w/v) and centrifugated at 5000 × g for 10 min at 4 °C. Protein content in homogenates was measured as described by Lowry et al. (1951). The homogenates were incubated in a mix reaction solution containing 1 mM mCB, glutathione *S*-transferase (GST) 1 U/ml, and the homogenate sample (33.3 μL); the mix reaction was incubated at room temperature for 30 min. Formation of the fluorescent GSH–mCB adduct was evaluated at 385 nm excitation and 478 nm emission in a Biotek Synergy HT spectrofluorometer every 15 min. GSH content in the samples was calculated with a standard curve of GSH in a range from 0.1 μM to 100 μM (Fernández-Checa and Kaplowitz, 1990). The fluorescent signal recorded over time was directly proportional to GSH concentration.

2.9. NO/cGMP pathway contribution to the cardioprotective effect of post-conditioning in ISO hearts

To evaluate the effect of NO/cGMP pathway in the post-conditioning protective effect, we administrated either the selective and irreversible heme-site inhibitor of soluble guanylate cyclase, 1 H-(1,2,4)oxadiazolo(4,3-a)quinoxalin-1-one (ODQ) or N5-[imino (nitroamino) methyl]-L-ornithine, methyl ester, monohydrochloride (L-NAME), a potent and reversible inhibitor of NOS. ODQ and L-NAME were perfused during 20 min prior to the ischemic period at doses of 50 and 10 μM, respectively. The hearts were then subjected to post-conditioning and to prolonged reperfusion with the compound. Other hearts, were perfused during reperfusion with 50 μM (Z)-1-[N-(2-aminoethyl)-N-(2-ammonioethyl)amino]diazen-1-ium-1,2-diolate (DETA-NO), a nitric oxide donor. This compound spontaneously dissociates in a pH-dependent, first-order process at 37 °C and pH 7.4, to liberate 2 mol of nitric oxide per mole of parent compound.

2.10. cGMP and nitric oxide content in post-conditioned ISO hearts

cGMP content was assayed with commercial kits purchased from Roche Diagnostics, Switzerland. Nitrate and nitrite were measured as indicators of nitric oxide concentration in deproteinized heart samples by measuring NADPH oxidase-dependent reduction of nitrate to nitrite. Values were calculated with a standard curve of nitrites with the reactive of Griess (Muñoz et al., 2003).

2.11. Mitochondrial permeability transition was evaluated by measuring calcium dynamics in mitochondria

Mitochondrial Ca^{2+} accumulation and retention was evaluated spectrophotometrically in a double-beam spectrophotometer at 675–685 nm by using the metallochromic dye arsenazo III (50 μM). Two mg of mitochondrial protein were incubated into a medium containing 125 mM KCl, 10 mM HEPES, 3 mM Pi, 10 mM succinate, 160 μM ADP, 50 μM Ca^{2+} and 5 μg rotenone pH 7.3. Where indicated 0.1 μM cyclosporine A (specific inhibitor of mitochondrial permeability transition pore) was added to correlate the activity of this channel with increased Ca^{2+} permeability. Cytochrome c release was measured according to Correa et al. (2007).

2.12. Data analysis

Statistical analysis was performed by analysis of variance (ANOVA), using the data analysis and technical program Microcal™ Origin™ from Microcal Software, Inc. (1999). Results were expressed as mean ± S.D. P values <0.05 were considered significant.

3. Results

3.1. Histological studies

ISO-treated animals showed infarct-like damage of circumferential type in the subendocardium, at the apex region of the left ventricle, as measured by triphenyltetrazolium chloride (TTC) staining. Infarct areas were clearly defined in the apex of all experimental animals (Fig. 1A, upper panel). Subepicardium damage was minimal, and there was no transmural infarction, since the lesion affected, on average, one third of the thickness of the ventricular wall. None of the control animals presented evidence of myocardial damage. Eosin–hematoxylin staining reveled coagulative necrosis, fiber fragmentation, inflammation and edema, associated with isoproterenol-induced acute myocardial infarction (Fig. 1A, bottom panel). Echocardiography analysis showed diminution of left ventricular shortening after one day of ISO-treatment (68% vs. 80% in control hearts), that decreased to 55% after two weeks (Fig. 1B).

3.2. Cardiac function in post-conditioned heart from ISO-treated rats

The double product of ISO hearts subjected only to perfusion during 110 min decreased from 26,607 mmHg beats min^{-1} to 16,785 mmHg beats min^{-1}. Function collapsed in ISO-hearts during the first min of reperfusion after ischemia to 4642 mmHg beats min^{-1}, in remarkable contrast to the ISO hearts subjected to the post-conditioning cycles, which maintained double products of 25,178 mmHg beats min^{-1} after 60 min of reperfusion. There was no significant difference between double product of ISO+I/R+PC hearts before ischemia and after reperfusion, against control heart function (Fig. 2).

3.3. Effect of PC and ON/GMPc inhibitors ON mitochondrial structure

The ultrastructural study showed in comparison with the control group (Fig. 3A), edema and mitochondrial membrane fragmentation, as well as fibrils disruption in the ISO-treatment

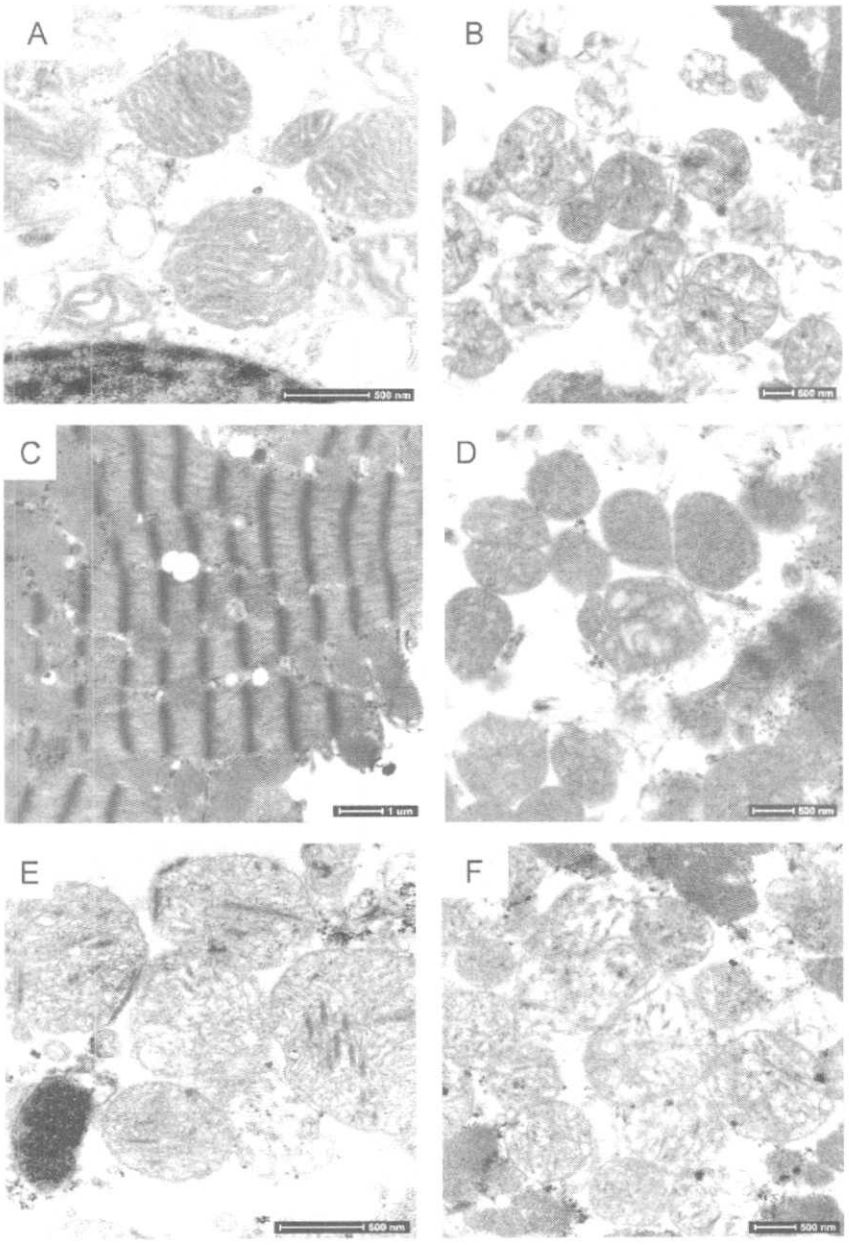

Fig. 3. Representative ultrastructural micrographs of the different groups. (A) Normal mitochondria located in the cytoplasm of cardiomyocytes from control group. (B) Swollen mitochondria with membrane rupture obtained from the ISO-treated group. (C) Well preserved myofibrils and intact mitochondria is observed in the post-conditioned ISO-treated group (D). Extensive mitochondrial damage is seen in the post-conditioned ISO-groups treated either with the inhibitor of guanylate cyclase (E) or NOS (F).

group (Fig. 3B). In contrast, the post-conditioned ISO-group showed well preserved mitochondria and myofibrils, with occasional swelled mitochondria (Fig. 3C and D); while extensive mitochondrial edema and membrane disruption were observed in the groups of post-conditioned ISO-groups treated with the inhibitor of guanylate cyclase (ODQ) (Fig. 3E) or NOS (L-NAME) (Fig. 3F).

3.4. Mitochondrial integrity in post-conditioned ISO hearts

At the end of the protocols, hearts were dismounted and mitochondria were obtained to evaluate oxygen consumption. There was a slight increase in basal respiratory rates (State 4) of ISO mitochondria as compared with control mitochondria when using succinate plus rotenone, although no difference was observed between ISO and ISO+I/R oxygen consumption. Mitochondria from I/R+ISO+PC hearts showed similar state 4 respiratory rates as the control group. ISO+I/R mitochondria was not stimulated by ADP, contrasting with mitochondria obtained from ISO+I/R +PC hearts that showed increased state 3 respiratory rates, such values were similar to oxygen consumption in control mitochondria. Respiratory control (RC), an indicator of the mitochondrial electron transport coupling to ADP phosphorylation was also determined. RC values in control mitochondria was 6.1 and 3.2 in C+ISO mitochondria, whereas in mitochondria isolated from ISO+I/R hearts this value diminished 66%. In contrast, ISO+I/R+PC mitochondria reached RC values of 5.2 (Fig. 4A).

We also measured mitochondrial aconitase activity, a Fe–S cluster enzyme that is inactivated by superoxide and peroxynitrite, to evaluate mitochondrial damage by oxidative stress. Activity in

A

Succinate + Rotenone	State4 $ngAtO_2$/min/mg	State 3 $ngAtO_2$/min/mg	R.C
control	8.1± 1.4	48.5 ± 7.5	6.1 ± 0.2
ISO	21.2 ± 6#	67.6 ± 10#	3.2± 0.5#
ISO + I/R	11.4 ± 5	11.4 ± 3*	1± 0*
ISO + I/R + PC	8.2 ± 2.3	44.0 ± 5.2	5.2± 0.8

B

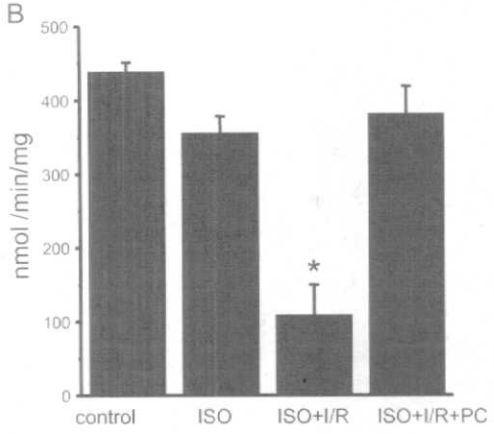

Fig. 4. Mitochondrial integrity in post-conditioned ISO hearts. (A) Oxygen consumption in mitochondria from ISO hearts was evaluated with succinate plus rotenone as substrate, nanograms atoms of oxygen ($ngAtO_2$) per min per mg of mitochondrial protein. $n=4$. $^*P \leq 0.05$ vs. ISO+I/R+PC; $^\#P \leq 0.05$ vs. control. (B) Aconitase activity in mitochondria from ISO hearts. $n=4$. $^*P \leq 0.05$ vs. all groups.

ISO+I/R mitochondria was significantly lower than in mitochondria obtained from control and ISO hearts (120 ± 42 nmol/min/mg vs. 438 ± 12 nmol/min/mg and 366 ± 12 nmol/min/mg, respectively). Conversely, aconitase activity in ISO+I/R+PC mitochondria was similar (380 ± 37 nmol/min/mg) to that observed in mitochondria from control and ISO hearts (Fig. 4B). It is worth to mention, that we do not observed any effect in aconitase activity or oxygen consumption in mitochondria obtained from ISO hearts treated with the inhibitors (Supplemental Fig. 2).

3.5. Activity of catalase and SOD in post-conditioned ISO-hearts

We evaluated catalase content (Fig. 5A) and activity (Fig. 5B) in cytosolic fractions of ISO hearts. Both content and activity diminished if compared with control hearts. Further decrease was observed after ischemia and reperfusion, which was prevented by post-conditioning. The same behavior was observed in both SOD isoforms (Fig. 5A and B). These results suggest sequential inactivation of superoxide ions and hydrogen peroxide in hearts subjected to post-conditioning (ISO+I/R+PC).

3.6. Total glutathione (GSH) content in post-conditioned ISO hearts

Changes in GSH content of ISO hearts are shown in Fig. 6. GSH levels diminished after the reperfusion protocol (ISO+I/R) and were recovered in post-conditioning hearts (ISO+I/R+PC), this enhancement was comparable with GSH content in isoproterenol hearts (ISO).

3.7. Role of the nitric oxide/cGMP pathway in post-conditioned ISO hearts function

We evaluated the effect of guanylate cyclase (GC) and nitric oxide synthase (NOS) inhibition on the cardioprotective effect of post-conditioning in ISO hearts. Cardiac function diminished in post-conditioned ISO hearts at the end of reperfusion in the presence of ODQ (9,375 ± 1,953 mmHg · beats · min^{-1}) as compared with ISO+I/R+PC hearts (25,000 ± 3,125 mmHg beats · min^{-1}), although it remain significantly higher than that observed in ISO+I/R hearts (4,687 ± 1,640 mmHg beats min^{-1}). L-NAME also exerted a dramatic effect on the double product of ISO+I/R+PC hearts, as cardiac function was totally abolished at the end of reperfusion, decreasing even at lower levels than ISO+I/R hearts (859 ± 681 mmHg beats min^{-1} vs. 4,687 ± 1,640 mmHg beats min^{-1}) (Fig. 7A). Perfusion of the nitric oxide donator (DETA-NO) mimics the effect of the PC maneuver when administrated to ISO+I/R during reperfusion, whereas hearts with previous ODQ treatment partially recovered function (Fig. 7B), indicating that NO may exert both cGMP-dependent and independent cardioprotective effects. We also observed that the NO/GC dependent pathway activated is highly regulated during PC, as ODQ administration during reperfusion did not abolished the cardioprotective effect of PC (Fig. 8A), whereas eNOS inhibition during PC abrogated cardioprotection (Fig. 8B).

It is worth to mention that at the doses used here, perfusion of ODQ and L-NAME did not modified the double product of ISO hearts non-subjected to ischemia and reperfusion (Supplemental Fig. 1). We neither observed any effect in aconitase activity or oxygen consumption in mitochondria obtained from ISO hearts treated with the inhibitors (Supplemental Fig. 2)

3.8. Effect of ODQ and L-NAME on cGMP and nitric oxide (NO) content in post-conditioned ISO hearts

At the end of reperfusion we evaluated cGMP and NO content in hearts subjected to post-conditioning in the presence of the abovementioned inhibitors. ISO+I/R hearts showed lower levels of cGMP than untreated ISO hearts. ISO+I/R+PC recovered cGMP content at ISO hearts levels (7.6 ± 1.1 pmol/g tissue vs. 6.5 ± 1.04 pmol/g tissue). As expected, the inhibition of GC and NOS diminished such levels to 2.9 ± 1 pmol/g tissue and 0.79 ± 1.7 pmol/g tissue, respectively (Fig. 9A). A similar response was observed in nitrite content, although the inhibitors did not promote total depletion of this metabolite (Fig. 9B).

3.9. Effect of nitric oxide pathway inhibition on mitochondrial function in post-conditioned ISO hearts

We evaluated the mitochondrial transition permeability by measuring calcium dynamics. Mitochondria from ISO+ I/R hearts presented a low calcium retention capacity and fast calcium release as compared with ISO and ISO+I/R+PC mitochondria, which was only partially prevented by cyclosporine A (CSA) a specific inhibitor of mPTP. L-NAME and ODQ administration to the post-conditioned group produce the loss of the protected status and consequent opening of the permeability transition pore (Fig. 10A).

Open and closed states of the permeability transition pore were related with changes in cytochrome c content (Fig. 10B).

4. Discussion

Overstimulation of α-adrenergic receptors by isoproterenol (ISO) has been related with oxidative stress induction. The reactive intermediates formed during catecholamine oxidation may influence development of several heart diseases (Costa et al., 2011). It is

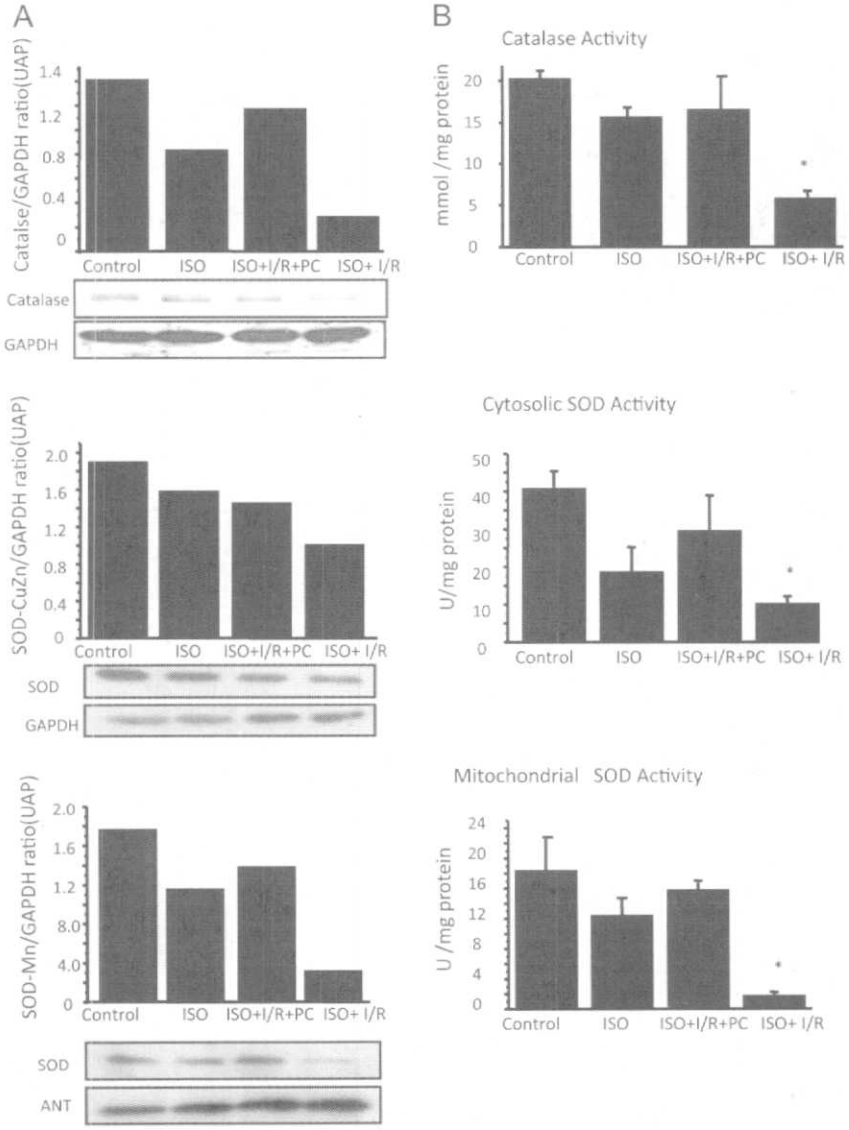

Fig. 5. Content and activity of catalase and SOD in post-conditioned ISO-hearts. (A) Representative western blots of catalase, SOD–CuZn and SOD–Mn content in ISO hearts subjected to post-conditioning. Bars show the ratio between the antioxidant enzymes and control loading markers. GAPDH in cytosol and ANT in mitochondria. (B) Antioxidant enzymes activity, $n=4$. $^{*}P \leq 0.05$ vs. ISO+I/R+PC.

known for example, that oxidation of catecholamine's hydroxyl groups leads to quinone conversion and subsequent formation of adrenochromines. During this reaction highly toxic oxygen derived free radicals, detrimental to extra and intracellular enzymes and proteins are produced causing cell necrosis and contractile failure in rat heart (Díaz-Muñoz et al., 2006; Rona et al., 1959). Furthermore, free radicals initiate the peroxidation of membrane bound polyunsaturated fatty acids, increasing functional and structural myocardial injury.

The pathophysiological and morphological changes that take place in rat's heart following MI induced by ISO has been described to be comparable to the changes that takes place in human myocardial infarct (Kannan and Quine, 2011a). In this sense, previous studies demonstrated that myocardium injury induced by isoproterenol in experimental rats is strongly associated with deterioration of hemodynamic and LV contractile function (Kannan and Quine, 2011b, 2013; Whalen and Lewis, 1999).

Therefore, in this work we used the infarct-like damage model induced by ISO that is developed 24 h after the administration of a single dose of the catecholamine (Chagoya et al., 1997) to determine if postconditioning (PC) may exert a cardioprotective response against reperfusion in previously damaged hearts. PC has become a watershed in cardioprotection since it was discovered that the application of brief cycles of occlusion and reperfusion in the left anterior descending artery (LAD) after ischemia and before long reperfusion in normal dog hearts, produced reduction in infarct size and preserved endothelial function (Zhao et al., 2003). PC-conferred cardioprotection is driven at the onset of myocardial reperfusion by the activation of cell surface receptors and recruitment of signaling kinases that regulate mitochondrial function (Hausenloy and Yellon, 2009). The nitric oxide (NO)/soluble guanylate cyclase (GC)/cyclic guanosine monophosphate (cGMP)/protein kinase G (PKG) pathway has been extensively studied in PC. However, recent reports indicate that the mechanisms by which PC activates this pathway are differentially regulated in healthy hearts, depending on the species. It was observed for example, that cardioprotection is only blunted by the NOS inhibitor L-NAME and abolished by ODQ (a GC antagonist) in rat hearts (Penna et al., 2006), whereas both NOS and GC inhibition abrogated the post-conditioning infarct-sparing effect in rabbit hearts

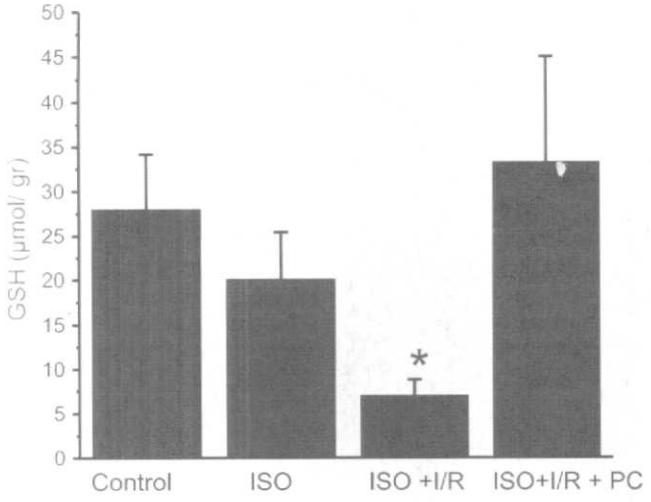

Fig. 6. GSH content in post-conditioned ISO hearts. Levels of glutathione were measured at end of reperfusion protocol, $n=4$. $^{*}P \leq 0.05$ vs. ISO+I/R+PC.

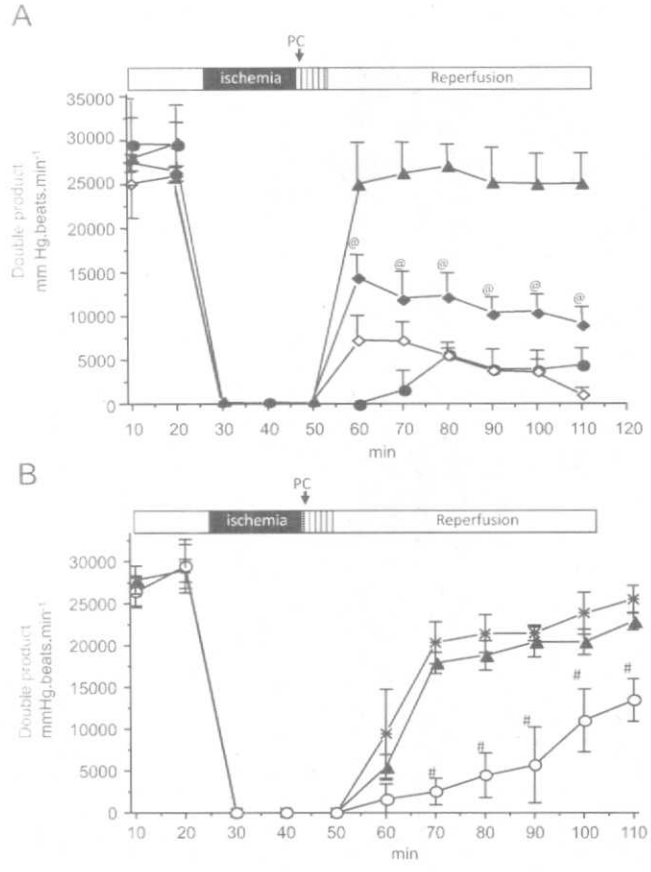

Fig. 7. Heart function in post-conditioned ISO hearts perfused with L-NAME, ODQ and DETA-NO. (A) 50 µM L-NAME (◇) or 10 µM ODQ (◆) were administrated during all the protocol. It is also shown that heart function of post-conditioned ISO hearts (▲) and (●) ISO+I/R B) 50 µM DETA-NO (○) was administrated to ODQ-treated PC hearts during reperfusion; It is also shown that heart function of post-conditioned ISO hearts (▲) and the effect of the DETA-NO on ISO/I/R hearts (*), $n=4$. $^{@}P \leq 0.05$ vs. ISO+I/R+PC; $^{\#}P \leq 0.05$ vs. ISO+I/R+DETA-NO and ISO+I/R+PC.

(Yang et al., 2005, 2004). Our results show that post-conditioning promoted cardioprotection in rat hearts with previous infarct-like damage by both cGMP-dependent and cGMP-independent pathways, as the effect of PC was partially maintained in presence of

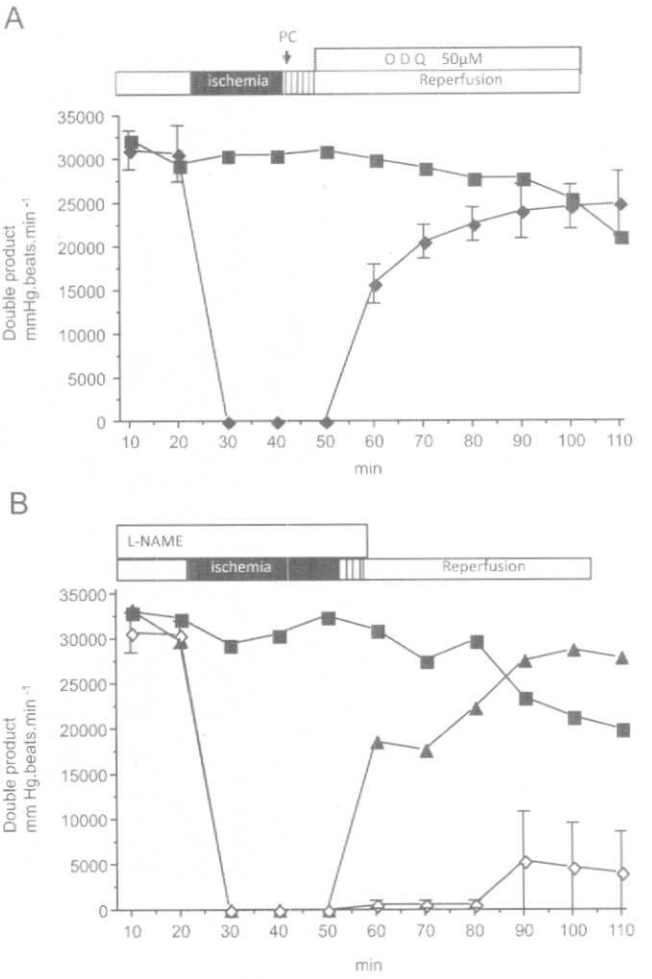

Fig. 8. Heart function in post-conditioned ISO hearts perfused with L-NAME previous to reperfusion and with ODQ during reperfusion. (A) 50 µM ODQ was administrated only during reperfusion to ISO+I/R hearts (◆). (B) 10 µM L-NAME was perfused during the stabilization period and post-conditioning (◇). It is also shown heart function from control ISO hearts (■) and ISO+I/R+PC hearts (▲), $n=4$.

ODQ (Fig. 7A), whereas treatment with L-NAME, completely inhibited the protective effect of post-conditioning. Although a correlation between low cGMP levels during reperfusion and total abolition of PC-cardioprotection in rat hearts treated with ODQ has previously reported, here we observed that ODQ did not abolish the protective effect of PC, using the same concentration and administration scheme. Besides, perfusion of the NO donor (DETA-NO) to hearts in which GC was previously inhibited, restored partially PC-conferred cardioprotection, suggesting that NO may exert protection independently of cGMP. In this regard, and while the present manuscript was in preparation, it was reported that in ischemic preconditioning (IPC) the protective NO effect, rather to be related with GS/cGMP/PKC signaling pathway, was driven through S-nitrosylation signaling (Sun et al., 2013). As it is known that both PC and ischemic pre-conditioning (IPC) recruit similar signaling pathways, it is tempting to speculate that in ISO-hearts, NO cardioprotective mechanisms may include protein S-nitrosylation (Haosenloy and Yellon, 2009).

In this work we also showed that the antioxidant machinery is preserved providing a mean to keep the balance between NO and ROS generation in post-conditioned ISO hearts. In this sense, we and others have previously demonstrated a close dependence between mitochondrial integrity and oxidative stress diminution in healthy post-conditioned hearts (Hermann et al., 2012; Correa

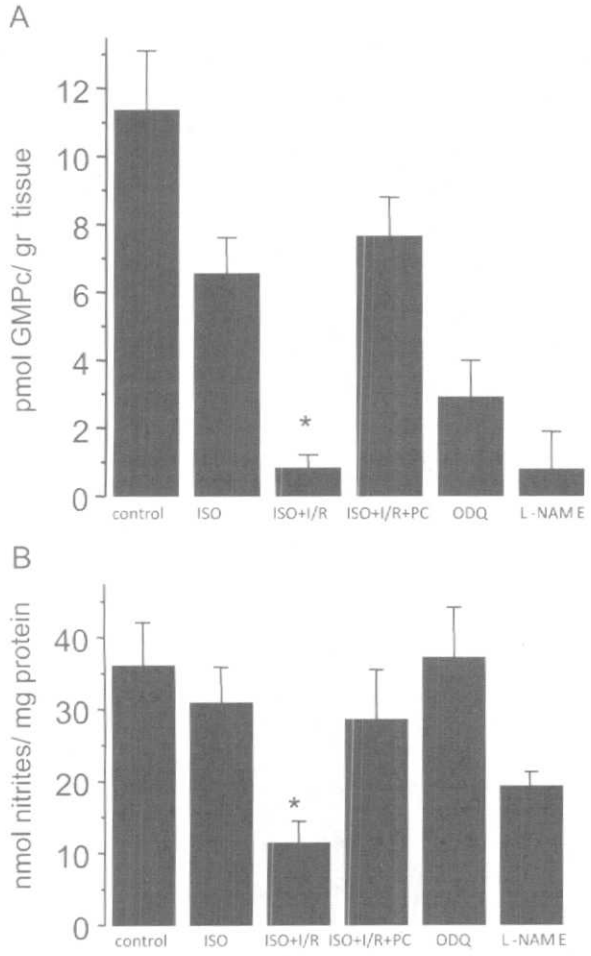

Fig. 9. Post-conditioning effect in cGMP and NO content in ISO hearts. Mean ± SD of cGMP (A) and NO (B) levels measured at the end of the reperfusion, $n=5$. $^{*}P \leq 0.05$ vs. control, ISO, ISO+I/R+PC.

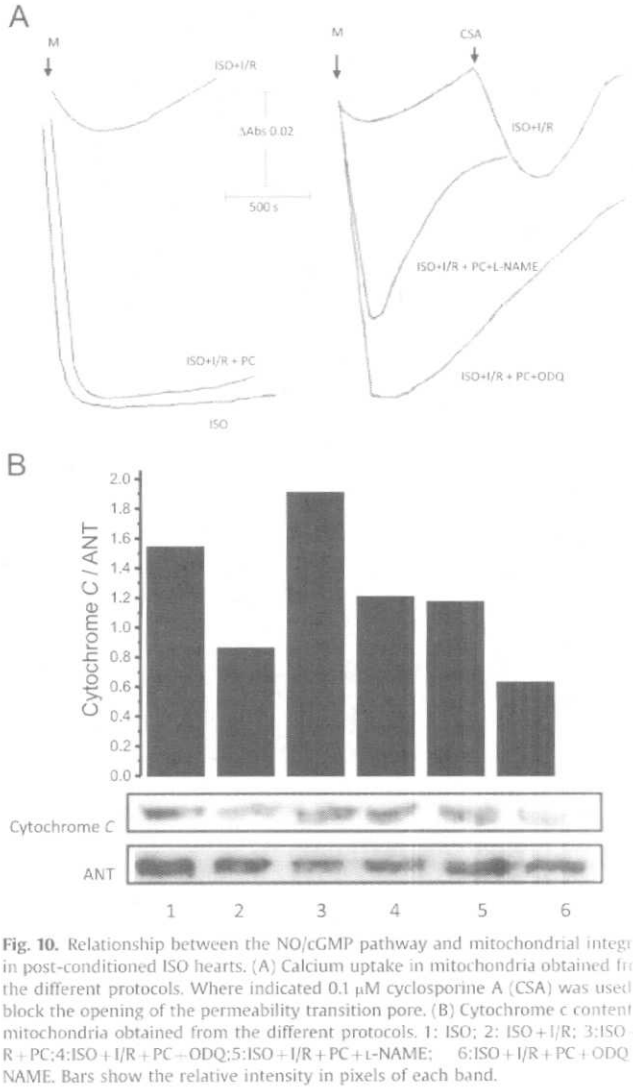

Fig. 10. Relationship between the NO/cGMP pathway and mitochondrial integrity in post-conditioned ISO hearts. (A) Calcium uptake in mitochondria obtained from the different protocols. Where indicated 0.1 μM cyclosporine A (CSA) was used to block the opening of the permeability transition pore. (B) Cytochrome c content in mitochondria obtained from the different protocols. 1: ISO; 2: ISO+I/R; 3:ISO+I/R+PC;4:ISO+I/R+PC+ODQ;5:ISO+I/R+PC+L-NAME; 6:ISO+I/R+PC+ODQ+L-NAME. Bars show the relative intensity in pixels of each band.

et al., 2008 and Serviddio et al., 2005). In fact, it has been reported that ROS and high intramitochondrial Ca^{2+} may act together to trigger the mitochondrial permeability transition (mPTP) (Duchen, 2000; Doran and Halestrap, 2000; Crompton, 1999). The mPTP is a non-specific mega channel that induces depolarization of the mitochondrial inner membrane leading to ATP depletion and enhancing colloidal osmotic pressure in the mitochondrial matrix, producing matrix swelling and rupture of the mitochondrial outer membrane (Hernández-Reséndiz et al., 2013). The mechanism by which PC inhibits mPTP opening has been suggested to occur through the activation of protein kinases, such as Akt, GSK-3β (Jabůrek et al., 2006; Juhaszova et al., 2004), which are downstream kinases of eNOS. Some reports proposed that PC prevents mPTP opening at the start of reperfusion by reducing ROS levels and oxidative stress diminution, possibly mediated by PKC. However, the mechanism by which this is achieved remains to be elucidated.

On the other hand, it has been reported that high NO concentration favors the opening of the mPTP, whereas physiological NO levels favors mPTP closure (Davidson and Duchen, 2006; Brookes et al., 2000). High NO concentrations may induce mPTP opening by disulfide bonds formation and through the oxidizing effect of peroxynitrite; whereas physiological NO concentration may inhibit the mPT by S-nitrosylation-related mechanisms (Ohtani et al., 2012). The mPTP induces mitochondrial swelling and membrane depolarization and provides a mechanism for cytochrome c release, a hallmark signal protein of mitochondrial apoptosis pathway (Correa et al., 2007). In this sense, we observed that cytochrome c content was regulated by both L-NAME and ODQ in post-conditioned ISO hearts; therefore NO might reduce necrosis and apoptosis by preventing mPTP opening.

We acknowledge that the model used in this work has some limitations, as it does not reflect common clinical myocardial infarction (MI) in patients. However the pathophysiological and morphological changes that take place in rat's heart following MI induced by ISO are comparable to the change that takes place in human MI.

Our results show that post-conditioning may be an effective strategy to reduce reperfusion injury in hearts with previous infarct-like damage and, that such protection is sustained by cGMP-dependent and cGMP-independent pathways, that maintained mitochondrial structure and function.

5. Conclusion

Post-conditioning exerts cardioprotection in hearts with previous infarct by maintaining mitochondrial structure and function through NO-dependant pathways.

Competing Interest

The authors declare that there is no conflict of interests regarding the publication of this paper.

Acknowledgments

This work was partially supported by Grant 181593 and 090742 to FC and 177525 to CZ from the National Council of Science and Technology (CONACyT, Mexico).

Appendix A. Supplementary material

Supplementary data associated with this article can be found in the online version at http://dx.doi.org/10.1016/j.ejphar.2015.09.018.

References

Brookes, P.S., Salinas, E.P., Darley-Usmar, K., Eiserich, J.P., Freeman, B.A., Darley-Usmar, V.M., Anderson, P.G., 2000. Concentration-dependent effects of nitric oxide on mitochondrial permeability transition and cytochrome c release. J. Biol. Chem. 275, 20474–20479.

Chagoya de Sánchez, V., Hernández-Muñoz, R., López-Barrera, F., Yañez, L., Vidrio, S., Suárez, J., Cota-Garza, M.D., Aranda-Fraustro, A., Cruz, D., 1997. Sequential changes of energy metabolism and mitochondrial function in myocardial infarction induced by isoproterenol in rats: a long-term and integrative study. Can. J. Physiol. Pharmacol. 75 (12), 1300–1311.

Chien, K.R., Abrams, J., Serroni, A., Martin, J.T., Farber, J.L., 1978. Accelerated phospholipid degradation and associated membrane dysfunction in irreversible, ischemic liver cell injury. J. Biol. Chem. 253, 4809–4817.

Correa, F., García, N., Robles, C., Martínez-Abundis, E., Zazueta, C., 2008. Relationship between oxidative stress and mitochondrial function in the post-conditioned heart. J. Bioenerg. Biomembr. 40 (6), 599–606.

Correa, F., Soto, V., Zazueta, C., 2007. Mitochondrial permeability transition relevance for apoptotic triggering in the post-ischemic heart. Int. J. Biochem. Cell Biol. 39 (4), 787–798.

Costa, A.D., Pierre, S.V., Cohen, M.V., Downey, J.M., Garlid, K.D., 2008. cGMP signalling in pre- and post-conditioning: the role of mitochondria. Cardiovasc. Res. 77 (2), 344–352.

Costa, V.M., Carvalho, F., Bastos, M.L., Carvalho, R.A., Carvalho, M., Remião, F., 2011. Contribution of catecholamine reactive intermediates and oxidative stress to the pathologic features of heart diseases. Curr. Med. Chem. 18 (15), 2272–2314.

Crompton, M., 1999. The mitochondrial permeability transition pore and its role in cell death. Effects of the AMP-activated protein kinase inhibitor compound C on the postconditioned rat heart. Biochem. J. 341, 233–249.

Davidson, S.M., Duchen, M.R., 2006. Effects of NO on mitochondrial function in cardiomyocytes: Pathophysiological relevance. Cardiovasc. Res. 71, 10–21.

de Velasco, J., Cosín, J., López Sendón, J.L., de Teresa, E., de Oya, M., Carrasco, J.L., Navarro, A., 1997. La prevención secundaria del infarto de miocardio en España. Estudio PREVESE. Rev. Esp. Cardiol. 50, 406–415.

Díaz-Muñoz, M., Alvarez-Pérez, M.A., Yáñez, L., Vidrio, S., Martínez, L., Rosas, G., Yáñez, M., Ramirez, S., de Sánchez, V.C., 2006. Correlation between oxidative stress and alteration of intracellular calcium handling in isoproterenol-induced myocardial infarction. Mol. Cell. Biochem. 289 (1–2), 125–136.

Doran, E., Halestrap, A.P., 2000. Cytochrome c release from isolated rat liver mitochondria can occur independently of outer-membrane rupture: possible role of contact sites. Biochem. J. 348, 343–350.

Duchen, M.R., 2000. Mitochondria and Ca^{2+} in cell physiology and pathophysiology. Cell Calcium 28, 339–348.

Fernández-Checa, J.C., Kaplowitz, N., 1990. The use of monochlorobimane to determine hepatic GSH levels and synthesis. Anal. Biochem. 190, 212–219.

Hausenloy, D.J., Yellon, D.M., 2009. Preconditioning and postconditioning: underlying mechanisms and clinical application. Atherosclerosis. 204 (2), 334–341.

Hausladen, A., Fridovich, I., 1994. Superoxide and peroxynitrite inactive aconitine, but nitric oxide does not. J. Biol. Chem. 269 (47), 29405–29408.

Hermann, R., Marina Prendes, M.G., Torresin, M.E., Vélez, D., Savino, E.A., Varela, A., 2012. Effects of the AMP-activated protein kinase inhibitor compound C on the postconditioning rat heart. J. Physiol. Sci. 62 (4), 333–341.

Hernández-Reséndiz, S., Buelna-Chontal, M., Correa, F., Zazueta, C., 2013. Targeting mitochondria for cardiac protection. Curr. Drug Targets 14 (5), 586–600.

Jabůrek, M., Costa, A.D., Burton, J.R., Costa, C.L., Garlid, K.D., 2006. Mitochondrial PKC epsilon and mitochondrial ATP-sensitive K^{+} channel copurify and coreconstitute to form a functioning signaling module in proteoliposomes. Circ. Res. 99 (8), 878–883.

Juhaszova, M., Zorov, D.B., Kim, S.H., Pepe, S., Fu, Q., Fishbein, K.W., Ziman, B.D., Wang, S., Ytrehus, K., Antos, C.L., Olson, E.N., Sollott, S.J., 2004. Glycogen synthase kinase-3 beta mediates convergence of protection signaling to inhibit the mitochondrial permeability transition pore. J. Clin. Investig. 113, 1535–1549.

Kannan, M.M., Quine, S.D., 2011a. Pharmacodynamics of ellagic acid on cardiac troponin-T, lyosomal enzymes and membrane bound ATPases: mechanistic clues from biochemical, cytokine and in vitro studies. Chem. Biol. Interact. 193 (2), 154–161.

Kannan, M.M., Quine, S.D., 2011b. Ellagic acid ameliorates isoproterenol induced oxidative stress: evidence from electrocardiological, biochemical and histological study. Eur. J. Pharmacol. 659 (1), 45–52.

Kannan, M.M., Quine, D.S., 2013. Ellagic acid inhibits cardiac arrhythmias, hypertrophy and hyperlipidaemia during myocardial infarction in rats. Metabolism 62, 52–61.

Kumbhani, D.J., Wells, B.J., Lincoff, A.M., Jain, A., Arrigain, S., Yu, C., Goormastic, M., Ellis, S.G., Blackstone, E., Kattan, M.W., 2013. Predictive models for short- and long-term adverse outcomes following discharge in a contemporary population with acute coronary syndromes. Am. J. Cardiovasc. Dis. 3 (1), 39–52.

Lowry, O.H., Rosenbrough, N.J., Farr, A.L., Randall, L.J., 1951. Protein measurement with the folin phenol reagent. J. Biol. Chem. 193, 265–275.

Muñoz, R.M., Vargas, F., Bobadilla, N.A., 2003. Valoración de un método para determinar nitritos y nitratos en muestras biológicas. Rev. Invest. Clin. 55 (6), 670–676.

Ohtani, H., Katoh, H., Tanaka, T., Saotome, M., Urushida, T., Satoh, H., Hayashi, H., 2012. Effects of nitric oxide on mitochondrial permeability transition pore and thiol-mediated responses in cardiac myocytes. Nitric Oxide 26 (2), 95–101.

Pedraza-Chaverri, J., Granados-Silvestre, M.D., Medina-Campos, O.N., Hernandez-Pando, R., 1999. Effect of the in vivo catalase inhibition on aminonucleoside nephrosis. Free Radic. Biol. Med. 27, 245–253.

Penna, C., Cappello, S., Mancardi, D., Raimondo, S., Rastaldo, R., Gattullo, D., Losano, G., Pagliaro, P., 2006. Post-conditioning reduces infarct size in the isolated rat heart: role of coronary flow and pressure and the nitric oxide/cGMP pathway. Basic Res. Cardiol. 101 (2), 168–179.

Prabhu, S., Jainu, M., Sabitha, K.E., Devi, C.S., 2006. Role of mangiferin on biochemical alterations and antioxidant status in isoproterenol-induced myocardial infarction in rats. J. Ethnopharmacol. 107, 126–133.

Remondino, A., Kwon, S.H., Communal, C., Pimentel, D.R., Sawyer, D.B., Singh, K., Colucci, W.S., 2003. Beta-adrenergic receptor-stimulated apoptosis in cardiac myocytes is mediated by reactive oxygen species/c-Jun NH2-terminal kinase-dependent activation of the mitochondrial pathway. Circ. Res. 92 (2), 136–138.

Rona, G., Chappel, C.I., Balazs, T., Gaudry, R., 1959. An infarct-like myocardial lesion and other toxic manifestations produced by isoproterenol in the rat. AMA Arch. Pathol. 67 (4), 443–455.

Serviddio, G., Di Venosa, N., Federici, A., D'Agostino, D., Rollo, T., Prigigallo, F., Altomare, E., Fiore, T., Vendemiale, G., 2005. Brief hypoxia before normoxic reperfusion (postconditioning) protects the heart against ischemia-reperfusion injury by preventing mitochondria peroxyde production and glutathione depletion. FASEB J. 19 (3), 354–361.

Stelzner, T.J., Welsh, C.H., Berger, E., McCullough, R.G., Morris, K., Repine, J.E., Weil, J. V., 1987. Antiarrhythmic agents diminish thiourea-induced pulmonary vascular protein leak in rats. J. Appl. Physiol. 63, 1877–1883.

Sun, J., Aponte, A.M., Kohr, M.J., Tong, G., Steenbergen, C., Murphy, E., 2013. Essential role of nitric oxide in acute ischemic preconditioning: S nitros(yl)ation versus sGC/cGMP/PKG signaling? Free Radic. Biol. Med. 54, 105–112.

Sushamakumari, S., Jayadeep, A., Kumar, J.S., Menon, V.P., 1989. Effect of carnitine on malondialdehyde, taurine and glutathione levels in heart of rats subjected to myocardial stress by isoproterenol. Indian J. Exp. Biol. 27, 134–137.

Tappia, P.S., Hata, T., Hozaima, L., Sandhu, M., Panagia, V., Dhalla, N.S., 2001. Role of oxidative stress in catecholamine-induced changes in cardiac sarcolemmal Ca2+ transport. Arch. Biochem. Biophys. 387, 85–92.

Todd, G.L., Cullan, G.E., Cullan, G.M., 1980. Isoproterenol-induced myocardial necrosis and membrane permeability alterations in the isolated perfused rabbit heart. Exp. Mol. Pathol. 33, 43–54.

Whalen, E.J., Lewis, S.J., 1999. In vivo evidence that isoproterenol may increase heart rate in the rat by mechanisms in addition to activation of cardiac beta(1)- or beta(2)-adrenoceptors. Eur. J. Pharmacol. 382, 207–210.

Yang, X.-M., Proctor, J.B., Cui, L., Krieg, T., Downey, J.M., Cohen, M.V., 2004. Multiple, brief coronary occlusions during early reperfusion protect rabbit hearts by targeting cell signalling pathways. J. Am. Coll. Cardiol. 44 (5), 1103–1110.

Yang, X.M., Philipp, S., Downey, J.M., Cohen, M.V., 2005. Postconditioning's protection is not dependent on circulating blood factors or cells but involves adenosine receptors and requires PI3-kinase and guanylyl cyclase activation. Basic Res. Cardiol. 100, 57–63.

Zhao, Z.Q., Corvera, J.S., Halkos, M.E., Kerendi, F., Wang, N.P., Guyton, R.A., Vinten-Johansen, J., 2003. Inhibition of myocardial injury by ischemic postconditioning during reperfusion: comparison with ischemic preconditioning. Am. J. Physiol. Heart Circ. Physiol. 285, H579–H588.

Hindawi Publishing Corporation
Evidence-Based Complementary and Alternative Medicine
Volume 2015, Article ID 917435, 16 pages
http://dx.doi.org/10.1155/2015/917435

Research Article

Curcumin Attenuates Gentamicin-Induced Kidney Mitochondrial Alterations: Possible Role of a Mitochondrial Biogenesis Mechanism

Mario Negrette-Guzmán,[1] Wylly Ramsés García-Niño,[2] Edilia Tapia,[3] Cecilia Zazueta,[2] Sara Huerta-Yepez,[4] Juan Carlos León-Contreras,[5] Rogelio Hernández-Pando,[5] Omar Emiliano Aparicio-Trejo,[1] Magdalena Madero,[6] and José Pedraza-Chaverri[1]

[1]*Departamento de Biología, Facultad de Química, UNAM, 04510 Ciudad de México, DF, Mexico*
[2]*Departamento de Biomedicina Cardiovascular, Instituto Nacional de Cardiología "Ignacio Chávez", 14080 Ciudad de México, DF, Mexico*
[3]*Laboratorio de Fisiopatología Renal, Instituto Nacional de Cardiología "Ignacio Chávez", 14080 Ciudad de México, DF, Mexico*
[4]*Unidad de Investigación en Enfermedades Oncológicas, Hospital Infantil de México "Federico Gómez", 06720 Ciudad de México, DF, Mexico*
[5]*Departamento de Patología, Instituto Nacional de Ciencias Médicas y Nutrición "Salvador Zubirán", 14000 Ciudad de México, DF, Mexico*
[6]*Departamento de Nefrología, Instituto Nacional de Cardiología "Ignacio Chávez", 14080 Ciudad de México, DF, Mexico*

Correspondence should be addressed to José Pedraza-Chaverri; pedraza@unam.mx

Received 7 May 2015; Revised 3 July 2015; Accepted 15 July 2015

Academic Editor: Jian-Li Gao

It has been shown that curcumin (CUR), a polyphenol derived from *Curcuma longa*, exerts a protective effect against gentamicin- (GM-) induced nephrotoxicity in rats, associated with a preservation of the antioxidant status. Although mitochondrial dysfunction is a hallmark in the GM-induced renal injury, the role of CUR in mitochondrial protection has not been studied. In this work, LLC-PK1 cells were preincubated 24 h with CUR and then coincubated 48 h with CUR and 8 mM GM. Treatment with CUR attenuated GM-induced drop in cell viability and led to an increase in nuclear factor (erythroid-2)-related factor 2 (Nrf2) nuclear accumulation and peroxisome proliferator-activated receptor gamma coactivator-1 alpha (PGC-1α) cell expression attenuating GM-induced losses in these proteins. *In vivo*, Wistar rats were injected subcutaneously with GM (75 mg/Kg/12 h) during 7 days to develop kidney mitochondrial alterations. CUR (400 mg/Kg/day) was administered orally 5 days before and during the GM exposure. The GM-induced mitochondrial alterations in ultrastructure and bioenergetics as well as decrease in activities of respiratory complexes I and IV and induction of calcium-dependent permeability transition were mostly attenuated by CUR. Protection of CUR against GM-induced nephrotoxicity could be in part mediated by maintenance of mitochondrial functions and biogenesis with some participation of the nuclear factor Nrf2.

1. Introduction

Curcumin (CUR) is the most active compound in *Curcuma longa* (turmeric or curcuma), an herbaceous plant popularly used as a culinary spice and traditional remedy. Chemically, curcumin is a bis-α, β-unsaturated β-diketone that also features two methoxy groups, two phenolic hydroxyl groups, and two double-conjugated bonds that play important roles in its well-known physiological benefits [1]. Among its reported biological properties, curcumin includes anticarcinogenic [2, 3], anti-inflammatory [4], antimicrobial [5], antiatherosclerotic [6], and antifibrotic [7] effects. Most of the anti-inflammatory and cytoprotective reports have been linked to the antioxidant activity of curcumin, which is a bifunctional antioxidant [8]. On one hand, curcumin can react directly with reactive oxygen species (ROS) thanks to

the phenolic groups in its structure. On the other hand, curcumin is able to induce an upregulation of various cytoprotective and antioxidant proteins by activation of nuclear factor (erythroid-2)-related factor 2 (Nrf2), a master regulator of the cell antioxidant response [1, 9].

As was documented by our group and others, curcumin protective properties against different kinds of damage models in several tissues might be also mediated by mechanisms that involve preservation in mitochondrial integrity and functions [10]. Indeed, fails in heart performance induced by cardiac reperfusion [11] and 5/6-nephrectomy in rats [12] were improved with curcumin treatment in correlation with attenuated oxidative stress, recovery of antioxidant enzymes activities, and preservation of the respiratory capacity in isolated mitochondria. In addition, cardiotoxicity induced by catecholamine [13] and anoxia-reoxygenation in rats [14] was attenuated by curcumin-mediated inhibition of the mitochondrial permeability transition (MPT) pore and preserving energy production, respectively. In rat kidney and liver, hexavalent chromium-induced injury was attenuated through maintenance of bioenergetic status, calcium retention capacity, and activity of the respiratory complexes [15, 16]. Pretreatment with curcumin rendered similar results in a rat model of indomethacin-induced enteropathy [17]. Interestingly, Kuo et al. [18] and Liu et al. [19] found that the curcumin treatment normalized the mitochondrial biogenesis altered in a liver steatosis obese mice model and a cerebral ischemia reperfusion rat model, respectively, as markers like nuclear respiratory factor 1 (NRF1) and mitochondrial transcription factor A (Tfam) were preserved after the treatment.

Renal protection by curcumin has been well established [1]. There are numerous animal trials that showed nephroprotection by curcumin in some common health complications and in exposures to drugs and chemicals. For its clinical relevance, the protective effect of curcumin against gentamicin- (GM-) induced renal injury is highlighted [20, 21]. Nephrotoxicity is one of the main side effects of this aminoglycoside antibiotic and occurs in 10%–20% of therapeutic regimes. GM is one of the best known nephrotoxic drugs and its association with mitochondrial dysfunction in proximal tubules has been well studied [22]. Mitochondrial membrane potential disruption [23], oxygen consumption anomalies, adenosine triphosphate (ATP) yield decrease, MPT pore formation, mitochondrial cytochrome c release, intrinsic apoptosis, and mitochondrial antioxidant status impairment have been observed both in culture tubular cells and in rat kidneys exposed to GM [23–26]. On the other hand, some reports suggest that curcumin protective effect against GM nephrotoxicity is associated with preservation of the renal antioxidant status and with modulation of the inflammatory response mediated by NF-κB, rather than with protection of renal mitochondrial function [20, 21, 27].

In the present work, we investigate the unexplored effect of curcumin treatment on alterations induced by GM in renal mitochondria in both cells and rats. Because inducers of nuclear translocation of Nrf2 like curcumin have been proposed as inducers of mitochondrial biogenesis [28], we evaluated Nrf2 and peroxisome proliferator-activated receptor gamma coactivator-1 alpha (PGC-1α) expression. PGC-1α is a central stimulator of mitochondrial biogenesis [29]. Ultrastructural mitochondrial changes, bioenergetic status, and respiratory complexes activities as well as calcium-dependent MPT pore opening were also evaluated. Our results evidence that the protective effect of CUR against GM-induced renal injury and dysfunction could be mediated by maintenance of kidney mitochondrial biogenesis, structure, and functions.

2. Materials and Methods

2.1. Chemicals and Reagents. CUR (Cat. no. C1386, batch 081M1611V), 3-(4,5-dimethylthiazol-2-yl)-2,5-diphenyltetrazolium bromide (MTT), dimethyl sulfoxide (DMSO), glutaraldehyde, sodium cacodylate, osmium tetroxide (OsO_4), paraformaldehyde, bovine serum albumin, potassium succinate, sodium glutamate, sodium malate, adenosine diphosphate (ADP), N-(2-hydroxyethyl)piperazine-N′-(2-ethanesulfonic acid) (HEPES), rotenone, carbonyl cyanide m-chlorophenylhydrazone (CCCP), decylubiquinone, nicotinamide adenine dinucleotide reduced form (NADH), potassium cyanide (KCN), antimycin A, sucrose, phenazine methosulfate (PMS), cytochrome c from equine heart, ascorbic acid, tetramethyl-p-phenylenediamine (TMPD), manganese(II) chloride tetrahydrate, safranin O, arsenazo III, cyclosporine A (CsA), 3-(N-morpholino) propane-sulfonic acid (MOPS), and ethylene glycol-bis(2-aminoethylether)-*N,N,N′,N′*-tetraacetic acid (EGTA) were purchased from Sigma-Aldrich (St. Louis, MO, USA). GM (Garamicina G.U. 120 mg/1.5 mL, batches 2DPDA006 and 1DPDA002) was obtained from Schering-Plough (Mexico City, DF, Mexico). Dulbecco's Modified Eagle Medium (DMEM), fetal bovine serum (FBS), trypsin, antibiotic (10,000 U/mL penicillin and 10,000 μg/mL streptomycin), and other tissue culture reagents were purchased from Gibco (Mexico City). Rabbit polyclonal anti-Nrf2 antibody (C-20, Cat. no. sc-722) was obtained from Santa Cruz Biotechnology, Inc. (Santa Cruz, CA, USA). Rabbit polyclonal anti-PGC-1α antibody (Cat. no. ab54481) was purchased from Abcam, Inc. (Cambridge, MA, USA). Normal goat serum blocking solution (S-1000) and Avidin/Biotin Blocking Kit (SP-2001) were obtained from Vector Laboratories, Inc. (Burlingame, CA, USA). Biotinylated Link Universal, Streptavidin-HRP, and 3,3′-diaminobenzidine (DAB) were obtained from Dako (Carpinteria, CA, USA). Potassium chloride (KCl), sodium citrate, dextrose, and ethylenediaminetetraacetic acid disodium salt dihydrate (EDTA) were acquired from J.T. Baker (Xalostoc, Edo. Mex, Mexico). All other reagents and chemicals used were of the highest grade of purity commercially available.

2.2. Cell Culture and Viability. Lily Laboratory Culture Porcine Kidney (LLC-PK1) porcine renal epithelial cells were obtained from American Type Culture Collection (Rockville, MD, USA). This cell line is an accepted model to study toxicity of aminoglycosides [23, 30]. LLC-PK1 cells were maintained in DMEM supplemented with 10% FBS and 1% of antibiotic and cultured under permissive conditions:

37°C and 5% CO_2. In order to evaluate the effect of CUR on GM-induced toxicity, cells were seeded at a density of 3×10^4 cells/cm^2 onto either 96-well or 6-well plates and used for the experiment on the following day. Cells were incubated for 24 h with CUR (10–30 μM) or medium before the GM addition. At the end of preincubation period, CUR or culture medium was replaced by fresh CUR or medium, adding 8 mM GM to some cell groups in order to induce toxicity. CUR treatment and GM exposure were maintained for 48 h by replacing the first medium with fresh medium at 24 h. Cell viability was assessed by MTT reduction. At the end of 72 h of experiment, medium was removed and cells were washed twice with phosphate-buffered saline (PBS) pH 7.4. In 96-well plates, cells were incubated in medium containing MTT (0.125 mg/mL) at 37°C for 1 h in humidified air supplemented with 5% CO_2. Medium was then discarded and the formazan crystals deposited in each well bottom were dissolved in 100 μL of 0.1 N HCl in isopropanol. Absorbance was determined at 570 nm using an EnSpire multimode plate reader (PerkinElmer Inc., Waltham, MA, USA). Cells incubated in 6-well plates were trypsinized and resuspended in PBS at a proportion of 20 000 cells/10 μL. Spots of 20 000 cells were seeded on slides, left drying at room temperature, fixed in 4% formaldehyde at 4°C, and washed three times in PBS for posterior immunocytochemical analysis.

2.3. Immunocytochemistry. Immunocytochemical staining for Nrf2 and PGC-1α was performed in LLC-PK1 cells fixed with formaldehyde pH 7.4 on slides. Antigens were recuperated by boiling for 20 min in 0.01% sodium citrate solution, pH 6.0. Background staining was reduced by blocking with 3% H_2O_2 solution in methanol for 30 minutes, incubation in a 2% solution of normal goat serum in PBS (PBS-NGS) for 2 hours, and treatment with avidin and biotin for 10 min each. Slides were incubated overnight at room temperature with anti-Nrf2 (1 : 100) and anti-PGC-1α (1 : 250) primary antibodies. The following day, slides were washed five times for 5 min in PBS 1X pH 7.4. After washing, slides were incubated for 30 min at room temperature with universal biotinylated link and for 30 min at room temperature with streptavidin conjugated to HRP. For color developing, DAB was used from 1 to 5 min. The reaction was stopped with distilled water and the slides were counterstained with hematoxylin. Finally, cells were dehydrated and fixed with Mount E-2 medium (Shandon Laboratory, Pittsburgh, PA, USA). Slides were analyzed under a microscope Olympus BX40 and immunopositive cells were quantified by simple counting.

2.4. Animals. Male Wistar rats with an initial body weight of 200–220 g were used. Animals were maintained under 12-h light/dark cycles at controlled temperature, having *ad libitum* access to water and standard food. Local Committee for the Care and Use of Laboratory Animals approved this experimental study (FQ/CICUAL/038/12), which was conducted according to the guidelines of Mexican Official Norm Guide for the use and care of laboratory animals (NOM-062-ZOO-1999) and for the disposal of biological residues (NOM-087-SEMARNAT-SSA1-2002).

2.5. Experimental Design. Animals were randomly divided into four groups: (i) control group (CT) was injected subcutaneously (s.c.) with isotonic saline solution (ISS, vehicle for GM) every 12 h for 7 days and administered with carboxymethyl cellulose (vehicle of CUR) by oral gavage once a day during five days previous to any ISS injection and between the daily ISS injections. (ii) Gentamicin group (GM) was administered s.c. with GM at a dose of 75 mg/Kg/12 h [31] and carboxymethyl cellulose was given like in CT group. (iii) CUR + GM group was injected with GM as in the GM group but received oral CUR (400 mg/Kg) in carboxymethyl cellulose [15] 5 days before GM exposure and between the two daily GM injections (14 doses). (iv) CUR group was administered s.c. with ISS during 7 days and with CUR during 12 days. On the thirteenth day of treatment, rats were euthanized by anesthetization with sodium pentobarbital (60 mg/Kg) and bled via abdominal aorta using a syringe containing heparin and a needle #18 at room temperature. Plasma was separated and stored at −20°C until the markers of renal damage, plasma creatinine, and blood urea nitrogen (BUN) were measured.

2.6. Analytical Methods. Creatinine and BUN in plasma were determined by spectrophotometric assays using commercial Spinreact kits as previously reported [23]. Creatinine determination in plasma is based on the reaction of this compound with sodium picrate forming a red complex whose intensity is proportional to the creatinine concentration. However, urea present in the plasma reacts with o-phthalaldehyde forming a colored complex which is quantified at 510 nm.

2.7. Ultrastructural Study. To study the mitochondrial ultrastructural morphology, immediately after animal sacrifice, thin kidney tissue slices were obtained and immersed into 4% glutaraldehyde dissolved in 1 mM cacodylate buffer pH 7.2. Then, the kidney cortex was selected and sectioned in small tissue fragments that were deposited into glass tubes and fixed by immersion in the same solution during 24 hr at 4°C. Then, tissue fragments were postfixed with 2% OsO_4 buffer, dehydrated in graded ethyl alcohol solutions, and embedded in Epon Resin (London Resin Company, London, UK). Thin sections from 70 to 90 nm were placed on cooper grids, contrasted with lead and uranium salts, and examined with a FEI Tecnai G2 Spirit transmission electron microscope (Hillsboro, OR, USA).

2.8. Mitochondria Isolation. Kidneys were quickly removed and maintained in cold isolation buffer (250 mM sucrose, 10 mM HEPES, 1 mM EGTA, pH 7.3). The renal cortex was separated and utilized for mitochondria isolation. Tissue was ground and then homogenized in a Glass/Teflon Potter Elvehjem homogenizer in the same buffer. Mitochondria were obtained by differential centrifugation and the protein content was measured by Biuret method [15].

2.9. Mitochondrial Bioenergetics. Oxygen consumption was measured using a Clark type oxygen electrode (Yellow Springs Instruments, Yellow Springs, OH, USA) and two

different respiratory substrates. To evaluate respiration driven by complex I, 1 mg of mitochondrial protein was added to 1.7 mL of basic medium containing 125 mM KCl, 10 mM HEPES, 3 mM inorganic phosphate (Pi), 10 mM sodium malate, and 10 mM sodium glutamate at pH 7.3. Oxygen consumption sustained by complex II was evaluated replacing malate and glutamate with 10 mM succinate plus 1 μg/mL rotenone. State 4 was registered in basic medium, while state 3 respiration was stimulated with ADP (final concentration 200 μM) [32]. Respiratory control index (RCI) was calculated as the ratio state 3/state 4. Uncoupled respiration was obtained by adding 1 μM of CCCP. Phosphorylation efficiency (ADP/O ratio) was calculated from the added amount of ADP and the total amount of oxygen utilized during the developed state 3 [16].

2.10. Activity of Mitochondrial Respiratory Complexes and Aconitase. Effects on mitochondrial enzyme activities were evaluated as previously described [15]. Complex I activity was measured by following the decrease in absorbance due to oxidation of NADH to NAD^+ at 340 nm. The reaction was initiated by adding 60 μM decylubiquinone in 1.7 mL of standard reaction medium (125 mM KCl, 10 mM HEPES, 3 mM inorganic phosphate, pH 7.3) supplemented with 0.1 μg antimycin A, 1 mM KCN, 100 μM NADH, and 0.5 mg of mitochondrial protein. Complex II activity was determined polarographically by recording oxygen consumption. PMS was used as an artificial electron acceptor and succinate as a donor. The reaction was initiated by adding 1 mM PMS in 1.7 mL of standard reaction medium supplemented with 5 mM succinate, 2 μM rotenone, 0.1 μg antimycin A, 1 mM KCN, 1 μM CCCP, and 0.5 mg of mitochondrial protein. Complex III activity was performed by following the increase in absorbance at 550 nm resulting from the reduction of cytochrome c. The assay included oxidized cytochrome c as electron acceptor and decylubiquinol as donor. The reaction was carried out in 2 mL of reaction medium (25 mM K_2HPO_4, 1 mM EDTA, pH 7.6) supplemented with 1 mM KCN, 20 μM cytochrome c, 2 μM rotenone, and 10 μg of mitochondrial protein. The reaction was initiated by the addition of 25 μM decylubiquinol. An extinction coefficient value of 18.7 mM^{-1} cm^{-1} was used for reduced cytochrome c. Complex IV activity was followed polarographically. TMPD was used as an artificial electron mediator that accelerates the transfer of electrons from ascorbate to membrane-bound cytochrome c. The reaction was carried out in 1.7 mL of the standard reaction medium supplemented with 5 mM ascorbic acid, 2 μM rotenone, 1 μM CCCP, 0.5 μg antimycin A, 25 μM cytochrome c, and 2.5 mM TMPD. The reaction was initiated by the addition of 50 μg of mitochondrial protein. The activity of aconitase was assayed by determining the rate of formation of the intermediate product, *cis*-aconitate, from the interconversion of L-citrate and isocitrate at 240 nm. Briefly, the reaction was carried out in 1 mL of reaction medium containing 25 mM KH_2PO_4 + 0.05% Tween, 1 mM sodium citrate, and 0.6 mM $MnCl_2$. The reaction was initiated by the addition of 50 μg of mitochondrial protein. An extinction coefficient for *cis*-aconitate of 3.6 mM^{-1} cm^{-1} was used.

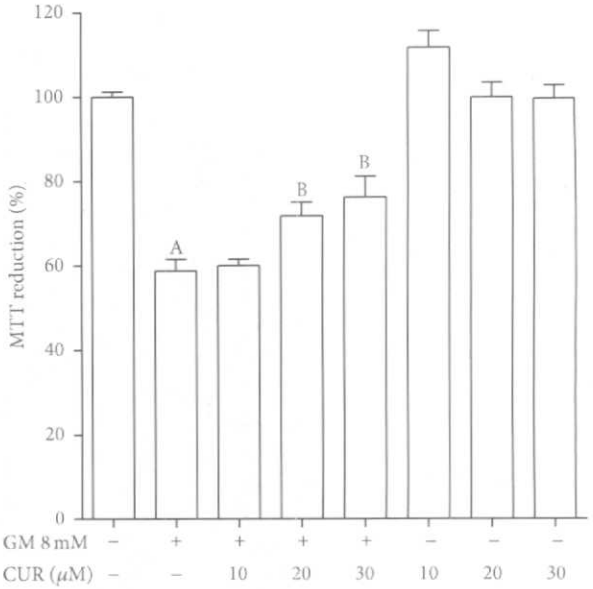

FIGURE 1: CUR attenuates GM-induced cell viability drop in LLC-PK1 cells. Cells were preincubated with 10–30 μM CUR during 24 h and then coincubated with 10–30 μM CUR and 8 mM GM during further 48 h. Viability was measured as percentage of MTT reduction compared to control cells (CT). Data are mean ± SEM, $n = 3$. $^{A}P < 0.001$ versus CT; $^{B}P < 0.05$ versus GM-treated cells.

2.11. Ca^{2+}-Dependent MPT. Effects on the opening of MPT pore induced by Ca^{2+} overload were evaluated in a double-beam spectrophotometer UV-2401 Shimadzu (Kyoto, Japan), as previously described [15]. Ca^{2+} retention capacity was determined monitoring the absorbance changes at 625–675 nm of the dye arsenazo III (60 μM) in 2.8 mL of medium containing 125 mM KCl, 10 mM HEPES, 3 mM Pi, 10 mM succinate, 1.8 μg/mL rotenone, and 200 μM ADP (pH 7.3). Mitochondria (2 mg of mitochondrial protein) were added and then challenged with 100 μM $CaCl_2$. In a similar way, Ca^{2+}-induced membrane potential dissipation was evaluated spectrophotometrically at 525–575 nm using 10 μM safranin O. Both assays were also performed in presence of 1 μM CsA, a known inhibitor of the MPT pore. Depolarization of the membrane potential was induced by CCCP addition at the end of the assays [15].

2.12. Statistics. Results are expressed as mean ± SEM. Data were analyzed by one-way ANOVA followed by Bonferroni's multiple comparisons test using the software Prism 5.0 (GraphPad, San Diego, CA, USA). A P value less than 0.05 was considered statistically significant.

3. Results and Discussion

3.1. Viability of LLC-PK1 Cells. Incubation for 48 h with GM decreased cell viability (expressed as MTT reduction) to 58.8% compared to untreated cells (Figure 1). A cytoprotective effect was observed when LLC-PK1 cells were pre- and coincubated with 20 and 30 μM CUR (viabilities of

71.6% and 76.1%, resp.). Viability of cells only incubated with CUR was not significantly different from control cells. Minor concentrations were assayed but no protection was found. On the other hand, concentrations of 40 and 50 μM were also tested but they were seemingly toxic as viability decreased in cells incubated only with CUR and the protection against GM was not observed (data not shown).

3.2. Nrf2 Nuclear Accumulation and PGC-1α Expression. CUR is a bifunctional antioxidant that induces nuclear accumulation of the factor Nrf2 in LLC-PK1 cells [33]. In order to confirm its role in this cell culture model, we evaluated the nuclear immunoprevalence of Nrf2 at the end of the CUR-GM scheme. After 72 h of 30 μM CUR incubation, nuclear translocation of Nrf2 significantly increases compared to CT cells (Figures 2(a) and 2(d)). Nuclear accumulation is inhibited in GM cells as expression is mainly located in cytoplasm but not in nucleus (Figure 2(b)). Immunopositive nuclei fell from 28.3% in CT cells to 9.8% in GM cells (Figure 2(e)). However, pre- and coincubation with 30 μM CUR in cells exposed to GM (CUR + GM cells) prevented this effect ($P < 0.05$). Hereafter, it could be considered that Nrf2 plays a role in the effects observed.

The coactivator PGC-1α has been well identified as a potent inducer of mitochondrial biogenesis *trans*-activating target genes of nuclear factors like NRF1 and NRF2, involved in the program of respiratory gene expression. Also, PGC-1α induces transcripts of these factors, confirming its important integrative role upstream of biogenic program [29]. In Figures 3(a) and 3(b), it can be noticed that GM induced a strong drop in PGC-1α-expressing cells (from 88.5% in CT to 16.9% in GM). This effect was entirely prevented with the CUR treatment; nevertheless, it seems that CUR does not induce *per se* an increase in cells expressing PGC-1α (Figure 3(e)).

Connection between Nrf2 and mitochondrial biogenesis has been established. It was reported that 5′-UTR for NRF1 contains binding motifs for Nrf2, antioxidant response elements (AREs). Nuclear translocation of Nrf2 was followed by NRF1 induction and mitochondrial biogenesis that enabled rescuing mice from doxorubicin-induced cardiomyopathy and lethal *Staphylococcus aureus* sepsis, effects accompanied by an induction in PGC-1α [34, 35]. The conservation of PGC-1α levels in CUR + GM LLC-PK1 cells could be associated with the curcumin-induced Nrf2 nuclear translocation. This *in vitro* approach could work in involving mitochondrial biogenesis in the following observations *in vivo*.

3.3. Rat Renal Function. Figure 4 shows the protective effect of CUR against GM-induced renal dysfunction in rats. GM induced an 8-fold increase in plasma creatinine level (Figure 4(a)). This notable GM-elicited change was attenuated in the CUR + GM group that showed plasma creatinine values 37% lower than those found in the GM group ($P < 0.05$ versus GM). A similar trend was observed in BUN (Figure 4(b)). An increase about 10-fold above CT value was obtained in the rats injected with GM, which was attenuated by 37% in the CUR + GM rats ($P < 0.05$). Animals administered only with CUR showed no changes in these parameters.

Previous works carried out by Ali et al. [20] and Farombi and Ekor [21] where a different GM administration scheme was used, with daily single doses of 80 mg/Kg intramuscularly during 6 days [20] and 100 mg/Kg intraperitoneally for 7 days [21], showed that creatinine and BUN levels in animals treated with GM increase 2–4.4-fold compared to CT group. Nevertheless, in rats cotreated with GM and CUR, those levels were similar to CT group. In our study, we observed that creatinine and BUN levels were about 10-fold greater in GM group than those observed in the CT animals after daily administration of 150 mg/Kg, which was distributed in two injections, to approach a clinical multidoses system. In this regard, some meta-analysis studies have shown that monodoses system (one daily single dose) correlates with less nephrotoxicity than multidoses system [36]. We choose the administration of a higher GM dose by a multidose system to achieve significant mitochondrial dysfunction and then evaluate the protective effect of curcumin in this condition. Successfully, CUR treatment ameliorates the GM-induced increase on both plasma creatinine and BUN levels in the GM + CUR group in spite of the high toxicity induced for this antibiotic.

3.4. Mitochondrial Ultrastructure. In well agreement with these determinations, the electron microscopy study showed extensive damage in the mitochondrial morphology produced by GM, characterized by effacement of inner membrane (cristae) (Figure 5(b)), while GM + CUR group showed higher number of mitochondria with almost normal structure; just some swollen mitochondria were seen (Figure 5(c)). The mitochondrial ultrastructure of proximal tubules from CT rats (Figure 5(a)) and treated with CUR (Figure 5(d)) was well preserved. In addition, it was observed that CUR treatment increases the number of rounded mitochondria having electron dense matrices and tightly packed cristae (Figures 5(c) and 5(d)).

In this connection, there are several *in vivo* studies on rodents that demonstrate the protective effect of CUR on mitochondrial ultrastructure injury [37–41], in a similar way to our results. Besides, it has been previously confirmed that CUR increases mitochondrial biogenesis [18, 42, 43]. Liu et al. [19] suggested that this mechanism could be responsible for neuroprotection in a model of ischemia/reperfusion on brain. Thus, CUR attenuates GM-induced mitochondrial alterations by a mitochondrial biogenesis mechanism.

3.5. Mitochondrial Bioenergetics. Oxygen consumption profiles of rat renal mitochondria representatives of each experimental group are indicated for the two respiratory substrate conditions, malate/glutamate (Figure 6(a)) and succinate (Figure 6(b)). Oxygen consumption coupled to phosphorylation was reduced in mitochondria obtained from the GM-treated group as compared with CT mitochondria. CCCP stimulated respiratory rates in all conditions except in GM mitochondria oxidizing NADH-linked substrates (Figure 6(a)). At both substrates conditions, it can be graphically noted that the healthy behavior is partially preserved in mitochondria from rats cotreated with CUR and GM.

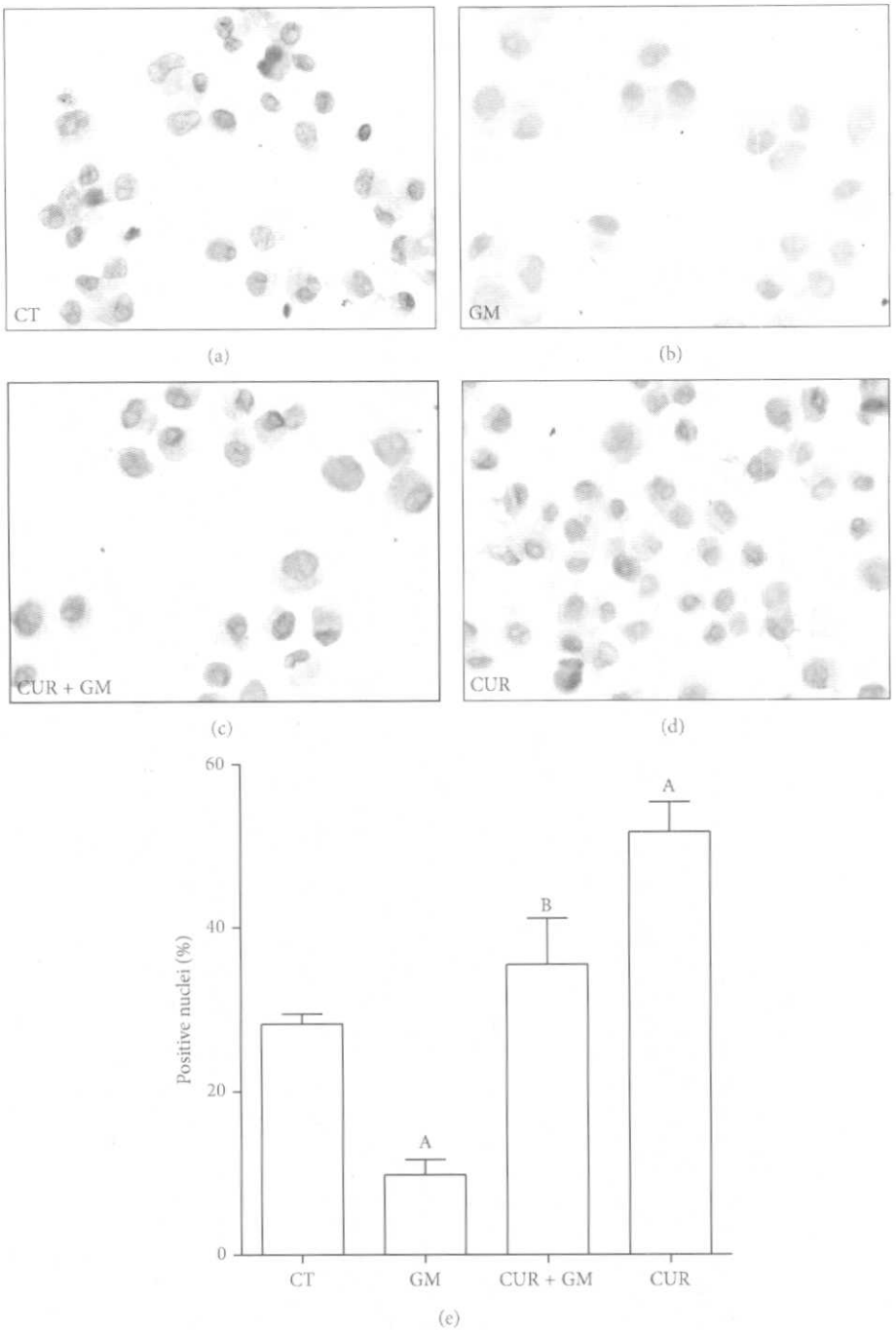

FIGURE 2: CUR induces an increase in nuclear accumulation of Nrf2 and prevented the GM-induced drop in Nrf2 expression and nuclear accumulation in LLC-PK1 cells. Cells were preincubated with 30 μM CUR during 24 h and then coincubated with 30 μM CUR and 8 mM GM during further 48 h. Expression of Nrf2 was detected by immunocytochemical technique. (a) CT. (b) GM. (c) CUR + GM. (d) CUR. (e) Quantification of positive nuclei. Data are mean ± SEM, $n = 3$. $^{A}P < 0.05$ versus CT; $^{B}P < 0.01$ versus GM.

Besides, there were no relevant differences between CUR and CT mitochondria (data not shown).

Outcomes for the major bioenergetics parameters obtained by oxygen consumption measurements are shown in Figure 7 (using malate/glutamate as substrate) and in Figure 8 (using succinate as substrate). State 3 decreased by 30% in mitochondria from rats treated with GM (Figures 7(a) and 8(a), $P < 0.05$ versus CT). ADP-stimulated oxygen consumption was preserved in CUR + GM by 73% in mitochondria supplied with malate/glutamate and around 61% in mitochondria supplied with succinate. Basal respiration was maintained in mitochondria from all groups

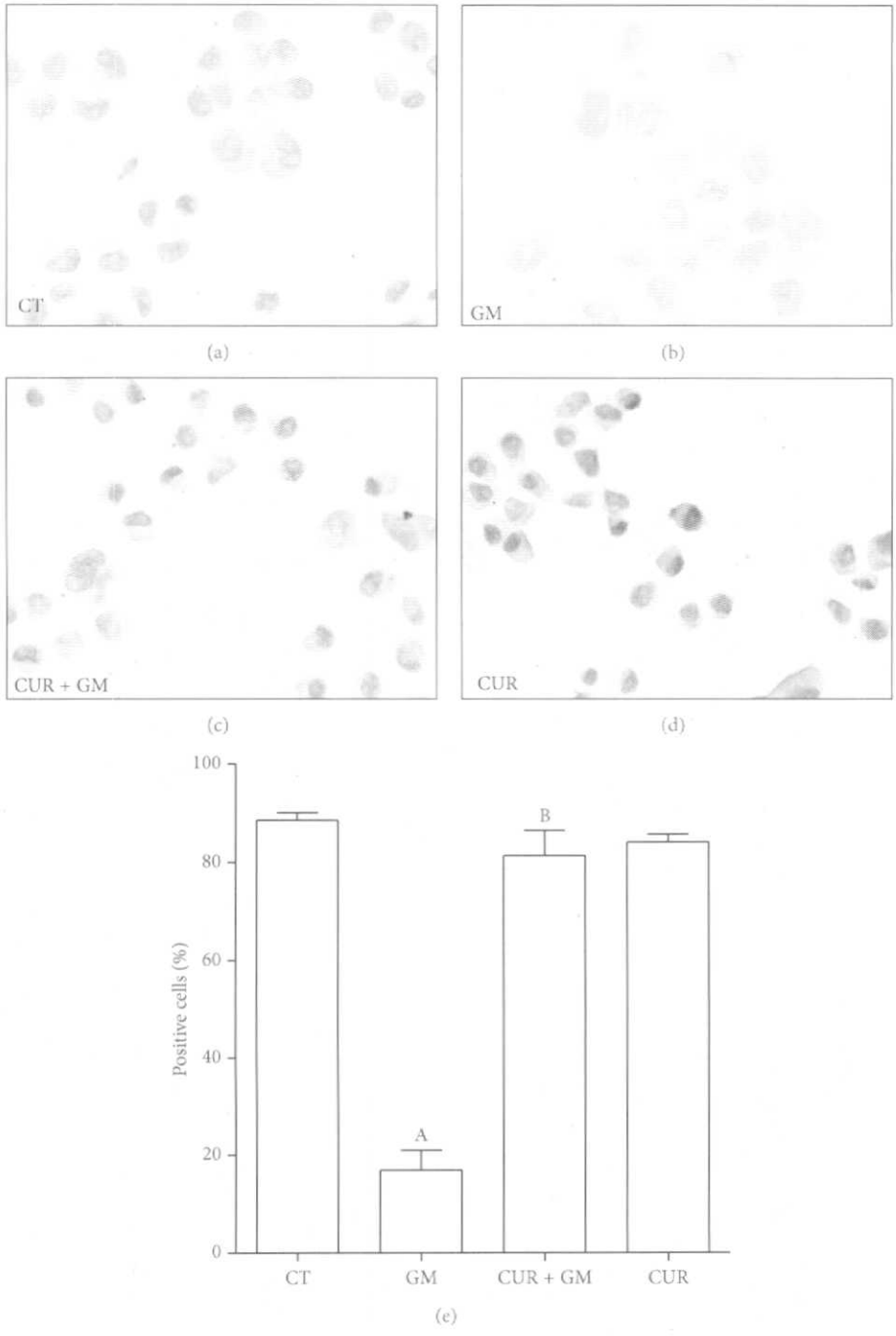

FIGURE 3: CUR prevents GM-induced drop in expression of the coactivator PGC-1α in LLC-PK1 cells. Cells were preincubated with 30 μM CUR during 24 h and then coincubated with 30 μM CUR and 8 mM GM during further 48 h. Expression of PGC-1α was detected by immunocytochemical technique. (a) CT. (b) GM. (c) CUR + GM. (d) CUR. (e) Quantification of positive cells. Data are mean ± SEM, $n = 3$. $^{A}P < 0.001$ versus CT; $^{B}P < 0.001$ versus GM.

fed with malate/glutamate (Figure 7(b)). In contrast, state 4 was lower in mitochondria from the GM group oxidizing succinate. State 4 rates were not completely reestablished in CUR + GM, while similar values of oxygen consumption between CT and CUR were observed under these conditions (Figure 8(b)). However, using either substrate, these values lead to significant differences in the RCI between the GM group and the CT group and between CUR + GM group and GM group. RCI falls from 4.7 in CT mitochondria to 1.4 (30%) in GM mitochondria and was recovered to

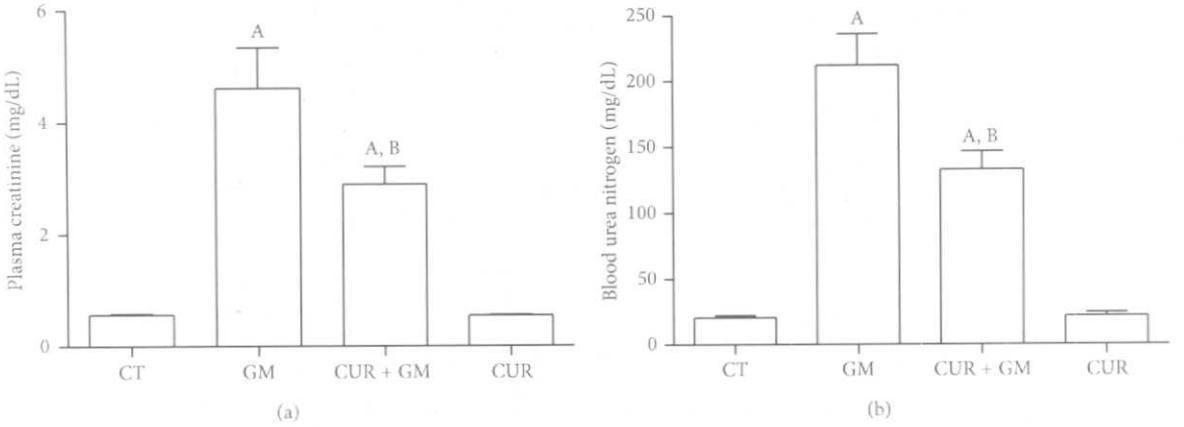

FIGURE 4: CUR ameliorates GM-induced renal dysfunction in rats. (a) Plasma creatinine. (b) Blood urea nitrogen. Data are mean ± SEM, $n = 6$. $^{A}P < 0.01$ versus CT; $^{B}P < 0.05$ versus GM.

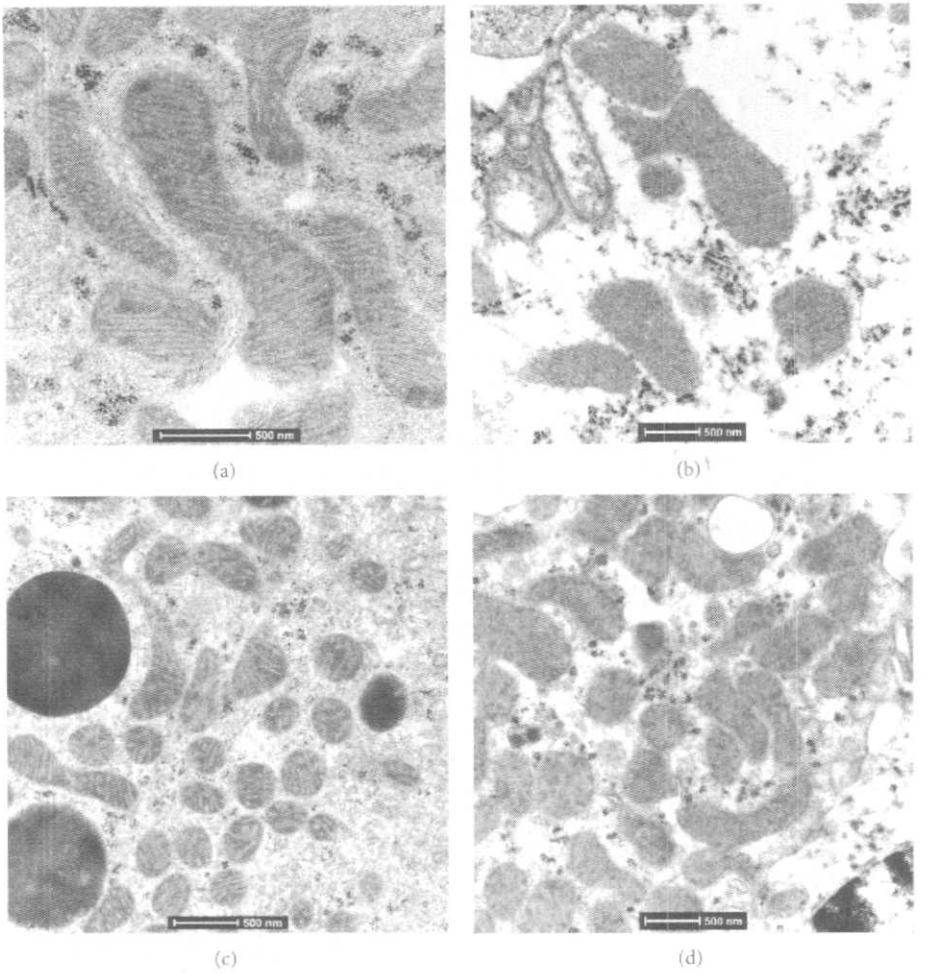

FIGURE 5: Representative micrographs of mitochondrial ultrastructure from convoluted proximal tubules. (a) Normal mitochondria structure in epithelial cell from convoluted proximal tubule from control rat. (b) In contrast, mitochondria show total cristae effacement in an animal treated with GM. (c) Convoluted proximal epithelial cell from a rat treated with CUR + GM shows numerous mitochondria with well-preserved morphology. (d) Similar mitochondrial morphology to CT animal is observed in rat only treated with CUR.

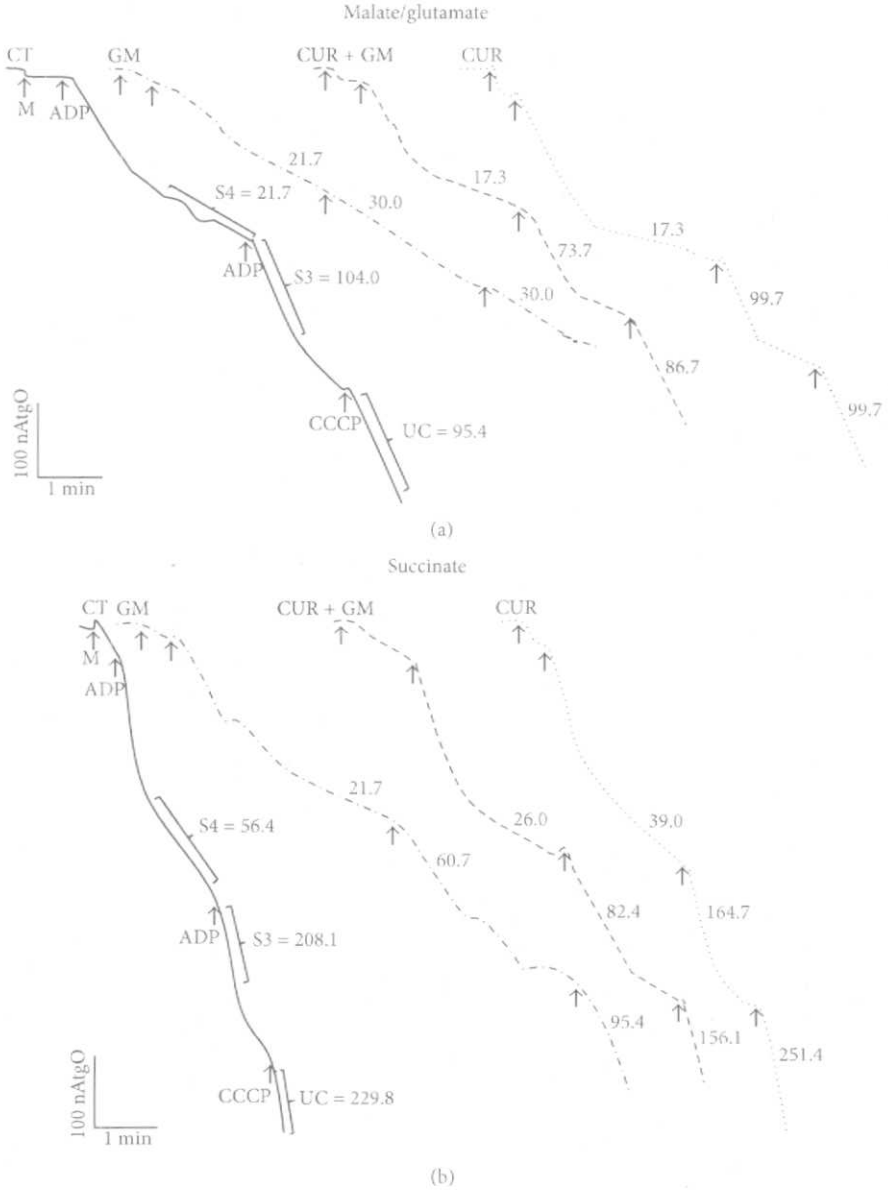

FIGURE 6: Representative tracings for oxygen consumption profiles of renal mitochondria using (a) malate/glutamate or (b) succinate as substrates. Values on tracings belong to punctual observations and are not means. M: mitochondria; ADP: adenosine diphosphate; CCCP: carbonyl cyanide m-chlorophenylhydrazone; S3: state 3; S4: state 4; UC: uncoupled respiration; CT: control; GM: gentamicin; CUR: curcumin. Units of S3, S4, and UC are ngAtO/min/mg protein.

3.8 (81% compared with CT) in CUR + GM mitochondria (Figure 7(c)) with malate/glutamate, whereas RCI of GM group falls to 67% of CT and renal mitochondria from the CUR + GM group reached 86% of untreated rats RCI (Figure 8(c), $P < 0.05$ versus GM) when using succinate.

Uncoupled respiration was lower (24% of CT group) in GM mitochondria oxidizing malate/glutamate (Figure 7(d), $P < 0.05$ versus CT) and such diminution was prevented with curcumin. A similar trend was observed when succinate was supplemented, but the drop was lesser and was slightly attenuated by CUR treatment (Figure 8(d)).

ADP/O ratio in GM mitochondria oxidizing NADH-linked substrates showed lower phosphorylation rates as compared with CT mitochondria. Mitochondria from CUR + GM group recovered phosphorylation rates (Figure 7(e)). On the other hand, ADP/O values were similar in all experimental groups when succinate was the energizing substrate (Figure 8(e)). The CUR group had a behavior similar to that for CT group in all of evaluated bioenergetics parameters.

Oxidative phosphorylation is controlled by the activity of ATP turnover (adenine nucleotide translocase, phosphate

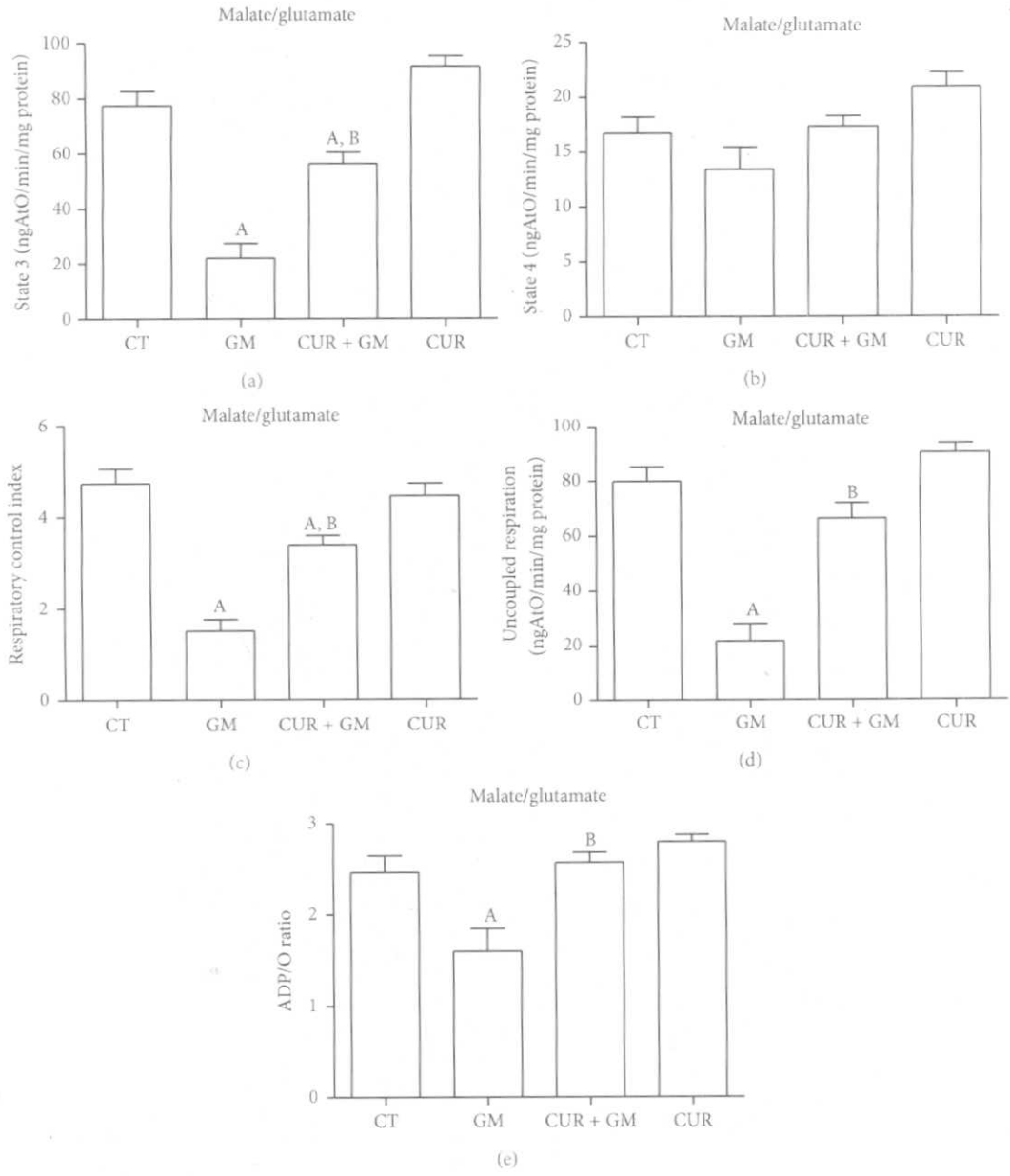

FIGURE 7: CUR attenuates GM-induced alterations in renal mitochondrial site I (malate/glutamate as a respiratory substrate) bioenergetics. (a) State 3. (b) State 4. (c) Respiratory control index. (d) Uncoupled respiration. (e) ADP/O ratio. Data are mean ± SEM, $n = 6$–8. $^{A}P < 0.05$ versus CT; $^{B}P < 0.01$ versus GM.

transporter, and ATP synthase) and substrate oxidation (substrate uptake, processing enzymes, relevant electron-transport chain complexes, pool sizes of ubiquinone and cytochrome c, and O_2 concentration) [44]. Simmons et al. [45] and Weinberg and Humes [46] determined that GM inhibits oxidative phosphorylation in renal cortical mitochondria related with the inhibition in maximal rates of electron transport mainly in the input components of the chain. Consequently, our results showed that mitochondria from GM-treated rats presented alterations in oxygen consumption by decreasing state 3 rates using malate/glutamate and succinate as substrates, which was noticeably recovered after curcumin treatment. Previously, it has been reported that curcumin restored mitochondrial state 3 rates in a model of renal dysfunction induced by hexavalent chromium [15]. On the other hand, in GM mitochondria, no significant change was registered on state 4 in glutamate/malate-dependent oxygen consumption. In contrast, state 4 in mitochondria from GM-treated rats presented lower values of oxygen consumption using succinate as a substrate. Morales et al. [25] reported a similar reduction on state 4 rates in rats treated with GM. Studies in isolated mitochondria from rat

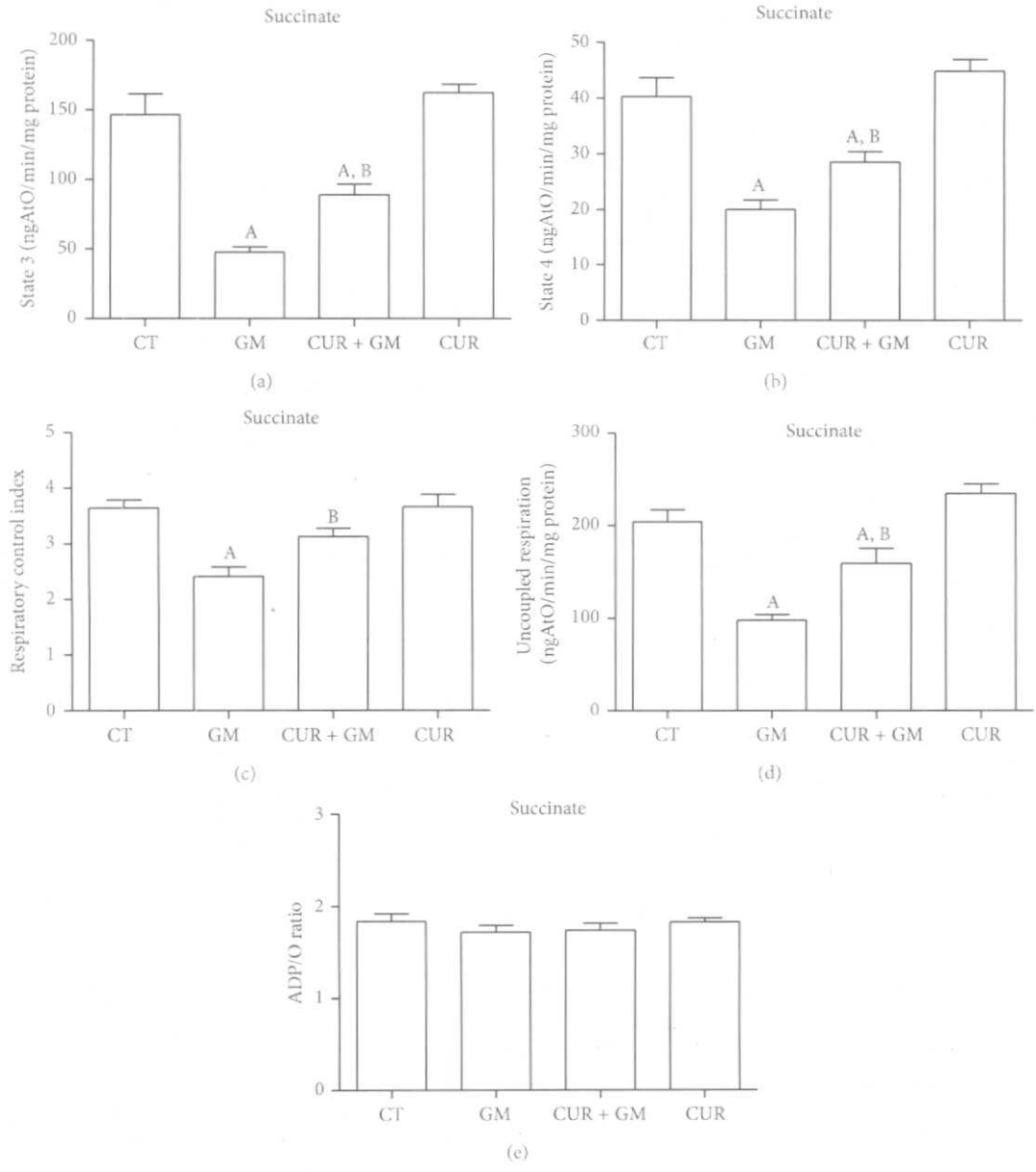

FIGURE 8: CUR attenuates GM-induced alterations in renal mitochondrial site II (succinate as a respiratory substrate) bioenergetics. (a) State 3. (b) State 4. (c) Respiratory control index. (d) Uncoupled respiration. (e) ADP/O ratio. Data are mean ± SEM, $n = 6$–8. $^{A}P < 0.05$ versus CT; $^{B}P < 0.05$ versus GM.

renal cortex incubated with GM showed increment in state 4 dependent on the antibiotic concentration [46, 47].

RCI is the single most useful general measure of function in isolated mitochondria. High RCI indicates good function and low RCI usually indicates uncoupling [44]. Mitochondria from GM-treated rats showed dysfunction when using both malate/glutamate or succinate and curcumin attenuated strongly such dysfunction. Uncoupled respiration was substantially reduced below CT values in GM group and recovered in CUR + GM group, mainly when malate/glutamate were used. This is a parameter controlled exclusively by substrate oxidation and detects dysfunction in respiratory chain components, substrate translocases, or dehydrogenases [44]. Accordingly, ADP/O ratio in mitochondria oxidizing malate/glutamate was decreased in GM group and recovered in mitochondria from cotreated rats. Curcumin prevents mitochondrial dysfunction by maintaining redox homeostasis or by protecting the mitochondrial respiratory complexes [17, 48]; nevertheless, biogenic recuperation of complexes could be another way.

3.6. Activity of Respiratory Complexes and Aconitase. We also evaluated the activity of the respiratory complexes and found that GM induced reduction in the activity of complexes

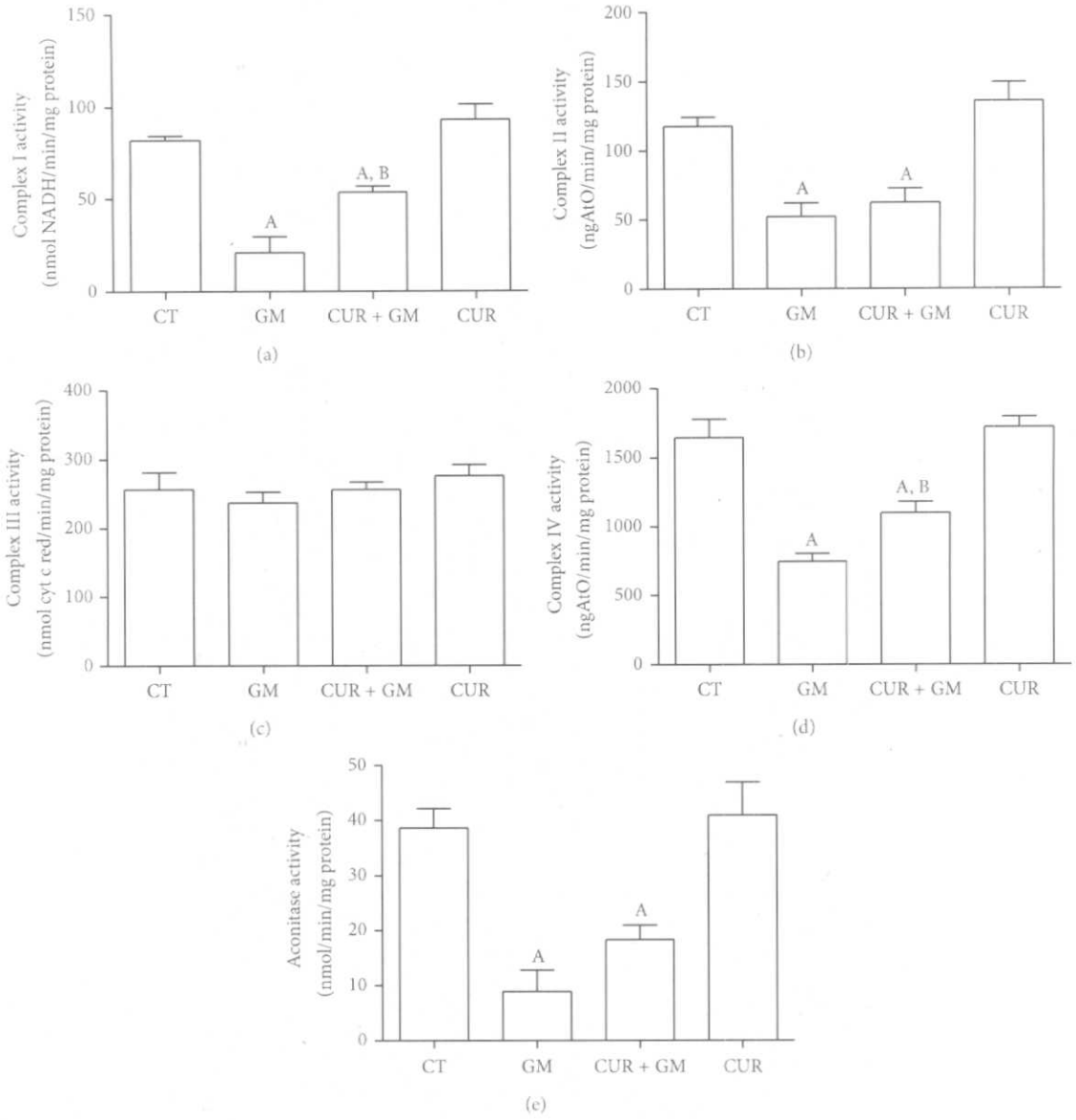

FIGURE 9: Effect of CUR treatment over GM-induced changes in the activity of renal respiratory complexes and of aconitase. (a) Complex I. (b) Complex II. (c) Complex III. (d) Complex IV. (e) Aconitase. Data are mean ± SEM, $n = 5$-6. $^{A}P < 0.05$ versus CT; $^{B}P < 0.05$ versus GM.

I, II, and IV. Activity of complex I in the GM group was the most affected retaining 25% of the activity observed in CT mitochondria ($P < 0.05$) (Figure 9(a)). Activity of complexes II and IV declined close to 45% of that observed in the CT group (Figures 9(b) and 9(d)). Curcumin treatment recovered the activities of complexes I and IV (Figures 9(a) and 9(d)), but no recovery was observed in complex II (Figure 9(b)). Retrievals reached approximately 67% of the respective CT value ($P < 0.05$ versus GM). Respiratory complexes from CUR-administered rats had similar activities to those corresponding to untreated animals.

In Figure 9(e) it is shown that the GM exposure in rats leads to a significant loss of aconitase activity in relation to the CT ($P < 0.05$). Even though a weak trend toward activity recuperation is observed in the CUR + GM group, this was not significantly different. Aconitase activity in mitochondria of rats treated only with CUR showed similar values to CT group.

We have already discussed the components of RCI, state 3 and state 4, and with the results of complexes activity assays we will identify the primary causes of mitochondrial dysfunction. According to oxygen consumption analysis, we observed that GM decreased the activity of complexes I and II which may explain the diminution in state 3 rates, RCI, and uncoupled respiration (Figures 7 and 8). These effects induced by GM on complexes I and II were recently known [49]. The absence of complex III activity alterations is in agreement with the previous observation of absence

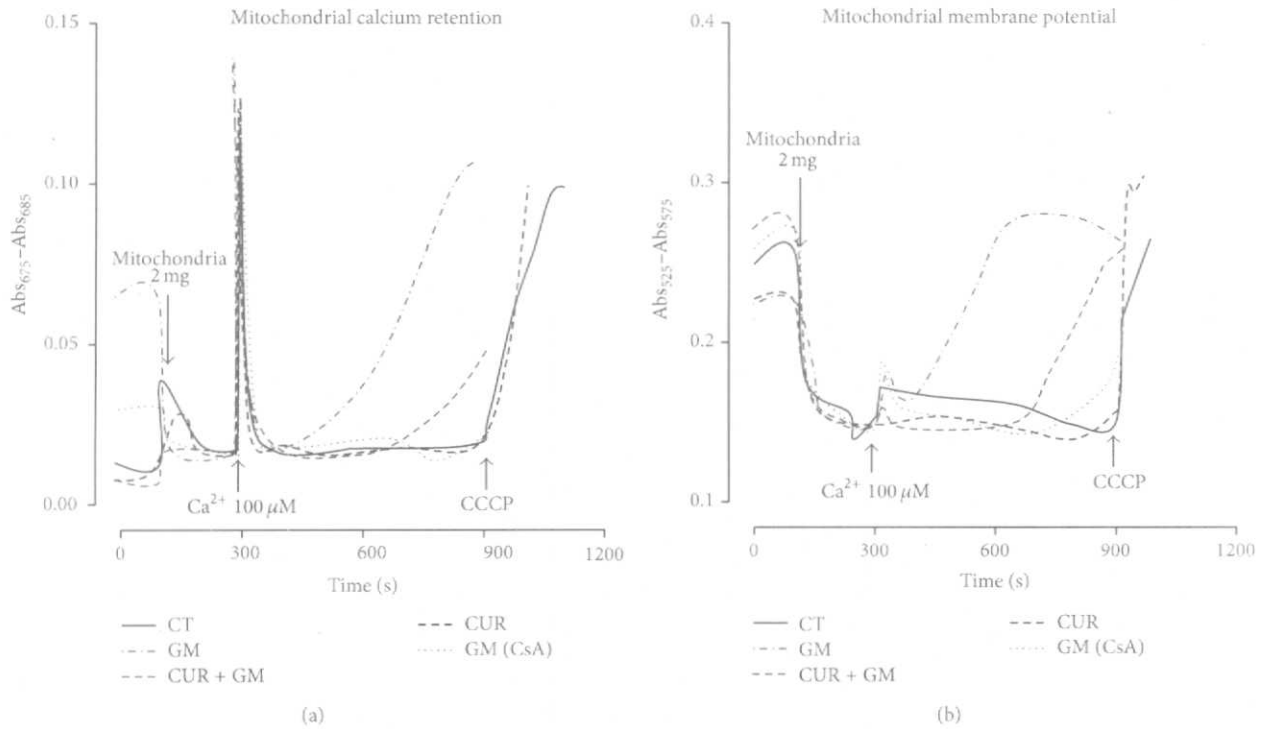

FIGURE 10: CUR treatment delays the Ca^{2+}-dependent mitochondrial permeability transition in renal cortex of GM-exposed rats. (a) Representative tracings of Ca^{2+} retention capacity obtained by arsenazo III assay and (b) representative tracings of mitochondrial membrane potential responsive to Ca^{2+} overload obtained by safranin O assay. CCCP: carbonyl cyanide m-chlorophenylhydrazone; CT: control; GM: gentamicin; CUR: curcumin; CsA: cyclosporine A.

of changes in ascorbate-TMPD-supported respiration in isolated mitochondria exposed to GM [46]. Notwithstanding, complex IV activity was altered by GM exposure countering the statement that the terminal components of respiratory chain are relatively insensitive to GM effect [46]. Indeed, it has been demonstrated that cytochrome oxidase (complex IV) concentration and its activity decreased significantly after GM treatment in rats [49, 50]. Curcumin attenuating action in complex IV activity was consistent with its effects on state 3 and uncoupled respiration. Besides, several studies have shown the potential protective effect of curcumin on the respiratory chain complexes [10].

On the other hand, it is known that anion superoxide ($O_2^{\bullet-}$) generation is an important event in mitochondria exposed to GM *in vitro* [51]. Results in Figure 9(e) support this idea in our model as aconitase activity was strongly inhibited in GM group. Aconitase is an enzyme belonging to the tricarboxylic acids pathway and its activity can be used as a measure of mitochondrial oxidative stress [52]; specifically, aconitase activity inhibition can be used to indirectly determine $O_2^{\bullet-}$ production [32]. However, curcumin treatment produced a marginal nonsignificant recovery in aconitase activity probably because of the high sensitivity of this enzyme to GM-induced ROS production [25].

3.7. Ca^{2+}-Dependent MPT. The effects of Ca^{2+} overload on the opening of the MPT pore evaluated as Ca^{2+} retention mitochondrial capacity and mitochondrial membrane potential are shown in Figures 10(a) and 10(b), respectively. Calcium was rapidly accumulated and maintained in mitochondria in all the experimental groups; however, high calcium concentration promoted the opening of the MPT pore in GM mitochondria, as CsA totally prevents this condition (Figure 10(a)). CUR partially mitigated Ca^{2+} release induced by GM. Ca^{2+} overload promotes membrane permeabilization and abolition of the mitochondrial membrane potential. In Figure 10(b), tracing GM evidences membrane potential dissipation next to Ca^{2+} addition. Unlike GM, CT and CUR tracings maintained their potential 600 s after Ca^{2+} addition, until CCCP was added. In CUR + GM mitochondria, depolarization was delayed as compared with GM mitochondria. The absence of this pattern in GM mitochondria with CsA confirms that potential loss is mediated by the formation of the MPT pore.

Ca^{2+} retention mitochondrial capacity and the membrane potential disruption by Ca^{2+} overload could be associated with the phenomenon of MPT as a triggering mechanism of cell death [53]. MPT pore opening is induced under pseudopathological conditions of oxidative stress. ROS production sensitizes mitochondria toward the MPT induction that, in turn, increases Ca^{2+} release which may enhance ROS production [54–56]. Thus, our results confirmed that mitochondria from GM-treated rats presented MPT pore opening, as previously described [57, 58]. CUR treatment

favorably ameliorates the MPT pore opening from GM-treated rats protecting them from the noxious effects generated from this antibiotic by preserving mitochondrial integrity.

4. Conclusions

The main finding of this work was that the attenuation of GM-induced nephrotoxicity by curcumin was associated with an improvement of mitochondrial dysfunction. This improvement could be probably linked to a maintenance in the program of gene expression for mitochondrial components involved in respiratory chain that could result minimized by GM. Curcumin treatment attenuated the GM-induced alterations in mitochondrial energy-linked functions of renal cortex of rats, which are associated with protection of mitochondrial chain complexes and preserving mitochondrial integrity. Despite the well-known antioxidant properties of curcumin that can protect mitochondrial proteins against oxidative stress, another presumptive protective mechanism could be the preservation of mitochondrial biogenesis which would guarantee an opportune replacement of impaired structures. Mitochondrial biogenesis could be diminished by GM and curcumin would prevent this effect with participation of Nrf2 in some extension, another proposed mechanism of protection against GM-induced nephrotoxicity.

Disclosure

The authors alone are responsible for the content and writing of the paper.

Conflict of Interests

The authors report no conflict of interests.

Authors' Contribution

Mario Negrette-Guzmán and Wylly Ramsés García-Niño contributed equally to this work and should be considered as first authors.

Acknowledgments

This work was supported by PAPIIT (Grant IN210713) and CONACYT (Grants nos. 167949, 177527, 252008, and 220046).

References

[1] J. Trujillo, Y. I. Chirino, E. Molina-Jijón, A. C. Andérica-Romero, E. Tapia, and J. Pedraza-Chaverrí, "Renoprotective effect of the antioxidant curcumin: recent findings," *Redox Biology*, vol. 1, no. 1, pp. 448–456, 2013.

[2] M. Singh and N. Singh, "Molecular mechanism of curcumin induced cytotoxicity in human cervical carcinoma cells," *Molecular and Cellular Biochemistry*, vol. 325, no. 1-2, pp. 107–119, 2009.

[3] J.-M. Kim, E.-M. Noh, K.-B. Kwon et al., "Curcumin suppresses the TPA-induced invasion through inhibition of PKCα-dependent MMP-expression in MCF-7 human breast cancer cells," *Phytomedicine*, vol. 19, no. 12, pp. 1085–1092, 2012.

[4] H. Nishikawa, J. Tsutsumi, and S. Kitani, "Anti-inflammatory and anti-oxidative effect of curcumin in connective tissue type mast cell," *Journal of Functional Foods*, vol. 5, no. 2, pp. 763–772, 2013.

[5] S. Z. Moghadamtousi, H. Abdul Kadir, P. Hassandarvish, H. Tajik, S. Abubakar, and K. Zandi, "A review on antibacterial, antiviral, and antifungal activity of curcumin," *BioMed Research International*, vol. 2014, Article ID 186864, 12 pages, 2014.

[6] S.-K. Shin, T.-Y. Ha, R. A. McGregor, and M.-S. Choi, "Long-term curcumin administration protects against atherosclerosis via hepatic regulation of lipoprotein cholesterol metabolism," *Molecular Nutrition and Food Research*, vol. 55, no. 12, pp. 1829–1840, 2011.

[7] M. R. Smith, S. R. Gangireddy, V. R. Narala et al., "Curcumin inhibits fibrosis-related effects in IPF fibroblasts and in mice following bleomycin-induced lung injury," *The American Journal of Physiology—Lung Cellular and Molecular Physiology*, vol. 298, no. 5, pp. L616–L625, 2010.

[8] S. González-Reyes, S. Guzmán-Beltrán, O. N. Medina-Campos, and J. Pedraza-Chaverri, "Curcumin pretreatment induces Nrf2 and an antioxidant response and prevents hemin-induced toxicity in primary cultures of cerebellar granule neurons of rats," *Oxidative Medicine and Cellular Longevity*, vol. 2013, Article ID 801418, 14 pages, 2013.

[9] W. R. García-Niño and J. Pedraza-Chaverrí, "Protective effect of curcumin against heavy metals-induced liver damage," *Food and Chemical Toxicology*, vol. 69, pp. 182–201, 2014.

[10] J. Trujillo, L. F. Granados-Castro, C. Zazueta, A. C. Andérica-Romero, Y. I. Chirino, and J. Pedraza-Chaverrí, "Mitochondria as a target in the therapeutic properties of curcumin," *Archiv der Pharmazie*, vol. 347, no. 12, pp. 873–884, 2014.

[11] A. González-Salazar, E. Molina-Jijón, F. Correa et al., "Curcumin protects from cardiac reperfusion damage by attenuation of oxidant stress and mitochondrial dysfunction," *Cardiovascular Toxicology*, vol. 11, no. 4, pp. 357–364, 2011.

[12] F. Correa, M. Buelna-Chontal, S. Hernández-Reséndiz et al., "Curcumin maintains cardiac and mitochondrial function in chronic kidney disease," *Free Radical Biology and Medicine*, vol. 61, pp. 119–129, 2013.

[13] M. Izem-Meziane, B. Djerdjouri, S. Rimbaud et al., "Catecholamine-induced cardiac mitochondrial dysfunction and mPTP opening: protective effect of curcumin," *The American Journal of Physiology—Heart and Circulatory Physiology*, vol. 302, no. 3, pp. H665–H674, 2012.

[14] P. H. Xu, Y. L. Yao, P. J. Guo, T. Wang, B. W. Yang, and Z. Zhang, "Curcumin protects rat heart mitochondria against anoxia-reoxygenation induced oxidative injury," *Canadian Journal of Physiology and Pharmacology*, vol. 91, no. 9, pp. 715–723, 2013.

[15] E. Molina-Jijón, E. Tapia, C. Zazueta et al., "Curcumin prevents Cr(VI)-induced renal oxidant damage by a mitochondrial pathway," *Free Radical Biology and Medicine*, vol. 51, no. 8, pp. 1543–1557, 2011.

[16] W. R. García-Niño, E. Tapia, C. Zazueta et al., "Curcumin pretreatment prevents potassium dichromate-induced hepatotoxicity, oxidative stress, decreased respiratory Complex i activity, and membrane permeability transition pore opening," *Evidence-Based Complementary and Alternative Medicine*, vol. 2013, Article ID 424692, 19 pages, 2013.

[17] N. Sivalingam, J. Basivireddy, K. A. Balasubramanian, and M. Jacob, "Curcumin attenuates indomethacin-induced oxidative stress and mitochondrial dysfunction," *Archives of Toxicology*, vol. 82, no. 7, pp. 471–481, 2008.

[18] J.-J. Kuo, H.-H. Chang, T.-H. Tsai, and T.-Y. Lee, "Positive effect of curcumin on inflammation and mitochondrial dysfunction in obese mice with liver steatosis," *International Journal of Molecular Medicine*, vol. 30, no. 3, pp. 673–679, 2012.

[19] L. Liu, W. Zhang, L. Wang et al., "Curcumin prevents cerebral ischemia reperfusion injury via increase of mitochondrial biogenesis," *Neurochemical Research*, vol. 39, no. 7, pp. 1322–1331, 2014.

[20] B. H. Ali, N. Al-Wabel, O. Mahmoud, H. M. Mousa, and M. Hashad, "Curcumin has a palliative action on gentamicin-induced nephrotoxicity in rats," *Fundamental and Clinical Pharmacology*, vol. 19, no. 4, pp. 473–477, 2005.

[21] E. O. Farombi and M. Ekor, "Curcumin attenuates gentamicin-induced renal oxidative damage in rats," *Food and Chemical Toxicology*, vol. 44, no. 9, pp. 1443–1448, 2006.

[22] Y. Quiros, L. Vicente-Vicente, A. I. Morales, J. M. López-Novoa, and F. J. López-Hernández, "An integrative overview on the mechanisms underlying the renal tubular cytotoxicity of gentamicin," *Toxicological Sciences*, vol. 119, no. 2, pp. 245–256, 2011.

[23] M. Negrette-Guzmán, S. Huerta-Yepez, O. N. Medina-Campos et al., "Sulforaphane attenuates gentamicin-induced nephrotoxicity: role of mitochondrial protection," *Evidence-Based Complementary and Alternative Medicine*, vol. 2013, Article ID 135314, 17 pages, 2013.

[24] H. Servais, P. Van Der Smissen, G. Thirion et al., "Gentamicin-induced apoptosis in LLC-PK1 cells: involvement of lysosomes and mitochondria," *Toxicology and Applied Pharmacology*, vol. 206, no. 3, pp. 321–333, 2005.

[25] A. I. Morales, D. Detaille, M. Prieto et al., "Metformin prevents experimental gentamicin-induced nephropathy by a mitochondria-dependent pathway," *Kidney International*, vol. 77, no. 10, pp. 861–869, 2010.

[26] J. Chen, H. S. Wong, H. Y. Leung et al., "An ursolic acid-enriched extract of *Cynomorium songaricum* protects against carbon tetrachloride hepatotoxicity and gentamicin nephrotoxicity in rats possibly through a mitochondrial pathway: a comparison with ursolic acid," *Journal of Functional Foods*, vol. 7, no. 1, pp. 330–341, 2014.

[27] R. Manikandan, M. Beulaja, R. Thiagarajan, A. Priyadarsini, R. Saravanan, and M. Arumugam, "Ameliorative effects of curcumin against renal injuries mediated by inducible nitric oxide synthase and nuclear factor kappa B during gentamicin-induced toxicity in Wistar rats," *European Journal of Pharmacology*, vol. 670, no. 2-3, pp. 578–585, 2011.

[28] M. Negrette-Guzmán, S. Huerta-Yepez, E. Tapia, and J. Pedraza-Chaverri, "Modulation of mitochondrial functions by the indirect antioxidant sulforaphane: a seemingly contradictory dual role and an integrative hypothesis," *Free Radical Biology and Medicine*, vol. 65, pp. 1078–1089, 2013.

[29] R. C. Scarpulla, "Transcriptional paradigms in mammalian mitochondrial biogenesis and function," *Physiological Reviews*, vol. 88, no. 2, pp. 611–638, 2008.

[30] H. Servais, Y. Jossin, F. Van Bambeke, P. M. Tulkens, and M.-P. Mingeot-Leclercq, "Gentamicin causes apoptosis at low concentrations in renal LLC-PK 1 cells subjected to electroporation," *Antimicrobial Agents and Chemotherapy*, vol. 50, no. 4, pp. 1213–1221, 2006.

[31] P. D. Maldonado, D. Barrera, I. Rivero et al., "Antioxidant S-allylcysteine prevents gentamicin-induced oxidative stress and renal damage," *Free Radical Biology and Medicine*, vol. 35, no. 3, pp. 317–324, 2003.

[32] E. Martínez-Abundis, N. García, F. Correa, S. Hernández-Reséndiz, J. Pedraza-Chaverri, and C. Zazueta, "Effects of α-mangostin on mitochondrial energetic metabolism," *Mitochondrion*, vol. 10, no. 2, pp. 151–157, 2010.

[33] E. Balogun, M. Hoque, P. Gong et al., "Curcumin activates the haem oxygenase-1 gene via regulation of Nrf2 and the antioxidant-responsive element," *Biochemical Journal*, vol. 371, no. 3, pp. 887–895, 2003.

[34] C. A. Piantadosi, M. S. Carraway, A. Babiker, and H. B. Suliman, "Heme oxygenase-1 regulates cardiac mitochondrial biogenesis via nrf2-mediated transcriptional control of nuclear respiratory factor-1," *Circulation Research*, vol. 103, no. 11, pp. 1232–1240, 2008.

[35] N. C. MacGarvey, H. B. Suliman, R. R. Bartz et al., "Activation of mitochondrial biogenesis by heme oxygenase-1-mediated NF-E2-related factor-2 induction rescues mice from lethal *Staphylococcus aureus* sepsis," *The American Journal of Respiratory and Critical Care Medicine*, vol. 185, no. 8, pp. 851–861, 2012.

[36] J. Palomino and J. Pachón, "Aminoglucósidos," *Enfermedades Infecciosas y Microbiología Clínica*, vol. 21, no. 2, pp. 105–115, 2003.

[37] J. Feng, T. Tao, W. Yan, C. S. Chen, and X. Qin, "Curcumin inhibits mitochondrial injury and apoptosis from the early stage in EAE mice," *Oxidative Medicine and Cellular Longevity*, vol. 2014, Article ID 728751, 10 pages, 2014.

[38] A. M. Sanli, E. Turkoglu, G. Serbes et al., "Effect of curcumin on lipid peroxidation, early ultrastructural findings and neurological recovery after experimental spinal cord contusion injury in rats," *Turkish Neurosurgery*, vol. 22, no. 2, pp. 189–195, 2012.

[39] P. Srivastava, R. S. Yadav, L. P. Chandravanshi et al., "Unraveling the mechanism of neuroprotection of curcumin in arsenic-induced cholinergic dysfunctions in rats," *Toxicology and Applied Pharmacology*, vol. 279, no. 3, pp. 428–440, 2014.

[40] J. Pan, H. Li, J.-F. Ma et al., "Curcumin inhibition of JNKs prevents dopaminergic neuronal loss in a mouse model of Parkinson's disease through suppressing mitochondria dysfunction," *Translational Neurodegeneration*, vol. 1, article 16, 2012.

[41] M. Abdul-Hamid and N. Moustafa, "Protective effect of curcumin on histopathology and ultrastructure of pancreas in the alloxan treated rats for induction of diabetes," *The Journal of Basic & Applied Zoology*, vol. 66, no. 4, pp. 169–179, 2013.

[42] J.-J. Kuo, H.-H. Chang, T.-H. Tsai, and T.-Y. Lee, "Curcumin ameliorates mitochondrial dysfunction associated with inhibition of gluconeogenesis in free fatty acid-mediated hepatic lipoapoptosis," *International Journal of Molecular Medicine*, vol. 30, no. 3, pp. 643–649, 2012.

[43] L. Gibellini, E. Bianchini, S. De Biasi, M. Nasi, A. Cossarizza, and M. Pinti, "527209," *Evidence-Based Complementary and Alternative Medicine*, vol. 2015, Article ID 527209, 13 pages, 2015.

[44] M. D. Brand and D. G. Nicholls, "Assessing mitochondrial dysfunction in cells," *Biochemical Journal*, vol. 435, no. 2, pp. 297–312, 2011.

[45] C. F. Simmons Jr., R. T. Bogusky, and H. D. Humes, "Inhibitory effects of gentamicin on renal mitochondrial oxidative phosphorylation," *The Journal of Pharmacology and Experimental Therapeutics*, vol. 214, no. 3, pp. 709–715, 1980.

[46] J. M. Weinberg and H. D. Humes, "Mechanisms of gentamicin induced dysfunction of renal cortical mitochondria. I. Effects of mitochondrial respiration," *Archives of Biochemistry and Biophysics*, vol. 205, no. 1, pp. 222–231, 1980.

[47] J. M. Weinberg, P. G. Harding, and H. D. Humes, "Mechanisms of gentamicin-induced dysfunction of renal cortical mitochondria. II. Effects on mitochondrial monovalent cation transport," *Archives of Biochemistry and Biophysics*, vol. 205, no. 1, pp. 232–239, 1980.

[48] H. Raza, A. John, E. M. Brown, S. Benedict, and A. Kambal, "Alterations in mitochondrial respiratory functions, redox metabolism and apoptosis by oxidant 4-hydroxynonenal and antioxidants curcumin and melatonin in PC12 cells," *Toxicology and Applied Pharmacology*, vol. 226, no. 2, pp. 161–168, 2008.

[49] B. D. Sahu, S. Tatireddy, M. Koneru et al., "Naringin ameliorates gentamicin-induced nephrotoxicity and associated mitochondrial dysfunction, apoptosis and inflammation in rats: possible mechanism of nephroprotection," *Toxicology and Applied Pharmacology*, vol. 277, no. 1, pp. 8–20, 2014.

[50] L. M. Mela-Riker, L. L. Widener, D. C. Houghton, and W. M. Bennett, "Renal mitochondrial integrity during continuous gentamicin treatment," *Biochemical Pharmacology*, vol. 35, no. 6, pp. 979–984, 1986.

[51] C.-L. Yang, X.-H. Du, and Y.-X. Han, "Renal cortical mitochondria are the source of oxygen free radicals enhanced by gentamicin," *Renal Failure*, vol. 17, no. 1, pp. 21–26, 1995.

[52] C. E. Guerrero-Beltrán, M. Calderón-Oliver, E. Martínez-Abundis et al., "Protective effect of sulforaphane against cisplatin-induced mitochondrial alterations and impairment in the activity of NAD(P)H: quinone oxidoreductase 1 and γ glutamyl cysteine ligase: studies in mitochondria isolated from rat kidney and in LLC-PK1 cells," *Toxicology Letters*, vol. 199, no. 1, pp. 80–92, 2010.

[53] A. P. Halestrap, G. P. McStay, and S. J. Clarke, "The permeability transition pore complex: another view," *Biochimie*, vol. 84, no. 2-3, pp. 153–166, 2002.

[54] M. Crompton, "The mitochondrial permeability transition pore and its role in cell death," *The Biochemical Journal*, vol. 341, part 2, pp. 233–249, 1999.

[55] S. Orrenius, "Reactive oxygen species in mitochondria-mediated cell death," *Drug Metabolism Reviews*, vol. 39, no. 2-3, pp. 443–455, 2007.

[56] A. Rasola and P. Bernardi, "Mitochondrial permeability transition in Ca^{2+}-dependent apoptosis and necrosis," *Cell Calcium*, vol. 50, no. 3, pp. 222–233, 2011.

[57] N. Dehne, U. Rauen, H. De Groot, and J. Lautermann, "Involvement of the mitochondrial permeability transition in gentamicin ototoxicity," *Hearing Research*, vol. 169, no. 1-2, pp. 47–55, 2002.

[58] A. Muthuraman, S. K. Singla, A. Rana, A. Singh, and S. Sood, "Reno-protective role of flunarizine (mitochondrial permeability transition pore inactivator) against gentamicin induced nephrotoxicity in rats," *Journal of the Pharmaceutical Society of Japan*, vol. 131, no. 3, pp. 437–443, 2011.

Tuberculosis 95 (2015) 562–569

Contents lists available at ScienceDirect

Tuberculosis

journal homepage: http://intl.elsevierhealth.com/journals/tube

IMMUNOLOGICAL ASPECTS

Effect of cortisol and/or DHEA on THP1-derived macrophages infected with *Mycobacterium tuberculosis*

Bettina Bongiovanni [a, *], Dulce Mata-Espinosa [b], Luciano D'Attilio [a], Juan Carlos Leon-Contreras [b], Ricardo Marquez-Velasco [c], Oscar Bottasso [a], Rogelio Hernandez-Pando [b], María Luisa Bay [a]

[a] Instituto de Inmunología Clínica y Experimental de Rosario (IdICER-CONICET), Universidad Nacional de Rosario, Suipacha 590, Rosario, Argentina
[b] Sección de Patología Experimental, Departamento de Patología, Instituto Nacional de Ciencias Médicas y Nutrición Salvador Zubirán, Av. Vasco De Quiroga 15, Tlalpan, México D.F., Mexico
[c] Departamento de Inmunología, Instituto Nacional de Cardiología Ignacio Chávez, Juan Badiano 1, Tlalpan, México D.F., Mexico

ARTICLE INFO

Article history:
Received 26 March 2015
Accepted 19 May 2015

Keywords:
Macrophages
Mycobacterium tuberculosis
Dehydroepiandrosterone
Cortisol
Autophagy

SUMMARY

Tuberculosis (TB) is a major health problem requiring an appropriate cell immune response to be controlled. Macrophages play a central role in the response against *Mycobacterium tuberculosis* (Mtb).

Given our prior studies in which adrenal steroids were found to modify the cellular immune responses from TB patients, it was sensible to analyze the immunomodulatory capability of cortisol and DHEA on macrophages infected with Mtb. The human macrophage-like THP-1 cells were infected with the H37Rv strain of Mtb and treated with Cortisol and DHEA at different doses. We monitored phagocytosis, intracellular-bacterial growth, autophagosoma formation, as well as cytokine gene expression and production.

Cultures exposed to cortisol showed a decreased production of IL-1β, TNF-α, with DHEA being unable to modify the pattern of cytokine production or to reverse the cortisol inhibitory effects. Interestingly the intra-macrophagic bacterial burden was found reduced by DHEA treatment. While this effect was not related to a different cytokine pattern, in terms their production or mRNA expression, DHEA treatment did promote autophagy in Mtb-infected macrophages, irrespective of Cortisol presence.

In essence, the better control of Mtb load by DHEA-treated macrophages seems to be dependent on an autophagic mechanism. The present results are relevant for two reasons as autophagy is not only important for clearance of mycobacteria but also for the prevention of tissue damage.

1. Introduction

Tuberculosis (TB) constitutes an important health problem today. In 2014, an estimated 8.6 million people developed TB and 1.3 million died from the disease (including 320 000 deaths among HIV-positive people). The number of TB deaths is unacceptably large given that most are preventable [1]. This disease is caused by *Mycobacterium tuberculosis* (Mtb), a facultative intracellular bacterium that is capable of surviving and persisting within host mononuclear cells [2].

In most cases, the immune response against Mtb is adequate and avoids the development of active disease. However, complete clearance of the pathogen is frequently not achieved. Macrophages comprise a niche cell for mycobacterial infection, yet they may also contribute to elimination of bacilli via numerous mechanisms, including the successful acidification and maturation of phagosomes [3–5]. However, Mtb ensures its survival within host macrophages by arresting the maturation pathway that leads to phagosome–lysosome fusion, thus avoiding the phagolysosome that is rich in acid hydrolases capable of microbicidal degradation, and creating a suitable environment for bacillary survival and replication [6–8]. As yet, while Mtb can block phagosome maturation, the induction of autophagy facilitates phagosome-lysosome fusion and the bacilli clearance [9,10].

Among modulators of the immune response, hormones like the steroid hormones of the adrenal and gonadal glands, and neurotransmitters are known to play an influential role in this regard [11,12]. In analyzing the immune-endocrine profile of TB patients, we

* Corresponding author.
E-mail address: bettina.bongiovanni@gmail.com (B. Bongiovanni).

http://dx.doi.org/10.1016/j.tube.2015.05.011
1472-9792/

carried out a series of studies in newly diagnosed, untreated patients with different degrees of lung compromise. Plasma levels of interferon gamma (IFN-γ), interleukin (IL) 10, and IL6 were increased, whereas testosterone and dehydroepiandrosterone (DHEA) levels were profoundly decreased in these patients, more evident in those with an advanced disease. In parallel there were modest increases in the concentrations of cortisol and estradiol [13]. These endocrine changes may partly account for the deficient control of the inflammatory response and the gradual loss of protective responses that TB patients present with disease progression [14].

More recent studies in patients undergoing specific therapy revealed a more balanced cortisol/DHEA and cortisol/DHEAS ratio, implying that etiologic treatment encompasses favorable immune and endocrine changes, which may account for its beneficial effects [15].

Macrophages play a central role in the defense against TB through phagocytosis, intracellular killing of mycobacteria, and antigen presentation to lymphocytes [16,17]. Since adrenal steroids are much likely to modify such responses, it was sensible to analyze the immunoregulatory capability of cortisol and DHEA on macrophages infected with Mtb.

In addressing this issue we have employed a model able to mimic the macrophage-Mtb interaction. Hence, we infected the human macrophage-like THP-1 cells with Mtb strain H37Rv and treated with Cortisol and DHEA at different doses. We monitored phagocytosis, intracellular-bacterial growth, autophagosoma formation, cytokines gene expression and production. This approach provided new insight on the steroid hormones effects on the intracellular fate of Mtb.

2. Materials and methods

2.1. Bacterial cultures

M. tuberculosis strain H37Rv (ATCC 25618) was used in all experiments. For *in vitro* cell infection, frozen H37Rv *M. tuberculosis* was prepared in Middlebrook 7H9 (Difco Laboratories) culture medium supplemented with ADC (Difco Laboratories) during 48 h. Bacilli were then placed in bottles containing 60 ml of the same culture medium and incubated at 70 rpm 35 °C during 7–10 days until reaching a 600 nm OD. To prepare a suspension with single bacteria and disrupt mycobacterial clump formation, bacterial pellets were then resuspended in RPMI with 6% glycerol and vortexed for 5 min in the presence of five sterile 3-ml glass beads. The resulting suspension of mycobacteria was centrifuged at 900 g for 10 min to remove any remaining large clumps. Supernatants with disaggregated mycobacterial stock cultures were then divided into aliquots and stored at −70 °C until use. Mean concentrations of *M. tuberculosis* strain H37Rv stock suspensions were determined by counting colony-forming units (CFU) on 7H10 agar plates in triplicate serial dilutions of declumped stock suspensions between Days 21 and 28. This declumping procedure was performed in each experiment to ensure use of single-bacterial-cell suspensions and to establish the input amounts of bacteria for the infections at 5:1 of multiplicities of infection [MOI], [18].

2.2. Cell preparations

The characteristics of THP-1, a human monocytic leukemia cell line, have been described previously in detail [19]. This cell line was grown in suspension cultures in Tissue Culture Medium RPMI-1640 supplemented with 10% of heat-inactivated fetal bovine serum and kanamycin (60 μg/ml, Gibco) at 37 °C in 5% CO2. THP-1 cells/ml were cultured in complete RPMI-1640 containing 30 ng/ml phorbol-12-myristate-13-acetate (PMA, Sigma Chemical Co., St. Louis, MO, USA) and plated for differentiation to macrophages. Twenty four hours later supernatants were removed and complete RPMI-1640 was added for 48 h before the infection.

2.3. Infection with M. tuberculosis and stimulation of macrophages with cortisol and DHEA

Macrophages were infected with Mtb at Multiplicity of Infection (MOI) of 5:1 (5 bacteria/1 cell) for 3 h, in presence or absence of steroid hormones. In line with our earlier work [20], hormones were employed within the range of physiological concentrations, Cortisol (10^{-6} M, Sigma Chemical Co.) and/or DHEA (10^{-6}or 10^{-7} M, Sigma Chemical Co.) in RPMI with 10% of heat-inactivated fetal bovine serum and kanamycin (60 μg/ml) and cultured at37 °C in 5% CO_2. Cells were then washed 4 times with complete RPMI-1640 to remove extracellular bacilli. According to the study purposes, experimental approaches were as follows:

a) To assess Mtb phagocytosis, the macrophages (1×10^6 cells/wells in chamber slide) were stained by Ziehl Neelsen after 3 h of infection in presence or absence of hormones and 1 h more with RPMI-1640 alone. The rate of infection was measured by quantifying the number of bacteria phagocytosed per cell, 100 cells/field were counted in triplicate.
b) To evaluate the control of mycobacterial intracellular growth, infected macrophages (3×10^5 cells/well in round bottom 96-well polystyrene plates) were incubated for 1 h (Day 0), 24 h (Day 1) and 96 h (Day 4) in presence or absence of hormones. Cells were lysed with 1% SDS followed by 20% BSA, serially diluted in Middlebrook 7H9 medium and plated in triplicate over 7H10 medium to quantify colony forming units (CFU). To take into account the phagocytosis of bacteria, the intracellular growth fold change was calculated as CFU at Day 1 or Day 4 post-infection, and also at Day 0, after 21 days of culture.
c) For cytokine gene expression and production, 5×10^6 cells plated in 24-well dishes under the above described conditions were incubated during 24 h more with hormones. Supernatants were collected to assess cytokine production and cells were preserved for mRNA extraction.
d) For transmission electron microscopy examination, 4×10^6 macrophages cultured in polypropylene tubes under the same conditions were treated during 24 h more with Cortisol and/or DHEA and then fixed and prepared for electron microscopy. In addition, infected cells were treated with muramyldipeptide (MDP, Sigma Chemical Co.) for 24 h post-infection for positive control of autophagy.

2.4. RNA isolation, cDNA synthesis and real-time PCR for cytokines gene expression

Total RNA was isolated by using RNeasy Mini® Kit (Quiagen, Carlsbad, CA, USA) according to the manufacture's recommendations. RNA pellets were dissolved in DEPC sterile water and stored at −80 °C until analysis. RNA quantity was calculating by OD 260 spectrophotometry (NanoVuePlus Spectrophotometer, GE Healthcare, Little Chalfont, UK). The integrity of the purified RNA was determined by 2% agarose gel electrophoresis. cDNA was synthesized from 5 μg of total RNA using 200 U M-MLV reverse transcriptase (USB Corporation, Cleveland, USA) and specific reverse primers (Table 1). Briefly, 5X M-MLV Reaction Buffer, 0.4 mMdNTP (Amersham Biosciences, Piscataway, NJ, USA); 21.5 U RNAasa Inhibitor (RNAguard, Amersham Biosciences), 0.4 μM of each reverse primer; 2 mM $MgCl_2$ (Invitrogen, Camarillo, CA, USA) and DEPC sterile water for 50 μl of final volume. Retrotranscription

Table 1
Real Time nucleotide primer sequence.

Transcripts	Primer forward	Primer reverse	Size (pb)	NCBI reference sequence
TGF-beta1	TACCTGAACCCGTGTTGCTC	GCGAAAGCCCTCAATTTCCC	224	NM_000660.5
IL-23a	CCCAAGGACTCAGGGACAAC	TGGGACTGAGGCTTGGAATC	222	NM_016584.2

programmes consisted of 5 min at 65 °C, 1 h at 40 °C followed by enzyme inactivation at 95 °C for 3 min cDNA was stored at − 80 °C until use it. qPCRwas performed with the ABI PRISM® 7500 Real Time PCR System (Applied Biosystems, Foster City, CA, USA) using 10 μl dilution 1/200 of cDNA, 0.4 μM of each primer and 25 μl of SYBR Green PCR Master Mix 2X at a final volume of 50 μl. Thermal cycling conditions were: 2 min at 50 °C, 10 min at 95 °C followed by 45 PCR cycles of denaturing at 95 °C for 15 s, annealing and elongation at 60 °C for 1 min. Fluorescence readings were performed on annealing/elongation steps. Data were expressed as arbitrary units -AU-, where 1 AU equals to 1 μg of standard mRNA [21].

2.5. Cytokine detection

Cytokines IL1-β, IL6, IL10, TNF-α and soluble TNFR type I (sTNFRI) were measured in culture supernatants employing commercially available ELISA kits according to the instructions of the manufacturer (BioLegend Company, CA, USA for IL1-β, IL6, IL10, TNF-α and R&D Systems, Inc. MN, USA for sTNFRI). Detection limits were: 2.0 pg/ml for IL1-β; 4.0 pg/ml for IL6; 2.0 pg/ml for IL10, 2.0 pg/ml for TNF-α and 15.0 pg/ml for sTNFRI.

2.6. Electron microscopy

Cells were prepared for transmission electron microscopy (TEM) by pelleting the various cell preparations by centrifugation for 1 min/6000 rpm. Cells were fixed in 1% glutaraldehyde dissolved in 0.1 M cacodylate buffer (pH 7); postfixed in 2% osmium tetroxide; dehydrated with increasing concentrations of ethanol and gradually infiltrated with Epon resin (Pelco). Thin sections were contrasted with uranyl acetate and lead citrate. In order to confirm autophagosomes, the subcellular localization of its specific marker LC3 protein was investigated by immunoelectronmicroscopy [22]. Briefly, cells were fixed in 4% paraformaldehyde in 0.2 M Sörensen buffer; dehydrated with different concentrations of ethylic alcohol and infiltrated with LR-White hydrosoluble resin (London Resin Co., Hampshire, United Kingdom). Sections of 60 to 80 nm thick were placed on nickel grids. The grids were incubated overnight at 4 °C with specific polyclonal rabbit anti-LC3 antibodies. After rinsing with PBS, the grids were incubated for 2 h at room temperature with goat anti-rabbit IgG (Sigma Chemical Co) conjugated to 5-nm gold particles (Sigma Chemical Co) diluted 1:20 in PBS. The grids were contrasted with uranyl acetate (Electron Microscopy Sciences, Fort Washington, PA) and examined with an M-10 Zeiss electron microscope (Karl Zeiss, Jena Germany). For morphometry, 30 cells from each condition were random selected at day one of incubation with steroids and photographed at 40,000x magnification, then the total number of phagosomes, autophagosomes and lysosomes were counted in each experimental group. From the total number of these vacuolar structures, the number and mean of autophagosomes was quantified and compared among the groups.

2.7. Statistical analysis

There were 5 independent rounds of experiments. Data are shown as means ± SEM. Statistical comparisons were performed by the Kruskall-Wallis and Mann-Whitney U tests. A p value <0.05 was considered statistically significant except the morphometric study, where the Student t test was used. A $p < 0.05$ was considered statistically significant.

3. Results

3.1. Effects of steroid hormones on phagocytosis in cells infected with M. tuberculosis

Adherent cells were infected with Mtb H37Rv at an infection ratio of 5 bacteria/1 macrophage for 3 h and treated with Cortisol (Gc) and/or DHEA. As depicted in Figure 1, Cortisol decreased the phagocytosis of Mtb while the phagocytic capacity of macrophages was increased by DHEA but it was not significant. The combination of Cortisol 10^{-6} M and DHEA at 10^{-6} M significantly reverted the Cortisol inhibitory effect.

3.2. Effects of steroid hormones on the intracellular-bacterial growth of cells infected with M. tuberculosis

After infection, cultures treated with Cortisol or DHEA showed significant differences at Day 0, where treatment with DHEA at 10^{-7} M resulted in increased CFU numbers respect cultures exposed to Mtb alone (Figure 2, panel A). The same was true when comparing cultures treated with Gc + DHEA vs. those only infected with Mtb (Figure 2, panel A).

Considering culture timing, macrophages exposed to Mtb alone showed an increase in the CFU numbers from day 1 to day 4 By opposite, in cultures exposed to DHEA at 10^{-7} a trend to a decreased bacterial low as time elapsed was found, but differences remained statistically insignificant (Figure 3 panel A). Assessment at day 4 revealed that cultures treated with Gc + DHEA had significantly reduced CFU numbers with reference to their untreated counterparts (Figure 2 panel C). Moreover, at day 4 there was a significant CFU decrease ($p < 0.01$) respect to day 1 in the cultures infected and treated with Gc + DHEA (Figure 3 panel B).

3.3. Effects of steroids hormones on cytokines and sTNFR release in cells infected with M. tuberculosis H37Rv

Cells were incubated for 24 h in the presence or absence of Cortisol (10^{-6} M) and/or DHEA (10^{-6} M or 10^{-7} M) before *M. tuberculosis* infection (MOI 5:1). In cultures left uninfected and treated with hormones (Gc and/or DHEA), cytokines and sTNFR were undetectable (data not shown). As shown in Figure 5, Mtb-infected cultures had increased amounts of TNF-α, sTNFR, IL1-β and IL10. Except for sTNFR levels, which were significantly higher in Cortisol-treated cultures, this hormone decreased TNF-α, IL1-β and IL-10 levels respect to infected cultures left without hormones (Figure 4). In general terms, values in DHEA-treated cultures remained within the range seen in cells exposed to Mtb (Figure 4). Cultures treated with Gc + DHEA continued to show lesser amounts of TNF-α, IL1-β and IL10 together with higher quantities of sTNFR (Figure 4). IL6 levels were undetectable at this infection time point.

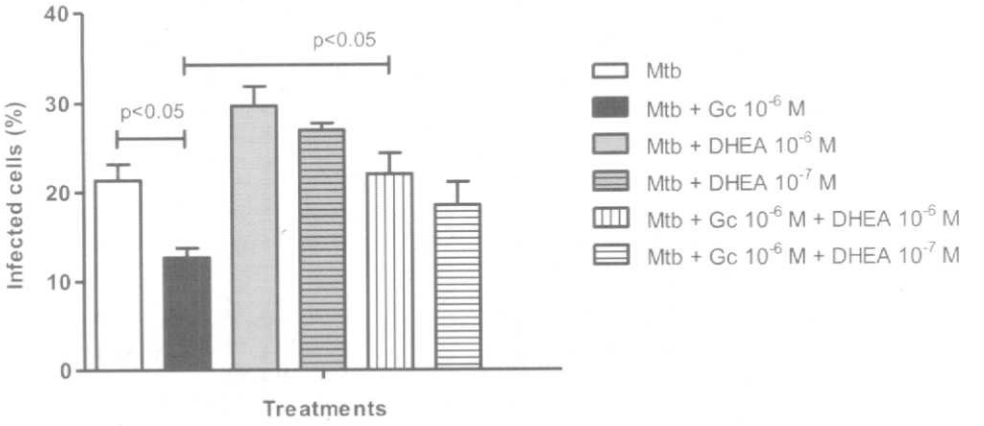

Figure 1. Effects of steroid hormones on phagocytosis by cells infected with *M. tuberculosis*. Cells were infected with *M. tuberculosis* H37Rv at an infection ratio of 5 bacteria/1 macrophage for 3 h and treated with Cortisol and/or DHEA. Non-phagocytosed bacteria were washed away and macrophages were fixed and stained. The values are means ± SEM (n = 5); $p < 0.05$. Mtb: *M. tuberculosis*; Gc: Cortisol 10^{-6} M; DHEA: DHEA 10^{-6} M or 10^{-7} M.

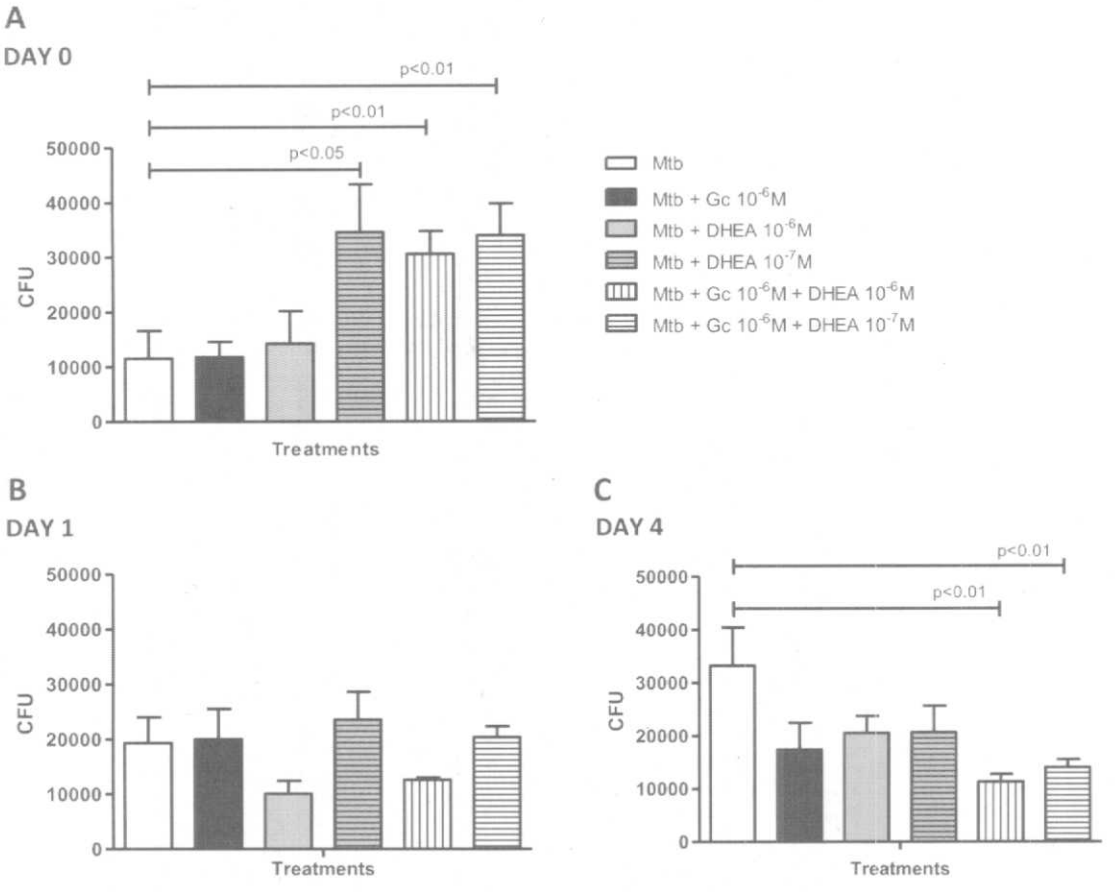

Figure 2. Effects of steroid hormones on CFU in cells infected with *M. tuberculosis*. Cells were infected with *M. tuberculosis* H37Rv at an infection ratio of 5 bacteria/1 macrophage for 3 h and treated with Cortisol and/or DHEA. Non-phagocytosed bacteria were washed away and macrophages were treated again with steroid hormones or medium. The values are means ± SEM (n = 5); Mtb: *M. tuberculosis*; Gc: Cortisol 10^{-6} M; DHEA 10^{-6} M or 10^{-7} M.

3.4. *Effects of steroids hormones on cytokine gene expression in cells infected with M. tuberculosis*

We next proceeded to analyze gene expression levels for a couple of cytokines also relevant in the macrophage response against pathogens. Data from Figure 6 revealed that Mtb induced the expression of TGF-β and IL23, with cortisol inhibiting the expression of the latter cytokine. DHEA failed to reverse such inhibitory effect. The pattern of IL23 expression in DHEA-treated cultures was similar to the one seen in *M. tuberculosis*-infected cultures (Figure 5 panel A). Infection with Mtb also led to a significant expression of TGF-β, although in this case treatment with Cortisol and/or DHEA resulted in no gross changes when compared with infected cultures left without hormones (Figure 5 panel B).

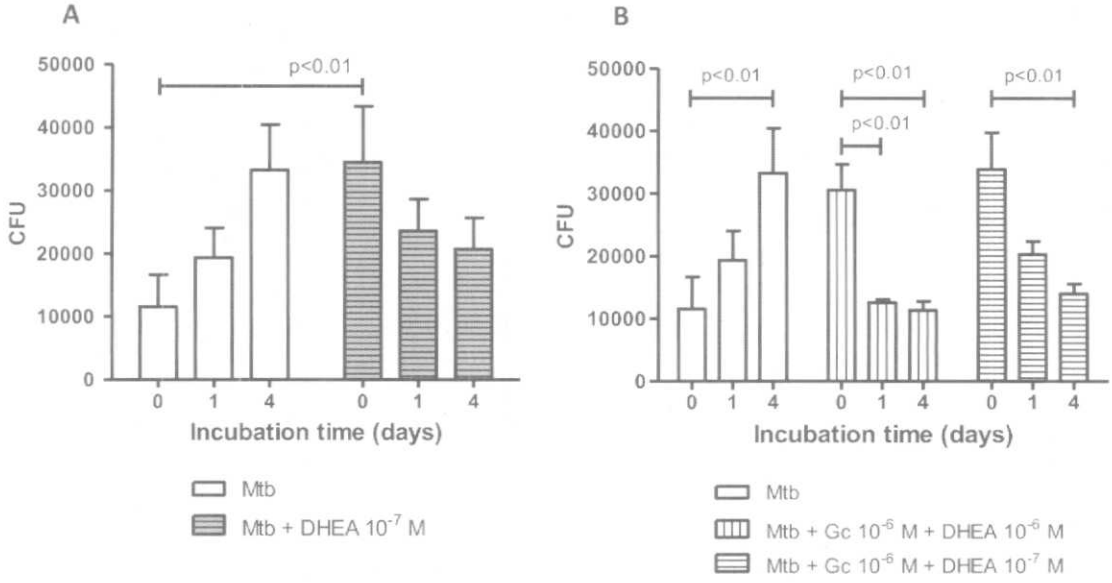

Figure 3. Effects of DHEA with or without Cortisol on CFU in cells infected with *M. tuberculosis*. **A)** Cells were infected with *M. tuberculosis* H37Rv for 3 h and treated with DHEA 10^{-7} M. Non-phagocytosed bacteria were washed away and macrophages were treated again with steroid hormones or medium. **B)** Cells were infected with *M. tuberculosis* H37Rv for 3 h and treated with Cortisol and DHEA. Non-phagocytosed bacteria were washed away and macrophages were treated again with the steroid hormone or medium. The values are means ± SEM (n = 5); Mtb: *M. tuberculosis*; Gc: Cortisol 10^{-6} M; DHEA 10^{-6} M or 10^{-7} M.

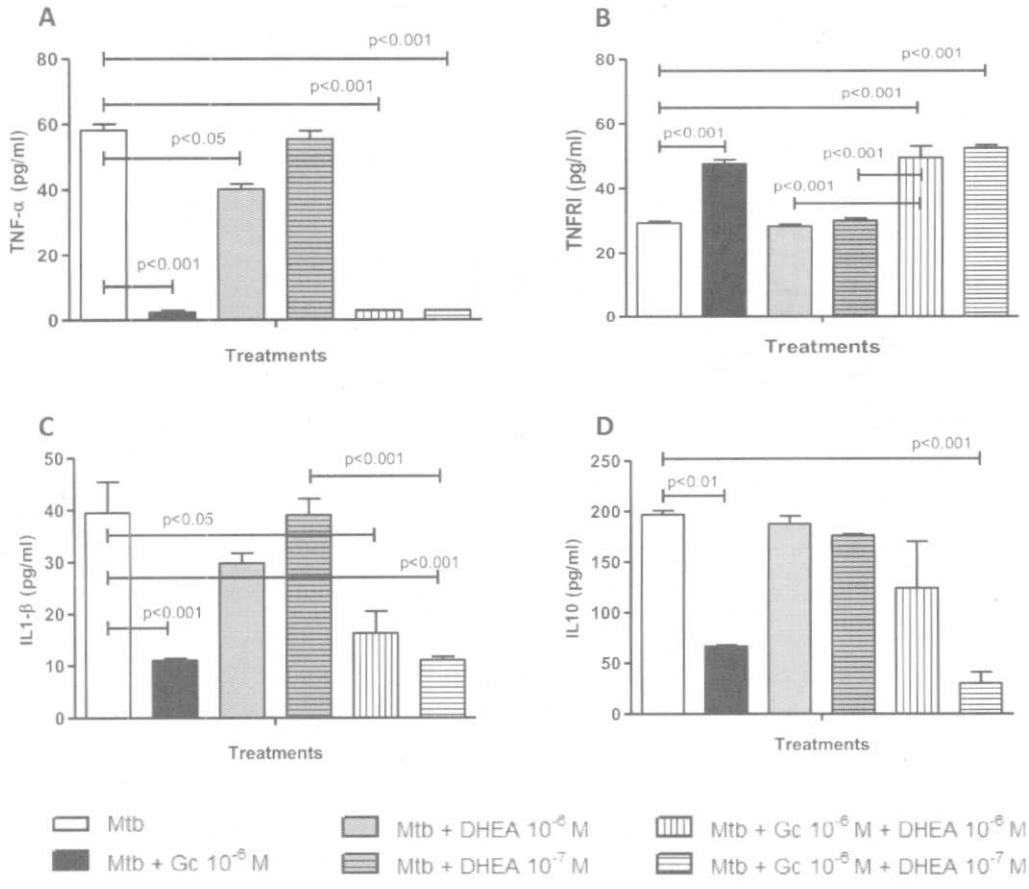

Figure 4. Effects of steroid hormones on cytokine release and sTNFRI levels in cells infected with *M. tuberculosis* H37Rv. Cells were incubated for 24 h in the presence or absence of Cortisol (10^{-6} M) and/or DHEA (10^{-6} M or 10^{-7} M) before Mtb infection (MOI 5:1). Production of TNFα, sTNFRI, IL1-β and IL10 (pg/ml) was measured in culture supernatants using ELISAs kits. The values are means ± SEM (n = 5). Mtb: *M. tuberculosis*; Gc: Cortisol 10^{-6} M; DHEA: DHEA 10^{-6} M or 10^{-7} M.

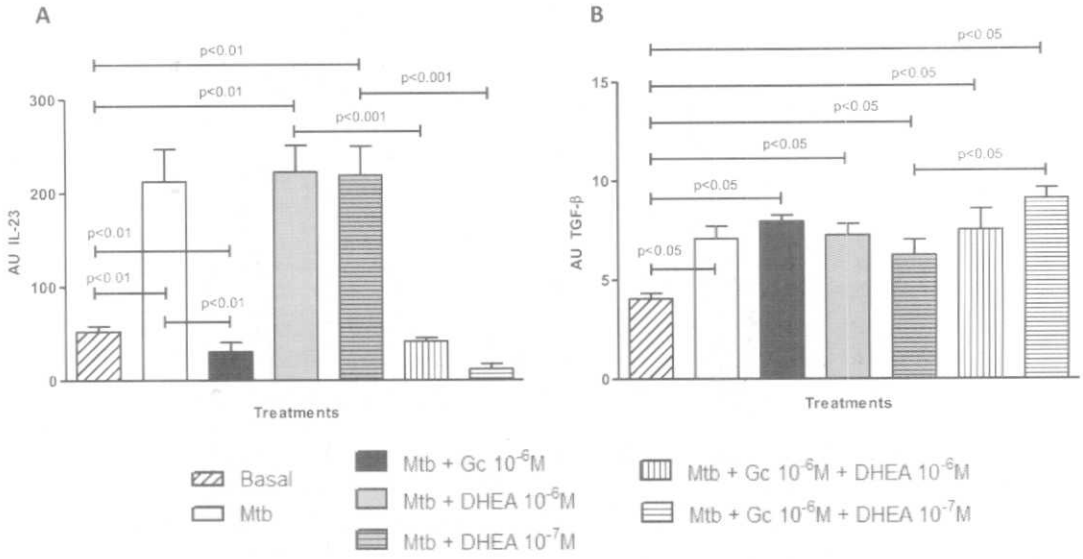

Figure 5. Effects of steroid hormones on cytokine gene expression in cells infected with *M. tuberculosis* H37Rv. Cells were incubated for 24 h in the presence or absence of Cortisol (10^{-6} M) and/or DHEA (10^{-6} M or 10^{-7} M) before Mtb infection (MOI 5:1). Gene expression of IL23 and TGF-β was measured in cells using real time RT-PCR. The values are means ± SEM (n = 5), of arbitrary units (**AU**). Mtb: *M. tuberculosis*; Gc: Cortisol 10^{-6} M; DHEA: DHEA 10^{-6} M or 10^{-7} M.

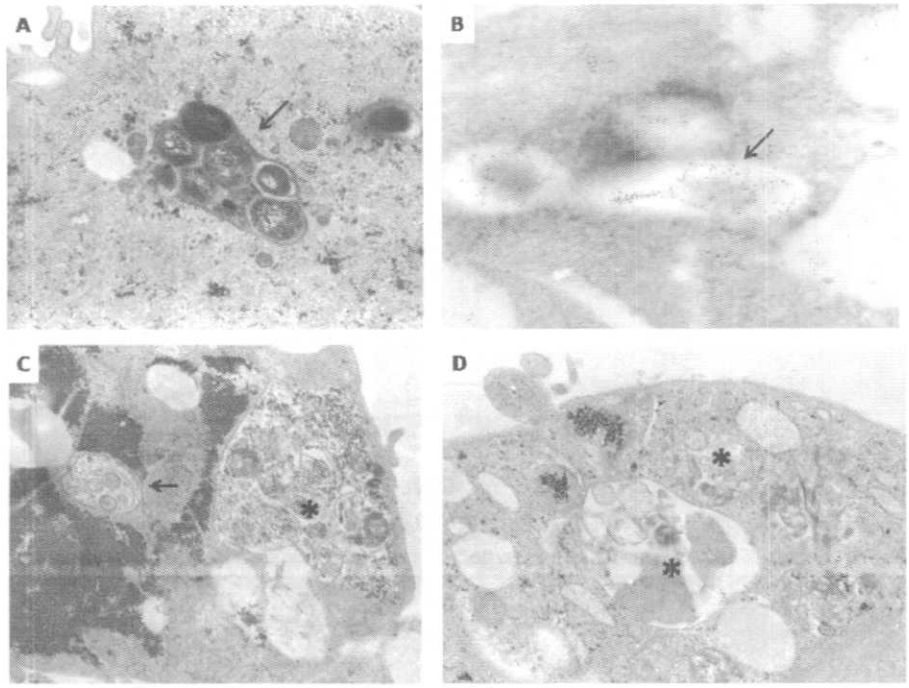

Figure 6. Representative electronmicroscopy and immunoelectronmicroscopy micrographs from infected macrophages incubated during 24h with adrenal steroids. A) The cytoplasm from an infected macrophage shows multi-vesicular structures corresponding to an autophagosome (arrow) (31,000x). B) These vacuoles show small black dots that correspond to immunogold labeling to the specific autophagosome specific marker LC3 (arrow) (63,000x). C) The cytoplasm from an infected macrophage incubated with DHEA (10^{-7} M) shows isolated (arrow) or conglomerate of autophagosomes (asterisk) (20,000x). D) Large autophagosomes (asterisks) are seen in the cytoplasm of macrophage incubated with Gc 10^{-6} M + DHEA 10^{-7} M (25,000x).

3.5. *Autophagosome formation*

Infected macrophages showed numerous cytoplasmic vacuoles, like primary lysosomes, phagosomes and autophagosomes. These latter organelles corresponded to multivescicular structures in which it was possible to recognize phagosomes associated with mitochondria, primary lysosomes or endoplasmic reticulum vacuoles. Autophagosomes were confirmed by the detection of the protein LC3 by immunoelectron microscopy an specific marker of these structures (Figure 6).

The total number of lysosomes, phagosomes and autophagosomes were assessed in 30 cells by experimental condition and the

number of autophagosomes was compared with the total number of cytoplasmic vacuoles. Control infected macrophages showed a mean of 13 ± 2 autophagosomes. A similar number was found when analyzing infected macrophages incubated with cortisol, whereas DHEA-treated macrophages displayed increased autophagosome numbers, in 10^{-6} M and 10^{-7} M concentrations, respectively, $p < 0.01$ (Figure 7). Some of these cells show bigger phagosomes forming large conglomerates (Figure 6).

Respect to cells infected and treated with both hormones (Gc + DHEA), the Gc 10^{-6} M + DHEA 10^{-6} M combination displayed values similar to infected cultures without hormones. Unlike this, Gc 10^{-6} M + DHEA 10^{-7} M had a higher amount of autophagosomes, some of them larger than those exhibited by infected macrophages without steroid hormones in the culture medium (Figure 6). Uninfected cells revealed no autophagosomes (data not shown).

4. Discusion

Macrophages engulf invading bacteria and kill them by the intracellular degradation system. However, some species of microorganisms, including *M. tuberculosis*, have strategies for evading intracellular degradation. These microorganisms can thrive in host phagocytes, favoring the development of infectious disease [23,24].

As with all complex organisms, single biological systems rarely work in isolation. There is extensive cross-talk between the immune and endocrine axis, together with the neural system, to form the major communication network in the body [25]. Cortisol is a glucocorticoid hormone secreted by the adrenal gland and plays a role in the stress response being also immunosuppressive [26]. DHEA and its sulphated precursor (DHEAS) have opposing actions to cortisol and may protect individuals from negative effects of aging and inflammation. They are secreted from the adrenal cortex and, in smaller amounts from testes and ovaries [27]. Confirming and extending former observations we here observed that cortisol has an immunosuppressive/anti-inflammatory effect given the decreased production of IL-1β, TNF-α in cultures exposed to this steroid. While, DHEA was unable to modify the pattern of cytokine production or to reverse the cortisol inhibitory effects; interestingly the intra-macrophagic bacterial burden was found reduced by DHEA treatment. This result adds further support to the beneficial effect of DHEA seen in previous studies from our group and other laboratories [13,14,28,29]. Studies during experimental tuberculosis also proved a protective effect of androstenediol and DHEA when administrated for 3 weeks, which is coincident with the phase of adrenal hyperplasia. Collectively, it follows that adrenal steroids are implicated in the pathogenesis of tuberculosis [30].

As regards the hormonal effects on phagocytosis, while cortisol decreased such function DHEA seemed to increase it in a dose-dependent manner. It is known that Mtb surface proteins interact with different receptors from host cell surface to mediate invasion beyond phagocytosis; i.e.,Toll-like receptors, mannose receptors, scavenger receptors, surfactant protein A and D receptors and complement receptors 1, 3 and 4 [31–33]. Whether DHEA is likely to modify receptor expressions and hence favoring Mtb entry without phagocytosis, remains to be established.

In relation to the reduced intra-macrophagic bacterial burden seen in single DHEA-treated cultures such findings could not be ascribed to a different cytokine pattern, in terms of their production or mRNA expression, suggesting that other mechanisms are accounting for the diminished bacterial load.

As regards to the mechanisms dealing with mycobacterial clearance, the induction of both apoptotic and necrotic cell death has been reported during the onset of tuberculosis in Mtb–infected macrophages. Necrotic cell death may cause dissemination of intracellular pathogens, from the site of infection. In contrast, apoptotic cell death is accompanied by complete packaging of the pathogens within apoptotic bodies, which are immediately engulfed by neighboring phagocytes [34–38]. Added to it, autophagy has also been implicated in several physiological processes, with perturbations in the autophagy phenomenon being associated to different diseases including the infectious ones [39–41]. Vesicle expansion and formation of autophagosomes is controlled by two ubiquitin-like conjugation processes: the Atg12-Atg5-Atg16L1 complex formation, and the conjugation of Atg8/LC3 to phosphatidylethanolamine. Finally, the newly formed autophagosomes fuse with lysosomes in a process that requires recruitment of the small GTPase Rab7 [42–44]. Studies have demonstrated that stimulation of autophagy suppressed the intracellular survival of Mtb *in vitro*. Upon infection of macrophages, Mtb block phagosome maturation in order to survive but induction of autophagy facilitates phagosome-lysosome fusion and degradation of pathogen [9]. In our hands, a lower dose of DHEA promoted autophagy in Mtb-infected macrophages, regardless of cortisol, suggesting that the CFU decrease from 1-4 days may be achieved through this mechanism.

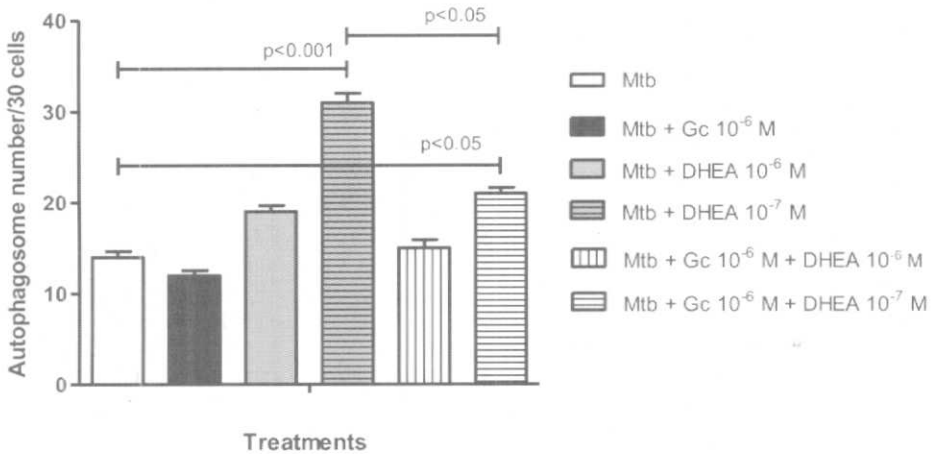

Figure 7. Effects of steroid hormones on autophagosome formation in cells infected with *M. tuberculosis* H37Rv. Cells were incubated for 24 h in the presence or absence of Cortisol (10^{-6} M) and/or DHEA (10^{-6} M or 10^{-7} M) before Mtb infection (MOI 5:1). Quantification of autophagosome numbers is represented in the graph. Values correspond to means ± SEM (n = 30 cells). Mtb: *M. tuberculosis*; Gc: Cortisol 10^{-6} M; DHEA: DHEA 10^{-6} M or 10^{-7} M.

In conclusion, DHEA in physiological conditions (that is in presence of cortisol) leads to autophagy induction and hence a better Mtb control. These results sound interesting since autophagy is not only important for bacterial clearance but also for the prevention of tissue damage [45]. Last but not least, present results add support to the use of DHEA as an adjuvant therapy for TB.

Funding: None.

Competing interests: None declared.

Ethical approval: Not required.

Acknowledgments

This study was supported by grants from the Consejo Nacional de Ciencia y Tecnología (CONACYT 253053) of México, Agencia de Promoción Científica y Tecnológica Argentina (PID160, ANPCyT) and Secretaria de Estado de Ciencia, Tecnología e Innovación de la Provincia de Santa Fe, Argentina [2010-140-11]. We thank Esmeralda Juarez PhD for her advice in Microbiology topics.

References

[1] World Health Organization. Global tuberculosis report. WHO report 2014. Available at: http://apps.who.int/iris/bitstream/10665/137094/1/9789241564809_eng.pdf?ua=1.
[2] Comstock GW. Epidemiology of tuberculosis. Am Rev Respir Dis 1982;125:8–15.
[3] Hestvik AL, Hmama Z, Av-Gay Y. Mycobacterial manipulation of the host cell. FEMS Microbiol Rev 2005;29:1041–50.
[4] Russell DG. Mycobacterium tuberculosis: here today, and here tomorrow. Nat Rev Mol Cell Biol 2001;2:569–77.
[5] Jordao L, Bleck CK, Mayorga L, Griffiths G, Anes E. On the killing of mycobacteria by macrophages. Cell Microbiol 2008;10:529–48.
[6] Clemens DL, Horwitz MA. Characterization of the *Mycobacterium tuberculosis* phagosome and evidence that phagosomal maturation is inhibited. J Exp Med 1995;181:257–70.
[7] Rohde K, Yates RM, Purdy GE, Russell DG. *Mycobacterium tuberculosis* and the environment within the phagosome. Immunol Rev 2007;219:37–54.
[8] de Chastellier C. The many niches and strategies used by pathogenic mycobacteria for survival within host macrophages. Immunobiology 2009;214:526–42.
[9] Gutierrez MG, Master SS, Singh SB, Taylor GA, Colombo MI, Deretic V. Autophagy is a defense mechanism inhibiting BCG and *Mycobacterium tuberculosis* survival in infected macrophages. Cell 2004;119(6):753–66.
[10] Castillo EF, Dekonenko A, Arko-Mensah J, Mandell MA, Dupont N, Jiang S, Delgado-Vargas M, Timmins GS, Bhattacharya D, Yang H, Hutt J, Lyons CR, Dobos KM, Deretic V. Autophagy protects against active tuberculosis by suppressing bacterial burden and inflammation. Proc Natl Acad Sci USA 2012;109(46):E3168–76.
[11] Cutolo M, Straub RH, Bijlsma JW. Neuroendocrine-immune interactions in synovitis. Nat Clin Pract Rheumatol 2007;3:627–34.
[12] Loria RM. Beta-androstenes and resistance to viral and bacterial infections. Neuroimmunomodulation 2009;16(2):88–95.
[13] del Rey A, Mahuad CV, Bozza VV, Bogue C, Farroni MA, Bay ML, Bottasso OA, Besedovsky HO. Endocrine and cytokine responses in humans with pulmonary tuberculosis. Brain Behav Immun 2007;21:171–9.
[14] Bottasso O, Bay ML, Besedovsky H, Del Rey A. Adverse neuro-immune-endocrine interactions in patients with active tuberculosis. Mol Cell Neurosci 2013;53:77–85.
[15] Bongiovanni B, Díaz A, D'Attilio L, Santucci N, Didoli G, Nannini JL, Gardeñez W, Bogue C, Besedovsky H, del Rey A, Bottasso O, Bay ML. Changes in the immune-endocrine response in patients with pulmonary tuberculosis undergoing specific treatment. Ann N Y AcadSci 2012;1262(1):10–5.
[16] Pieters J. *Mycobacterium tuberculosis* and the macrophage: maintaining a balance. Cell Host Microbe 2008;3:399–407.
[17] Fenton MJ, Vermeulen MW. Immunopathology of tuberculosis: roles of macrophages and monocytes. Infect Immun 1996;64:683–90.
[18] Carranza C, Juarez E, Torres M, Ellner J, Sada E. Mycobacterium tuberculosis growth control by lung macrophages and CD8 cells from patient contacts. Am J Respir Crit Care Med 2006;173:238–45.
[19] Tuchiya S, Yamabe M, Yamaguchi Y, Kobayashi Y, Konno T, Tada K. Establishment and characterization of a human acute monocytic leukemia cell line (THP-1). Int J Cancer 1980;26:171–6.
[20] Mahuad C, Bay ML, Farroni MA, Bozza V, Del Rey A, Besedovsky H, Bottasso OA. Cortisol and dehydroepiandrosterone affect the response of peripheral blood mononuclear cells to mycobacterial antigens during tuberculosis. Scand J Immunol 2004;60:639–46.
[21] D'Attilio L, Trini E, Bongiovanni B, Didoli G, Gardeñez W, Nannini L, Giri A, Bottasso A, Bay ML. mRNA expression of alpha and beta isoforms of glucocorticoid receptor in peripheral blood mononuclear cells of patients with TB and its relation with components of the immunoendocrine response. Brain Behav Immun 2011;25:461–7.
[22] Rivas-Santiago B, Schwander SK, Sarabia C, Diamond G, Klein-Patel ME, Hernandez-Pando R, Ellner JJ, Sada E. Human {beta}-defensin 2 is expressed and associated with *Mycobacterium* tuberculosis during infection of human alveolar epithelial cells. Infect Immun 2005;73:4505–11.
[23] Vergne I, Chua J, Lee HH, Lucas M, Belisle J, Deretic V. Mechanism of phagolysosome biogenesis block by viable *Mycobacterium tuberculosis*. Proc Natl Acad Sci USA 2005;102:4033–8.
[24] Divangahi M, Chen M, Gan H, Desjardins D, Hickman TT, Lee DM, Fortune S, Behar SM, Remold HG. Mycobacterium evades macrophage defenses by inhibiting plasma membrane repair. Nat Immunol 2009;10:899–906.
[25] Straub RH, Cutolo M, Zietz B, Scholmerich J. The process of aging changesthe interplay of the immune, endocrine and nervous systems. Mech Ageing Dev 2001;122(14):1591–611.
[26] Phillips AC, Carroll D, Gale CR, Lord JM, Arlt W, Batty GD. Cortisol, DHEAsulphate, their ratio, and all-cause and cause-specific mortality in theVietnam experience Study. Eur J Endocrinol 2010;163(2):285–92.
[27] Baylis D, Bartlett D, Patel H, Roberts H. Understanding how we age: insights intoinflammaging. Longev &Healthspan 2013;2:1–8.
[28] Mahuad C, Bozza V, Pezzotto SM, Bay ML, Besedovsky H, del Rey A, Bottasso O. Impaired immune responses in tuberculosis patients are related to weight loss that coexists with an immunoendocrineimbalance. Neuroimmunomodulation 2007;14(3–4):193–9.
[29] D'Attilio L, Bozza VV, Santucci N, Bongiovanni B, Didoli G, Radcliffe S, Besedovsky H, del Rey A, Bottasso O, Bay ML. TGF-β neutralization abrogates the inhibited DHEA production mediated by factors released from M. tuberculosis-stimulated PBMC. Ann N Y Acad Sci 2012;1262:1–9.
[30] Hernandez-Pando R, De La Luz Streber M, Orozco H, Arriaga K, Pavon L, Al-Nakhli SA, Rook GA. The effects of androstenediol and dehydroepiandrosterone on the course and cytokine profile of tuberculosis in BALB/c mice. Immunology 1998;95(2):234–41.
[31] Ernst JD. Macrophage receptors for *Mycobacterium tuberculosis*. Infec Immun 1998;66:1277–81.
[32] Rooyakkers AW, Stokes RW. Absence of complement receptor 3 results in reduced binding and ingestion of *Mycobacterium tuberculosis* but has no significant effect on the induction of reactive oxygen and nitrogen intermediates or on the survival of the bacteria in resident and interferon-gamma activated macrophages. Microb Pathog 2005;39:57–67.
[33] Ocampo M, Aristizábal-Ramírez D, Rodriguez DM, Muñoz M, Curtidor H, Vanegas M, Patarroyo MA, Patarroyo ME. The role of Mycobacterium tuberculosis Rv3166cprotein-derived high-activity binding peptidesin inhibiting invasion of human cell lines. Protein Eng Des Sel 2012;25(5):235–42.
[34] Fratazzi C, Arbeit RD, Carini C, Remold HG. Programmed celldeath of *Mycobacterium aviumserovar* 4-infected human macrophages preventsmycobacteria from spreading and induces mycobacterial growth inhibition byfreshly added, uninfected macrophages. J Immunol 1997;158:4320–7.
[35] Danelishvili L, McGarvey J, Li YJ, Bermudez LE. *Mycobacterium tuberculosis* infection causes different levels of apoptosis and necrosis in human macrophages and alveolar epithelial cells. Cell Microbiol 2003;5:649–60.
[36] Gil DP, Leon LG, Correa LI, Maya JR, París SC, García LF, Rojas M. Differential induction of apoptosis and necrosis in monocytes from patients with tuberculosis and healthy control subjects. J Infect Dis 2004;189:2120–8.
[37] Zhang J, Jiang R, Takayama H, Tanaka Y. Survival of virulent *Mycobacterium tuberculosis* involves preventing apoptosis induced by Bcl-2 upregulation and release resulting from necrosis in J774 macrophages. Microbiol Immunol 2005;2005(49):845–52.
[38] Iyoda T, Takada M, Fukatsu Y, Kumokoshi S, Fujisawa T, Shimada T, Shimokawa N, Matsunaga T, Makino K, Doi N, Terada H, Fukai F. A novel mechanism underlying the basic defensive response of macrophages against *Mycobacterium* infection. J Immunol 2014;192(9):4254–62.
[39] Pengo N, Scolari M, Oliva L, Milan E, Mainoldi F, Raimondi A, Fagioli C, Merlini A, Mariani E, Pasqualetto E, Orfanelli U, Ponzoni M, Sitia R, Casola S, Cenci S. Plasma cells require autophagy for sustainable immunoglobulin production. Nat Immunol 2013;14(3):298–305.
[40] Deretic V. Autophagy in immunity and cell-autonomous defense against intracellular microbes. Immunol Rev 2011;240(1):92–104.
[41] Levine B, Mizushima N, Virgin HW. Autophagy in immunity and inflammation. Nature 2011;469(7330):323–35.
[42] Deretic V, Saitoh T, Akira S. Autophagy in infection, inflammation and immunity. Nat Rev Immunol 2013;13:722–37.
[43] Perot BP, Ingersoll MA, Albert ML. The impact of macroautophagy on CD8(−) T-cell-mediated antiviral immunity. Immunol Rev 2013;255:40–56.
[44] Tang D, Kang R, Coyne CB, Zeh HJ, Lotze MT. PAMPs and DAMPs: signal 0s that spur autophagy and immunity. Immunol Rev 2012;249:158–75.
[45] Deretic V. Autophagy in tuberculosis. Cold Spring Harb Perspect Med 2014;4(11). http://dx.doi.org/10.1101/cshperspect.a018481.

Biochimica et Biophysica Acta 1848 (2015) 1157–1164

Contents lists available at ScienceDirect

Biochimica et Biophysica Acta

journal homepage: www.elsevier.com/locate/bbamem

Prolactin and the dietary protein/carbohydrate ratio regulate the expression of SNAT2 amino acid transporter in the mammary gland during lactation

Laura A. Velázquez-Villegas [a], Adriana M. López-Barradas [a], Nimbe Torres [a], Rogelio Hernández-Pando [b], Juan Carlos León-Contreras [b], Omar Granados [a], Victor Ortíz [a], Armando R. Tovar [a,*]

[a] Departamento de Fisiología de la Nutrición, Instituto Nacional de Ciencias Médicas y Nutrición Salvador Zubirán, México D.F. 14000, Mexico
[b] Departamento de Patología, Instituto Nacional de Ciencias Médicas y Nutrición Salvador Zubirán, México D.F. 14000, Mexico

ARTICLE INFO

Article history:
Received 17 November 2014
Received in revised form 24 January 2015
Accepted 10 February 2015
Available online 17 February 2015

Keywords:
Amino acid transport
Dietary protein/carbohydrate ratio
Lactation
Mammary gland
Prolactin
SNAT2

ABSTRACT

The sodium coupled neutral amino acid transporter 2 (SNAT2/SAT2/ATA2) is expressed in the mammary gland (MG) and plays an important role in the uptake of alanine and glutamine which are the most abundant amino acids transported into this tissue during lactation. Thus, the aim of this study was to assess the amount and localization of SNAT2 before delivery and during lactation in rat MG, and to evaluate whether prolactin and the dietary protein/carbohydrate ratio might influence SNAT2 expression in the MG, liver and adipose tissue during lactation. Our results showed that SNAT2 protein abundance in the MG increased during lactation and this increase was maintained along this period, while 24 h after weaning it tended to decrease. To study the effect of prolactin on SNAT2 expression, we incubated MG explants or T47D cells transfected with the SNAT2 promoter with prolactin, and we observed in both studies an increase in the SNAT2 expression or promoter activity. Consumption of a high-protein/low carbohydrate diet increased prolactin concentration, with a concomitant increase in SNAT2 expression not only in the MG during lactation, but also in the liver and adipose tissue. There was a correlation between SNAT2 expression and serum prolactin levels depending on the amount of dietary protein/carbohydrate ratio consumed. These findings suggest that prolactin actively supports lactation providing amino acids to the gland through SNAT2 for the synthesis of milk proteins.

1. Introduction

Lactation is a physiological process necessary to provide all nutrients to the newborns. This process is fundamental for all mammals, and it requires large amounts of building block substrates for the synthesis of proteins, triglycerides and lactose among others for the milk synthesis. Thus, circulating amino acids from the mother are actively taken up for protein synthesis. It has been evidenced that during the lactation period the most abundant amino acids transported into the mammary gland are alanine and glutamine [1] and are particularly important in regulating the amino acid intracellular pool. Specifically, glutamine is an efflux substrate for other amino acid transporters like the amino acid heteroexchanger system L (LAT1), facilitating the uptake of branched-chain amino acids, particularly leucine that activates the TOR pathway involved in protein synthesis [2,3].

These amino acids, alanine and glutamine, as well as other small neutral amino acids are mainly transported across membranes through System A which is comprised by three subtypes known as SNATs (sodium-coupled neutral amino acid transporters) 1, 2 and 4 [4]. However, SNAT2, which represents the classical characteristics of System A, is widely expressed in mammalian cells and is Na^+-dependent [5–7]. Additionally, SNAT2 is regulated by environmental conditions, proliferative stimuli, developmental changes, and hormonal signals [8].

Several studies showed that the mammary glands possess characteristics of System A activity [9,10], determined by using the non-metabolizable analog MeAIB. In addition, SNAT2 in the mammary gland shows a unique characteristic of this transport system observed in other cell types called adaptive regulation [11].

Abbreviations: BSA, bovine serum albumin; cAMP, cyclic adenosine monophosphate; CRE, cAMP response element; DAB, diaminobenzidine; ECL, enhanced chemiluminescence; HPRT1, hypoxanthine phosphoribosyl transferase 1; HPR, horseradish peroxidase; JaK2, janus kinase 2; MAPK, mitogen-activated protein kinase; MeAIB, methylaminoisobutyric acid; MG, mammary gland; MMLV, Moloney murine leukemia virus; PBS, phosphate-buffered saline; PI3K, phosphatidylinositol-4,5-bisphosphate 3-kinase; PKA, protein kinase A; PKB, protein kinase B; PVDF, polyvinylidene difluoride; RIA, radioimmunoassay; RIPA, radio-immunoprecipitation assay; RT-PCR, real time polymerase chain reaction; SNAT2, sodium-coupled neutral amino acid transporter 2; STAT5, signal transducer and activator of transcription 5; TBS, Tris-buffered saline

* Corresponding author at: Departamento de Fisiología de la Nutrición, Instituto Nacional de Ciencias Médicas y Nutrición Salvador Zubirán, Vasco de Quiroga No. 15 Col. Sección XVI, México D.F. 14000, Mexico. Tel./fax: +52 55 56553038.
E-mail address: tovar.ar@gmail.com (A.R. Tovar).

http://dx.doi.org/10.1016/j.bbamem.2015.02.011
0005-2736/

Several hormones play an important role in the regulation of SNAT2 gene expression in the mammary gland. There is evidence during gestation of an increase in the SNAT2 mRNA abundance in this tissue that is associated with concomitant changes in serum estradiol levels [12]. Recently, it has been demonstrated that upregulation of SNAT2 gene expression during gestation is mediated by the estrogen receptor α bound to the coactivator glyceraldehyde 3-phosphate dehydrogenase that specifically binds to an estrogen response element found in the SNAT2 gene promoter [13]. Interestingly, we have evidence that after gestation, there is a second increase of SNAT2 mRNA that reaches its maximal in the peak of lactation in the mammary gland [12]. There is preliminary evidence that suggests that prolactin could be responsible for the maintenance and regulation of this amino acid transporter during lactation, however this has not been established.

Prolactin is a single polypeptide with a molecular weight of 23 kDa that is produced in the pituitary gland [14]. This hormone is secreted with a pulsatile pattern during this physiological stage [15]. Prolactin has two receptor isoforms, a long- and a short-isoform [16]. Interestingly, the mammary gland during lactation mainly expresses the long-isoform which activates several signaling pathways, particularly those involving JAK2/STAT5, PI3K/PKB and MAPK [14]. It is known that prolactin is involved in the activation of the expression of several genes that include the β-casein gene to synthesize one of the most abundant proteins in milk *via* the STAT5 transcription factor [17]. Therefore, in order to sustain an elevated rate of milk protein synthesis, the supply of large amounts of amino acids is necessary. There is evidence that the expression of several amino acid transporters is up-regulated during lactation, including SNAT2 [18–20].

Interestingly, It has been demonstrated that incubation of mammary gland explants with prolactin increases the uptake of amino acids transported *via* System A [21]. However, there are no studies that have established whether prolactin in fact increases the expression of SNAT2 in the mammary gland.

Moreover, it has been demonstrated that the circulating levels of prolactin are dependent on the amount of dietary protein consumed. The lower the amount of protein, the lower the concentration of serum prolactin [22]. As a result there is a decrease in milk production that is reflected in the growth pattern of the pups. It is important to study whether the changes in the dietary protein/carbohydrate ratio may affect the expression of SNAT2 not only in the mammary gland but also in other tissues such as the adipose tissue and liver. It has been demonstrated that the prolactin receptor is present in these tissues among others [23–27]. However, there is no knowledge whether during lactation the SNAT2 gene is regulated in a similar fashion in these tissues compared with the mammary gland.

Therefore, the aim of the present work was to demonstrate if there are changes in SNAT2 protein abundance before delivery and during lactation, to study if prolactin was able to increase the expression and promoter activity of SNAT2 in mammary gland explants and T47D cells and finally, to establish whether the dietary protein/carbohydrate ratio may influence serum prolactin levels and SNAT2 gene expression in the mammary gland, liver and adipose tissue.

2. Materials and methods

The experimental design and procedures of this study were reviewed and approved by the Animal Care Committee of the Instituto Nacional de Ciencias Médicas y Nutrición, México, in accordance with the international guidelines for the use of animals in research.

2.1. Animals

This study was divided into two independent studies in order to achieve the objectives described.

2.1.1. Study 1

This study was designed to determine the change in SNAT2 gene expression during late gestation and lactation. Female Wistar rats weighing 200–250 g were obtained from the animal research facility at the Instituto Nacional de Ciencias Médicas y Nutrición. The animals were housed in individual stainless steel cages at 21 °C with a 12:12 h light–dark cycle. The animals were allowed free access to water and chow diet. Gestational age was determined by vaginal smear to detect spermatozoa. Mammary gland explants were obtained as previously reported [11] from pregnant rats at day 20, lactating rats at days 5, 12, and 18, or weaning (rats 21 days postpartum separated from their pups for 24 h). After normal pregnancy and delivery, the litter size was adjusted to 8 pups/dam. Five rats per group were used.

2.1.2. Study 2

This study was designed to determine if dietary protein modifies SNAT2 protein abundance during late gestation and lactation. The rat strain, the maintenance thereof, and the gestational age determination were the same as study 1. The animals were allowed free access to water and to a low-protein/high-carbohydrate (10/73%), normal-protein/normal-carbohydrate (20/63%) or high-protein/low-carbohydrate (30/53%) diets, according to the American Institute of Nutrition (AIN93) lab rodent diet recommendations [28]. The adipose tissue, liver and mammary gland were obtained from pregnant rats on day 20, or rats that had been lactating for 5 and 12 days. After delivery, the litter size was adjusted to 8 pups/dam. Five rats per group were used. The food intake of the dams was recorded daily, and the dams and pups were weighed every other day.

2.2. Quantitative real-time PCR

Total RNA was extracted from the mammary gland by the guanidinium thiocyanate–cesium chloride method as previously described [12]. The RNA concentration was measured using a NanoDrop spectrophotometer 1000 (ND-1000; Thermo Scientific, Wilmington, De, USA). RNA integrity was corroborated by visualizing the 28S and 18S ribosomal subunits in a 1% (w/v) agarose gel and quality was assessed with the 260/280 nm ratio absorbance of 2.0. RNA (3 μg) was reverse-transcribed to cDNA by the use of Moloney murine leukemia virus (MMLV) reverse transcriptase (Invitrogen). For the real-time PCR analyses, 300 ng of cDNA was used in a final reaction volume of 10 μl per reaction. Predesigned TaqMan assay (Applied Biosystems, Foster City, CA, USA) probes for sodium-coupled neutral amino acid transporter SNAT2 (Rn00710421_m1) and HPRT1 (hypoxanthine phosphoribosyl transferase 1) (Rn01527840_m1) were used. RT-PCR was performed using the following PCR amplification conditions: denaturation for 5 min at 95 °C, annealing for 1 min at 56.2 °C, extension for 1.30 min at 72 °C for 34 cycles; and final extension for 7 min at 72 °C. The amplification and detection of specific products was performed with the ABI PRISM 7000 (Applied Biosystems). The mRNA level of the SNAT2 was normalized to the HPRT1 gene. HPRT1 was used as a housekeeping gene since cyclophilin or β-actin showed great variation among samples. The relative amount of mRNA was calculated using the comparative CT method (User Bulletin no. 2; PE Applied Biosystems).

2.3. Western blot

Proteins were extracted from the mammary gland, liver and adipose tissue using RIPA (radio-immunoprecipitation assay) lysis buffer containing the following: 50 mmol/l Tris–HCl, pH 7.4, 150 mmol/l NaCl, 1% NP40, 0.25% Na-deoxycholate, and 1 mmol/l PMSF. We added a 1× Roche mini complete protease mixture. The protein concentration was measured in duplicate using the Lowry method. Before being loaded, the samples were prepared by mixing 40 μg of protein with Laemmli buffer in a 1:1 ratio and heated at 80 °C for 5 min.

The proteins were separated by electrophoresis on a polyacrylamide gel (8% v/v), and transferred onto a polyvinylidene difluoride (PVDF) membrane (Amersham GE Healthcare). For gel electrophoresis and semi-dry transfer, we used a Tris/glycine buffer. After transfer, the membranes were blocked with 5% (w/v) non-fat milk blocking solution with 1 × Tris-buffered saline (TBS) and 0.1% Tween 20 for 1 h. The membranes were incubated overnight at 4 °C with the different primary antibodies as follows: SNAT2 (Santa Cruz Biotechnology, sc-166366, 1:800), and β-actin (Santa Cruz Biotechnology, sc-1615, 1:1000), which were diluted in TBS, 5% (w/v) non-fat milk and 0.1% Tween 20. We used different secondary HRP (horseradish peroxidase) conjugated antibodies as follows: anti-mouse IgG-HRP (Santa Cruz Biotechnology, sc-2005, 1:3500) and anti-goat IgG-HRP (Santa Cruz Biotechnology, sc-2768, 1:3500) diluted in TBS, 5% (w/v) non-fat milk and 0.1% Tween 20. The chemiluminescence produced was measured using the Amersham Enhanced Chemiluminescence (ECL) detection reagents by exposure to X-ray film.

2.4. Immunohistochemistry

For the immunohistochemistry examination, rat mammary gland was obtained from pregnant rats at day 20, or lactating rats at 5 and 12 days. Before staining, tissue sections were immersed in 10% (v/v) hydrogen peroxide (H_2O_2)/methanol for 15 min, washed in two changes of distilled water (2 × 5 min) and deparaffinized through xylene and different percentages of ethanol (100, 95, and 70% twice). Sections were rinsed in phosphate-buffered saline (PBS), pH 7.4, and blocked for 30 min in 3% (v/v) bovine serum albumin (BSA) in PBS. The primary antibody used was mouse polyclonal affinity-purified IgG anti-SNAT2 or 0.1 MPBS instead of primary antibodies for negative controls. Primary antibodies were incubated overnight for 18 h at 4 °C. Conventional immunohistochemistry was performed using a biotinylated goat anti-mouse secondary antibody. After extensive wash using PBS, the color reaction was developed with diaminobenzidine (DAB; Sigma-Aldrich) in PBS and 30% (v/v) H_2O_2 for about 10 min. Slides were washed with deionized water, air-dried, and counterstained.

2.5. Preparation of mammary tissue explants

Mammary tissue explants were prepared as described previously [11]. Briefly, rats were anesthetized and the mammary gland was immediately removed and placed at 37 °C in 30 ml of Krebs–Ringer bicarbonate buffer, pH 7.4, equilibrated with 95% O_2–5% CO_2 and contained the following (in mmol/l): 141 NaCl, 5.6 KCl, 3.0 $CaCl_2$, 1.4 KH_2PO_4, 1.4 $MgSO_4$, 24.6 $NaHCO_3$, and 11 glucose. After the removal of the connective tissue, the mammary tissue was diced into 2- to 5-mg explants. The tissue explants were rinsed repeatedly with buffer at 37 °C prior to assay. The explants were incubated in the presence of 0, 25, 250 or 2500 ng/ml of prolactin for 1 h. Subsequently, the mammary tissue was used to determine the SNAT2 gene expression by quantitative real-time PCR and western blot techniques as mentioned above.

2.6. Transfection and reporter gene assays

Human T47D mammary gland ductal carcinoma cells that express the prolactin receptor were grown in RPMI (Roswell Park Memorial Institute) medium supplemented with 5% fetal bovine serum, L-glutamine (2 mM), penicillin (100 U/ml), and streptomycin (100 μg/ml) at 37 °C in a 5% CO_2 incubator. The p-SNAT2 promoter (−1872 to +265 bp) construct was inserted in the pGL3 basic vector (Promega, Fitchburg, WI, USA), which contained a luciferase reporter gene. T47D cells (150,000 cells/well) were plated in 12-well plates in RPMI medium, supplemented with 5% fetal bovine serum (FBS) 24 h before transfection. Transient transfection on Human T47D cells was performed with 0.25 μg of the p-SNAT2 luciferase reporter gene construct and 0.01 μg of pRL-TK Renilla expression vector (Promega, Fitchburg, WI, USA), used as an internal control to normalize the transfection efficiency, using the PolyFect (Qiagen) reagent according to the manufacturer's instructions. After transfection, the cells were incubated with different concentrations of prolactin (2, 20, 200, 2000 or 20,000 ng/ml) or without prolactin referred as control. Luciferase activity was measured as relative light units with a Veritas microplate luminometer (Turner Biosystems, Sunnyvale, CA). Each transfection was performed in triplicate, and three independent experiments were performed for each construct.

2.7. Serum prolactin quantification

Prolactin determinations were done in duplicate by specific radioimmunoassay (RIA) using reagents and protocols provided by the National Hormone and Peptide Program (Torrance, CA 90509, USA). The results are expressed in terms of the international reference standard NIDDK-rPRL-RP-3. The coefficients of variation intra- and interassay were 8.7 and 14.1, respectively. All samples were analyzed together to eliminate interassay variability.

2.8. Statistical analysis

The results are reported as the means ± SEM and gene expression data were tested using a 1-way and 2-way ANOVA, and significant differences among groups were analyzed by Bonferroni adjustments. The linear regression method was used to analyze correlations. Differences were considered significant at $P < 0.05$.

3. Results

3.1. Protein expression of SNAT2 in the mammary gland during gestation and lactation

The western blot analysis revealed that SNAT2 protein abundance in the mammary gland increased during lactation. From delivery until day 5 of lactation, there was an increase of about 11.7-fold, and this was maintained until the peak of lactation (days 12 and 18). After 24-h weaning SNAT2 protein tended to decrease however it did not reach statistical significance (Fig. 1A, B). To determine the cellular localization of SNAT2, immunohistochemistry was performed in the mammary gland from pregnant, lactating and weaning rats. The mammary gland from rats after delivery showed a poor SNAT2 immunostaining (Fig. 1C). In contrast, at days 5 and 12 of lactation (Fig. 1D, E respectively) a strong SNAT2 immunostaining was seen in alveolar cells, while during weaning a decrease of immunoreactivity was observed (Fig. 1F). These results well correlated with the expression of SNAT2 protein studied with western blot (Fig. 1A, B).

3.2. Effect of prolactin on the expression of SNAT2

Prolactin stimulated SNAT2 mRNA and protein abundance in mammary gland explants. Incubation of explants with 25 ng/ml for 6 h significantly stimulated SNAT2 concentration by approximately 24%, and with 250 ng/ml the increment in the protein abundance was about 49%. Further increase in the concentration of prolactin did not have an additional stimulation in the SNAT2 protein concentration (Fig. 2A).

We then performed a time course analysis to assess the effect of prolactin on the expression of SNAT2 in mammary gland explants. For this study we added 250 ng/ml of prolactin to the explants. Our data clearly showed that prolactin was able to significantly stimulate SNAT2 expression in mammary gland explants, and this response initiated at about 6 h of incubation reaching the maximal response after 8 h of incubation by approximately 4.5-fold. Then, after 10 h of incubation we observed a sharp decrease in the expression of this transporter (Fig. 2B).

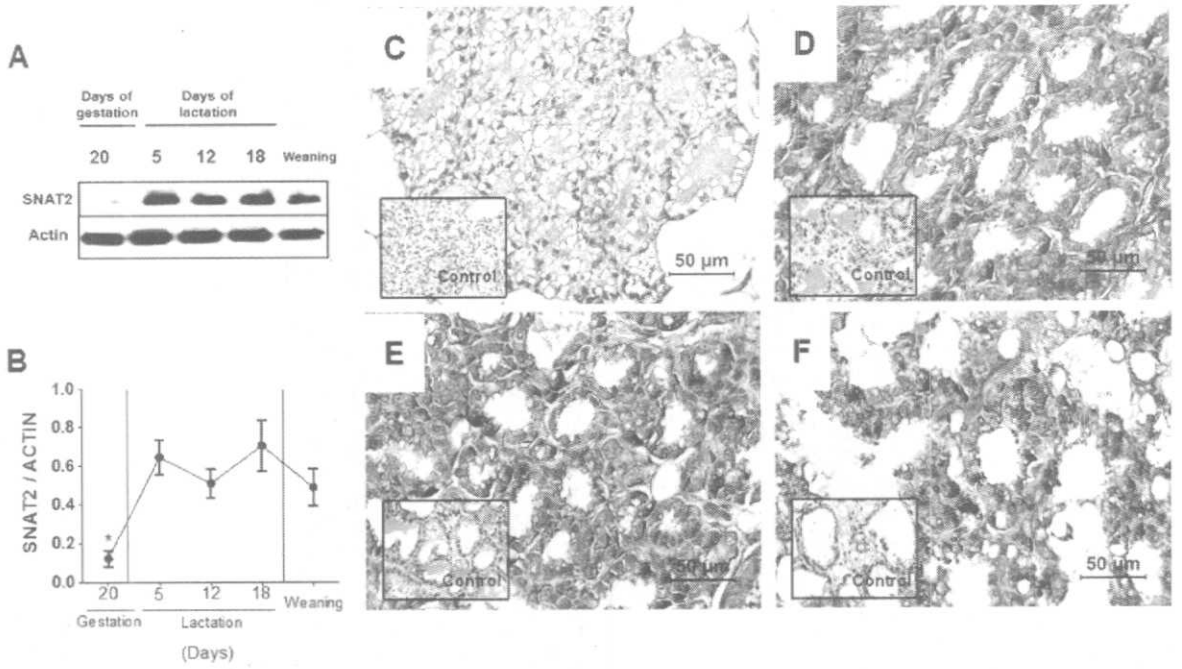

Fig. 1. SNAT2 protein abundance in rat mammary gland. A) A representative immunoblot of SNAT2 and actin as constitutive protein of gestation day 20; lactation days 5, 12, and 18; and weaning. B) Western blot densitometric analysis of SNAT2/actin. Values are the mean ± SEM of three different blots. n = 5. Representative immunohistochemistry of SNAT2 detection in different physiological phases of the mammary gland. C) Day 20 of gestation shows almost negative SNAT2 detection D) at day 5 and E) day 12 of lactation there is a strong SNAT2 immunostaining in lobular epithelial cells. F) During weaning there is a mild SNAT2 immunostaining (all micrograph scale bars: 50 µm).

In addition, luciferase reporter gene assays in T47D cells using the SNAT2 promoter region showed a significant increase in the luciferase activity after incubating with 20, 200, 2000 and 20,000 ng/ml compared to the control without prolactin stimulus. The maximum effect was observed with 200 ng/ml concentration having a two-fold increase in the SNAT2 promoter activity (Fig. 2C). These results demonstrate that prolactin is able to activate SNAT2 transcription *in vitro*.

3.3. Effect of the dietary protein/carbohydrate ratio in the diet on the expression of SNAT2

To determine whether the supply of the amino acid/carbohydrate ratio, provided by the consumption of different amounts of dietary protein, could modify SNAT2 expression after delivery and during lactation in different tissues (mammary gland, liver and white adipose tissue), we measured the expression of the SNAT2 protein abundance in these tissues from rats fed with a low-protein/high-carbohydrate (10/73%), or a normal-protein/normal-carbohydrate (20/63%) or a high-protein/low-carbohydrate (30/53%) diet. We observed that SNAT2 was expressed in the mammary gland, as well as in the white adipose tissue and liver as has been previously reported [29]. In the mammary gland we found the same SNAT2 protein abundance just before delivery independently of the amount of dietary protein/carbohydrate ratio consumed. Interestingly, during the lactation period SNAT2 protein abundance increased as the dietary protein/carbohydrate ratio increased, particularly on days 5 and 12 of lactation (Fig. 3A).

In the liver and adipose tissue we observed a different expression pattern depending on the dietary protein/carbohydrate ratio before delivery. Rats fed with a high-protein/low-carbohydrate (30/53%) diet showed a significant increase in the SNAT2 protein abundance, in contrast with the results observed in the mammary gland. However, during lactation, SNAT2 protein expression followed a similar trend than the observed in the mammary gland with a significant increase of the SNAT2 protein depending on the dietary protein/carbohydrate ratio (Fig. 3B, C).

3.4. Prolactin concentration during lactation increased as the dietary protein/carbohydrate ratio increased and correlated with SNAT2 expression

To determine whether the increase in SNAT2 expression was associated with an increase in prolactin concentration as a consequence of the dietary protein/carbohydrate ratio, we measured serum prolactin concentration during lactation. We observed that serum prolactin levels increased as dietary protein/carbohydrate ratio increased during lactation (Fig. 3D). Interestingly, we found a significant correlation between SNAT2 protein concentration and serum prolactin levels ($r^2 = 0.9854$, 0.8935 and 0.9177 in the mammary gland, adipose tissue and liver respectively) on day 12 of lactation (Fig. 4A–C).

4. Discussion

Amino acids are essential nutrients for protein synthesis and other metabolic functions. Particularly, during the lactation period there is a sharp increase in the amino acid requirements to support the milk protein synthesis in the mammary gland. Amino acids are captured into the cells by amino acid transporters, which play an important role in this physiological period to supply the amount of amino acids required. In our study we showed that the expression of SNAT2, one of the most abundant amino acid transporters, was regulated in the mammary gland by prolactin stimuli as well as by the dietary protein/carbohydrate ratio during lactation.

We observed an increase of the SNAT2 protein abundance in the mammary gland on day 5 of lactation. It is known that prolactin rapidly rises in the first days of lactation as we also demonstrated by measuring the serum levels of this hormone; therefore prolactin could contribute to the up-regulation of SNAT2 protein abundance. In fact, we also showed that prolactin can regulate the expression of this transporter in mammary gland explants by incubating the tissue in the presence of physiological levels reached by this hormone during the lactation period. It is important to discuss that in this study, we decided to use mammary gland explants from lactating rats because they are mainly

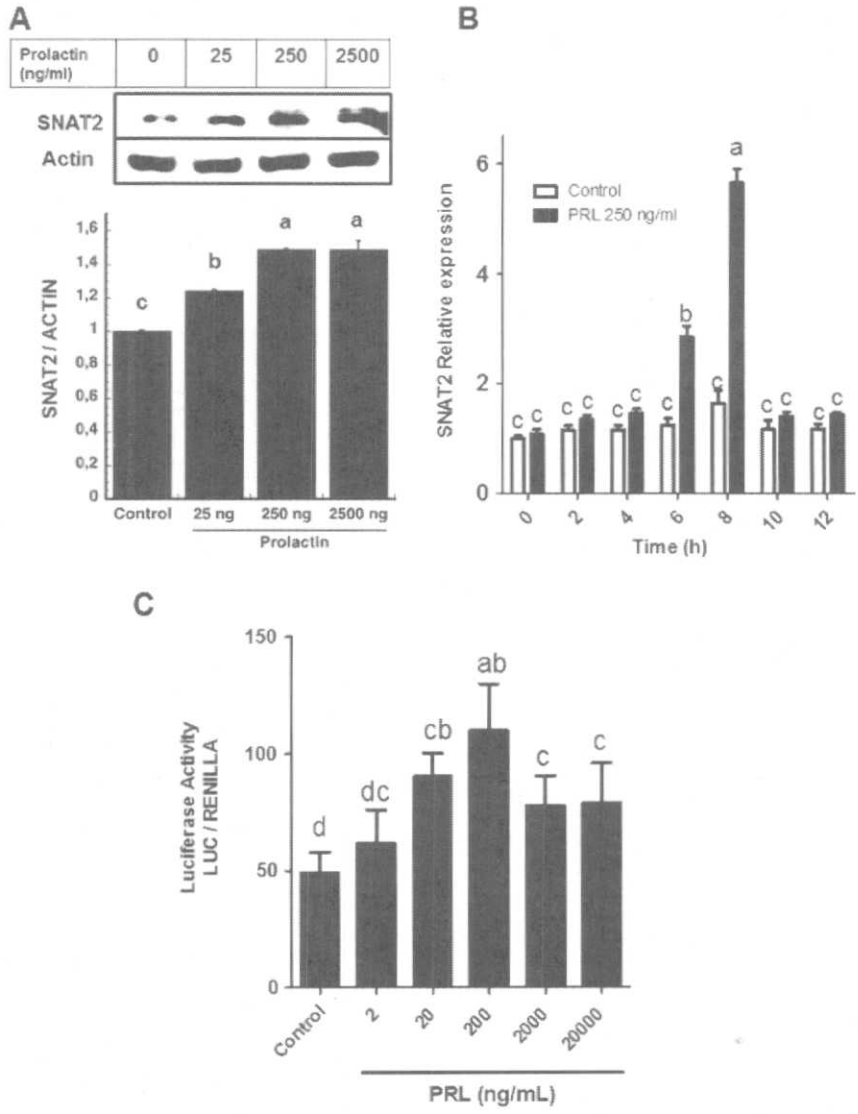

Fig. 2. Effect of prolactin in SNAT2 expression in rat mammary gland and T47D cells. A) A representative immunoblot of SNAT2 and actin, as constitutive protein, of mammary gland explants at day 12 of lactation incubated with 25, 250 and 2500 ng/ml of prolactin and western blot densitometric analysis of SNAT2/actin of mammary gland explant lactation day 12 in the presence of different concentrations of prolactin. B) Time course (0, 2, 4, 6, 8, 10, 12 h) of SNAT2 relative mRNA levels in rat mammary gland explants incubated with 250 ng/ml of prolactin. Values are the mean ± SEM of three different blots. n = 5. C) Effect of prolactin (PRL) on SNAT2 promoter activity in T47D mammary ductal carcinoma cells co-transfected with SNAT2 promoter–reporter construct and pRL-TK (Renilla expression vector for normalization), and incubated in the presence of different concentrations (2, 20, 200, 2000 or 20,000 ng/ml) of PRL or without stimulus (control). The results are the mean ± SEM of 3 independent experiments. Different letters differ: a > b > c > d. $P < 0.05$.

conformed by epithelial cells, in comparison to non-lactating mammary glands which have a considerable amount of adipose tissue. However, the effect of exogenous prolactin in this experiment could be misinterpreted by using already lactating dams that have been stimulated *in vivo* by the endogenous increase of this hormone. To clarify the effect of prolactin in SNAT2 expression we performed additional *in vitro* studies in T47D cells using the promoter region of this gene, and incubating the cells in the presence or absence of prolactin. Our results demonstrated that physiological levels during lactation of this hormone were able to significantly increase SNAT2 promoter activity in T47D cell line.

Viña and colleagues reported arteriovenous changes of amino acids across the mammary gland, and that prolactin can regulate the amino acid uptake by this tissue. Interestingly they observed a decrease in the uptake of the SNAT2 substrates, specially alanine and glutamine by adding the prolactin inhibitor bromocriptine [1]. Our data as well as those observed by other authors suggest that the activity of SNAT2 could be stimulated by prolactin during the first days of lactation in the mammary gland.

Interestingly, the SNAT2 protein abundance in the mammary gland on day 12 of lactation, which corresponds to the maximal peak of milk production in the rat, was dependent on the dietary protein/carbohydrate ratio consumed. It has been explored whether the amount of dietary protein could affect the levels of circulating prolactin. Moretto et al. clearly demonstrated that in fact when rats consumed a low protein diet, the concentration of serum prolactin was significantly reduced [22]. Our results also demonstrated that the dietary protein/carbohydrate ratio influences the serum prolactin concentration. This may imply that the reduction of prolactin decreases SNAT2 expression or that the dietary protein/carbohydrate ratio can directly modulate the expression of this gene possibly *via* cAMP, as has been reported in the liver [30]. Further studies are needed to dissect this mechanism.

Interestingly, the mechanisms involved in the regulation of SNAT2 expression in the mammary gland during gestation and lactation are

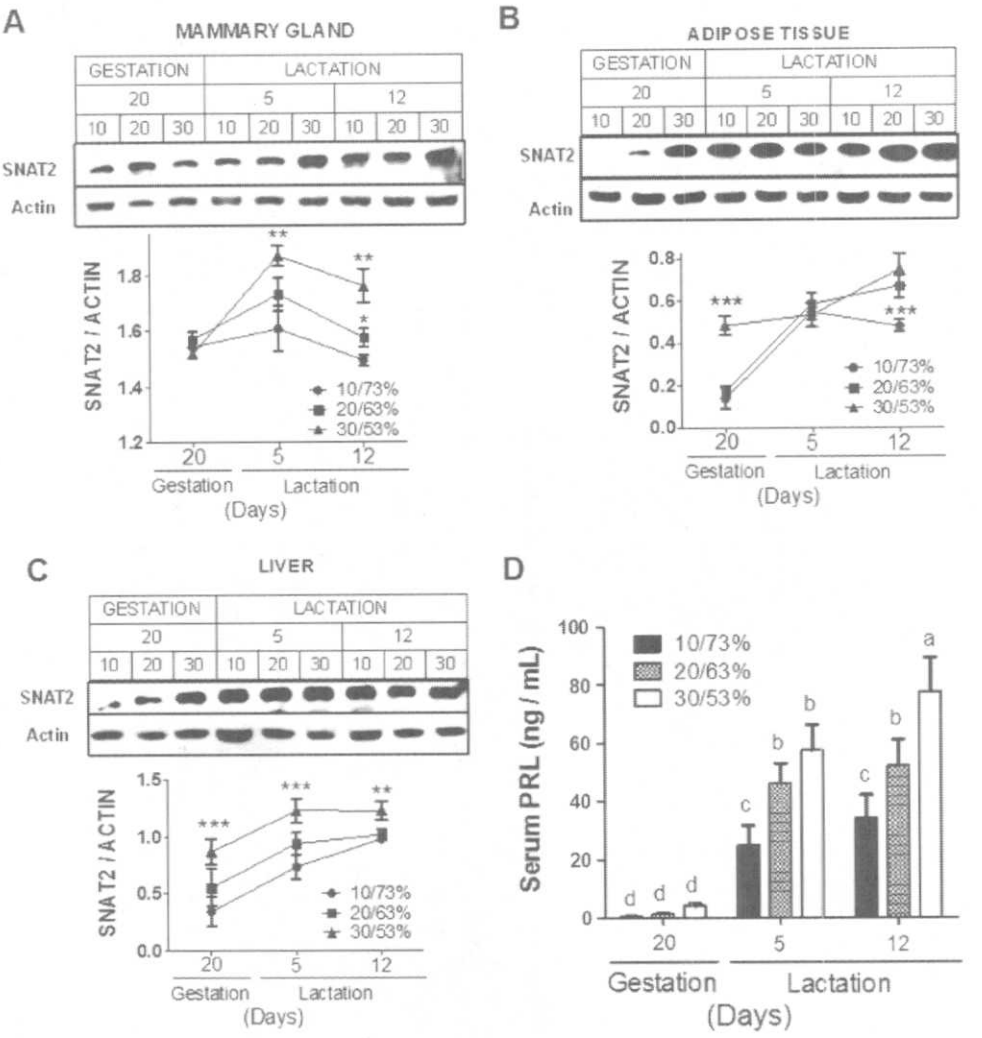

Fig. 3. Effect of dietary protein/carbohydrate ratio in SNAT2 protein abundance and serum prolactin levels. A representative immunoblot and western blot densitometric analysis of SNAT2/Actin in rat A) mammary gland, B) adipose tissue and C) liver; and D) prolactin serum levels during gestation day 20 and lactation days 5 and 12 of rats fed a low-protein/high-carbohydrate (10/73%), normal-protein/normal-carbohydrate (20/63%), or high-protein/low-carbohydrate (30/53%) diet. Values are the mean ± SEM of three different blots. n = 5. *P < 0.05, **P < 0.01, ***P < 0.001. Different letters differ: a > b > c > d. P < 0.05.

not systemic. The SNAT2 protein abundance followed a different pattern of expression in the liver and adipose tissue with respect to the mammary gland during the last day of gestation. Before delivery, the expression of this transporter was not modified in the mammary gland due to the dietary protein/carbohydrate ratio consumed, whereas during lactation there was an increase in SNAT2 expression that was dependent on this ratio. It is known, that during lactation rats increase their food intake by 300% [31,32]. Therefore, the supply of amino acids is significantly increased when rats consumed a high protein diet as has been previously reported [33]. It has been demonstrated that an increase in the amount of dietary protein, stimulates the serum glucagon levels, which in turn upregulates the expression of SNAT2 *via* PKA in the liver, since the SNAT2 promoter gene contains a cAMP response element (CRE) at −48 bp [30].

On the other hand, serum prolactin levels, modulated by the dietary protein/carbohydrate ratio, can directly regulate the expression of this transporter by activating its classical pathway mediated by the prolactin receptor not only in the mammary gland but also in other tissues such as the liver and adipose tissue. The long form of the prolactin receptor is expressed in the liver and adipose tissue [34,35], and prolactin plays important roles in these organs during lactation. Moreno-Carranza and colleagues demonstrated that prolactin promotes hepatic cell proliferation and survival, especially in neonates and lactating female rodents [36]. In these stages, SNAT2 amino acid transporter regulated by this hormone could be involved in this process. In the adipose tissue it is known that prolactin receptor is increased during lactation and differentiation, and that prolactin favors the adipogenesis process [37]. During the lactation period prolactin decreases lipogenesis and glucose uptake in the adipose tissue favoring the contribution of energy substrates to the mammary gland [38]. Further studies are needed to identify possible prolactin response elements in the SNAT2 gene to elucidate the molecular mechanism by which this hormone regulates its expression during lactation. *In silico* analysis revealed that the SNAT2 promoter contains a putative STAT3 response element that could be involved in the induction of this gene. We are conducting studies to understand the possible molecular mechanism by which prolactin stimulates the transcription of SNAT2 and its implication in several tissues during the lactation period.

5. Conclusion

The mammary gland during the lactation period requires an active uptake of amino acids to support the newborn needs. Our results suggest that prolactin actively supports lactation by providing amino

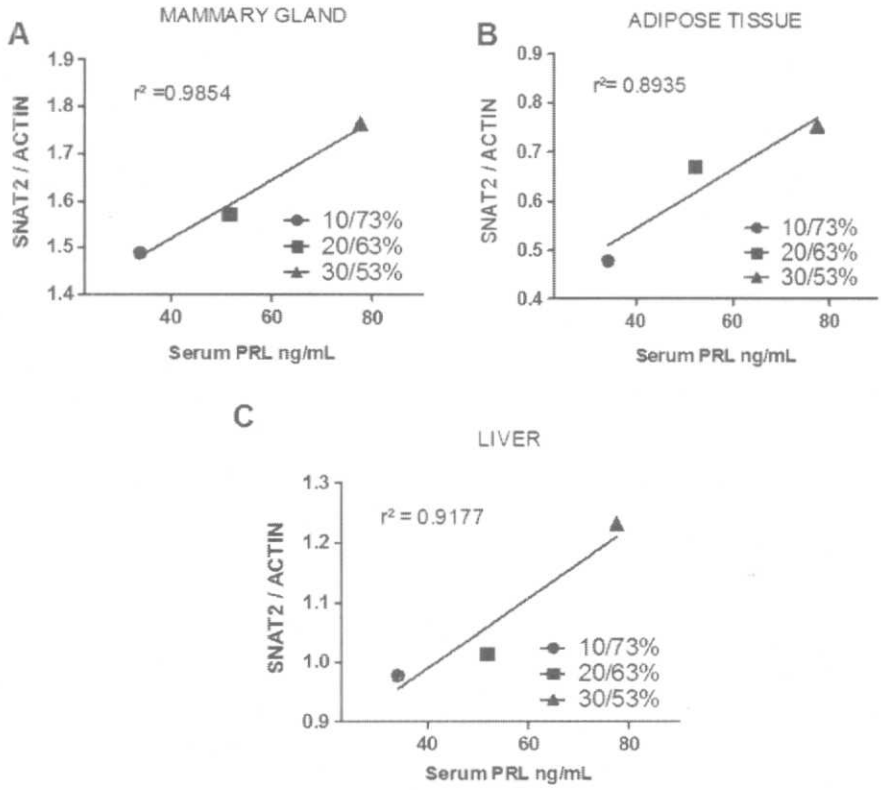

Fig. 4. Correlation between SNAT2 protein abundance and serum prolactin levels. Linear regression of rat A) mammary gland, B) adipose tissue and C) liver SNAT2 protein concentration and serum prolactin levels during lactation day 12 in rats fed a low-protein/high-carbohydrate (10/73%), normal-protein/normal-carbohydrate (20/63%), or high-protein/low-carbohydrate (30/53%) diet.

acids into the mammary epithelium through the activation of the expression of amino acid transporters, particularly SNAT2, for the synthesis of milk proteins. The dietary protein/carbohydrate ratio consumed also influenced SNAT2 abundance and correlated with serum prolactin levels not only in the mammary gland, but also in the liver and adipose tissue indicating a new way of regulation of this amino acid transporter expression.

Author contributions

ART and NT design research. LAVV, AMLB, JCLC and OG performed research. LAVV, AMLB, RHP and ART analyzed and interpreted the data. LAVV, AMLB, RHP and ART wrote the manuscript. All authors revised critically the manuscript and approved the final version to be submitted.

Disclosure statement

All authors declare no conflict of interest.

Transparency document

The Transparency document associated with this article can be found, in the online version.

Acknowledgments

This work was supported by the Consejo Nacional de Ciencia y Tecnología (CONACYT) Grant 154939 to ART. LAVV is grateful for a fellowship granted by CONACYT.

References

[1] J. Vina, I.R. Puertes, G.T. Saez, J.R. Vina, Role of prolactin in amino acid uptake by the lactating mammary gland of the rat, FEBS Lett. 126 (1981) 250–252.
[2] O. Bussolati, V. Dall'Asta, R. Franchi-Gazzola, R. Sala, B.M. Rotoli, R. Visigalli, J. Casado, M. Lopez-Fontanals, M. Pastor-Anglada, G.C. Gazzola, The role of system A for neutral amino acid transport in the regulation of cell volume, Mol. Membr. Biol. 18 (2001) 27–38.
[3] J. Pinilla, J.C. Aledo, E. Cwiklinski, R. Hyde, P.M. Taylor, H.S. Hundal, SNAT2 transceptor signalling via mTOR: a role in cell growth and proliferation? Front. Biosci. 3 (2011) 1289–1299.
[4] B. Mackenzie, J.D. Erickson, Sodium-coupled neutral amino acid (system N/A) transporters of the SLC38 gene family, Pflugers Arch. 447 (2004) 784–795.
[5] R.J. Reimer, F.A. Chaudhry, A.T. Gray, R.H. Edwards, Amino acid transport system A resembles system N in sequence but differs in mechanism, Proc. Natl. Acad. Sci. U. S. A. 97 (2000) 7715–7720.
[6] M. Sugawara, T. Nakanishi, Y.J. Fei, W. Huang, M.E. Ganapathy, F.H. Leibach, V. Ganapathy, Cloning of an amino acid transporter with functional characteristics and tissue expression pattern identical to that of system A, J. Biol. Chem. 275 (2000) 16473–16477.
[7] D. Yao, B. Mackenzie, H. Ming, H. Varoqui, H. Zhu, M.A. Hediger, J.D. Erickson, A novel system A isoform mediating Na^+/neutral amino acid cotransport, J. Biol. Chem. 275 (2000) 22790–22797.
[8] S.S. Palii, H. Chen, M.S. Kilberg, Transcriptional control of the human sodium-coupled neutral amino acid transporter system A gene by amino acid availability is mediated by an intronic element, J. Biol. Chem. 279 (2004) 3463–3471.
[9] M.C. Neville, C.J. Lobitz, E.A. Ripoll, C. Tinney, The sites for alpha-aminoisobutyric acid uptake in normal mammary gland and ascites tumor cells: a comparative study of mouse tissues in vitro, J. Biol. Chem. 255 (1980) 7311–7316.
[10] D.B. Shennan, S.A. McNeillie, Characteristics of alpha-aminoisobutyric acid transport by lactating rat mammary gland, J. Dairy Res. 61 (1994) 9–19.
[11] A.R. Tovar, E. Avila, S. DeSantiago, N. Torres, Characterization of methylaminoisobutyric acid transport by system A in rat mammary gland, Metabolism 49 (2000) 873–879.
[12] A. Lopez, N. Torres, V. Ortiz, G. Aleman, R. Hernandez-Pando, A.R. Tovar, Characterization and regulation of the gene expression of amino acid transport system A (SNAT2) in rat mammary gland, Am. J. Physiol. Endocrinol. Metab. 291 (2006) E1059–E1066.
[13] L.A. Velazquez-Villegas, V. Ortiz, A. Strom, N. Torres, D.A. Engler, R. Matsunami, D. Ordaz-Rosado, R. Garcia-Becerra, A.M. Lopez-Barradas, F. Larrea, J.A. Gustafsson, A.R. Tovar, Transcriptional regulation of the sodium-coupled neutral amino acid

transporter (SNAT2) by 17beta-estradiol, Proc. Natl. Acad. Sci. U. S. A. 111 (2014) 11443–11448.
[14] C. Bole-Feysot, V. Goffin, M. Edery, N. Binart, P.A. Kelly, Prolactin (PRL) and its receptor: actions, signal transduction pathways and phenotypes observed in PRL receptor knockout mice, Endocr. Rev. 19 (1998) 225–268.
[15] S.R. Valdez, A.B. Penissi, R.P. Deis, G.A. Jahn, Hormonal profile and reproductive performance in lactation deficient (OFA hr/hr) and normal (Sprague–Dawley) female rats, Reproduction 133 (2007) 827–840.
[16] J.F. Trott, A. Schennink, W.K. Petrie, R. Manjarin, M.K. VanKlompenberg, R.C. Hovey, Triennial Lactation Symposium: prolactin: the multifaceted potentiator of mammary growth and function, J. Anim. Sci. 90 (2012) 1674–1686.
[17] M. Wartmann, N. Cella, P. Hofer, B. Groner, X. Liu, L. Hennighausen, N.E. Hynes, Lactogenic hormone activation of Stat5 and transcription of the beta-casein gene in mammary epithelial cells is independent of p42 ERK2 mitogen-activated protein kinase activity, J. Biol. Chem. 271 (1996) 31863–31868.
[18] G. Aleman, A. Lopez, G. Ordaz, N. Torres, A.R. Tovar, Changes in messenger RNA abundance of amino acid transporters in rat mammary gland during pregnancy, lactation, and weaning, Metabolism 58 (2009) 594–601.
[19] D.B. Shennan, I.D. Millar, D.T. Calvert, Mammary-tissue amino acid transport systems, Proc. Nutr. Soc. 56 (1997) 177–191.
[20] C.R. Baumrucker, Amino acid transport systems in bovine mammary tissue, J. Dairy Sci. 68 (1985) 2436–2451.
[21] R. Sharma, V.K. Kansal, Characteristics of transport systems of L-alanine in mouse mammary gland and their regulation by lactogenic hormones: evidence for two broad spectrum systems, J. Dairy Res. 66 (1999) 385–398.
[22] V.L. Moretto, M.O. Ballen, T.S. Goncalves, N.H. Kawashita, L.F. Stoppiglia, R.V. Veloso, M.Q. Latorraca, M.S. Martins, M.H. Gomes-da-Silva, Low-protein diet during lactation and maternal metabolism in rats, ISRN Obstet. Gynecol. 2011 (2011) 876502.
[23] G.A. Jahn, M. Edery, L. Belair, P.A. Kelly, J. Djiane, Prolactin receptor gene expression in rat mammary gland and liver during pregnancy and lactation, Endocrinology 128 (1991) 2976–2984.
[24] C. Ling, G. Hellgren, M. Gebre-Medhin, K. Dillner, H. Wennbo, B. Carlsson, H. Billig, Prolactin (PRL) receptor gene expression in mouse adipose tissue: increases during lactation and in PRL-transgenic mice, Endocrinology 141 (2000) 3564–3572.
[25] C. Ling, L. Svensson, B. Oden, B. Weijdegard, B. Eden, S. Eden, H. Billig, Identification of functional prolactin (PRL) receptor gene expression: PRL inhibits lipoprotein lipase activity in human white adipose tissue, J. Clin. Endocrinol. Metab. 88 (2003) 1804–1808.
[26] M. Nagano, P.A. Kelly, Tissue distribution and regulation of rat prolactin receptor gene expression. Quantitative analysis by polymerase chain reaction, J. Biol. Chem. 269 (1994) 13337–13345.
[27] J. Yu, F. Xiao, Q. Zhang, B. Liu, Y. Guo, Z. Lv, T. Xia, S. Chen, K. Li, Y. Du, F. Guo, PRLR regulates hepatic insulin sensitivity in mice via STAT5, Diabetes 62 (2013) 3103–3113.
[28] P.G. Reeves, F.H. Nielsen, G.C. Fahey Jr., AIN-93 purified diets for laboratory rodents: final report of the American Institute of Nutrition ad hoc writing committee on the reformulation of the AIN-76A rodent diet, J. Nutr. 123 (1993) 1939–1951.
[29] R. Hyde, G.R. Christie, G.J. Litherland, E. Hajduch, P.M. Taylor, H.S. Hundal, Subcellular localization and adaptive up-regulation of the system A (SAT2) amino acid transporter in skeletal-muscle cells and adipocytes, Biochem. J. 355 (2001) 563–568.
[30] V. Ortiz, G. Aleman, M. Escamilla-Del-Arenal, F. Recillas-Targa, N. Torres, A.R. Tovar, Promoter characterization and role of CRE in the basal transcription of the rat SNAT2 gene, Am. J. Physiol. Endocrinol. Metab. 300 (2011) E1092–E1102.
[31] L. Barbosa, S. De Santiago, Effect of food consumption restriction in adult rats on the growth and tissue composition of their suckling offspring, Arch. Latinoam. Nutr. 44 (1994) 98–104.
[32] P.E. Millican, R.G. Vernon, V.M. Pain, Protein metabolism in the mouse during pregnancy and lactation, Biochem. J. 248 (1987) 251–257.
[33] L.A. Velazquez-Villegas, A.R. Tovar, A.M. Lopez-Barradas, N. Torres, The dietary protein/carbohydrate ratio differentially modifies lipogenesis and protein synthesis in the mammary gland, liver and adipose tissue during gestation and lactation, PLoS ONE 8 (2013) e69338.
[34] M.C. Barber, R.A. Clegg, E. Finley, R.G. Vernon, D.J. Flint, The role of growth hormone, prolactin and insulin-like growth factors in the regulation of rat mammary gland and adipose tissue metabolism during lactation, J. Endocrinol. 135 (1992) 195–202.
[35] N. Carre, N. Binart, Prolactin and adipose tissue, Biochimie 97 (2014) 16–21.
[36] B. Moreno-Carranza, M. Goya-Arce, C. Vega, N. Adan, J. Triebel, F. Lopez-Barrera, A. Quintanar-Stephano, N. Binart, G. Martinez de la Escalera, C. Clapp, Prolactin promotes normal liver growth, survival, and regeneration in rodents: effects on hepatic IL-6, suppressor of cytokine signaling-3, and angiogenesis, Regul. Integr. Comp. Physiol. 305 (2013) R720–R726.
[37] D. Fleenor, R. Arumugam, M. Freemark, Growth hormone and prolactin receptors in adipogenesis: STAT-5 activation, suppressors of cytokine signaling, and regulation of insulin-like growth factor I, Horm. Res. 66 (2006) 101–110.
[38] L.A. Nilsson, C. Roepstorff, B. Kiens, H. Billig, C. Ling, Prolactin suppresses malonyl-CoA concentration in human adipose tissue, Horm. Metab. Res. = Horm. Stoffwechselforschung = Horm. Metab. 41 (2009) 747–751.

Mol Cell Biochem (2015) 406:183–197
DOI 10.1007/s11010-015-2436-9

C-phycocyanin prevents cisplatin-induced mitochondrial dysfunction and oxidative stress

Berenice Fernández-Rojas[1] · Daniela Sarai Rodríguez-Rangel[1] · Luis Fernando Granados-Castro[1] · Mario Negrette-Guzmán[1] · Juan Carlos León-Contreras[2] · Rogelio Hernández-Pando[2] · Eduardo Molina-Jijón[3] · José L. Reyes[3] · Cecilia Zazueta[4] · José Pedraza-Chaverri[1]

Received: 29 January 2015 / Accepted: 6 May 2015 / Published online: 14 May 2015

Abstract The potential of C-phycocyanin (C-PC) to prevent cisplatin (CP)-induced kidney mitochondrial dysfunction was determined in CD-1 male mice. The CP-induced mitochondrial dysfunction was characterized by ultrastructural abnormalities and by decrease in the following parameters in isolated kidney mitochondria: adenosine diphosphate (ADP)-induced oxygen consumption (state 3), respiratory control ratio, ADP/oxygen (ADP/O) ratio, adenosine triphosphate synthesis, membrane potential, calcium retention, glutathione (GSH) content, and activity of respiratory complex I, aconitase, catalase, and GSH peroxidase. These mitochondria also showed increase in hydrogen peroxide production, malondialdehyde, and 3-nitrotyrosine protein adducts content. The above-described changes, as well as CP-induced nephrotoxicity, were attenuated in mice pretreated with a single injection of C-PC. Our data suggest that the attenuation of mitochondrial abnormalities is involved in the protective effect of C-PC against CP-induced nephrotoxicity. This is the first demonstration that C-PC pretreatment prevents CP-induced mitochondrial dysfunction in mice.

Keywords Functional food · C-phycocyanin · Mitochondrial oxygen consumption · Mitochondrial membrane potential · Nephrotoxicity · Cisplatin

Introduction

C-phycocyanin (C-PC) is a protein from the phycobiliprotein family [1] characterized by its antioxidant activity [2] and by an intense blue color (it has a characteristic absorption peak at 620 nm) and is one of the main pigments of the algae *Spirulina*, which is used as a dietary supplement due to its high content of protein. *Spirulina* may be considered a functional food. The role of functional foods and their components in the prevention, treatment, and promotion of human health has been currently accepted [3–5]. Functional foods contain one or more nutraceuticals, and these are defined as "compounds or products that have been isolated or purified from food sources that are health-promoting" [6]. C-PC has several nutraceutical properties such as renoprotective (against oxalate and cisplatin, CP) [7, 8], anti-inflammatory [9], and hepatoprotective (against carbon tetrachloride) [10] and others [11]. Recently, we have shown that C-PC prevents CP-induced nephrotoxicity in mice that was associated with attenuation of oxidative damage and preservation of the activity of antioxidant enzymes in kidney [2]. CP is a potent antineoplastic agent discovered in the laboratory of Barnett Rosenberg in 1965 [12]. It is widely used worldwide for cancer treatment, including testicular, ovarian, bladder, neck, endometrium, non-small cell lung adenocarcinoma, melanoma, penile, and adrenal carcinoma [13,

✉ José Pedraza-Chaverri
pedraza@unam.mx

1 Department of Biology, Facultad de Química, UNAM, Ciudad Universitaria, 04510 Mexico, D.F., Mexico

2 Experimental Pathology Section, Instituto Nacional de Ciencias Médicas y Nutrición "Salvador Zubirán", 14000 Mexico, D.F., Mexico

3 Department of Physiology, Biophysics and Neurosciences, Center for Research and Advanced Studies of the National Polytechnic Institute (Cinvestav-IPN), 07360 Mexico, Mexico

4 Department of Cardiovascular Biomedicine, Instituto Nacional de Cardiología "Ignacio Chávez", 14080 Mexico, D.F., Mexico

14]. However, its therapeutic use is limited mainly because it is capable to induce renal damage. Several mechanisms are involved in the CP-induced renal damage including oxidative stress, mitochondrial dysfunction, inflammation, and apoptosis [15–19].

Mitochondria are the principal organelles involved in the production of reactive oxygen species (ROS) and are the major source of adenosine triphosphate (ATP) production by coupling electron transport chain (ETC) with ATP synthesis [20, 21]. Several lines of research have proved that CP accumulates in kidney mitochondria decreasing ATP synthesis and increasing ROS production that finally leads to cell damage [22, 23]. In fact, mitochondria are both a target and an early event in CP-induced nephrotoxicity [19, 24, 25]. Several studies have shown the prevention of CP-induced mitochondrial dysfunction by the use of synthetic or natural antioxidants such as carvedilol [26], sulforaphane [27], and 5-aminolevulinic acid [28]. Based on the above information, the hypothesis was made that C-PC may prevent the CP-induced kidney mitochondrial alterations. In this work, the effect of C-PC on CP-induced renal mitochondrial dysfunction in mice was studied.

Materials and methods

Reagents

The C-PC (Lt number 044/13-14) used was a generous gift from Valensa International (Orlando, FL, USA). CP was obtained from Aldrich (Cat. No. 479306-1G, Lt MKBH5984V). Amplex red, horseradish peroxidase (HRP), nicotinamide, dinucleotide phosphate (NADPH and $NADP^+$), glutathione (GSH), glucose, glucose 6 phosphate dehydrogenase (G6PDH), hexokinase, GSH reductase (GR), glutamic acid, malic acid, xanthine, xanthine oxidase, monochlorobimane, D-mannitol, sodium succinate dibasic, 4-(2-hydroxyethyl)-1-piperazineethanesulfonic acid (HEPES), fat free bovine serum albumin (BSA), adenosine 5′-diphosphate sodium salt (ADP), carbonyl cyanide 4-(trifluoromethoxy) phenylhydrazone (FCCP), rotenone, sucrose, 2,6-dichlorophenolindophenol sodium salt hydrate (DCPIP), Percoll®, antimycin A, β-nicotinamide adenine dinucleotide (NADH), decylubiquinone (DuB), sodium phosphate dibasic (Na_2HPO_4), sodium phosphate monobasic (NaH_2PO_4), nitroblue tetrazolium (NBT), potassium cyanide (KCN), carbonyl cyanide *m*-chlorophenylhydrazone (CCCP), glutathione-*S*-transferase (GST), sodium dodecyl sulfate (SDS), and safranin O were purchased from Sigma-Aldrich (St. Louis, MO, USA). Calcium chloride ($CaCl_2$) was from Research Organics, Inc. (Cleveland, OH, USA). Arsenazo III was acquired from ICN Biomedicals, Inc. (Aurora, OH, USA). Cyclosporine A (CsA) was purchased from Enzo Life Sciences (Farmingdale, NY, USA). Magnesium chloride ($MgCl_2$) and sodium dithionite were from Merck (HES, Germany). Potassium phosphate dibasic (K_2HPO_4) and potassium chloride (KCl) were from Mallinckrodt (NY, USA). Protein assay (500-0006) from Bio-Rad Laboratories (Hercules, CA, USA) was used for protein quantification. Ethylenediaminetetraacetic acid disodium salt (Na_2EDTA), sodium carbonate (Na_2CO_3), and hydrogen peroxide (H_2O_2) were from JT Baker (Xalostoc, Edo. Mexico, Mexico). Glutaraldehyde, cacodylate buffer, and osmium tetroxide were form Electron Microscopy Science (Hatfield, PA, USA). Primary antibodies anti-malondialdehyde (MDA), anti-3-nitrotyrosine (3-NT), and anti-adenine nucleotide translocase (ANT) 1/2 were from Abcam (Boston, MA, USA), Cayman Chemical Co. (Ann Arbor, MI, USA), and Santa Cruz Biotechnology, Inc. (Santa Cruz, CA, USA), respectively. Commercial kits for the measurement of blood urea nitrogen (BUN) (UREA-37) and plasma creatinine (CREATININE-J) concentration were from Spinreact (Girona, Spain). Sodium pentobarbital (Sedalphorte^{MR}), used as sedative, was from Salud y Bienestar Animal S.A. de C.V. (Mexico City). Other compounds and reagents used were of high purity and were obtained commercially.

Experimental model

Twenty CD-1 male mice (30–35 g, 8–9 week-old) were used. They were randomly divided into four experimental groups of five mice each: (1) control group (CT) received only 0.9 % sodium chloride solution (SS), (2) CP group received a single dose of 22 mg/kg of CP, (3) C-phycocyanin (C-PC) + CP (C-PC + CP) group received phycocyanin 30 mg/kg 1 h prior to CP administration (22 mg/kg), and (4) C-PC group received a single dose of 30 mg/kg of C-PC. All treatments were by intraperitoneal (i.p.) administration. The doses and treatment times of C-PC and CP were based on our previous work [2]. Seventy-two hours after CP or SS administration, mice were anesthetized with sodium pentobarbital (70 mg/kg, i.p.) and euthanized by exsanguinations in the axillary artery. Blood was collected directly in heparinized Eppendorf tubes and was centrifuged at $10{,}000 \times g$ for 10 min; the obtained plasma was used for determination of renal function markers (BUN and creatinine). Both kidneys were immediately dissected and were prepared for mitochondrial isolation.

Renal function

BUN and plasma creatinine levels were determined by spectrophotometric assays using commercial Spinreact kits. Urea present in the plasma reacts with *o*-phthalaldehyde in acid medium, and colored complex formed is quantified spectrophotometrically at 510 nm [29].

Creatinine determination in plasma is based on the reaction of this compound with sodium picrate as described by Jaffé [30]. Creatinine reacts with alkaline picrate forming a red complex whose intensity is proportional to the creatinine concentration [30, 31].

Electron microscopy studies of mitochondria in renal tissue

After mice were euthanized, the kidneys were immediately obtained, sectioned into thin slide of 1 mm of thickness; several small cubes of the kidney cortex were obtained and immediately fixed by immersion in 4 % (v/v) glutaraldehyde dissolved in 1 mM cacodylate buffer, pH 7.4 for 4 h at 4 °C, postfixed in 2 % (v/v) osmium tetroxide, dehydrated in graded ethyl alcohol, and embedded in epoxy resins. Sections of 1 μm were stained with toluidine blue and examined with a light microscopy to select representative areas from which ultrathin sections were obtained [32]. These sections were contrasted with uranyl acetate and lead citrate and examined with a FEI Tecnai™ G2 transmission electron microscope (Hillsboro, OR, USA).

Isolation of renal mitochondria

Renal mitochondria were isolated using Percoll® gradients, based mainly in a lung mitochondria isolation method with minor modifications [33]. The animals were euthanized, and both kidneys were immediately rinsed in cold isolation buffer with the following composition: 225 mM D-mannitol, 75 mM sucrose, 1 mM Na_2EDTA, 11 mM HEPES, and 0.1 % BSA, pH 7.4. The isolation procedure was performed at 4 °C. The kidney capsule was removed; kidneys were cut and homogenized in a glass Potter–Elvehjem homogenizer using a motor driven Teflon pestle with 2 mL of isolation buffer. Then the homogenates were centrifuged at 4000×*g* for 5 min. The supernatant was mixed with Percoll® to form an 8 % (v/v) solution that was stratified with a 15 % (v/v) Percoll® solution carefully added through the walls. Afterward, tubes were centrifuged at 12,500×*g* for 10 min without centrifuge brake. The mitochondrial-enriched fraction (bottom) was resuspended in 1 mL of BSA-free isolation buffer and centrifuged at 10,000×*g* for 10 min. Finally, the pellet was resuspended in 100 μL of BSA-free isolation buffer. The mitochondrial protein content was measured according to the Bradford technique [34] adapted to a 96-well plate, to assure the use of equal protein quantity in the following determinations.

Electron microscopy studies of isolated mitochondria

The mitochondrial pellet obtained from control mice was fixed in a 10 % glutaraldehyde solution dissolved in cacodylate buffer pH 7.2 for 4 h at 4 °C, postfixed in 2 % (v/v) osmium tetroxide, dehydrated in graded ethyl alcohol, and embedded in epoxy resin [35]. Ultrathin sections were obtained with a Sorvall MT-6000 ultramicrotome, contrasted with uranyl acetate and lead citrate and examined with an electron microscope FEI Tecnai G2.

Mitochondrial bioenergetics

The mitochondrial functionality was evaluated by measuring the rate of mitochondrial oxygen consumption in state 3 (with ADP) and state 4 (without ADP). The ratio of states 3/4, known as respiratory control ratio (RCR), was calculated; this ratio expresses the coupling degree between ETC and ATP synthesis. The ADP/oxygen (ADP/O) ratio was also calculated; this is another important mitochondrial functionality parameter that expresses the relationship between the amount of added ADP (mol) and the consumed oxygen (mol) during state 3 [33]. Measurement of mitochondrial respiration was performed using a Clark-type electrode (Strathkelvin Instruments, ML, Scotland) at 37 °C. Mitochondria (15 μg of protein) were suspended in 100 μL of respiration buffer, which contain 70 mM sucrose, 220 mM mannitol, 1 mM Na_2EDTA, 10 mM K_2HPO_4, 5 mM HEPES, 5 mM $MgCl_2$, 0.2 % BSA; pH 7.2 [33]. To evaluate respiration driven by complex I, 10 mM glutamate + 5 mM malate was employed. Oxygen consumption sustained by complex II was evaluated using 10 mM succinate + 2 mM rotenone. State 3 was induced by adding 115 μM ADP; afterward, the state 4 was reached when the respiration decreased because the ATP synthesis was no longer taking place as direct consequence of the ADP depletion. Rates of oxygen consumption in states 3 and 4 were expressed in ng O_2/(min μg protein).

Activity of complex I (NADH:ubiquinone oxidoreductase)

The enzymatic activity of complex I was assayed spectrophotometrically at 37 °C with 2.5 μg of isolated kidney mitochondria. Mitochondria were broken with four freezing and thawing cycles, and the activity of mitochondrial complex I was carried out independently in a 96-well plate (final volume of 300 μL), with and without 13 μM rotenone, an inhibitor of complex I. Specific activity was determined by subtraction of the inhibited activity to the total non-inhibited one, and the values are reported as mmol/(min* mg protein). Mitochondrial protein was incubated for 5 min at 37 °C with a solution containing 41 mM potassium phosphate buffer, 3.5 mg/mL BSA, 67 μM DCPIP, 1 μM antimycin A, 0.2 mM NADH, and 0.2 mM KCN. Afterward, a kinetic reading at 600 nm for 2 min monitored the base line; the reaction was started by the

addition of 3.12 mM DuB and was followed for 3 min [33, 36]. The decrease in absorbance is proportional to DCPIP reduction.

Mitochondrial membrane potential ($\Delta\Psi$) and calcium retention

Evaluation of $\Delta\Psi$ was determined by changes in absorbance of the cationic dye safranin O produced by the membrane potential state. The measurements were carried out in a buffer solution (pH 7.3) containing 2 mg of mitochondrial protein, 125 mM KCl, 10 mM HEPES, 3 mM Pi, 1.8 μg/mL rotenone, 200 μM ADP, and 10 mM potassium succinate as respiratory substrate. Absorbance tracings were obtained and displayed in a double beam spectrophotometer at 525–575 nm. Mitochondrial calcium movement was analyzed by a similar assay but the absorbance tracings were determined at 675–685 nm using arsenazo III (60 μM) dye as indicator [27]. In both cases, the reaction was initiated by the addition of 100 μM Ca^{2+}. The experiments in the CP group were performed in the presence or absence of 1 μM CsA, a known inhibitor of the mitochondrial permeability transition pore (mPTP) opening. Depolarization of the $\Delta\Psi$ was induced by CCCP addition at the end of the assays of CT and C-PC groups [37].

ATP synthesis

The determination of ATP production was performed by coupled reactions between 9 U/mL hexokinase and 2.3 U/mL G6PDH in a medium containing 2 M glucose, 0.7 M succinate, and 1.8 mM $NADP^+$ dissolved in respiration buffer. The increase in absorbance of NADPH at 340 nm was proportional to mitochondrial ATP synthesis [35].

Mitochondrial H_2O_2 production

Mitochondrial H_2O_2 generation was measured by the technique previously described by Starkov [38]. The assay was performed with freshly isolated mitochondria (15 μg of protein), in a medium containing 125 mM KCl, 4 mM KH_2PO_4, 14 mM NaCl, 20 mM HEPES–NaOH, 1 mM $MgCl_2$, 0.2 % BSA, 1 mM EDTA, pH 7.2 in the presence of 0.7 mM succinate, 10 μM rotenone, 0.1 mM amplex red, and HRP (10 U/mL). Additionally, a standard curve with different H_2O_2 concentrations (20–140 nM) was employed. Amplex red is oxidized in the presence of H_2O_2 to produce resorufin, a fluorescent compound measured using an excitation filter 530/25 and emission 590/35 nm [2].

Oxidative stress markers

Aconitase activity and GSH content were measured in sonicated mitochondria, as previously reported [2]. The activity of aconitase was assayed by determining the rate of formation of the intermediate product, *cis*-aconitate, from the interconversion of L-citrate and isocitrate at 240 nm [27]. Briefly, the reaction was carried out in 1 mL of reaction medium containing 25 mM KH_2PO_4 + 0.05 % Tween, 1 mM sodium citrate, and 0.6 mM $MnCl_2$. Absorbance at 240 nm was recorded for 2 min with 30 s interval readings. The activity is reported as mU/mg protein [39]. Mitochondrial GSH content was evaluated by measuring fluorescent adducts of GSH with 1 mM monochlorobimane in the presence of 1 U/L GST [2]. A standard curve of GSH in Krebs–Henseleit (pH 7.4) solution was employed. The fluorescent adducts were read at 385 and 478 nm excitation and emission, respectively. Values are reported as μmol/mg protein. Western blot analyses of MDA and 3-NT protein adducts were performed as previously described by Molina-Jijón et al. [40]. Briefly, total proteins from isolated mitochondria from the four experimental groups were extracted with 200 μL of lysis buffer (RIPA, mM): 40 Tris–HCl pH 7.6, 150 NaCl, 2 EDTA, 10 % glycerol, 1 % Triton X-100, 0.5 % sodium deoxycholate, and 0.2 % SDS. Thereafter, samples were sonicated three times for 30 s each in a high-intensity ultrasonic processor (Vibra cell, Sonics and Materials, Inc., Danbury, CT, USA), centrifuged at 20,000×*g* and 4 °C, for 40 min, and supernatants were collected. Briefly, samples were denatured by boiling for 12 min and then diluted 1:5 in 5× Laemmli buffer with urea (5 M). Proteins were loaded on SDS-15 % polyacrylamide gel electrophoresis. Molecular weight standards (Amersham Pharmacia Biotech, Piscataway, NJ, USA) were run in parallel. Proteins were transferred to polyvinylidene fluoride membranes (Amersham Biosci, Uppsala, Sweden). Nonspecific protein binding was blocked by incubation with 5 % non-fat dry milk in phosphate buffer saline 1× containing 0.4 % Tween 20, for 1 h, at room temperature. Membranes were incubated overnight at 4 °C with the appropriate primary antibodies against MDA (dilution 1:1000), against 3-NT (1:1000 dilution) and against ANT (1:500 dilution). Thereafter, membranes were incubated with peroxidase-conjugated anti-rabbit, anti-mouse, or anti-goat (1:10,000 dilution) for 1 h; after washing, immunoblots were developed using the ECL™ prime western blotting detection reagent (Amersham™, GE Healthcare, Buckinghamshire, UK). Chemiluminescence was detected in an EC3 imaging system (UVP BioImaging Systems, Cambridge, UK). Protein band density was quantified by transmittance densitometry (UVP BioImaging Systems software, Cambridge, UK).

Activity of antioxidant enzymes

The activity of GSH peroxidase (GPx), catalase (CAT), and superoxide dismutase (SOD) was measured in sonicated

mitochondria using the previously described techniques [2]. Briefly, GPx activity was assessed by the disappearance of NADPH monitored at 340 nm in a coupled reaction, carried out in a reaction solution containing 1 mM GSH, 0.2 mM NADPH, and 1 U/mL of GR. Fifty μg of protein and 2.5 mM H_2O_2 were added to the reaction mixture. Twenty five μg of mitochondrial protein were used to evaluate CAT activity by measuring the disappearance of H_2O_2 at 240 nm in 10 mM phosphate buffered saline pH 7.0. Data were expressed as *k*/mg protein. SOD activity was determined by its ability to prevent formazan production from the reaction of NBT and superoxide anion (O_2^-) generated by the xanthine–xanthine oxidase system [41]. One hundred and fifty μg of mitochondrial protein or 50 mM phosphate buffer pH 7.0 (100 % formazan production) were added to the reaction mixture with the following composition: 90 μM xanthine, 16 mM Na_2CO_3, 2 mM KCN, 22.8 μM NBT, and 18 mM phosphate buffer; pH 7.0. The reaction was started by the addition of xanthine oxidase (168 U/L) followed by a 15 min incubation at 27 °C; finally, optical density was measured at 560 nm.

Statistical analyses

Results are expressed as mean ± standard error of the mean (SEM). One-way analysis of variance followed by multiple comparisons according to Bonferroni was employed using the software SigmaStat v. 11.0 (Systat Software, San José, CA, USA). A P value less than 0.05 was considered statistically significant.

Results

Renal function

Seventy-two hours after CP administration, plasma concentrations of creatinine and BUN were measured as kidney function markers (Fig. 1). Nephrotoxicity in the CP group was characterized by an increase in both markers. There was a significant increase (2–3-fold, $P < 0.05$) in both markers compared with the CT group. These data confirmed the development of CP-induced renal damage, which was attenuated by the pretreatment with C-PC. These data confirm the protective effect of C-PC against CP-induced nephrotoxicity. C-PC group showed similar values to the CT group.

Ultrastructural studies

The kidney of animals treated with CP showed numerous damaged proximal convoluted tubules, tubular epithelial cells exhibited extensive vacuolization, and mitochondrial swelling with internal membranes rupture (Fig. 2a, b). Other areas showed necrosis and cellular detachment. In contrast, animals treated with C-PC and CP showed occasional tubular epithelial cells with mild vacuolization and minimal mitochondrial abnormalities (Fig. 2c, d). Thus, the morphological study showed protective effect of C-PC against the mitochondrial damage induced by CP that closely correlated with the biochemical data.

Electronic microscopy study of isolated mitochondria

The quality of isolated mitochondrial fraction was also estimated by electronic microscopy. Figure 2e shows mitochondria obtained from the kidneys. Well-preserved internal and external membranes were found in the majority of the revised organelles, indicating well-preserved and higher efficiency of the mitochondria isolation method.

Mitochondrial bioenergetics

The mitochondrial oxygen consumption was measured immediately after mitochondrial isolation. Two substrates were employed to maintain the ETC: malate/glutamate and succinate for complexes I and II, respectively.

Succinate as ETC substrate

Figure 3a shows representative tracings of mitochondrial oxygen consumption using succinate as substrate. The data obtained for states 3 and 4, and uncoupled respiration obtained in the presence of FCCP are shown for each group. C-PC was able to attenuate the CP-induced decrease in state 3 and increase in state 4.

The mean for several experiments on respiratory parameters are shown in Fig. 3d–f. CP group was characterized by a significant decrease in state 3 and an increase in state 4 (8.1 ± 1.2 and 7.5 ± 1.0 ng O_2/min mg protein, respectively) compared to CT group (11.6 ± 0.4 and 2.5 ± 0.2 ng O_2/min mg protein, respectively), whereas the group pretreated with C-PC before CP showed similar values to CT group in state 3 (10.9 ± 1.7 ng O_2/min mg protein) and a slightly increased in state 4 (3.7 ± 0.2 ng O_2/min mg protein) (Fig. 3b, c). The RCR value (Fig. 3d) of CP group (1.4 ± 0.1) was significantly reduced versus CT group (4.7 ± 0.2). The pretreatment with C-PC prevented the RCR reduction induced by CP (3.8 ± 0.2). Accordingly, the ADP/O ratio (Fig. 3e) in the CP group was lower compared to the CT group (1.1 ± 0.05 and 2.1 ± 0.4, respectively), while in the C-PC + CP group (1.7 ± 0.1), the CP-induced reduction in this parameter was significantly prevented. Uncoupled respiration is presented in Fig. 3f. It is observed that C-PC prevented the

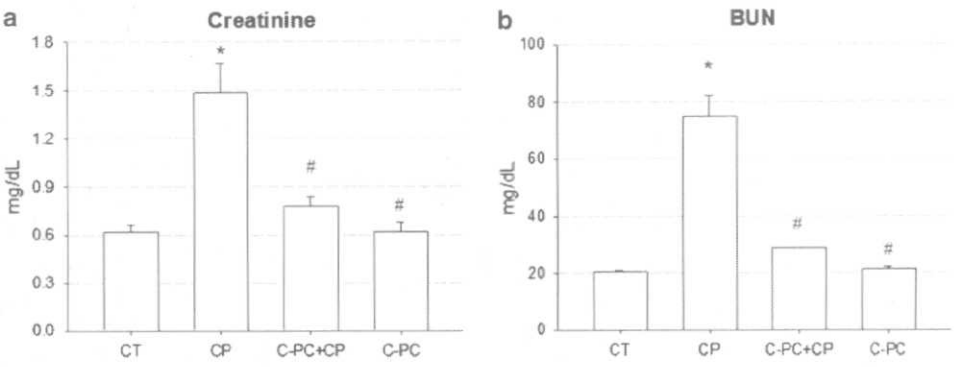

Fig. 1 Effect of C-phycocyanin (C-PC) on cisplatin (CP)-induced renal damage. **a** Plasma creatinine concentration and **b** blood urea nitrogen (BUN). *CT* control (vehicle). Data are presented as mean ± SEM, $n = 6$–10, $^{*}P < 0.05$ versus CT, $^{\#}P < 0.05$ versus CP

CP-induced decrease in FCCP-induced respiration. Treatment with C-PC alone did not alter any of the previously described parameters.

Malate–glutamate as ETC substrate

CP treatment decreased state 3 (2.0 ± 0.5 ng O_2/min mg protein) and increased state 4 (1.3 ± 0.3 ng O_2/min mg protein) compared to CT group values (4.8 ± 0.3 and 0.9 ± 0.1 ng O_2/min mg protein, respectively), while pretreatment with C-PC prevented the reduction of state 3 (4.8 ± 0.7 ng O_2/min mg protein); it did not modify the state 4 (1.3 ± 0.2 ng O_2/min mg protein). The respiration alterations induced by CP induced a reduction in the RCR value (1.6 ± 0.3) compared to CT group (5.2 ± 0.2); interestingly, pretreatment with C-PC prevented significantly this reduction (3.9 ± 0.4). Consistently with RCR results, ADP/O ratio was lower in the CP group (1.0 ± 0.02) compared to the CT group (2.6 ± 0.2), and the C-PC group prevented this reduction in the C-PC + CP group (2.3 ± 0.1). C-PC alone did not alter any of the previously described parameters (data not shown).

Activity of mitochondrial complex I

CP induced a significant decrease ($P < 0.05$) in the activity of mitochondrial complex I that was significantly attenuated by the pretreatment with C-PC. The C-PC treatment per se did not alter the activity compared to the control group (Fig. 4).

$\Delta\Psi$ and calcium retention

The addition of 100 μM Ca^{2+} to the mitochondrial preparation of the CP group led to a fast loss in $\Delta\Psi$ (Fig. 5a). Before completing 200 s of Ca^{2+} stimulus, mitochondria began to uncouple that was observed as an increase in absorbance difference at 525–575 nm. When the mitochondria from the CP group were incubated in the presence of CsA, the potential disruption was not observed (data not shown), which indicates the role of the mPTP formation in the loss of $\Delta\Psi$ induced by Ca^{2+}. The isolated mitochondria from C-PC + CP group were more resistant to $\Delta\Psi$ disruption in the presence of Ca^{2+} overload (Fig. 5a) compared to the CP group. Mitochondria from the CT (Fig. 5a) and C-PC (data not shown) groups were sensitive to Ca^{2+} addition up to 10 min. The above outcomes were similar to those obtained with arsenazo III at 675–685 nm (Fig. 5b). Mitochondrial Ca^{2+} retention capacity was lost in the CP group before 200 s post-Ca^{2+} addition (Fig. 5b) according with the results of membrane potential assay. The loss in mitochondrial Ca^{2+} retention capacity was attenuated in the CP group by the addition of CsA (data not shown) and in the C-PC + CP (Fig. 5b) suggesting that the C-PC pretreatment could inhibit the mPTP formation/opening (compared with the $\Delta\Psi$ results). CT (Fig. 5b) and C-PC (data not shown) groups maintain their Ca^{2+} retention capacity.

ATP synthesis

Figure 6a shows that ATP synthesis was decreased by CP treatment (169 ± 67 nmol/min mg protein) compared to the CT group (507 ± 65 nmol/min mg protein); this alteration was significantly prevented by the C-PC pretreatment. No significant changes were observed in mitochondria isolated from the C-PC group.

H_2O_2 production

Data of mitochondrial H_2O_2 production are shown in Fig. 6b. Compared to the CT group (40 ± 7 nmol H_2O_2/min mg protein), mitochondria from the CP group showed an important increase in H_2O_2 production (90 ± 3 nmol H_2O_2/min mg protein); interestingly, C-PC treatment was able to attenuate the mitochondrial H_2O_2 production (63 ± 11 nmol H_2O_2/min mg protein). C-PC group showed no significant alteration in mitochondrial H_2O_2 production (45 ± 3 nmol H_2O_2/min mg protein).

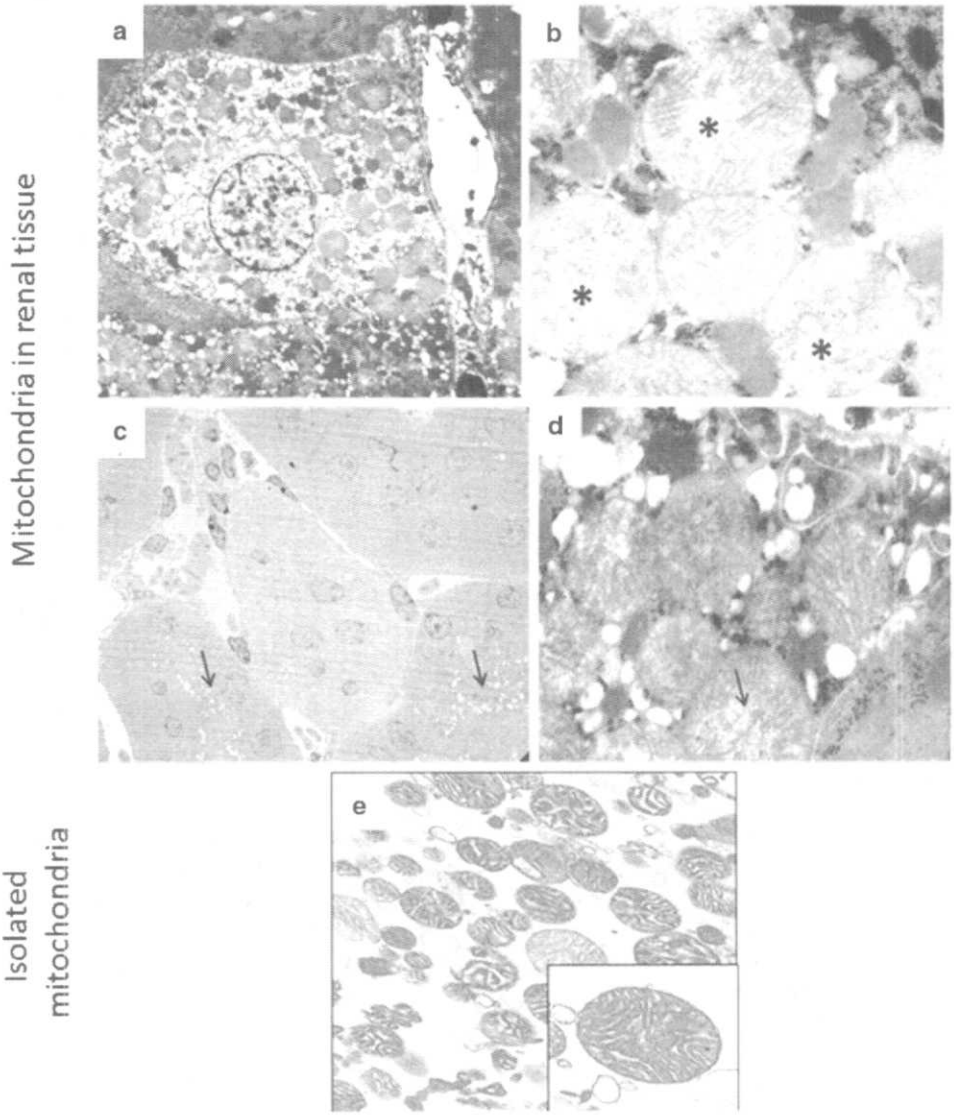

Fig. 2 Representative micrographs showing the effect of C-phycocyanin (C-PC) on cisplatin (CP)-induced ultrastructural kidney changes. **a** Tubular convoluted epithelial cell in mouse treated with CP shows swelling and extensive vacuolization (×15,000 magnification). **b** Higher magnification of cell showed in **a** exhibits swelling mitochondria with internal membranes disruption (*asterisks*, ×30,000). **c** Low-power micrograph from a mouse treated with C-PC and CP, occasional cells shows some cytoplasmic vacuoles (*arrows*, ×5000). **d** Higher magnification of epithelial tubular cells from kidney of mouse treated with C-PC and CP shows mitochondria with slight abnormalities, such as focal internal membrane disruption (*arrow*, ×50,000). **e** Ultrastructural analysis from mitochondria isolated forms control mice. The majority of structures correspond to well-preserved mitochondria (*inset*). ×50,000 magnification

Oxidative stress markers

CP treatment decreased the aconitase activity (36 ± 3 μU/mg protein) compared to the CT group (145 ± 6 μU/mg protein) but C-PC pretreatment (C-PC + CP group) was able to attenuate (69.5 ± 5.7 μU/mg protein) the reduction in aconitase activity induced by CP (Fig. 6c). C-PC treatment (129.3 ± 15.8 μU/mg protein) did not alter the aconitase activity. GSH content in mitochondria from the CP group was significantly reduced (0.8 ± 0.03 μmol/mg protein) compared to the CT group (1.3 ± 0.1 μmol/g protein: Fig. 6d). The C-PC pretreatment was able to prevent the CP-induced reduction in GSH content (1.13 ± 0.07 μmol/mg protein). C-PC treatment did not alter the mitochondrial GSH content (1.4 ± 0.1 μmol/mg protein). Furthermore and, consistently with the above data, C-PC was able to prevent the CP-induced increase in MDA (Fig. 7a, b) and 3-NT (Fig. 7c, d) protein adducts.

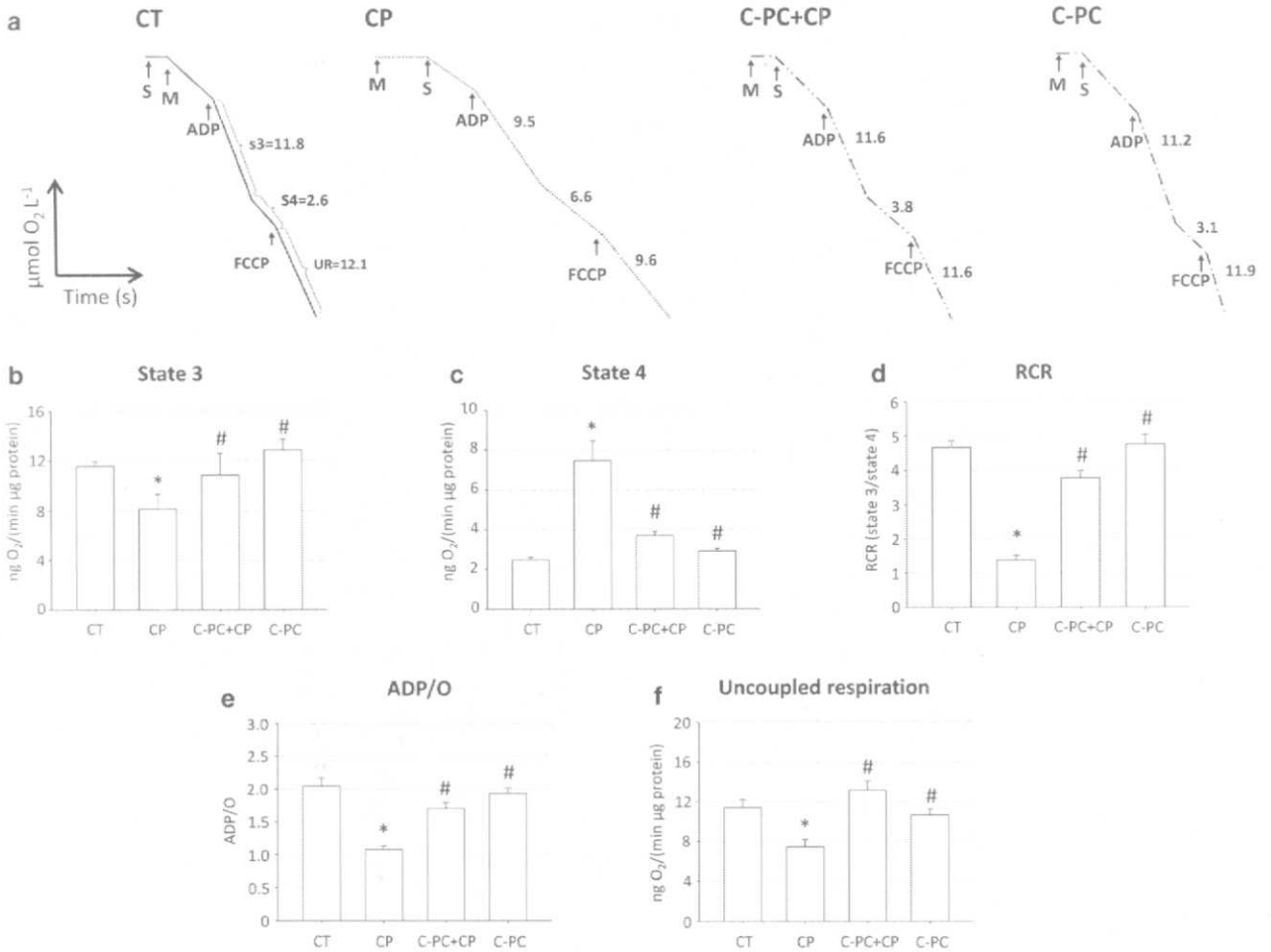

Fig. 3 Effect of C-phycocyanin (C-PC) on cisplatin (CP)-induced mitochondrial oxygen consumption alterations using succinate as substrate. **a** Representative graphic of mitochondrial oxygen consumption of the four groups of mice studied. One representative animal was chosen for each group. Sample and reagents were added to the chamber in the following order: (1) 15 µg of mitochondrial protein (M), (2) 10 mM succinate + 2 mM rotenone (S), (3) 115 µM adenosine diphosphate (ADP), and (4) carbonyl cyanide 4-(trifluoromethoxy) phenylhydrazone (FCCP) 20 nM were added to obtain the uncoupled respiration (UR). *State 3* (*S3*) was evident by an increase in respiration after ADP addition and *state 4* (*S4*) was evident by a decrease in oxygen consumption when all ADP added was phosphorylated into ATP. Measurements were conducted in a water-jacketed chamber (37 °C) connected to an oxymeter interfaced to a computer. **b** *State 3* of respiration, **c** *state 4* of respiration, **d** respiratory control ratio (*RCR*, *states 3/4*), **e** adenosine diphosphate/oxygen (*ADP/O*), and **f** uncoupled respiration. *CT* control (vehicle). Data are presented as mean ± SEM, $n = 4$–6, $^{*}P < 0.05$ versus CT, $^{\#}P < 0.05$ versus CP

Antioxidant enzymes

Figure 8 shows the enzymatic activity of GPx, CAT, and SOD in isolated mitochondria. CP induced a reduction in the activity of GPx (0.17 ± 0.01 U/mg protein) and CAT (1.3 ± 0.1 *k*/mg protein) compared to the CT group (GPx: 0.27 ± 0.02 U/mg protein, CAT: 2.3 ± 0.1 *k*/mg protein). The C-PC pretreatment prevented the CP-induced decrease in the activity of GPx and CAT (0.25 ± 0.02 U/mg protein and 2.3 ± 0.1 *k*/mg protein, respectively). In contrast, no significant changes were found in the activity of SOD.

Discussion

It has been found previously [2, 8] that C-PC prevents CP-induced nephrotoxicity and this was confirmed in the present study (Fig. 1). Moreover, it is known that CP-induced nephrotoxicity is characterized mitochondrial dysfunction [16, 19, 42–44] and that this may be an early event in the CP-induced acute renal failure [19, 25, 45]. CP-induced mitochondrial damage is characterized alterations in the activity of respiratory complexes (I–IV) and in mitochondrial membrane potential in renal cells in culture [43, 46], mitochondrial energy failure [24], ultrastructural

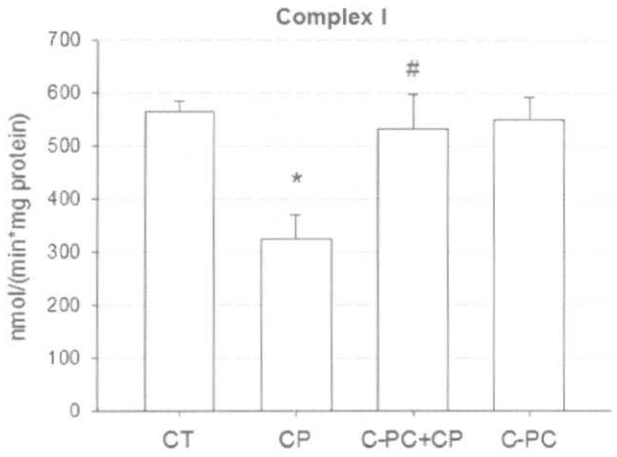

Fig. 4 Effect of C-phycocyanin (C-PC) on cisplatin (CP)-induced alterations in the activity of mitochondrial respiratory *complex I*. The experimental condition were 2.5 μg of mitochondrial protein was employed and incubated with a solution containing 67 μM 2,6-dichlorophenolindophenol (DCPIP), 1 μM antimycin A, 0.2 mM β-nicotinamide adenine dinucleotide (NADH), and 0.2 mM KCN; the reaction was started by the addition of 3.12 mM decylubiquinone (DuB). The non-enzyme activity was determined with 13 μM rotenone. *CT* control (vehicle). Data are presented as mean ± SEM, $n = 6$–9, $^{*}P < 0.05$ versus CT, $^{\#}P < 0.05$ versus CP

alterations characterized by decreased mitochondrial mass, disruption of cristae, and extensive mitochondrial swelling in proximal tubular epithelium [44], reduction of aconitase activity [27], reduction of antioxidant activity, and increase of oxidative damage [47] and ROS production [17].

Mitochondrial dysfunction has been recognized as a mediator of different types of pathological condition as well as aging by increasing ROS production leading to oxidation of deoxyribonucleic acid, lipids, and proteins [20, 48]. Approximately 2 % of the oxygen in the mitochondria is converted to $O_2^{\cdot-}$, mainly in the complexes I and III; most of it is converted to H_2O_2 by the mitochondrial SOD (Fig. 9) [49, 50]. H_2O_2 can easily pass across the mitochondrial membrane which can lead to the highly reactive hydroxyl radical production [51]. Due to its intermediary role in the mitochondrial ROS production process, the determination of the mitochondrial H_2O_2 production can give an idea of the general ROS production in the mitochondria. In fact, the oxidative damage induced by excessive ROS in mitochondria is related to mitochondrial dysfunction [19].

These earlier findings prompted us to investigate if C-PC was able to prevent CP-induced mitochondrial dysfunction. The main finding of our study was that C-PC attenuates CP-induced mitochondrial alterations and oxidative stress in mice and is summarized in the integrative schema of Fig. 9. These findings expand our previous data [2] and are relevant to explain the mechanism by which C-PC is attenuating CP-induced nephrotoxicity and oxidative stress.

The attenuation of CP-induced mitochondrial abnormalities was seen at both ultrastructural and functional levels. Representative micrographs (Fig. 2c, d) revealed that C-PC efficiently prevented the CP-induced

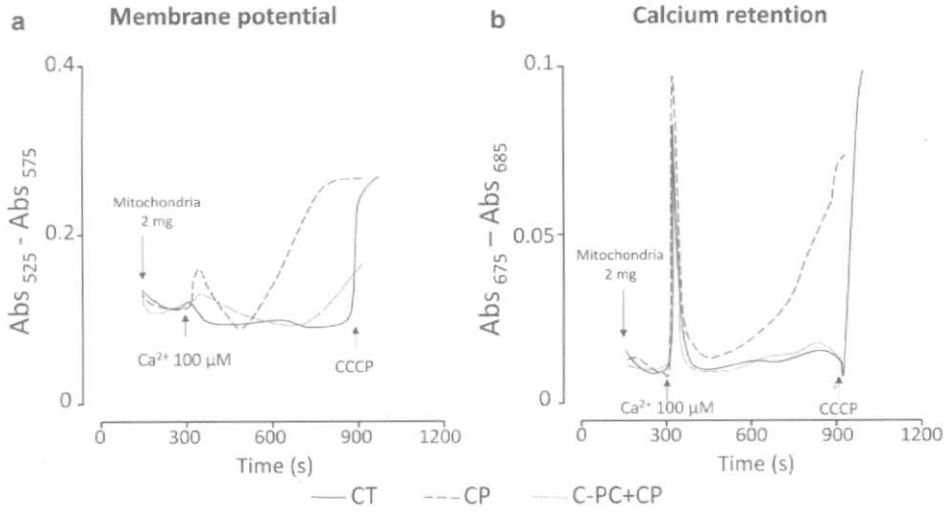

Fig. 5 Effect of C-phycocyanin (C-PC) on the cisplatin (CP)-induced alterations on the calcium-dependent mitochondrial permeability transition pore (mPTP). **a** Mitochondrial membrane potential ($\Delta\Psi$) and **b** calcium retention capacity. Both assays were performed with 2 mg of mitochondrial protein, 10 mM succinate, and 200 μM ADP. Mitochondrial permeability was induced by the addition of 100 μM Ca^{2+}, the loss of membrane potential, and the release of calcium were induced by the addition of carbonyl cyanide *m*-chlorophenylhydrazone (CCCP) to the control (CT) group. Tracings are representative of three independent experiments

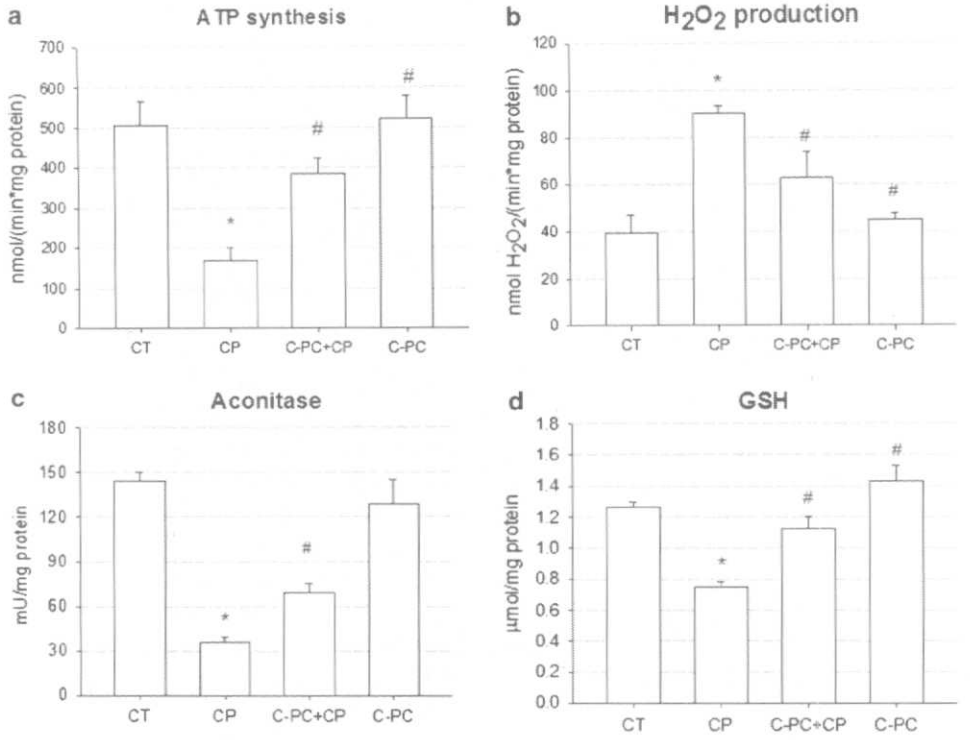

Fig. 6 Effect of C-phycocyanin (C-PC) on cisplatin (CP)-induced changes in mitochondrial **a** adenosine triphosphate (ATP) synthesis, **b** hydrogen peroxide (H_2O_2) production, **c** aconitase activity and **d** glutathione (GSH) content. **a** ATP synthesis was performed in medium containing 2 M glucose, 0.7 M succinate, and 1.8 mM $NADP^+$, $n = 4$–5, **b** H_2O_2 production was measured in the presence of 15 µg mitochondrial protein, 0.7 mM succinate, 10 µM rotenone, 0.1 mM amplex red, and horseradish peroxidase (10 U/mL), $n = 3$–6, **c** aconitase activity was monitored in the presence of 1 mM sodium citrate, 25 mM KH_2PO_4, 0.05 % Tween, and 0.6 mM $MnCl_2$, $n = 3$–5, and **d** GSH content was measurement with 1 mM monochlorobimane in the presence of 1 U/L of glutathione-*S*-transferase. $n = 5$–6. *CT* control (vehicle). Data are presented as mean ± SEM, $^*P < 0.05$ versus CT, $^\#P < 0.05$ versus CP

mitochondrial swelling and inner membrane rupture, which are characteristic structural abnormalities induced by CP [16, 42, 44].

Functional parameters were evaluated in isolated mitochondria whose purity was confirmed by electron microscopy studies (Fig. 2e). C-PC was able to attenuate the CP-induced alterations in the integrative parameters of mitochondrial function including decreased oxygen consumption (Fig. 3), ATP synthesis (Fig. 6), membrane potential, and calcium retention (Figs. 5, 9).

The main indicator of mitochondrial functionality is the RCR (states 3/4) as it expresses the coupling degree between the ETC and the ATP synthesis; a low value could indicate mitochondrial dysfunction which can be due to a failure in the mitochondrial membrane integrity and/or in the functionality of any of the mitochondrial complexes [52]. Another mitochondrial functionality indicator is the ADP/O ratio, which represents the number of ATP moles synthesized per mole of O_2 consumed [52]. The CP-induced mitochondrial dysfunction was characterized by alterations in oxygen consumption rates, using as substrates both glutamate/malate and succinate, consequently causing a reduction in RCR, ATP synthesis, ADP/O ratio, calcium transport, and $\Delta\Psi$. However, slight differences in some mentioned parameters values between both substrates employed were observed, as the different decrease in ADP/O ratio, which was more pronounced when malate/glutamate was used as substrate compared to succinate, probably due to the reduction in complex I activity (Fig. 4). In contrast, the high reduction of ADP/O rate when succinate was used as a substrate (Fig. 3) probably due to alterations in other respiratory complexes (II–IV) may also explain the decrease in state 3 respiration with succinate.

C-PC pretreatment prevented the alterations observed in the CP group, reestablishing the oxygen consumption rate of states 3 and 4 when succinate was used as substrate (Fig. 3b, c); nonetheless when malate/glutamate was used, only state 3 alterations were prevented. In general, it is agreed that during succinate oxidation, the main mechanism or ROS production in mitochondria is the reverse electron transport into complex I; however, some reports indicate that shifts in electron distribution and consequent changes in the rates of ROS production occur when the complex I inhibitor rotenone is included in the assay

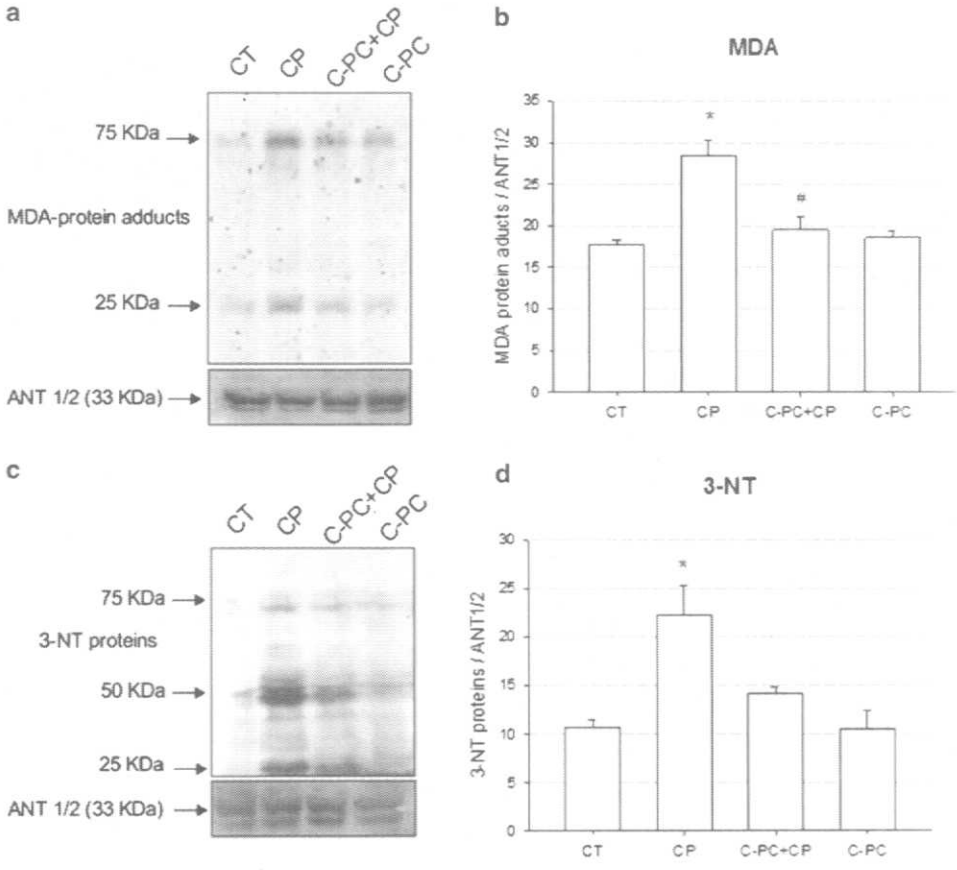

Fig. 7 Effect of C-phycocyanin (C-PC) on cisplatin (CP)-induced increase in **a**, **b** malondialdehyde (MDA)-protein adducts and **c**, **d** 3-nitrotyrosine (3-NT) proteins in isolated mitochondria from kidneys. Representative western blots for MDA and 3-NT are shown in **a** and **c**, respectively and densitometric quantification of MDA and 3-NT is shown in **b** and **d**, respectively. Adenine nucleotide translocase (ANT) 1/2 was used as loading control. *CT* control (vehicle). Data are presented as mean ± SEM, $n = 3$, $^{*}P < 0.05$ versus CT, $^{\#}P < 0.05$ versus CP

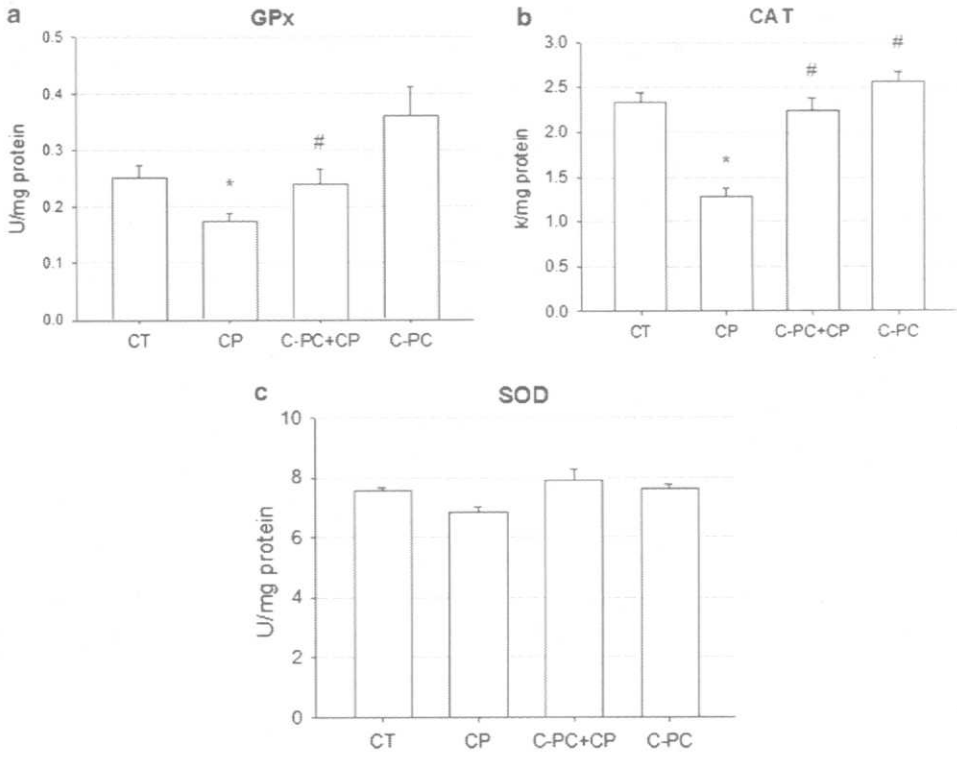

Fig. 8 Effect of C-phycocyanin (C-PC) on cisplatin (CP)-induced changes in the activity of antioxidant enzymes in isolated mitochondria from kidney. **a** Glutathione peroxidase (GPx) determination was carried out in a solution containing 1 mM GSH, 0.2 mM NADPH, and GR (1 U/mL), **b** catalase (CAT) activity was determined by the disappearance of H_2O_2, and **c** superoxide dismutase (SOD) activity was evaluated by ability to decrease formazan production induced by O_2^- generated by the xanthine–xanthine oxidase system. *CT*: control (vehicle). Data are presented as mean ± SEM, $n = 6$–9, $^{*}P < 0.05$ versus CT, $^{\#}P < 0.05$ versus CP

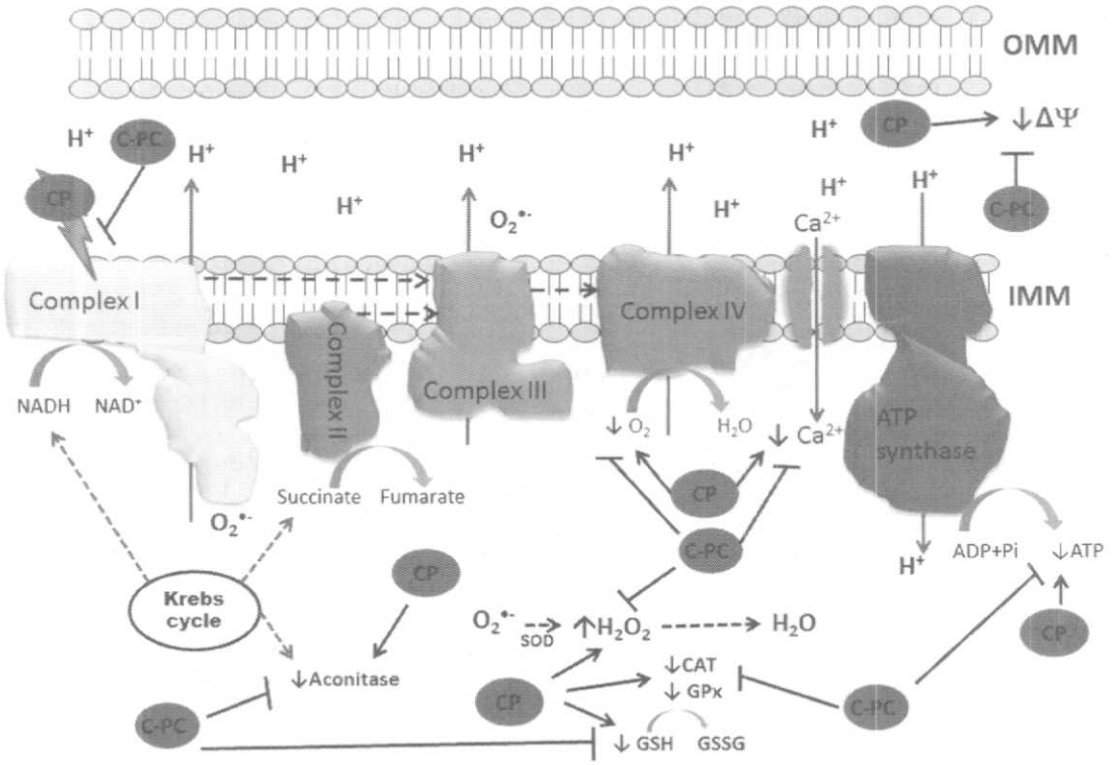

Fig. 9 Integrative schema showing the protective effect of C-phycocyanin (C-PC) against cisplatin (CP)-induced mitochondrial dysfunction. C-PC prevents the CP-induced decrease of activity of complex I, ATP synthesis rate, membrane potential ($\Delta\Psi$), oxygen consumption, calcium retention, and activity of antioxidant enzymes and of aconitase. C-PC also reduced oxidative stress and hydrogen peroxide (H_2O_2) production. *OMM* outer mitochondrial membrane, *IMM* inner mitochondrial membrane, *GSSG* glutathione disulfide, *GPx* glutathione peroxidase, *SOD* superoxide dismutase, *CAT* catalase, O_2^- superoxide anion

medium. Quinlan et al. [53] recently showed that in the presence of succinate plus rotenone, electron flow was diverted through complex III, whereas when using malate/glutamate as substrate, complexes I and III contribute equally to ROS production. In this sense, as we observed that mitochondria from the C-PC-treated group in the presence of succinate (but not when using NADH-linked substrates) markedly dropped the rate of oxygen consumption in state 4 respiring mitochondria, we hypothesize that the antioxidant treatment preserves in greater extent respiratory complex I function, failing to prevent from the combined stress generated by both complexes when succinate was oxidized. Under ADP-stimulated respiration, ROS production is decreased, which explains the protective effect of C-PC under this condition using both substrates.

Additionally, CP treatment reduced the activity of mitochondrial complex I. The low activity may explain the alterations in oxygen consumption and the low ATP synthesis rate. C-PC pretreatment prevented the decrease in ADP/O rate (Fig. 3e) and reestablished the activity of respiratory complex I (Fig. 4). As ATP synthesis determination relies on the ETC functionality and the C-PC pretreatment prevented changes on mitochondrial complex I activity, it was expected that C-PC pretreatment would also prevent the drop in ATP synthesis (Fig. 9), which was experimentally corroborated.

As oxidative stress indicators, content of MDA, 3-NT protein adducts and GSH, and the activity of aconitase and of some antioxidant enzymes were evaluated in isolated mitochondria (Fig. 9). MDA is a useful biomarker for detection of lipid peroxidation end-product, and 3-NT is a nitrosative modification of tyrosine that can be used as an indicator of the nitro-oxidative damage [40, 54, 55]. Aconitase is an iron–sulfur (Fe–S) protein whose catalytic activity is essential in Krebs cycle; it is a good indicator of oxidative stress damage since O_2^- is its principal inhibitor [56]. The low activity of aconitase suggests an increased O_2^- production in CP-treated animals (Fig. 9). On the other hand, the low-molecular weight tripeptide GSH is the cofactor of the antioxidant enzymes GPx and GST, maintains the environment of mitochondria in a reduced state, and prevents against the CP-induced mPTP [14]. GPx and CAT catalyze the decomposition of H_2O_2, and a decrease on its activity implies an accumulation of the H_2O_2 produced which can be interpreted as an increment in H_2O_2 production, as was observed in the isolated mitochondria from the CP group (Fig. 9). The antioxidant activity provided by

the C-PC pretreatment, just before CP administration, prevented the increase in MDA and 3-NT protein adducts, the drop in GSH level and the decrease in the activity of aconitase, GPx and CAT as well as the increase in H_2O_2 production (Fig. 9). We are tempting to speculate that the prevention of CP-mitochondrial oxidative stress by C-PC, documented in this study, may be involved, at least in part, in the prevention of renal oxidative stress by C-PC that was observed in the present and previous studies [2]. In fact, it has been shown that C-PC is direct scavenger of $O_2^{\cdot-}$, H_2O_2, singlet oxygen, peroxynitrite anion, nitric oxide, hypochlorous acid, and peroxyl radical [11, 57–59]. In addition, this nutraceutical has been located inside mitochondria [60] where it may exert its antioxidant effect.

The excessive mitochondrial H_2O_2 production in the CP group may explain the alterations in calcium retention and loss of the mitochondrial membrane potential that contribute to cellular injury with subsequent opening of the mPTP; all these processes are directly related with the mitochondrial membrane integrity. In this way, due to the C-PC antioxidant activity, the C-PC + CP group reduced H_2O_2 production and as consequence prevented mitochondrial dysfunction (Fig. 9). Earlier studies have found that C-PC is able to protect mitochondria in animal models. Gupta et al. [61] have described that C-PC (70 mg/kg i.p.) mitigates the mitochondrial membrane depolarization in thymocytes of tributyltin-treated rats and attenuates the pro-apoptotic event peculiar in the tributyltin treatment, and Marín-Prida et al. [62] found the preventive effect of C-PC (10–15 μM) on mitochondrial swelling, membrane potential dissipation, and ROS production in rat brain mitochondrial exposed to 3 mM phosphate and/or 100 μM Ca^{2+}. Other study showed that C-PC (20 mM) protection against oxalate induced alterations in mitochondrial membrane potential and ROS production in MDCK [63]. Recently, Lim et al. [8] have described the inhibitory effect of C-PC (50 mg/kg, i.p.) on apoptotic events induced by CP (12 mg/kg, i.p.) in mice.

Our study is the first to report that the nutraceutical C-PC as a protective agent against kidney mitochondrial dysfunction is induced by CP. Our data suggest that the attenuation of mitochondrial abnormalities is involved in the protective effect of C-PC against CP-induced nephrotoxicity due to its antioxidant activity. Consistently with our findings, it has been found that other antioxidant compounds [14, 23, 27, 64] are able to prevent mitochondrial dysfunction induced by CP. Further studies should be performed to establish if other mechanisms are involved in the protective effect of C-PC against CP-induced nephrotoxicity.

Acknowledgments This work was supported by Grants from PAPIIT (IN210713) and CONACYT (220046). The authors thank Dr. Enrique Pinzón and Dr. Ismael Torres for the technical support with the experimental animals.

Ethical Approval At any time of the research, the Official Mexican Standard Care and Use of Laboratory Animals (NOM-062-ZOO-1999) and the Mexican Official Standard NOM-087-ECOL-SSA1-2002-Infectious Bio Hazardous Waste-Classification and Specifications Handling were followed. This protocol was approved by the Local Ethics Committee (FQ/CICUAL/043/12).

References

1. Patel A, Mishra S, Pawar R, Ghosh PK (2005) Purification and characterization of C-Phycocyanin from cyanobacterial species of marine and freshwater habitat. Protein Expr Purif 40:248–255
2. Fernández-Rojas B, Medina-Campos ON, Hernández-Pando R, Negrette-Guzmán M, Huerta-Yepez S, Pedraza-Chaverri J (2014) C-Phycocyanin prevents cisplatin-induced nephrotoxicity through inhibition of oxidative stress. Food Funct 5:480–490
3. Griffiths JC, Abernethy DR, Schuber S, Williams RL (2009) Functional food ingredient quality: opportunities to improve public health by compendial standardization. J Funct Foods 1:128–130
4. Vulić JJ, Ćebović TN, Čanadanović-Brunet JM, Ćetković GS, Čanadanović VM, Djilas SM, Tumbas Šaponjac VT (2014) In vivo and in vitro antioxidant effects of beetroot pomace extracts. J Funct Foods 6:168–175
5. Zhuang H, Tang N, Yuan Y (2013) Purification and identification of antioxidant peptides from corn gluten meal. J Funct Foods 5:1810–1821
6. Lattanzio V, Kroon PA, Linsalata V, Cardinali A (2009) Globe artichoke: a functional food and source of nutraceutical ingredients. J Funct Foods 1:131–144
7. Farooq S, Asokan D, Sakthivel R, Kalaiselvi P, Varalakshmi P (2004) Salubrious effect of C-phycocyanin against oxalate-mediated renal cell injury. Clin Chim Acta 348:199–205
8. Lim BJ, Jeong JY, Chang Y-K, Na K-R, Lee KW, Shin Y-T, Choi DE (2012) C-phycocyanin attenuates cisplatin-induced nephrotoxicity in mice. Ren Fail 34:892–900
9. Romay C, Ledón N, González R (1998) Further studies on anti-inflammatory activity of phycocyanin in some animal models of inflammation. Inflamm Res 47:334–338
10. Ou Y, Zheng S, Lin L, Jiang Q, Yang X (2010) Protective effect of C-phycocyanin against carbon tetrachloride-induced hepatocyte damage in vitro and in vivo. Chem Biol Interact 185:94–100
11. Fernández-Rojas B, Hernández-Juárez J, Pedraza-Chaverri J (2014) Nutraceutical properties of phycocyanin. J Funct Foods 11:375–392
12. Long DF, Repta AJ (1981) Cisplatin: chemistry, distribution and biotransformation. Biopharm Drug Dispos 2:1–16
13. Naqshbandi A, Rizwan S, Khan F (2013) Dietary supplementation of flaxseed oil ameliorates the effect of cisplatin on rat kidney. J Funct Foods 5:316–326
14. Custódio JBA, Cardoso CMP, Santos MS, Almeida LM, Vicente JAF, Fernandes MAS (2009) Cisplatin impairs rat liver mitochondrial functions by inducing changes on membrane ion permeability: prevention by thiol group protecting agents. Toxicology 259:18–24
15. Barabas K, Milner R, Lurie D, Adin C (2008) Cisplatin: a review of toxicities and therapeutic applications. Vet Comp Oncol 6:1–18
16. Yao X, Panichpisal K, Kurtzman N, Kenneth N (2007) Cisplatin nephrotoxicity: a review. Am J Med Sci 334:115–124
17. Marullo R, Werner E, Degtyareva N, Moore B, Altavilla G, Ramalingam SS, Doetsch PW (2013) Cisplatin induces a mitochondrial-ROS response that contributes to cytotoxicity

depending on mitochondrial redox status and bioenergetic functions. PLoS ONE 8:e81162
18. Chirino YI, Pedraza-Chaverri J (2009) Role of oxidative and nitrosative stress in cisplatin-induced nephrotoxicity. Exp Toxicol Pathol 61:223–242
19. Santos NAG, Catão CS, Martins NM, Curti C, Bianchi MLP, Santos AC (2007) Cisplatin-induced nephrotoxicity is associated with oxidative stress, redox state unbalance, impairment of energetic metabolism and apoptosis in rat kidney mitochondria. Arch Toxicol 81:495–504
20. Brand MD, Orr AL, Perevoshchikova IV, Quinlan CL (2013) The role of mitochondrial function and cellular bioenergetics in ageing and disease. Br J Dermatol 169(Suppl 2):1–8
21. Wong HS, Chen J, Leong PK, Leung HY, Chan WM, Ko KM (2014) Cistanches Herba reduces the weight gain in high fat diet-induced obese mice possibly through mitochondrial uncoupling. J Funct Foods 10:292–304
22. Beeson CC, Beeson GC, Schnellmann RG (2010) A high-throughput respirometric assay for mitochondrial biogenesis and toxicity. Anal Biochem 404:75–81
23. Rodrigues MAC, Rodrigues JL, Martins NM, Barbosa F, Curti C, Santos NAG, Santos AC (2010) Carvedilol protects against the renal mitochondrial toxicity induced by cisplatin in rats. Mitochondrion 10:46–53
24. Ozaki T, Ishiguro S, Itoh H, Furuhama K, Nakazawa M, Yamashita T (2013) Cisplatin binding and inactivation of mitochondrial glutamate oxaloacetate transaminase in cisplatin-induced rat nephrotoxicity. Biosci Biotechnol Biochem 77:1645–1649
25. Brady HR, Kone BC, Stromski ME, Zeidel ML, Giebisch G, Gullans SR (1990) Mitochondrial injury: an early event in cisplatin toxicity to renal proximal tubules. Am J Physiol 258:1181–1187
26. Rodrigues MAC, Rodrigues JL, Martins NM, Barbosa F, Curti C, Santos NAG, Santos AC (2011) Carvedilol protects against cisplatin-induced oxidative stress, redox state unbalance and apoptosis in rat kidney mitochondria. Chem Biol Interact 189:45–51
27. Guerrero-Beltrán CE, Calderón-Oliver M, Martínez-Abundis E, Tapia E, Zarco-Márquez G, Zazueta C, Pedraza-Chaverri J (2010) Protective effect of sulforaphane against cisplatin-induced mitochondrial alterations and impairment in the activity of NAD(P)H: quinone oxidoreductase 1 and γ glutamyl cysteine ligase: studies in mitochondria isolated from rat kidney and in LLC-PK1 cells. Toxicol Lett 199:80–92
28. Terada Y, Inoue K, Matsumoto T, Ishihara M, Hamada K, Shimamura Y, Ogata K, Inoue K, Taniguchi Y, Horino T, Karashima T, Tamura K, Fukuhara H, Fujimoto S, Tsuda M, Shuin T (2013) 5-Aminolevulinic acid protects against cisplatin-induced nephrotoxicity without compromising the anticancer efficiency of cisplatin in rats in vitro and in vivo. PLoS ONE 8:e80850
29. Levinson SS (1978) Kinetic centrifugal analyzer and manual determination of serum urea nitrogen, with use of *o*-phthaldialdehyde reagent. Clin Chem 24:2199–2202
30. Husdan H, Rapoport A (1968) Estimation of creatinine by the Jaffe reaction. A comparison of three methods. Clin Chem 14:222–238
31. Toora BD, Rajagopal G (2002) Measurement of creatinine by Jaffe's reaction—determination of concentration of sodium hydroxide required for maximum color development in standard, urine and protein free filtrate of serum. Indian J Exp Biol 40:352–354
32. Pedraza-Chaverri J, Cruz C, Hernández-Pando R, Santana T, Arévalo AE, González L, Tapia E, Peña JC, Panduro A (1993) Angiotensina I-Converting enzyme activity in rats with carbon tetrachloride-induced acute renal failure. Ren Fail 15:19–26
33. Granados-Castro LF, Rodríguez-Rangel DS, Montaño M, Ramos C, Pedraza-Chaverri J (2015) Wood smoke exposure induces a decrease in respiration parameter and in the activity of respiratory complexes I and IV in lung mitochondria from guinea Pigs. Environ Toxicol 30:461–471
34. Bradford MM (1976) A rapid and sensitive method for the quantitation of microgram quantities of protein utilizing the principle of protein-dye binding. Anal Biochem 72:248–254
35. Cano-Ramírez D, Torres-Vargas CE, Guerrero-Castillo S, Uribe-Carvajal S, Hernández-Pando R, Pedraza-Chaverri J, Orozco-Ibarra M (2012) Effect of glycolysis inhibition on mitochondrial function in rat brain. J Biochem Mol Toxicol 26:206–211
36. Spinazzi M, Casarin A, Pertegato V, Salviati L, Angelini C (2012) Assessment of mitochondrial respiratory chain enzymatic activities on tissues and cultured cells. Nat Protoc 7:1235–1246
37. Zazueta C, García N, Martínez-Abundis E, Pavón N, Hernández-Esquivel L, Chávez E (2010) Reduced capacity of Ca^{2+} retention in liver as compared to kidney mitochondria. ADP requirement. J Bioenerg Biomembr 42:381–386
38. Starkov AA (2010) Measurement of mitochondrial ROS production. Methods Mol Biol 648:245–255
39. Molina-Jijón E, Tapia E, Zazueta C, El Hafidi M, Zatarain-Barrón ZL, Hernández-Pando R, Medina-Campos ON, Zarco-Márquez G, Torres I, Pedraza-Chaverri J (2011) Curcumin prevents Cr(VI)-induced renal oxidant damage by a mitochondrial pathway. Free Radic Biol Med 51:1543–1557
40. Molina-Jijón E, Rodríguez-Muñoz R, Namorado MDC, Bautista-García P, Medina-Campos ON, Pedraza-Chaverri J, Reyes JL (2015) All-*trans* retinoic acid prevents oxidative stress-induced loss of renal tight junction proteins in type-1 diabetic model. J Nutr Biochem 26(5):441–454
41. Jiménez-Osorio A, Picazo A, González-Reyes S, Barrera-Oviedo D, Rodríguez-Arellano M, Pedraza-Chaverri J (2014) Nrf2 and redox status in prediabetic and diabetic patients. Int J Mol Sci 15:20290–20305
42. Gordon JA, Gattone VH (1986) Mitochondrial alterations in cisplatin-induced acute renal failure. Am J Physiol 250:F991–F998
43. Kruidering M, Van de Water B, de Heer E, Mulder GJ, Nagelkerke JF (1997) Cisplatin-induced nephrotoxicity in porcine proximal tubular cells: mitochondrial dysfunction by inhibition of complexes I to IV of the respiratory chain. J Pharmacol Exp Ther 280:638–649
44. Zsengellér ZK, Ellezian L, Brown D, Horváth B, Kalyanaraman B, Parikh SM, Karumanchi SA, Stillman IE, Pacher P (2012) Cisplatin nephrotoxicity involves mitochondrial injury with impaired tubular mitochondrial enzyme activity. J Histochem Cytochem 60:521–529
45. Li-ping X, Skrezek C, Wand H, Reibe F (2000) Mitochondrial dysfunction at the early stage of cisplatin-induced acute renal failure in rats. J Zhejiang Univ Sci 1:91–96
46. Pourahmad J, Hosseini M-J, Eskandari MR, Shekarabi SM, Daraei B (2010) Mitochondrial/lysosomal toxic cross-talk plays a key role in cisplatin nephrotoxicity. Xenobiotica Fate Foreign Compd Biol Syst 40:763–771
47. Gaona-Gaona L, Molina-Jijón E, Tapia E, Zazueta C, Hernández-Pando R, Calderón-Oliver M, Zarco-Márquez G, Pinzón E, Pedraza-Chaverri J (2011) Protective effect of sulforaphane pretreatment against cisplatin-induced liver and mitochondrial oxidant damage in rats. Toxicology 286:20–27
48. Paradies G, Petrosillo G, Paradies V, Reiter RJ, Ruggiero FM (2010) Melatonin, cardiolipin and mitochondrial bioenergetics in health and disease. J Pineal Res 48:297–310
49. Inoue M, Sato EF, Nishikawa M, Park A-M, Kira Y, Imada I, Utsumi K (2003) Mitochondrial generation of reactive oxygen species and its role in aerobic life. Curr Med Chem 10:2495–2505
50. Klimova T, Chandel NS (2008) Mitochondrial complex III regulates hypoxic activation of HIF. Cell Death Differ 15:660–666

51. Ott M, Gogvadze V, Orrenius S, Zhivotovsky B (2007) Mitochondria, oxidative stress and cell death. Apoptosis 12:913–922
52. Brand MD, Nicholls DG (2011) Assessing mitochondrial dysfunction in cells. Biochem J 435:297–312
53. Quinlan CL, Perevoshchikova IV, Goncalves RLS, Hey-Mogensen M, Brand MD (2013) The determination and analysis of site-specific rates of mitochondrial reactive oxygen species production. Methods Enzymol 526:189–217
54. Ryberg H, Caidahl K (2007) Chromatographic and mass spectrometric methods for quantitative determination of 3-nitrotyrosine in biological samples and their application to human samples. J Chromatogr B 851:160–171
55. Chirino YI, Trujillo J, Sánchez-González DJ, Martínez-Martínez CM, Cruz C, Bobadilla NA, Pedraza-Chaverri J (2008) Selective iNOS inhibition reduces renal damage induced by cisplatin. Toxicol Lett 176:48–57
56. Orrenius S (2007) Reactive oxygen species in mitochondria-mediated cell death. Drug Metab Rev 39:443–455
57. Romay C, Gonzalez R, Pizarro M, Lissi E (2000) Kinetics of c-phycocyanin reaction with hypochlorite. J Protein Chem 19:151–155
58. Lissi E, Pizarro M, Aspee A, Romay C (2000) Kinetics of phycocyanine bilin groups destruction by peroxyl radicals. Free Radic Biol Med 28:1051–1055
59. Patel A, Sandhya M, Ghosh PK (2006) Antioxidant potential of C-phycocyanin isolated from cyanobacterial species *Lyngbya*, *Phormidium* and *Spirulina* spp. Indian J Biochem Biophys 43:25–31
60. Wang CY, Wang X, Wang Y, Zhou T, Bai Y, Li YC, Huang B (2012) Photosensitization of phycocyanin extracted from *Microcystis* in human hepatocellular carcinoma cells: implication of mitochondria-dependent apoptosis. J Photochem Photobiol B 117:70–79
61. Gupta M, Dwivedi UN, Khandelwal S (2011) C-Phycocyanin: an effective protective agent against thymic atrophy by tributyltin. Toxicol Lett 204:2–11
62. Marín-Prida J, Pentón-Rol G, Rodrigues FP, Alberici LC, Stringhetta K, Leopoldino AM, Naal Z, Polizello ACM, Llópiz-Arzuaga A, Rosa MN, Liberato JL, Dos Santos WF, Uyemura SA, Pentón-Arias E, Curti C, Pardo-Andreu GL (2012) C-Phycocyanin protects SH-SY5Y cells from oxidative injury, rat retina from transient ischemia and rat brain mitochondria from $Ca^{(2+)}$/phosphate-induced impairment. Brain Res Bull 89:159–167
63. Farooq SM, Boppana NB, Asokan D, Sekaran SD, Shankar EM, Li C, Gopal K, Bakar SA, Karthik HS, Ebrahim AS (2014) C-phycocyanin confers protection against oxalate-mediated oxidative stress and mitochondrial dysfunctions in MDCK cells. PLoS ONE 9:103361
64. Waseem M, Kaushik P, Parvez S (2013) Mitochondria-mediated mitigatory role of curcumin in cisplatin-induced nephrotoxicity. Cell Biochem Funct 31:678–684

Juárez et al. BMC Pulmonary Medicine 2014, 14:152
http://www.biomedcentral.com/1471-2466/14/152

BMC Pulmonary Medicine

RESEARCH ARTICLE Open Access

Nucleotide-oligomerizing domain-1 (NOD1) receptor activation induces pro-inflammatory responses and autophagy in human alveolar macrophages

Esmeralda Juárez[1], Claudia Carranza[1], Fernando Hernández-Sánchez[1], Elva Loyola[1], Dante Escobedo[2], Juan Carlos León-Contreras[3], Rogelio Hernández-Pando[3], Martha Torres[1] and Eduardo Sada[1*]

Abstract

Background: Nucleotide-binding oligomerizing domain-1 (NOD1) is a cytoplasmic receptor involved in recognizing bacterial peptidoglycan fragments that localize to the cytosol. NOD1 activation triggers inflammation, antimicrobial mechanisms and autophagy in both epithelial cells and murine macrophages. NOD1 mediates intracellular pathogen clearance in the lungs of mice; however, little is known about NOD1's role in human alveolar macrophages (AMs) or its involvement in *Mycobacterium tuberculosis* (Mtb) infection.

Methods: AMs, monocytes (MNs), and monocyte-derived macrophages (MDMs) from healthy subjects were assayed for NOD1 expression. Cells were stimulated with the NOD1 ligand Tri-DAP and cytokine production and autophagy were assessed. Cells were infected with Mtb and treated with Tri-DAP post-infection. CFUs counting determined growth control, and autophagy protein recruitment to pathogen localization sites was analyzed by immunoelectron microscopy.

Results: NOD1 was expressed in AMs, MDMs and to a lesser extent MNs. Tri-DAP stimulation induced NOD1 up-regulation and a significant production of IL1β, IL6, IL8, and TNFα in AMs and MDMs; however, the level of NOD1-dependent response in MNs was limited. Autophagy activity determined by expression of proteins Atg9, LC3, IRGM and p62 degradation was induced in a NOD1-dependent manner in AMs and MDMs but not in MNs. Infected AMs could be activated by stimulation with Tri-DAP to control the intracellular growth of Mtb. In addition, recruitment of NOD1 and the autophagy proteins IRGM and LC3 to the Mtb localization site was observed in infected AMs after treatment with Tri-DAP.

Conclusions: NOD1 is involved in AM and MDM innate responses, which include proinflammatory cytokines and autophagy, with potential implications in the killing of Mtb in humans.

Keywords: Human alveolar macrophages, Innate immunity, NOD1, IRGM, LC3, Autophagy, *Mycobacterium tuberculosis*

* Correspondence: eduardosadadiaz@yahoo.com
[1]Department of Microbiology, Instituto Nacional de Enfermedades Respiratorias Ismael Cosio Villegas, México City, México
Full list of author information is available at the end of the article

Background

Pathogen recognition and induction of innate immune responses are important for the efficient elimination of infection. The nucleotide-oligomerizing domain 1 (NOD1) pattern recognition receptor senses the cytosolic presence of meso-diaminopimelic acid (DAP)-containing peptidoglycan fragments derived predominantly from the cell walls of gram-negative bacteria and *M. tuberculosis* [1,2]. Following microbial sensing, NOD1 directly recruits a serine–threonine kinase, Receptor-interacting protein 2 (Rip2), which initiates a signal cascade that ultimately allows NF-κB to translocate to the nucleus [3]. Stimulating NOD1 induces the secretion of proinflammatory cytokines and chemokines (IL-6, IL-8, CXCL1, MIP-2, CCL2, and CCL5), the production of antimicrobial peptides (β-defensins), and autophagy in human epithelial cells [4-6].

Recent evidence reveals a major role for NOD1 in the resolution of respiratory infections. NOD1-deficient mice have an impaired ability to eliminate pulmonary *Legionella pneumophila* and to recruit neutrophils to the lungs [7]; clearance of *Streptococcus pneumoniae* and *Haemophilus influenzae* also occurs via a NOD1-dependent manner in a murine model of co-infection [8]. Rip2−/− mice show reduced iNOS expression and delayed neutrophil recruitment to the lungs and an inability to clear *Chlamydophila pneumoniae* infections, which subsequently lead to an increased rate of mortality [9]. Despite the evidence for NOD1's role in resolving pulmonary infections, there are no data to support its role in *M. tuberculosis* infections.

Alveolar macrophages (AMs) are responsible for microbial lung clearance by orchestrating inflammatory responses that stimulate epithelial lung cells to produce additional chemokines and antimicrobial peptides, which amplify innate responses and help recruit other cells, such as monocytes and neutrophils [10]. AMs are also the cells responsible for eliminating *M. tuberculosis*. Although antimicrobial activity may be induced by NOD1, the involvement of AMs in NOD1-mediated responses and the full spectrum of cellular mechanisms responsible for antimicrobial NOD1-dependent activity, in mice and humans, remain to be elucidated.

In the present study, we investigate the presence of NOD1 in human AMs and examine its involvement with inflammatory cytokines and the induction of antimicrobial autophagy. For comparison, we include monocytes and monocyte-derived macrophages, as human monocytic cells have been reported to initiate proinflammatory responses following NOD1 ligand recognition [11]. Because NOD1 and autophagy are involved in intracellular pathogen clearance, we also analyze the role of NOD1 activation in the control of *M. tuberculosis* infection. Finally, we describe a novel role for NOD1 in primary human AM innate responses.

Methods

Ethics statement

The subjects for this study were healthy nonsmokers with a median age of 24 (range 20–40) years, 25% female, 75% male, seronegative for HIV-1, and no history of pulmonary or cardiac disease or recent infections. These subjects were studied after giving a signed informed consent, according to the Declaration of Helsinki, for bronchoalveolar lavage and venipuncture. The National Institute for Respiratory Diseases (INER) Institutional Review Board in Mexico City approved this protocol.

Cells

Human bronchoalveolar cells were obtained by bronchoscopy, as previously described [12]. Cells were collected in sterile saline solutions and centrifuged at 400 × g for 15 minutes at 4°C. The pellets from the bronchoalveolar cells were suspended in culture medium, and the viability of the bronchoalveolar cells was assessed by Trypan blue exclusion (>98% in all cases). Bronchoalveolar cells were found to be 94.3 ± 2.8% alveolar macrophages according to flow cytometric analysis using a gate based on size and granularity. Therefore, we will refer to these cells as alveolar macrophages (AMs) in this study.

Monocyte-derived macrophages (MDMs) were obtained from peripheral blood mononuclear cells (PBMCs) that were prepared by centrifugation of whole heparinized venous blood diluted 1/1 with RPMI 1640 (Lonza, Walkersville, MD, USA) over a Lymphocyte separation solution (Lonza) gradient. PBMCs were plated in polystyrene dishes and incubated for 1 h at 37°C, in 5% CO_2. After discarding non-adherent cells and extensive washings, the monocytes were recovered using a cell lifter. The viability of the monocytes was assessed by Trypan blue exclusion and was greater than 98% in all cases. MN concentrations were adjusted to 10^6 cells/ml and were incubated on 24-well plates at 37°C, in 5% CO_2 for 7 days, which allowed them to differentiate into MDMs that adhered to plastic [13]. MNs and MDMs were assayed for NOD1 activation. In all of the experiments, the culture medium consisted of RPMI 1640 supplemented with 50 μg/mL gentamycin sulfate, 200 mM L-glutamine, and 10% heat-inactivated pooled human serum.

Cell stimulation

To assess ligand-induced responses, 10^6 AMs, MDMs, and MNs were cultured in a final volume of 1 mL in an ultra-low attachment polystyrene 24-well plate (Corning Inc., NY, USA). The cells were stimulated using 5 μg/mL of synthetic L-Ala-γ-D-Glu-meso-diaminopimelic acid (Tri-DAP) (InvivoGen, San Diego, CA, USA) for 24 h. Next, the supernatants were collected and kept frozen until the cytokine assessment; the cells were harvested and prepared for protein or mRNA extraction. Culture

medium alone was used as a negative control, and LPS was used as a positive control, as indicated. In selected experiments, 10 μM of Rip2/p38 inhibitor SB203580 (Promega, Madison, WI, USA), 20 μM of PI3K inhibitor LY294002 (Promega) and 20 μM of pan-caspases inhibitor Z-VAD-fmk (Calbiochem, La Joya, CA, USA) were added to the cells 30 minutes before Tri-DAP stimulation to block NOD1 signaling.

Reverse transcription and real-time PCR for gene expression

Total RNA was extracted and reverse transcribed as previously reported [13]. The cDNA was subjected to quantitative real-time PCR (qRT-PCR, TaqMan) to determine the NOD1, LC3 and IRGM mRNA expression levels using the comparative threshold cycle (ΔΔCt) as described previously [14]. Real-time PCR reactions were performed in duplicate wells according to the manufacturer's protocol for Taqman predesigned gene assays; NOD1 (Hs01036717_m1), LC3 (Hs00171082_m1 and IRGM (Hs01013699_s1) were purchased from Applied Biosystems (Carlsbad, CA, USA). The Ct values for each gene were normalized to the endogenous control gene 18S rRNA (4319413E).

Cytokine detection

Supernatants of 24-h cultures were assayed for the release of IL1β, IL6, IL8, IL10, IL12p70, IFNα2, and TNFα cytokines using the Milliplex human cytokine detection kit (Millipore, Billerica, MA, USA) according to the manufacturer's protocol.

Immunoblot

Proteins extracted from cytoplasmic lysates were separated by SDS-PAGE and transferred to polyvinylidene difluoride membranes, as previously described [14]. Briefly, membranes were blocked and incubated with the following antibodies: anti-human NOD1 (AdB serotec, Raleigh, NC, USA), IRGM (Abcam, Cambridge, MA), Atg9, and LC3 (Novus Biologicals, Littleton, CA, USA) or α-tubulin (Sigma-Aldrich, St. Louis, MO, USA) for 2 h followed by an incubation with peroxidase-conjugated anti-rabbit or anti-mouse IgG antibody (Sigma-Aldrich) for 1 h at room temperature. Specific bands were detected with the chemiluminescence SuperSignal system (Thermo, Rockford, IL, USA) and were revealed using autoradiographic films. Densitometry was performed using ImageJ 1.44o (National Institutes of Health, USA).

Transduction of p62 to assess autophagic flux

MDMs were seeded in 8-well chamber slides (Thermo) at 5×10^5 cells/well. The cells were transduced with 15 viral particles per cell for ectopical expression of p62-RFP (Premo Autophagy Sensor p62 kit, Molecular Probes, Carlsbad, CA). After 18 h, the cells were stimulated with 5 μg/ml of Tri-DAP and incubated for 5 or 24 h at 37°C and 5% CO_2. Chloroquine 60 μM and medium were used as controls. We used Lysotracker (Molecular Probes) to stain lysosomes and Hoescht 33342 (Enzo Life Sciences, Farmingdale, NY) to stain nuclei following the manufacturer's instructions. Cells were visualized in an AxioScope. A1 microscope (Carl Zeiss, Oberkochen, Germany) with the appropriate fluorescence filters. Images were acquired and analyzed with ZEN Pro software (Carl Zeiss).

Infection with *Mycobacterium tuberculosis* and post-infection treatment

M. tuberculosis (Mtb) strain H37Rv (ATCC 25618) was grown as previously described [12]. AMs (10^5) were infected with Mtb in RPMI with 30% non-heat-inactivated, pooled human AB serum at an infection ratio of 1–2 bacteria/20 cells in 96-well polystyrene plates; they were incubated for 1 h followed by three washes to remove any non-phagocytized bacteria. The cells were then cultured for another hour in RPMI supplemented with 10% heat-inactivated pooled human serum with or without 5 μg/ml of Tri-DAP. The infected macrophages were incubated after Tri-DAP treatment for 1 h (Day 0), 24 h (Day 1) and 96 h (Day 4) to evaluate the effects of macrophages on mycobacterial intracellular growth by quantifying the colony-forming units (CFUs). The intracellular growth index was calculated as the ratio of CFUs at Day 1 or 4 relative to the CFUs at Day 0.

AMs were infected with a multiplicity of infection (MOI) of 5 using 4×10^6 cells cultured in polypropylene tubes under the same conditions described above and analyzed by transmission electron microscopy. Cells were treated with Tri-DAP with or without prior inhibition of Rip2/p38 and PI3K for 24 h post-infection and fixed in preparation for electron microscopy detection and subcellular localization of proteins.

Electron microscopy

The subcellular localization of IRGM and LC3 proteins was performed using transmission electron microscopy (TEM), as previously described [15]. Briefly, cells were fixed in 4% paraformaldehyde in 0.2 M Sörensen buffer; the samples were dehydrated with increasing concentrations of ethylic alcohol and infiltrated with LR-White hydrosoluble resin (London Resin Co., Hampshire, United Kingdom). Sections that were 60- to 80-nm-thick were placed on nickel grids. The grids were incubated overnight at 4°C with specific polyclonal rabbit anti-IRGM (Abcam) and anti-LC3 (Novus Biologicals) antibodies followed by a 2 h incubation at room temperature with goat anti-rabbit IgG (Sigma-Aldrich) conjugated to 5-nm gold particles (Sigma-Aldrich) and diluted 1:20 in PBS. The grids were contrasted with uranyl acetate (Electron Microscopy

Sciences, Fort Washington, PA) and examined with an M-10 Zeiss electron microscope (Karl Zeiss, Jena, Germany). To quantitatively assess autophagy protein recruitment to the mycobacteria-containing vesicle, we performed morphometric analyses by counting gold particles that colocalized with bacteria in 10 randomly selected cells from each condition (10–18 bacteria/condition) using ImageJ software.

Statistical analysis

Data of paired samples from related subjects were analyzed by a non-parametric two-tailed Wilcoxon signed-rank test. Comparisons among non-related samples were analyzed using a Mann–Whitney U test. The colocalization of gold particles with bacteria between treatments was analyzed using a two-tailed paired *t*-test. The means and standard errors (SEs) were calculated where indicated. A p-value of $p < 0.05$ was considered a statistically significant difference. The statistical analyses were performed using SPSS 15.0 for Windows (SPSS, Chicago, IL, USA) and GraphPad Prism, version 5.0 (GraphPad Software Inc., San Diego, CA, USA).

Results

NOD1 is up-regulated in AMs and MDMs, but not in monocytes, after ligand stimulation

Differences in Toll-like receptor patterns have been previously described between differentiated macrophages and monocytes [13]; therefore, we investigated whether NOD1 was expressed in unstimulated AMs, MDMs, and MNs. We observed a basal protein expression in all cell populations studied (Figure 1A) and densitometry revealed that NOD1 was more abundant in AMs (Figure 1B). We did not observe significant differences in the relative abundance of NOD1 mRNA in unstimulated cells (Figure 1C). However, after stimulation with Tri-DAP, AMs significantly up-regulated their NOD1 mRNA levels relative to the unstimulated cells, while MDMs barely modulated their gene expression and MNs showed down-regulated NOD1 levels ($p < 0.05$ vs. AMs, Figure 1D).

NOD1 stimulation with Tri-DAP induces proinflammatory cytokines in AMs and MDMs

NOD1 pathogen recognition is typically accompanied by proinflammatory cytokine production [16]. AMs are responsible for initiating inflammatory responses, which recruit large numbers of neutrophils into the alveolar spaces to clear bacteria from entering terminal airways [17]. In this study, we have determined that Tri-DAP stimulation of macrophages in 24 h cultured supernatants results in pro-inflammatory cytokine production. We found that AMs release significant amounts of IL1β, IL6, TNFα, and IL8 ($p < 0.05$, Figure 2A). Meanwhile, MDMs released significant quantities of IL1β, TNFα, and IL8 ($p < 0.05$), and remarkably, MNs only produce significant amounts of IL1β in response to Tri-DAP

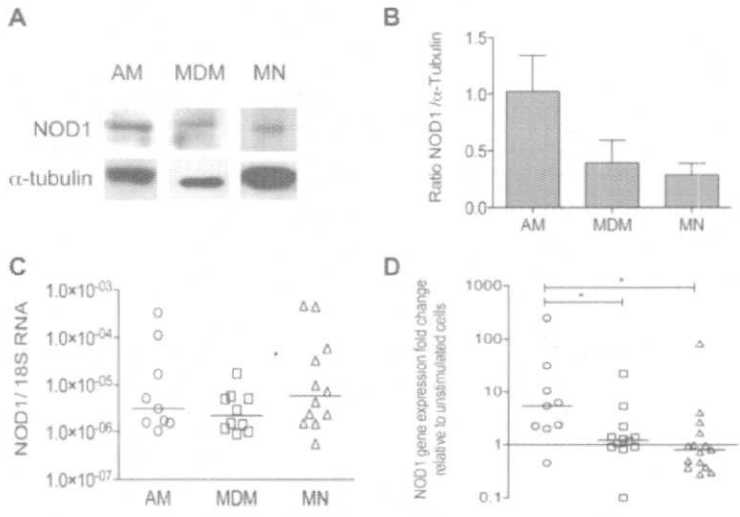

Figure 1 Differential NOD1 expression and response patterns between differentiated macrophages and monocytes. Unstimulated alveolar macrophages (AMs), monocyte-derived macrophages (MDMs) and monocytes (MNs) were lysed. NOD1 protein expression was measured from the cytosolic fractions by western blot analysis; one representative experiment out of three is depicted **(A)** and the mean ± SE of protein expression after normalized to tubulin is depicted; n = 3 **(B)**. Total RNA was extracted from cell lysates and reverse transcribed. NOD1 gene expression is depicted relative to the 18S RNA content of at least 9 subjects; the lines represent the median values **(C)**. Cells were incubated in the presence or absence of 5 μg/ml of Tri-DAP for 24 h. Up-regulation of NOD1 gene expression was assessed by quantitative PCR using the Taqman system and ΔΔCT for relative quantification. The fold changes of gene expression relative to the unstimulated cells of at least 9 subjects are depicted; the lines indicate the median values; *$p < 0.05$, Mann Whitney U test **(D)**.

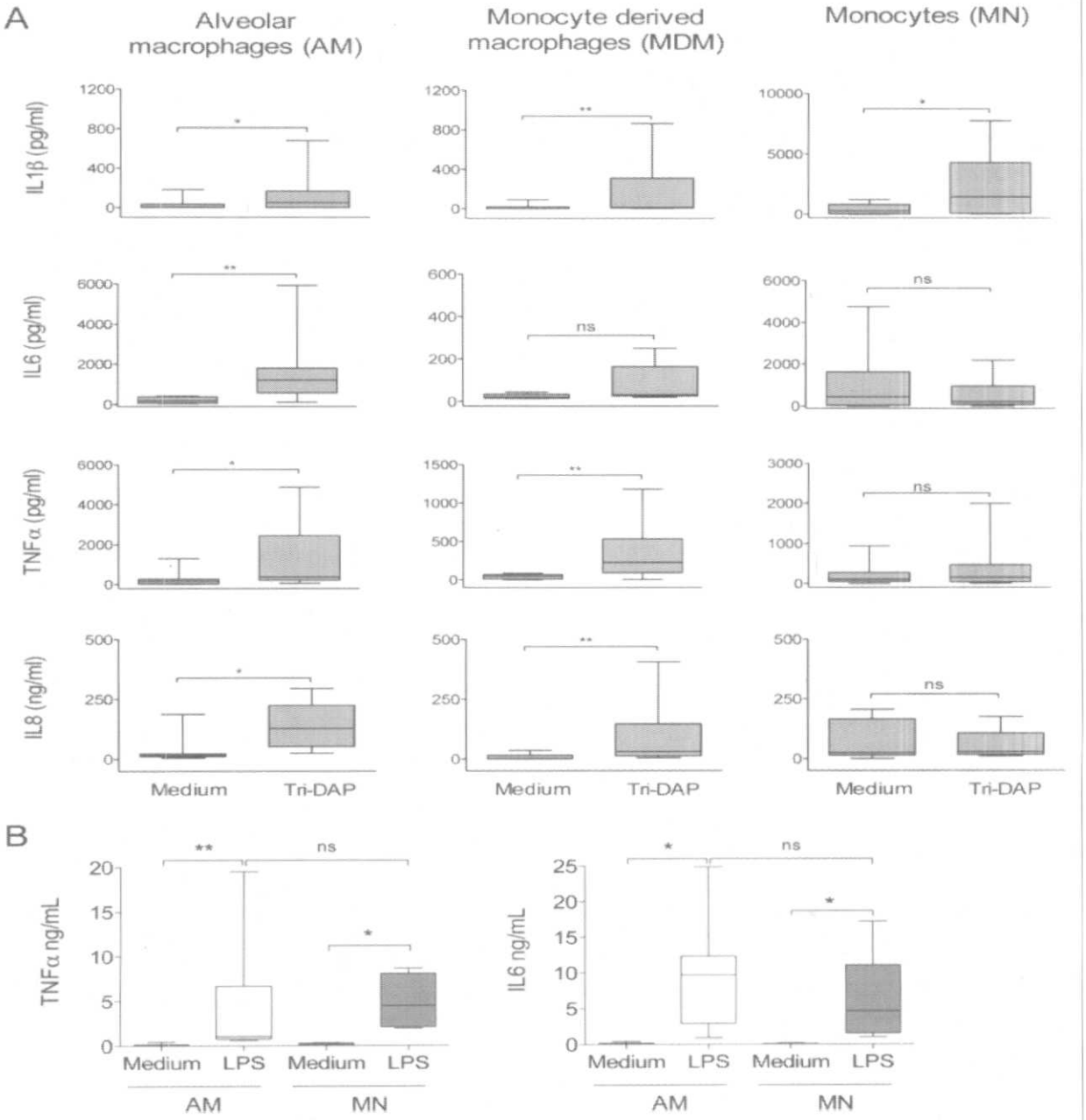

Figure 2 Macrophages stimulated with Tri-DAP release proinflammatory cytokines. Cells were incubated in the presence or absence of 5 μg/ml of Tri-DAP (n = 10, **A**) or 100 ng/ml of LPS (n = 8, **B**). The supernatants were collected after 24 h; cytokine production was measured using milliplex technology. Box plots indicate median and quartiles, *p < 0.05, **p < 0.01, ns = not significant Wilcoxon Rank test.

stimulation ($p < 0.05$). Interestingly, in all of the cell types tested, we did not find any anti-inflammatory production of IL10 after Tri-DAP exposure (data not shown). In addition, AMs, the maximum responders to Tri-DAP stimulation, were also assayed for IL12p70, IFNα, and IL17; we found that AMs do not produce these cytokines in response to NOD1 ligand binding (data not shown). To confirm the selectivity of NOD1's proinflammatory response, we stimulated AMs, the highest responders, and MNs, the lowest responders, with 100 ng/ml of LPS and observed that significant amounts of TNFα, IL6, and IL10 were released from both cell types ($p < 0.05$, compared to medium), and the levels of cytokine production were similar in both cells (Figure 2B). Cytokine responses were confirmed by qPCR using cell lysate-derived cDNAs (data not shown).

Macrophages increase their autophagy activity after stimulation with NOD1 ligand

NOD1 induces autophagy in epithelial cells [6], and we recently found that NOD2 activation induces autophagy in human AMs as part of their antibacterial pulmonary defense [14]. Thus, we evaluated the ability of NOD1 to induce autophagy in different macrophages by determining the expression of the autophagy proteins Atg9 and LC3 after Tri-DAP exposure. We found that the expression of Atg9 increased after NOD1 stimulation in AMs and MDMs (Figure 3A).

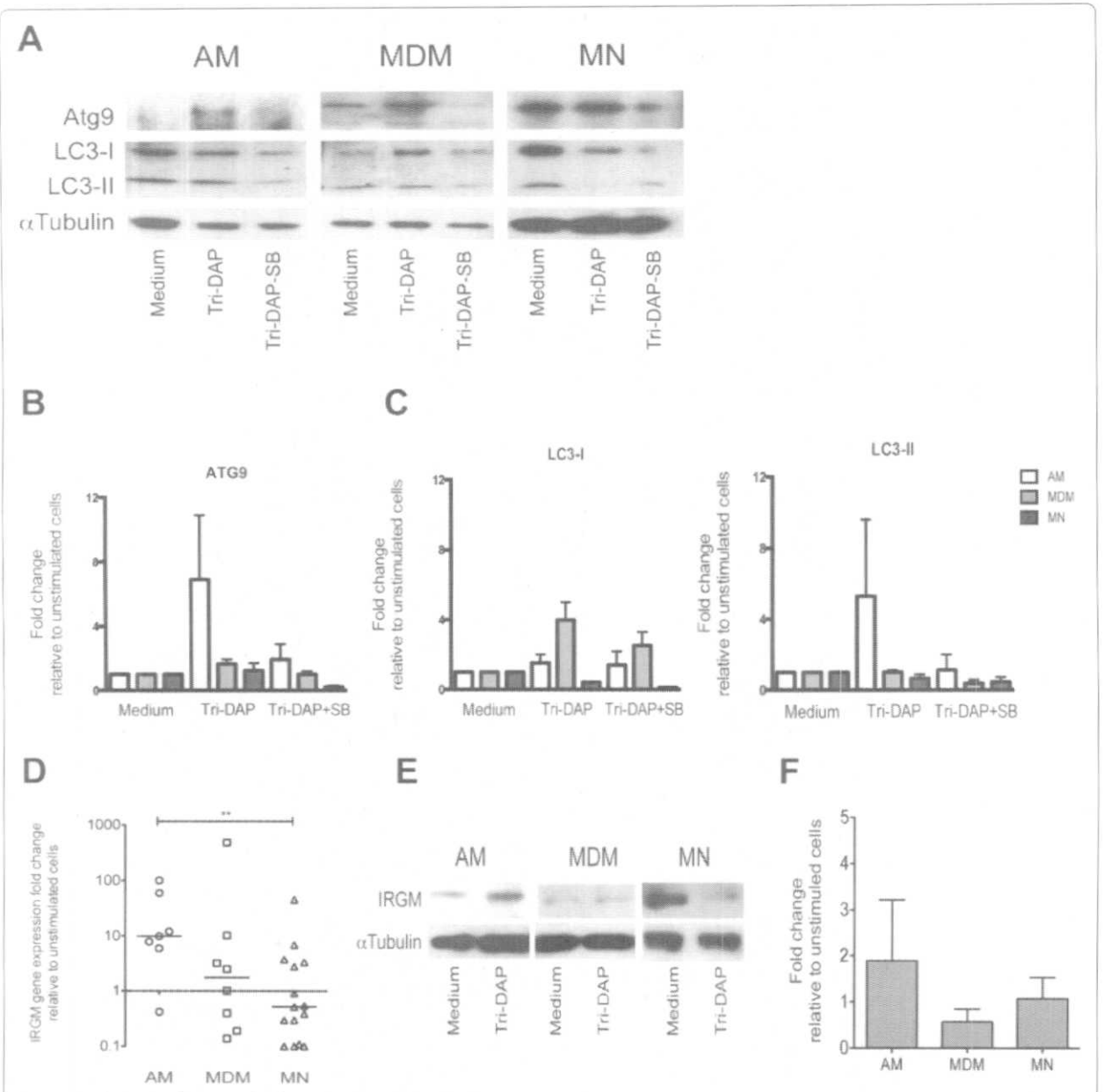

Figure 3 After stimulation with the NOD1 ligand, macrophages increased their expression of autophagy proteins Atg9, LC3 and IRGM. Alveolar macrophages (AMs), monocyte-derived macrophages (MDMs) and monocytes (MNs) were incubated in the presence of 5 μg/ml of Tri-DAP for 24 h. Cells were pre-incubated with Rip2/p38 inhibitor SB203580 (SB) for 30 min prior to Tri-DAP stimulation to block NOD1-mediated responses, as indicated. Atg9 and LC3 proteins were measured in the cytosolic fractions by western blot analysis **(A)**. The fold increases relative to the unstimulated cells were calculated after being normalized to tubulin, mean ± SE is depicted, n = 3 **(B, C)**. The up-regulation of IRGM gene expression was assessed after specific ligand recognition by quantitative PCR using the Taqman system and ΔΔCT method for relative quantification. The fold changes in gene expression relative to the unstimulated cells of at least 6 subjects are depicted; bold lines indicate medians, *$p < 0.05$ **(D)**. IRGM protein was measured in the cytosolic fractions of three subjects by western blot, and the fold increases relative to the unstimulated cells are indicated after being normalized to tubulin; mean + SE is depicted, n = 3 **(E, F)**.

Pretreatment of AMs and MDMs with the Rip2/p38 inhibitor SB203580 for 30 min prior to Tri-DAP stimulation blocked NOD1-mediated responses and blocked the increased expression of Atg9 (Figure 3A,B). NOD1 activation also induced an increment in LC3-I and II in AMs and MDMs (Figure 3A,C). In contrast, no increase in autophagy proteins was observed in MNs. The enzyme IRGM is a key autophagy component with antimicrobial functions. Thus, we analyzed IRGM expression levels and determined that IRGM gene expression was elevated in AMs after Tri-DAP exposure, slightly increased in MDMs, and decreased in MNs (Figure 3D). Consistent with the gene expression data, only the AMs overexpress IRGM protein after Tri-DAP stimulation (Figure 3E,F).

To confirm that autophagy was productive, we used ectopically expressed p62 in MDMs as an indicator of autophagic flux. The p62/SQSTM1 is a receptor for cargo destined to be degraded by autophagy [18]. Because the vector does not replicate within mammal cells, p62 is degraded when autophagy occurs and an accumulation of p62 positive vesicles indicate lack of autophagic flux. After 24 h of Tri-DAP treatment we observed cells with p62 puncta (Figure 4A). When we compared p62 puncta values obtained at 5 h to those of 24 h an evident reduction in p62 was observed confirming the development of productive autophagy (Figure 4B). In addition, most of the p62 puncta of Tri-DAP treated cells colocalyzed with lysotracker (Figure 4C). Chloroquine, as expected, induced autophagy but blocked the fusion autophagosomes-lysosome thus preventing the completion of the autophagic flux.

Tri-DAP stimulation confines *M. tuberculosis* to autophagic vesicles and helps control intracellular growth

Our results reveal that NOD1 activation induces an antibacterial state in AMs, which may improve the control of intracellular pathogenic infections. Therefore, we evaluated the role of NOD1 stimulation during *in vitro* infections with Mtb, one of the most successful intracellular pathogens. Previously, we demonstrated that Tri-DAP-treated AMs develop autophagy (Figures 3 and 4). Therefore, we

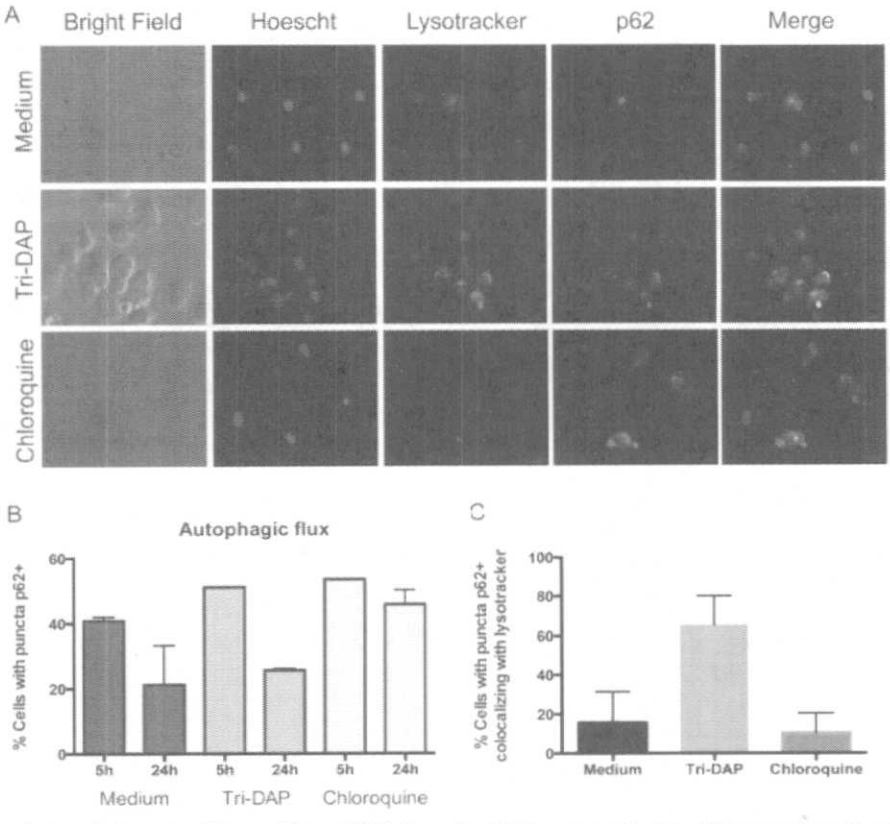

Figure 4 Autophagy induced after stimulation with the NOD1 ligand in MDMs was productive. MDMs were transduced with p62-RFP during 18 h. Cells were incubated in the presence of 5 μg/ml of Tri-DAP for 24 h. Accumulation of p62 in autophagosomes (puncta) was evaluated by fluorescence microscopy **(A)**. Lysotracker and Hoescht were used to stain lysosomes and nuclei, respectively. Choloroquine 60 μM was included as autophagic flux blocker. Transduction levels of p62 (5 h) and autophagy induction (24 h) were evaluated by counting cells with p62 puncta **(B)** and colocalization with lysotracker **(C)**. The mean ± SE of two independent experiments is depicted. Up to 300 cells were counted for each condition.

used immunoelectron microscopy to examine the recruitment of IRGM and LC3 to Mtb-containing vesicles in AMs infected with Mtb that were treated or non-treated with Tri-DAP. Our results demonstrate that when AMs are treated with Tri-DAP post-infection, the Mtb is enclosed in autophagic vesicles that are positive for autophagy proteins, such as IRGM and LC3, whereas a minimum recruitment of these proteins is observed in the untreated macrophages (Figure 5A-D). To confirm whether the recruitment of IRGM and LC3, as well as autophagy, were dependent on NOD1 signaling, we pre-incubated cells with Rip2/p38 (SB) and PI3K (LY) inhibitors prior to Tri-DAP stimulation (Additional file 1). The use of both inhibitors significantly diminished the recruitment of autophagy proteins to the Mtb-containing vesicle (Figure 5E, F). In absence of stimulation the expression of IRGM was very low, and LC3 was homogeneously distributed within the cytosol (Additional file 2).

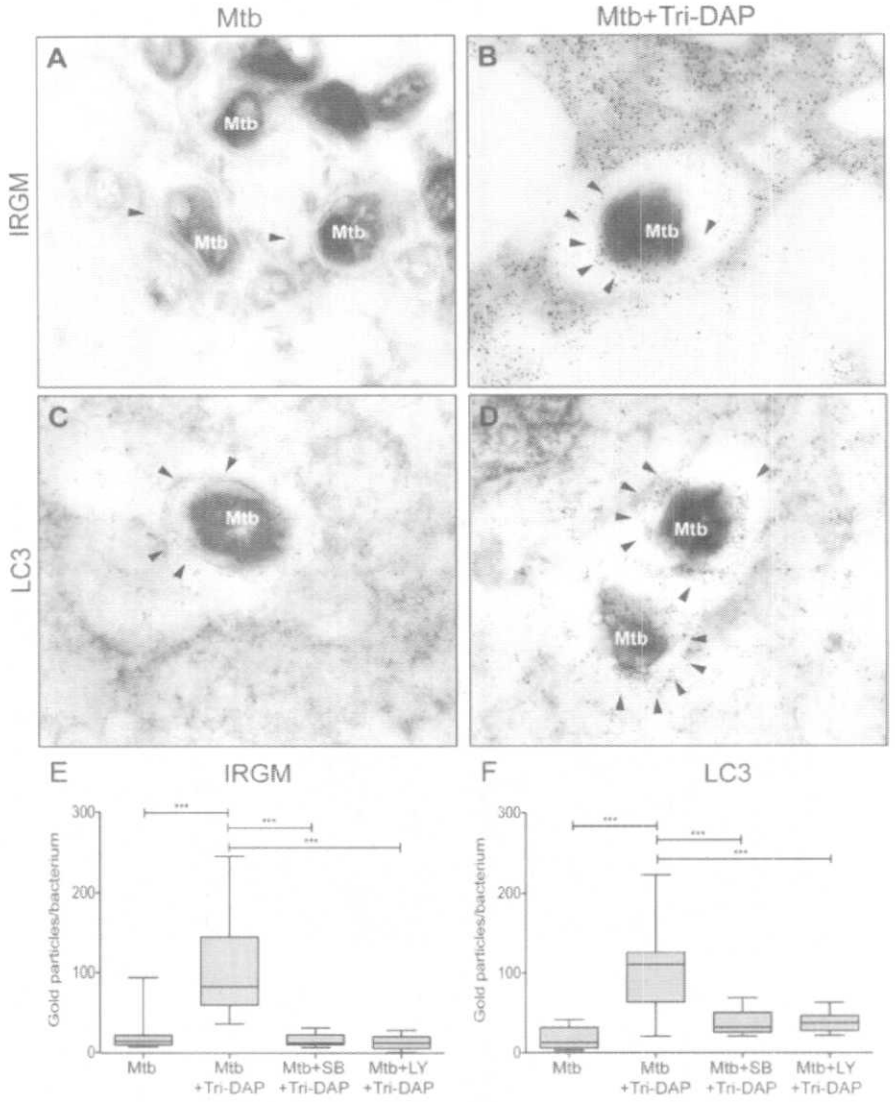

Figure 5 NOD1-dependent induction of autophagy contributes to IRGM and LC3 recruitment to Mtb-containing vesicles. AMs were infected with *M. tuberculosis* H37Rv using an infection ratio of 5 bacteria/macrophage for 1 h. Non-phagocytized bacteria were washed away. Then, the macrophages were treated with 5 μg/ml of Tri-DAP for 24 h. Cells were pre-incubated with Rip2/p38 inhibitor SB203580 (SB) or PI3K inhibitor LY294002 (LY) for 30 min prior to Tri-DAP stimulation which blocks NOD1- or autophagy-mediated responses, as indicated. The subcellular localization of autophagy proteins was observed in untreated **(A, C)** and Tri-DAP treated cells **(B, D)** using anti-IRGM and anti-LC3 antibodies, which were detected using a secondary antibody coupled to 5 nm gold particles (indicated with arrowheads; TEM X 62,000). Gold particles colocalizing with bacteria were manually counted in 10 macrophages of each condition **(E, F)** and the differences between the treatments are indicated: ***$p < 0.01$ and *$p < 0.05$ vs. Mtb, ++$p < 0.01$ vs. Tri-DAP, Wilcoxon Rank test. Box plots indicate median and quartiles.

Next, we investigated whether Tri-DAP treatment improves the control of Mtb-intracellular growth. The intracellular growth index revealed that bacterial growth was lower inside AMs when they were treated with Tri-DAP post-infection (Figure 6A) compared with the infected AMs that did not receive Tri-DAP stimulation. Moreover, Tri-DAP stimulation induced the release of significant amounts of TNFα and the overexpression of LC3 mRNA in AMs infected with Mtb (Figure 6B,C) that were not observed in AMs when they were not treated with Tri-DAP.

Discussion

The nucleotide-oligomerizing domain 1 (NOD1) pattern recognition receptor is essential in respiratory innate defense. NOD1 deficiencies cause severe respiratory diseases and impair antibacterial mechanisms in mouse models [7,9]. Human lung epithelial cells contribute to the clearance of attenuated *K. pneumoniae* by producing beta-defensins in a TLR2- and NOD1-dependent manner, which highlights the importance of NOD1 in respiratory pathogen elimination and in pathogen-evasion mechanisms in human pneumonia [19]. However, the role of NOD1 in human AM responses remains unknown. In the current study, we investigate the role of NOD1 in the primary human AM innate response, focusing on the proinflammatory effectors and the induction of autophagy.

First, we determined the intracellular expression of NOD1 in unstimulated primary human AMs and compared their NOD1 expression levels with those of MNs and MDMs. We determined that NOD1 was expressed in the cytosol of AMs, MNs, and MDMs. The NOD1 mRNA levels in unstimulated AMs are similar to those in MDMs and MNs, indicating that NOD1 expression is independent of cell differentiation and that AMs, MNs, and MDMs could potentially respond to stimulation by NOD1 ligands. However, NOD1 gene expression was only up-regulated in AMs after Tri-DAP stimulation; neither the MDMs nor the MNs increased their NOD1 gene expression, which suggests that regulation or the functional ability of the receptor is cell type-dependent.

In agreement with ligand-induced NOD1 overexpression, we observed a broader proinflammatory cytokine profile triggered by NOD1 in AMs. Alveolar macrophages produce significant quantities of TNFα, IL6, IL1β, and IL8; MDMs produce all of these cytokines except IL6; however, the MN response is restricted to IL1β. The low cytokine response observed in MNs is consistent with previous reports, which indicate that human PBMCs or purified MNs do not release pro-inflammatory cytokines after low concentrations of Tri-DAP stimulation. Instead, they synergize with TLR ligands to induce strong cytokine responses. However, increased Tri-DAP concentrations

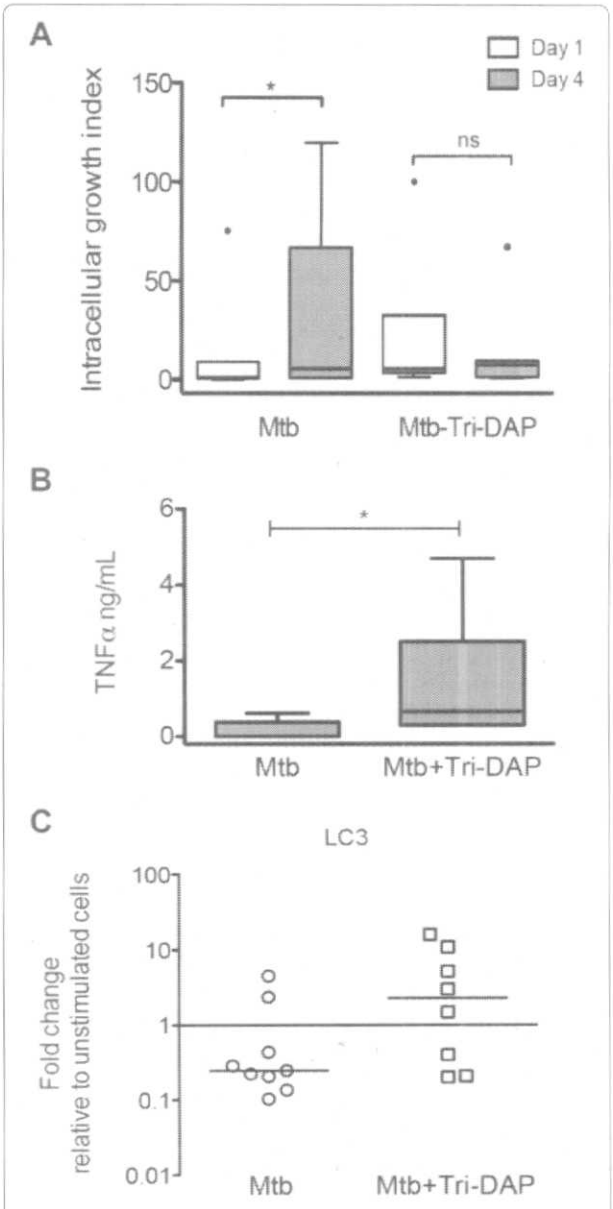

Figure 6 Tri-DAP treatment contributes to intracellular growth control of mycobacteria in alveolar macrophages. AMs were infected with *M. tuberculosis* H37Rv using an infection ratio of 1–2 bacteria/20 macrophages for 1 h. Non-phagocytized bacteria were washed away. Then, the macrophages were treated with 5 μg/ml of Tri-DAP for 24 h. The intracellular bacterial burden was measured by quantifying the colony-forming units, and the intracellular growth index was calculated after 1 and 4 days post-infection relative to the phagocytized bacteria at day 0; n = 7, *p < 0.05 **(A)**. TNFα production was determined by ELISA in 24 h supernatants, n = 7, *p < 0.05, box plots indicate median and quartiles **(B)**. LC3 gene expression was measured by quantitative PCR using the Taqman system and $\Delta\Delta$CT method for relative quantification. The fold changes in gene expression relative to the unstimulated cells of at least 8 subjects are depicted; bold lines indicate medians **(C)**.

induce cytokine responses in MNs [20,21]. Thus, the cytokine responses elicited by NOD1 stimulation depend on the stage of maturation and the specific requirements of the tissue. AMs produce increased levels of IL8, which suggests a role for NOD1-dependent neutrophil recruitment to human lungs. Meanwhile, other reports suggest that NOD1 responses induce not only neutrophil recruitment but also an increased neutrophil-killing capacity [22,23]. NOD1 induces the production of proinflammatory cytokines, which is critical for bacterial clearance in mice with *L. pneumophila* [24].

One of the antimicrobial mechanisms induced by innate receptors is autophagy, which is inducible by NOD1 in epithelial cells [6]. Therefore, we investigated whether macrophages could initiate autophagy in response to NOD1 ligand stimulation. We investigated the expression of the autophagy-related proteins Atg9, LC3, and IRGM after stimulation with Tri-DAP and found that AMs increase the expression of Atg9 and LC3. These results indicate that the autophagy process is involved because Atg9 is necessary for initiating autophagosome formation and LC3 is required to finalize autophagosome maturation [25,26]. Moreover, the degradation of p62 confirms the autophagy completion. In addition, NOD1 induces the overexpression of IRGM in AMs, which implies an antimicrobial component because human and murine IRGM not only induce autophagy but also collaborate to eliminate intracellular pathogens, including Mtb [27,28].

Taken together, our results suggest that AMs are highly responsive to NOD1 stimulation, MDMs elicit moderate innate responses after Tri-DAP stimulation, and MNs exhibit a limited response. Thus, although basal expression is similar, regulation of NOD1 expression levels, the quality and magnitude of NOD1-driven cytokine and autophagy responses are associated with the macrophage differentiation status and the tissue environment of the cell, which explains why higher responses are observed in AMs and MDMs.

Autophagy constitutes an important mechanism of defense against Mtb [29]. In this study, because autophagy was mainly induced in AMs, we evaluated the antimicrobial activity associated with autophagy in AMs. We infected AMs with Mtb as a model intracellular pathogen and evaluated the effect of NOD1 activation as an inducer of autophagy after an established infection. Some Mtb virulence factors inhibit autophagy in host macrophages to grant survival [30,31]. Therefore, Tri-DAP was added post-infection to overcome Mtb-associated inhibition of autophagy. After treating infected AMs with Tri-DAP, we observed recruitment of autophagy indicators, such as IRGM and LC3, to the pathogen-containing vesicles in a Rip2-dependent manner. Rip2-dependent and -independent responses have been documented for NOD1 and NOD2 [6]. LC3 and IRGM up-regulation have been used to measure autophagy because they are induced in human AMs after NOD2 activation [14]. Autophagy proteins did not increase and they were not recruited to pathogen-containing vesicles in the cells incubated with Rip2/p38 inhibitor prior to Tri-DAP stimulation. Therefore, our results indicate that the NOD1 ligand also induces autophagy in a Rip2-dependent manner in AMs. Autophagosomes become degradation compartments that influence phagosome maturation and pathogen degradation [32]. Therefore, the NOD1-dependent formation of autophagosomes may have improved the control of the intracellular mycobacterial burden that we observed in AMs.

Conclusions

The results of our study demonstrate the presence of NOD1 in AMs for the first time and show that this receptor is functionally active. These studies provide evidence that NOD1 induces the production of proinflammatory mediators and triggers autophagy mechanism in human alveolar macrophages. The antimicrobial profile activated by NOD1 may be of relevance, especially early after pulmonary microbe invasion. The induction of autophagy in AMs after NOD1 activation is a significant mechanism for eliminating intracellular microbes that enter the alveolar space, such as *M. tuberculosis*. NOD1 and NOD2 induce autophagy and recruitment of neutrophils and macrophages and have a role in defense against *M. tuberculosis* [33,34]; therefore, ligands of both receptors are potential candidates for use as immunomodulators in tuberculosis infection. Further studies are needed to elucidate whether activating the NOD1 receptor also induces other aspects of the AM immune response.

Additional files

Additional file 1: Tri-DAP-induced recruitment of IRGM (A-D) and LC3 (E-H) depends on NOD1 signaling and autophagy initiation.

Additional file 2: Detection of basal levels of IRGM and LC3 in unstimulated uninfected cells.

Abbreviations

AMs: Alveolar macrophages; MDMs: Monocyte-derived macrophages; MNs: monocytes; NOD1: Nucleotide-oligomerizing domain-1; IRGM: Immunity related GTPase M; Rip2: Receptor-interacting protein 2; p38: p38 mitogen-activated protein kinase; Tri-DAP: L-Ala-γ-D-Glu-meso-Diaminopimelic acid; LPS: Lipopolysaccharide.

Competing interests

The authors declare that they have no competing interests.

Authors' contributions

EJ performed the cell culture, cytokine detection and p62 transduction, participated in the molecular biology studies, performed the statistical analysis, and drafted the manuscript. CS, EL, FHS and DF participated in the immunoassays, the molecular biology studies, and western blotting. JL, RH performed and analyzed the electron microscopy measurements. ES conceived of the study; MT participated in the design and coordination of

INSTITUTO NACIONAL DE
CIENCIAS MÉDICAS
Y NUTRICIÓN
SALVADOR ZUBIRÁN

ausc

México, D.F. a 10 de Febrero de 2016

Dr. Rogelio Hernández Pando
Depto. Patología Experimental
Presente

Estimado Dr. Hernández:

Por este conducto le informo que su proyecto: **"INFRAESTRUCTURA DE APOYO A PROYECTOS RELACIONADOS CON LA EVALUACIÓN MORFOLÓGICA."**, con registro **CINVA: PAT-1300-14/15-1** finalizó en diciembre de 2015. Por lo que le solicito de la manera más atenta me haga saber si el proyecto requerirá una prórroga. En caso afirmativo, favor de enviar a la **CINVA** el periodo de extensión que solicita y de requerir un mayor número de animales especificar y justificar como se utilizarán y los procedimientos experimentales que se llevarán a cabo con los mismos. En caso de no requerir una prórroga favor de llenar el formato de cierre del protocolo que se anexa a la presente. De no recibir respuesta de su parte en el plazo de 30 días, el protocolo se dará por cerrado.

cerrado
10-marzo
2016

Sin otro particular por el momento, quedo de usted.

Atentamente,

Dra. Norma A. Bobadilla Sandoval
Coordinadora de la CINVA

INS. NACIONAL DE CIENCIAS MEDICAS Y NUTRICIÓN "SALVADOR ZUBIRÁN"
10 FEB 2016
DIRECCIÓN DE INVESTIGACIÓN

701
INSTITUTO NACIONAL DE CIENCIAS MEDICAS Y NUTRICIÓN
10 FEB 2016
INVESTIGACIÓN EXPERIMENTAL

INSTITUTO NACIONAL DE CIENCIAS MEDICAS Y NUTRICION "SALVADOR ZUBIRAN"
10 FEB 2016 11:54
DEPARTAMENTO DE ANATOMIA PATOLOGICA

c.c.p. Dr. Gerardo Gamba Ayala, Director de Investigación
MVZ Mariela Contreras Escamilla, Jefa del DIEB

NAB/nom

Avenida Vasco de Quiroga No. 15
Colonia Belisario Domínguez Sección XVI
Delegación Tlalpan
Codigo Postal 14080
Mexico, Distrito Federal
Tel. (52)54870900
www.incmnsz.mx

INSTITUTO NACIONAL DE CIENCIAS MÉDICAS Y NUTRICIÓN SALVADOR ZUBIRÁN

"2014 Año de Octavio Paz"

México, D.F. a 19 de junio de 2014.

DR. ROGELIO HERNÁNDEZ PANDO
Investigador en Ciencias Médicas F
Departamento de Patología
P r e s e n t e .

Estimado Doctor Hernández Pando:

Habiendo analizado detalladamente el Protocolo de Investigación Experimental titulado:

"Infraestructura de apoyo a proyectos relacionados con la evaluación morfológica ultraestructural de los efectos patogénicos de agentes infecciosos, químicos y nutricionales y sus posibles tratamientos.."

Este comité ha dictaminado **aprobar** el protocolo con la sugerencia a los autores de revisar y corregir el escrito ya que presenta muchas faltas de ortografía.

Su proyecto queda registrado en esta Institución como: **CINVA 1300: Clave: PAT-1300-14/15-1.**

Sin más por el momento quedo de usted.

INSTITUTO NACIONAL DE CIENCIAS MEDICAS Y NUTRICIÓN SALVADOR ZUBIRAN
INCMNSZ
23 JUN 2014
DEPARTAMENTO DE INVESTIGACIÓN EXPERIMENTAL Y BIOTERIO

Atentamente,

Dra. Norma A. Bobadilla Sandoval
Coordinadora de la Comisión de Investigación en Animales

INST NACIONAL DE CIENCIAS MEDICAS Y NUTRICION "SALVADOR ZUBIRAN"
23-JUN-14
DIRECCION DE INVESTIGACION

c.c.p. Dr. Gerardo Gamba A. Director de Investigación
Dr. Rafael Hernández. Jefe de Investigación Experimental y Bioterio

INSTITUTO NACIONAL DE CIENCIAS MEDICAS Y NUTRICION "SALVADOR ZUBIRAN"
P 23 JUN 2014 E
DEPARTAMENTO DE ANATOMIA PATOLOGICA
11:06

Vasco de Quiroga No. 15
Colonia Sección XVI
Delegación Tlalpan
México, D. F. 14000
Tel. (52)54870900
www.incmnsz.mx

01/2015

Instituto Nacional de Ciencias Médicas y Nutrición Salvador Zubirán	INSTITUTO NACIONAL DE CIENCIAS MÉDICAS Y NUTRICIÓN SALVADOR ZUBIRAN Dirección de Investigación FORMA ÚNICA PARA REGISTRO DE PROYECTOS

FECHA DE RECEPCIÓN: 03/06/2014 CLAVE: PAT-1300-14/15-1

TÍTULO: Infraestructura de apoyo a proyectos relacionados con la evaluación morfológica ultraestructural de los efectos patogénicos de agentes infecciosos, químicos y nutricionales y sus posibles tratamientos.

INVESTIGADOR RESPONSABLE: HERNANDEZ PANDO ROGELIO

DEPARTAMENTO O SERVICIO: DEPARTAMENTO DE PATOLOGÍA Y ANATOMÍA PATOLÓGICA

TIPO DE INVESTIGACIÓN: INVESTIGACIóN EXPERIMENTAL

PATROCINADORES:

Patrocinador	Cantidad
Consejo Nacional de Ciencia y Tecnología	$ 6,859,794.00

VIGENCIA DEL PROYECTO: Del 07/04/2014 al 28/05/2015

	Trimestre 1	Trimestre 2	Trimestre 3	Trimestre 4
Primer año	$ 0.00	$ 6,859,794.00	$ 0.00	$ 0.00

COSTO TOTALES DE LA INVESTIGACIÓN	
Personal	$ 0.00
(sueldos y sobresueldos al personal)	
Equipos	$ 6,859,794.00
(de laboratorio, cómputo, transporte, etc.)	
Materiales	$ 0.00
(reactivos, consumibles, desechables, etc.)	
Animales	$ 0.00
(adquisición, cuidado, procedimientos, etc.)	
Estudios	$ 0.00
(de laboratorio, gabinete,especiales,etc.)	
Viaticos	$ 0.00
(reuniones científicas y trabajo de campo)	

INSTITUCIONES PARTICIPANTES

FACULTAD DE QUIMICA, UNAM

FIRMAS

Investigador responsable		Jefe de Departamento
Comité de Investigación en Humanos		Comité de Investigación en Animales
Director de Investigación		Director General

I: 7/04/14
T: 28/05/15

Instituto Nacional de Ciencias Medicas y Nutricion
Salvador Zubirán

COMITÉ INSTITUCIONAL DE INVESTIGACIÓN BIOMÉDICA EN HUMANOS

FORMATO DE EVALUACIÓN DE PROYECTO DE INVESTIGACIÓN

No. de registro CIIBH: PAT-1300-14/15-1

1. Título del proyecto

Infraestructura de apoyo a proyectos relacionados con la evaluación morfológica ultraestructural de los efectos patogénicos químicos y nutricionales y sus posibles tratamientos.

2. Investigadores

2a. Identificación

INVESTIGADOR	Posición institucional	Posición en el proyecto	Teléfono (ext.)	Correo-E
HERNANDEZ PANDO ROGELIO	INVESTIGADOR EN CIENCIAS MED F	Investigador responsable		[redacted]
PEDRAZA CHAVARRI JOSÉ JORGE		Investigador invitado	(55) 5622	pedraza@unam.mx
TOVAR PALACIO ARMANDO ROBERTO	JEFE DE DEPARTAMENTO	Investigador asociado		[redacted]

Articulo 113 Fracción I de LFTAIP eleminado correo electronico por tratrarse de un dato personal

2b. Pertinencia del grupo de investigadores con respecto del proyecto

3. Instituciones participantes

- Campus Universitario Siglo XXI, Incorporado a la Universidad Autónoma de Estado de Mèxico
- Campus Universitario Siglo XXI, Incorporado a la Universidad Autónoma del Estado de Mèxico
- Centro de Investigación y de Estudios Avanzados del IPN
- Centro Medico ABC
- Centro Médico ABC
- Centro Médico Nacional Siglo XXI
- Centro Universitario del Sur, UdG
- Clínica Ruíz
- Comisión Coordinadora de los Institutos Nacionales de Salud y Hospitales de Alta Especialidad
- Departamento de Cirugia. Instituto Nacional de Ciencias Médicas y Nutrición Salvador Zubrian
- DEPARTAMENTO DE GASTROENTEROLOGIA, INSTITUTO NACIONAL DE CIENCIAS MEDICAS Y NUTRICIC
- Departamento de Infectología
- depto de urologia
- Depto. de infectómica, Centro de Estudios Avanzados del Instituto Politécnico Nacional, CINVESTAV-IPN (México)
- Dirección del Programa de Micobacteriosis
- Dirección del Programa de Salud en el Adulto y en el Anciano
- Facultad de Medicina, Universidad Nacional Autónoma de México
- Facultad de Psicología, UNAM
- FES Zaragoza
- FES Zaragoza
- Globla BioTherapeutics
- Hospital del Niño de niño DIF Hidalgo
- Hospital del Niño DIF Hidalgo

- Hospital del Niño DIF Hidalgo
- Hospital Gea Gonzalez
- Hospital Gea Gonzalez
- Hospital General Dr. Manuel Gea González
- Hospital General Dr. Manuel Gea Gonzalez
- Hospital General Dr. Manuel Gea González
- Hospital general Dr. Rúben Leñero
- Hospital general Gea Gonzalez
- Hospital General Tlaxcala Sesa
- Hospital General Tlaxcala Sesa
- Hospital Infantil de Tlaxcala
- Hospital Juárez de México
- Hospital Medica Sur
- Hospital Medica Sur
- Hospital Niño DIF
- INCMNSZ
- INCMNSZ
- INCMNSZ
- INCMNSZ
- INCMNSZ
- INCMNSZ
- INER
- INSITITUTO NACIONAL DE CIENCIAS MÉDICAS Y NUTRICIÓN SALVADOR ZUBIRÁN
- INSTITUO TECNOLOGICO Y DE ESTUDIOS SUPERIORES DE MONTERREY
- Instituto
- Instituto Nacional de Ciencias Médicas y Nutrición Salvador Zubirán
- INSTITUTO NACIONAL DE CIENCIAS MÉDICAS Y NUTRICIÓN SALVADOR ZUBIRÁN
- Instituto de Investigaciones Biomedicas
- Instituto de Investigaciones Biomédicas UNAM
- Instituto Mexicano del Seguro Social
- Instituto Nacional de Cardiología Ignacio Chávez
- Instituto Nacional de Ciencias Médicas y Nutrición
- Instituto Nacional de Ciencias Médicas y Nutrición
- instituto nacional de ciencias medicas y nutricion salvador zubirna
- INSTITUTO NACIONAL DE CIENCIAS MEDICAS Y NUTRICION, S.Z.
- Instituto Nacional de Enfermedades Respiratorias
- Instituto Nacional de Geriatría
- Instituto Nacional de Rehabilitacion
- Instituto Nacional de Salud pública
- ITESM-CCM
- jmedica sur
- Laboratorios Silanes S.A. de C.V.
- Laboratorios Silanes S.A. de C.V.
- Laboratorios Silanes S.A. de C.V.
- National Institutes of Health
- pasante licenciado en nutrición INCMNSZ
- Sin institución
- Sociedad Médica de medicina fisica y rehabilitación
- UNAM
- UNAM
- UNAM PME
- Universidad Autónoma de Guadalajara
- Universidad Autónoma de Nayarit, Unidad Académica de Medicina Veterinaria y Zootecnia
- Universidad Autónoma del Estado de Mèxico
- Universidad Autónoma del Estado de México
- Universidad Autónoma del Estado de México
- Universidad Autónoma Metropolitana
- Universidad Autónoma Metropolitana, Xochimilco
- Universidad de California
- Universidad de Colima

- Universidad de Colima
- Universidad de Colima
- Universidad de Guadalajara
- Universidad de Guanajuato, Campus León
- Universidad de Uppsala
- Universidad de Uppsala
- Universidad de Upssala
- Universidad Marista de Mérida
- UNIVERSIDAD NACIONAL AUTÓNOMA DE MÉXICO
- Universidad Nacional Autónoma de México
- Universidad Nacional Autónoma de México
- Universidad Nacional Autónoma de México
- Universidad Nacional Autónoma de México
- Universidad Nacional Autónoma de México
- Universidad Nacional Autónoma de México
- Universidad Nacional Autónoma de México
- Universidad Nacional Autonoma de Mexico
- Universidad Nacional de Rosario
- Universidad Rey Juan Carlos
- Universidad Rey Juan Carlos
- Universidas de Buenos Aires
- Washington University in Saint Louis

4. Patrocinio

4a. Organismos patrocinadores

- Consejo Nacional de Ciencia y Tecnología

4b. Especificar si los investigadores reciben pago (monetario o en especie) por su participación es investigación.

5. Marco teórico

ANTECEDENTES:

NO APLICA

DEFINICION DE PROBLEMAS :

Desde hace 30 años se adquirió para el Departamento de Patología del Instituto Nacional de la Nutrición un microscopio M-10, el cual ha dado un enorme servicio en el área de investigación específicamente en proyectos de Patol colaborativamente con diversas lineas de investigación del mismo Instituto y de otras instituciones nacionales y extranjer equipo ha contribuido enormemente en el diagnostico de diversas enfermedades neoplásicas, metabólicas y sobre todo décadas de servicio intenso, dicho microscopio es absolutamente obsoleto, de hecho se siguen utilizando rollos y pl actualmente ya no existen en el mercado y lo que se tiene en nuestro almacén esta a punto de agotarse con lo cual ya fotografías para ilustrar artículos de investigación y tampoco para los diagnósticos de los pacientes, material gráfico que para las sesiones anatomoclínicas que son de gran importancia para la formación de médicos especialistas. Se ha investigac o actualización de este microscopio tratando de adaptar sistemas de adquisición de imagen con cámara y computadora moc muy elevado y la garantía de que funcione es limitada, mas aun, diversos componentes básicos de este microscopio como b se producen y actualmente resulta imposible conseguirlos en el mercado nacional y extranjero, por lo que la eventual des de estos componentes implicaría la total incapacidad de este equipo para seguir funcionando. Por lo tanto se solicita la ad microscopio electrónico que permitirá continuar con el estudio ultraestructural de proyectos de investigación diversos, so las enfermedades infecciosas, metabólicas y por agentes tóxicos, aspectos en los que los proponentes han tenido una intensa y muy productiva; la adquisión de dicho equipo contribuirá también en la formación no solo de estudiantes de m diversos posgrados en investigacion biomedica si no ademas de especialistas médicos. El microscopio electrónico ha tenid lugar importante en la investigación experimental y el uso de técnicas especiales como la inmunoelectronmicroscopia cont substancialmente los resultados experimentales obtenidos con técnicas inmunológicas, bioquímicas o de biología mol aspectos morfológicos con moleculares. El resto del equipamiento como lo son ultramicrotomos y sistema de inclus experiencia en el uso de este equipo por el grupo solicitante es muy sólida, de manera que el equipo solicitado sera fu

prof. extensa colaborat

CONSEJO NACIONAL DE CIENCIA Y TECNOLOGÍA

SISTEMA DE FONDOS

IMPRESIÓN DE SOLICITUD

Fondo: I015B **Convocatoria:** INFR-2014-02 **Solicitud:** 000000000229779 **Modalidad:** INFRE

Estado de Solicitud: Propuesta

Programa Institucional: NO APLICA

Datos Generales de la Propuesta

T;tulo:	Infraestructura de apoyo a proyectos relacionados con la evaluación morfológica ultraestructural de los efectos patogénicos de agentes infecciosos, químicos y nutricionales y sus posibles tratamientos.
Registr; en otra convocatoria:	N
Registro Nacional de Instituciones y Empresas:	Si
N;mero de RENIECyT:	006
Instituci;n:	INSTITUTO NACIONAL DE CIENCIAS MEDICAS Y NUTRICION SALVADOR ZUBIRAN
Demandas Específicas:	Dato requerido
Fecha de Alta:	25/02/2014 11:59:53
Fecha de Envio:	25/02/2014 02:57:18

Breve Descripci;n:

Desde hace 30 años se adquirió para el Departamento de Patología del Instituto Nacional de la Nutrición un microscopio electrónico Carl Zeiss M-10, el cual ha dado un enorme servicio en el área de investigación específicamente en proyectos de Patología Experimental y colaborativamente con diversas líneas de investigación del mismo Instituto y de otras instituciones nacionales y extranjeras. Además el mismo equipo ha contribuido enormemente en el diagnóstico de diversas enfermedades neoplásicas, metabólicas y sobre todo renales. Después de 3 décadas de servicio intenso, dicho microscopio es absolutamente obsoleto, de hecho se siguen utilizando rollos y placas fotográficas que actualmente ya no existen en el mercado y lo que se tiene en nuestro almacén está a punto de agotarse con lo cual ya no se podrán obtener fotografías para ilustrar artículos de investigación y tampoco para los diagnósticos de los pacientes, material gráfico que también es utilizado para las sesiones anatomoclínicas que son de gran importancia para la formación de médicos especialistas. Se ha investigado sobre la renovación o actualización de este microscopio tratando de adaptar sistemas de adquisición de imagen con cámara y computadora modernas pero el costo es muy elevado y la garantía de que funcione es limitada, mas aun, diversos componentes básicos de este microscopio como bombas de vació ya no se producen y actualmente resulta imposible conseguirlos en el mercado nacional y extranjero, por lo que la eventual descompostura de alguno de estos componentes implicaría la total incapacidad de este

equipo para seguir funcionando. Por lo tanto se solicita la adquisición de un nuevo microscopio electrónico que permitirá continuar con el estudio ultraestructural de proyectos de investigación diversos, sobre todo en el área de las enfermedades infecciosas, metabólicas y por agentes tóxicos, aspectos en los que los proponentes han tenido una actividad colaborativa intensa y muy productiva; la adquisición de dicho equipo contribuirá también en la formación no solo de estudiantes de maestría y doctorado en diversos posgrados en investigación biomédica sino además de especialistas médicos. El microscopio electrónico ha tenido y sigue teniendo un lugar importante en la investigación experimental y el uso de técnicas especiales como la inmunoelectronmicroscopia contribuyen enriqueciendo substancialmente los resultados experimentales obtenidos con técnicas inmunológicas, bioquímicas o de biología molecular, integrando así aspectos morfológicos con moleculares. El resto del equipamiento como lo son ultramicrotomos y sistema de inclusión ya se tienen y la experiencia en el uso de este equipo por el grupo solicitante es muy sólida, de manera que el equipo solicitado será fundamentalmente para substituir al ya existente y así poder continuar con una productiva actividad de investigación y de servicio asistencial para una de las instituciones académicas de mayor trayectoria y prestigio de nuestro país.

Objetivo General:

1.- Contribuir con aspectos morfológicos ultraestructurales en la caracterización de los mecanismos patogénicos en modelos experimentales de enfermedades infecciosas (particularmente tuberculosis), agentes tóxicos (específicamente substancias químicas inductores de daño tisular por la generación de radicales libres de oxigeno) y metabólicos (sobre todo diabetes y obesidad). 2.- Aportar información morfológica ultraestructural como parte del estudio de nuevas modalidades terapéuticas en modelos experimentales de tuberculosis pulmonar, daño hepático y renal por substancias químicas oxidantes, obesidad y diabetes. 3.- Contribuir en el diagnóstico de pacientes con enfermedades diversas, sobre todo glomerulopatias, miopatías y respiratorias por anormalidades ciliares

Resultados Esperados:

1.- Publicación de cuando menos dos artículos en revistas indexadas por año durante el periodo de vida útil del equipo 2.- Graduación de estudiantes de maestría y doctorado cuyas tesis estén relacionadas con trabajo experimental en los que existan estudios ultraestructurales. 3.- Diagnostico de un promedio de 110 pacientes con enfermedades renales, miopatías y trastornos ciliares entre otras entidades

Periodo de Ejecuci;n (meses):	12
Palabras Clave:	-Patología experimental -Microscopia electónica -Modelos experimentales

Responsables de la Propuesta

DATOS DEL RESPONSABLE ADMINISTRATIVO	
Nombre:	MARTHA
Apellido Paterno:	ARREDONDO
Apellido Materno:	URZUA
Adscripción:	**Dato requerido**
Cargo:	**Dato requerido**
Calle:	VASCO DE QUIROGA 15
Número Exterior:	**Dato requerido**
Número Interior:	**Dato requerido**
Código Postal:	14000
Colonia:	SECCION XVI

Ciudad:	MEXICO
Estado:	DF
Delegación:	TLALPAN
Teléfono:	55.55133885
Extensión:	**Dato requerido**
Fax:	**Dato requerido**
e-mail:	cadi@quetzal.innsz.mx
DATOS DEL RESPONSABLE T;CNICO	
Nombre:	ROGELIO ENRIQUE
Apellido Paterno:	HERNANDEZ
Apellido Materno:	PANDO
Calle:	AV. PROLONGACION MORELOS # 11
Número Exterior:	0
Número Interior:	**Dato requerido**
Código Postal:	14500
Colonia:	SAN MIGUEL TOPILEJO
Ciudad:	MEXICO
Estado:	DF
Delegación:	TLALPAN
Teléfono:	**Dato requerido**
Extensión:	**Dato requerido**
Fax:	**Dato requerido**
e-mail:	[redacted]
Pertenece al SNI:	SI
Nivel de SNI:	Nivel 3
Edad:	57
Grado de estudios:	PostDoctorado
DATOS DEL RESPONSABLE LEGAL	
Nombre:	DAVID
Apellido Paterno:	KERSHENOBICH
Apellido Materno:	STALNIKOWITZ
Calle:	VASCO DE QUIROGA 15
Número Exterior:	0
Número Interior:	**Dato requerido**
Código Postal:	14000
Colonia:	SECCION XVI
Ciudad:	MEXICO
Estado:	DF
Delegación:	TLALPAN
Teléfono:	52.56232673.
Extensión:	**Dato requerido**
Fax:	**Dato requerido**
e-mail:	[redacted]

Articulo 113 Fracción I de LFTAIP eleminado correo electronico por tratrarse de un dato personal

Articulo 113 Fracción I de LFTAIP eleminado correo electronico por tratrarse de un dato personal

Grupo de Trabajo

Secuencia:	1
Nombre:	ROGELIO ENRIQUE
Apellido Paterno:	HERNANDEZ
Apellido Materno:	PANDO
Nivel Acad;mico:	Doctorado
Campo de Conocimiento:	260000 -
Disciplina:	0 -
Subdisciplina:	0 -
Especialidad:	Inmunopatología
Instituci;n:	INSTITUTO NACIONAL DE CIENCIAS MEDICAS Y NUTRICION SALVADOR ZUBIRAN
Pertenece al SNI:	SI
Nivel SNI:	Nivel 3
Producto que generar;:	No aplica
Informaci;n Relevante:	Médico especialista en Patología y Doctor en Inmunología, su línea de investigación: inmunopatología de la tuberculosis, jefe de la Sección de Patología Experimental del INCMNSZ, ha publicado 230 artículos en revistas internacionales, nivel III del SNI
Actividades Espec;ficas:	No aplica
Secuencia:	2
Nombre:	JOSE
Apellido Paterno:	PEDRAZA
Apellido Materno:	CHAVERRI
Nivel Acad;mico:	Doctorado
Campo de Conocimiento:	260000 -
Disciplina:	0 -
Subdisciplina:	0 -
Especialidad:	Bioquímica
Instituci;n:	UNIVERSIDAD NACIONAL AUTONOMA DE MEXICO
Pertenece al SNI:	SI
Nivel SNI:	Nivel 3
Producto que generar;:	No aplica
Informaci;n Relevante:	Doctor en Bioquímica, investigador titular de tiempo completo de Fac. de Química de la UNAM, su línea de investigación: daño tisular producido por radicales libres, ha publicado 216 artículos en revistas internacionales, es nivel III del SNI
Actividades Espec;ficas:	No aplica
Secuencia:	3
Nombre:	ARMANDO ROBERTO
Apellido Paterno:	TOVAR

Apellido Materno:	PALACIO
Nivel Acad;mico:	Doctorado
Campo de Conocimiento:	260000 -
Disciplina:	0 -
Subdisciplina:	0 -
Especialidad:	Biología Molecular
Instituci;n:	INSTITUTO NACIONAL DE CIENCIAS MEDICAS Y NUTRICION SALVADOR ZUBIRAN
Pertenece al SNI:	SI
Nivel SNI:	Nivel 3
Producto que generar;:	No aplica
Informaci;n Relevante:	Doctor en Biología Molecular, experto en aspectos moleculares de la nutrición, ha publicado 85 artículos en revistas internacionales, es nivel III del SNI y jefe de Fisiología de la Nutrición en la División de Nutrición del INCMNSZ
Actividades Espec;ficas:	No aplica

Fortalecimiento de Infraestructura

Secuencia:	1
Descripción:	Microscopio Electrónico de Transmisión con resolución de 0.2 nm Voltaje de aceleración 120kV PC de con sofware de operación para enfoque, y operación Monitor LCD estandar de 20" Lente objetiva de alto contraste optimizada para alta resolución. Sistema de alimentación ininterrumpible de corriente Powervar 15KV ups Hard-wired Cámara CCD para obtención de imágenes de 4 millones de pixeles CPU de 32 bits, con 4 G de RAM y 1 TB en DD, tarjeta de video de 512 megas con unidad de disco DVD Instalación y capacitación para el uso y manejo del equipo.
Justificación:	La microscopia electrónica es de gran importancia para el buen desarrollo de proyectos de Patología Experimental; de hecho el microscopio electrónico se ha utilizado sistemáticamente en nuestro Departamento tanto para fines de investigación como diagnóstico. El microscopio que actualmente tenemos tiene más de 30 años de uso intensivo, es un instrumento totalmente obsoleto y tiene un constante problema de mantenimiento pues muchas de las piezas ya no se producen debido a su antigüedad. Consideramos por lo tanto que para poder continuar con nuestro trabajo tanto de investigación como diagnóstico es necesario adquirir un nuevo microscopio con el que además se podrán ampliar y enriquecer diversos proyectos debido a las innovaciones tecnológicas que tienen los microscopios actuales.

Cronograma de Actividades

Presupuesto Solicitado

Número de Etapa:	001
Descripción:	Microscopio Electrónico
Duración (meses):	12
Descripción de la Etapa:	NO APLICA
Descripción de la Meta:	NO APLICA
Descripción de la Actividad:	NO APLICA
Productos de la Etapa:	NO APLICA

;

Desglose Financiero Propuesta

Presupuesto Solicitado

Etapa	Periodo	Tipo de Aportación	Tipo de Gasto	Rubro	Importe
001	001	SOLICITADAS AL FONDO	INVERSION	Equipo de laboratorio	$ 6,859,974.00

Justificación: La microscopia electrónica es de gran importancia para el buen desarrollo de proyectos de Patología Experimental; de hecho el microscopio electrónico se ha utilizado sistemáticamente en nuestro Departamento tanto para fines de investigación como diagnostico. El microscopio que actualmente tenemos tiene más de 30 años de uso intensivo, es un instrumento totalmente obsoleto y tiene un constante problema de mantenimiento pues muchas de las piezas ya no se producen debido a su antigüedad. Consideramos por lo tanto que para poder continuar con nuestro trabajo tanto de investigación como diagnostico es necesario adquirir un nuevo microscopio con el que además se podrán ampliar y enriquecer diversos proyectos debido a las innovaciones tecnológicas que tienen los microscopios actuales.

FONDO	CONCURRENTE	OTRAS
Gasto Corriente: $ Gasto Inversión: $ 6,859,974.00 Total: $ 6,859,974.00	Gasto Corriente: $ Gasto Inversión: $ Total: $	Gasto Corriente: $ Gasto Inversión: $ Total : $

Documentos Anexos

Clave Anexo:
ANX00001

Descripción:
Carta institucional de apoyo y compromisos,
Descripción Archivo:
Carta firmada por el Dr. Kershenobich
Archivo Anexo:
I015B_000000000229779_12_25_2014carta_institucional.pdf
Clave Anexo:
ANX00005
Descripción:
Carta de los líderes de los grupos de investigación o cuerpos académicos
Descripción Archivo:
Carta firmada por el Dr. Hernández Pando
Archivo Anexo:
I015B_000000000229779_22_25_2014carta_Dr_Hernandez_Pando.pdf
Clave Anexo:
ANX00005
Descripción:
Carta de los líderes de los grupos de investigación o cuerpos académicos
Descripción Archivo:
Carta de colaboración del Dr. Pedraza
Archivo Anexo:
I015B_000000000229779_32_25_2014carta_colaboracion_Dr_Pedraza.pdf
Clave Anexo:
ANX00005
Descripción:
Carta de los líderes de los grupos de investigación o cuerpos académicos
Descripción Archivo:
Carta de colaboración del Dr. Tovar
Archivo Anexo:
I015B_000000000229779_42_25_2014carta_colaboracion_Dr_Tovar.pdf
Clave Anexo:
ANX00003
Descripción:
Documento de Información indispensable para la solicitud, DESCARGAR, LLENAR y ADJUNTAR.
Descripción Archivo:
Formulario
Archivo Anexo:
I015B_000000000229779_52_25_2014EFormulario_Apoyos_equipos_APOYO_ESPECIAL.pdf

CON FUNDAMENTO EN EL ARTÍCULO 14, FRACCIÓN VI, ARTÍCULO 18, FRACCIONES I Y II, Y ARTÍCULO 21 DE LA LEY FEDERAL DE TRANSPARENCIA Y ACCESO A LA INFORMACIÓN PÚBLICA GUBERNAMENTAL, EL TIEMPO DE RESERVA DE LA PRESENTE INFORMACIÓN, QUE ES DE CARÁCTER CONFIDENCIAL, ES DE 10 AÑOS.

1300

Firmas de Convenio

Fondo I015B

Solicitud 000000000229779

Personalizar | Buscar | Primero 1-5 de 5 Último

	Fondo	Solicitud	Descripción	Codigo de Responsable	Firma	Fecha/Hora de firma	Requerido
1	I015B	000000000229779	FABILA CASTILLO,LUIS HUMBERTO	RC	☑	04/06/2014 18:07:43	☑
2	I015B	000000000229779	HERNANDEZ PANDO,ROGELIO ENRIQU	R. Técnico	☑	21/05/2014 10:10:23	☑
3	I015B	000000000229779	ARREDONDO URZUA,MARTHA	R. Admvo.	☑	27/05/2014 13:01:48	☑
4	I015B	000000000229779	KERSHENOBICH STALNIKOWITZ,DAVI	R. Legal	☑	04/06/2014 13:48:03	☑
5	I015B	000000000229779	TAGUEÑA PARGA,JULIA	S. Tecnic.	☑	04/06/2014 20:07:20	☑

Guardar | Volver a Buscar | Siguiente en Lista | Anterior en Lista | Notificar

CONVENIO DE ASIGNACIÓN DE RECURSOS

I010/186/2014

MOD.ORD./10/2014

GENERAL

INFR-2014-02

000000000229779

CONVENIO DE ASIGNACIÓN DE RECURSOS QUE CELEBRAN, POR UNA PARTE EL CONSEJO NACIONAL DE CIENCIA Y TECNOLOGÍA, EN LO SUCESIVO EL "CONACYT", REPRESENTADO EN ESTE ACTO POR LA DRA. JULIA TAGÜEÑA PARGA, EN SU CARÁCTER DE DIRECTORA ADJUNTA DE DESARROLLO CIENTÍFICO, ASISTIDA POR EL DR. LUIS HUMBERTO FABILA CASTILLO, DIRECTOR DE INVESTIGACIÓN CIENTÍFICA BÁSICA; Y POR LA OTRA, EL/LA INSTITUTO NACIONAL DE CIENCIAS MEDICAS Y NUTRICION SALVADOR ZUBIRAN, EN LO SUCESIVO EL "SUJETO DE APOYO", REPRESENTADO POR EL/LA DR. DAVID KERSHENOBICH STALNIKOWITZ, EN SU CALIDAD DE REPRESENTANTE LEGAL, INSTRUMENTO QUE SUJETAN AL TENOR DE LOS ANTECEDENTES, DECLARACIONES Y CLÁUSULAS SIGUIENTES:

ANTECEDENTES

1. El artículo 1°, fracciones I y II de la Ley de Ciencia y Tecnología (LCyT), regula los apoyos que el Gobierno Federal se encuentra obligado a otorgar para impulsar, fortalecer, desarrollar y consolidar la investigación científica, el desarrollo tecnológico y la innovación general en el país, así como determinar los instrumentos, mediante los cuales éste cumplirá con dicha obligación.
2. El 31 de diciembre de 2010 se publicaron en el Diario Oficial de la Federación las Reglas de Operación de los Programas del Consejo Nacional de Ciencia y Tecnología constituidos por el **"CONACYT"**, dentro de los cuales se contempla el programa denominado **"Apoyo al Fortalecimiento y Desarrollo de la Infraestructura Científica y Tecnológica"**, en adelante el **"PROGRAMA"**.
3. El numeral 5.4 de las Reglas de Operación del **"PROGRAMA"** establece lo relativo a las propuestas que podrán evaluarse y en su caso seleccionarse para recibir apoyos, que podrán ser en apego a la LCyT y a las propias Reglas que determinen los requisitos de participación establecidos en las Convocatorias o Convenio correspondiente.
4. El Plan Nacional de Desarrollo (PND) 2013-2018, publicado en el Diario Oficial de la Federación el 20 de mayo de 2013, establece en su Objetivo 3.5. Hacer del desarrollo científico, tecnológico y la innovación, pilares para el progreso económico y social sostenible.
5. Con fundamento en el artículo 13 de su Ley Orgánica, la canalización de recursos que haga **"CONACYT"**, para programas, apoyos, estudios, investigaciones específicas, otorgamiento de becas en sus diferentes modalidades y cualquier otro apoyo o ayuda de carácter económico que convenga o proporcione, estará sujeta a la celebración de un Convenio.
6. El **"CONACYT"**, a través de su página electrónica, publicó la Convocatoria denominada **"Apoyo al Fortalecimiento y Desarrollo de la Infraestructura Científica y Tecnológica 2014"**, con el propósito de proveer apoyo económico complementario a instituciones de educación superior y centros de investigación que desarrollen actividades de investigación y que requieran renovación o adquisición de equipo científico, a fin de fortalecer las líneas de investigación institucionales.
7. La Comisión de Evaluación, previo proceso de evaluación a que hace referencia la Convocatoria, en su

sesión de fecha 28 de marzo de 2014, aprobó la canalización de recursos a favor del **"SUJETO DE APOYO"**, por un monto de **$6,859,974.00 (SEIS MILLONES OCHOCIENTOS CINCUENTA Y NUEVE MIL NOVECIENTOS SETENTA Y CUATRO PESOS 00/100 MN)** para el desarrollo de la propuesta denominada **INFRAESTRUCTURA DE APOYO A PROYECTOS RELACIONADOS CON LA EVALUACIÓN MORFOLÓGICA ULTRAESTRUCTURAL DE LOS EFECTOS PATOGÉNICOS DE AGENTES INFECCIOSOS, QUÍMICOS Y NUTRICIONALES Y SUS POSIBLES TRATAMIENTOS.**, en lo sucesivo el **"PROYECTO"**.

DECLARACIONES

I. El "CONACYT" a través de su Representante, declara que:

A. Conforme a lo dispuesto por los artículos 1 y 2 de la Ley Orgánica del Consejo Nacional de Ciencia y Tecnología, es un organismo descentralizado del Estado, no sectorizado, con personalidad jurídica y patrimonio propio, que goza de autonomía técnica, operativa y administrativa, con sede en la Ciudad de México, Distrito Federal, entidad asesora del Ejecutivo Federal y especializada para articular las políticas públicas del Gobierno Federal y promover el desarrollo de la investigación científica y tecnológica, la innovación, el desarrollo y la modernización tecnológica del país.

B. La personalidad de la Dra. Julia Tagüeña Parga, Directora Adjunta de Desarrollo Científico, para suscribir el presente Convenio se acredita con el testimonio de la escritura pública número 46,337, de fecha 14 de mayo de 2013, otorgado ante la fe del Lic. Marco Antonio Espinoza Rommyngth, Notario Público número 97, de la Ciudad de México, Distrito Federal, en el que se hace constar el poder especial para la celebración de actos e instrumentos jurídicos que se deriven de las atribuciones que tiene asignadas en razón de su cargo en el **"CONACYT"**.

C. De conformidad con el presupuesto asignado al **"CONACYT"** en el Presupuesto de Egresos de la Federación del presente ejercicio fiscal, se cuenta con la suficiencia presupuestaria para canalizar al desarrollo del objeto del presente Convenio.

D. Para los efectos de este Convenio señala como su domicilio legal el ubicado en la Avenida Insurgentes Sur número 1582, Colonia Crédito Constructor, Delegación Benito Juárez, Código Postal 03940, de esta Ciudad de México, Distrito Federal.

II. El "SUJETO DE APOYO" a través de su Representante, declara que:

A. EL (LA) INSTITUTO NACIONAL DE CIENCIAS MEDICAS Y NUTRICION SALVADOR ZUBIRAN ES UN ORGANISMO PÚBLICO DESCENTRALIZADO, CON PERSONALIDAD JURÍDICA Y PATRIMONIO PROPIOS, DE CONFORMIDAD CON LO DISPUESTO EN LOS ARTÍCULOS 3, 9 Y 45 DE LA LEY ORGÁNICA DE LA ADMINISTRACIÓN PÚBLICA FEDERAL; 2, 14 Y 15 DE LA LEY FEDERAL DE LAS ENTIDADES PARAESTATALES; 1, 5 FRACCIÓN III; 9 FRACCIÓN III DE LA LEY DE LOS INSTITUTOS NACIONALES DE SALUD, PUBLICADA EN EL DIARIO OFICIAL DE LA FEDERACIÓN EL 26 DE MAYO DE 2000; 3 FRACCIONES I, II, XIV; 34 FRACCIÓN I DEL ESTATUTO ORGÁNICO DEL INSTITUTO, PUBLICADO EN EL DIARIO OFICIAL DE LA FEDERACIÓN EL 20 DE OCTUBRE DE 2009.

B. EL (LA) DR. DAVID KERSHENOBICH STALNIKOWITZ CUENTA CON LAS FACULTADES PARA SUSCRIBIR EL PRESENTE CONVENIO, TAL Y COMO SE DESPRENDE DE LA ESCRITURA PÚBLICA NÚMERO 137232, DE FECHA 21 DE JUNIO DE 2012, PASADA ANTE LA FE DEL LIC. IGNACIO SOTO BORJA, NOTARIO PÚBLICO NÚMERO 129, DEL DISTRITO FEDERAL, MÉXICO, D. F; MANIFESTANDO QUE A LA FECHA DE FIRMA DEL PRESENTE INSTRUMENTO, SUS FACULTADES NO LE HAN SIDO REVOCADAS NI MODIFICADAS EN FORMA ALGUNA

C. El Registro Federal de Contribuyentes inscrito en la Secretaría de Hacienda y Crédito Público es INC710101RH7.

D. Tiene establecido su domicilio en VASCO DE QUIROGA EXT/INT 15, SECCION XVI, TLALPAN,

C.P.14000, MEXICO, DISTRITO FEDERAL, mismo que señala para los fines y efectos legales de este Convenio.

E. En cumplimiento a lo dispuesto por los artículos 16 y 17 de la LCyT, se encuentra inscrito en el **Registro Nacional de Instituciones y Empresas Científicas y Tecnológicas (RENIECYT)**, a cargo del **"CONACYT"**, tal y como se acredita con la constancia de inscripción número 006.

F. El **"SUJETO DE APOYO"** manifiesta bajo protesta de decir verdad, que la celebración del presente instrumento jurídico lo realiza para su propio beneficio, por lo que no actúa como intermediario o para beneficio de otra persona física o moral u otras personas físicas o morales actúan como intermediarios para la presentación de la propuesta correspondiente; en el entendido que los recursos que otorga el **"CONACYT"** son públicos, a título personal y en beneficio del fomento de la investigación científica, tecnológica y la innovación en el país.

III. Declaración Conjunta:

ÚNICA. Las partes expresamente manifiestan su conocimiento al contenido de lo dispuesto por el artículo 12, fracción II de la LCyT, que a la letra dice: **"Los resultados de las actividades de investigación, desarrollo tecnológico e innovación que sean objeto de apoyos en términos de esta Ley serán invariablemente evaluados y se tomarán en cuenta para el otorgamiento de apoyos posteriores"**.

Expuesto lo anterior, las partes se obligan de acuerdo con las siguientes:

CLÁUSULAS

PRIMERA. OBJETO

El objeto del presente Convenio conforme a lo dispuesto por el artículo 1 de la LCyT, consiste en el establecimiento de las condiciones a que se sujeta la canalización de los recursos otorgados por el **"CONACYT"** en favor del **"SUJETO DE APOYO"**, para el desarrollo del **"PROYECTO"** denominado: **INFRAESTRUCTURA DE APOYO A PROYECTOS RELACIONADOS CON LA EVALUACIÓN MORFOLÓGICA ULTRAESTRUCTURAL DE LOS EFECTOS PATOGÉNICOS DE AGENTES INFECCIOSOS, QUÍMICOS Y NUTRICIONALES Y SUS POSIBLES TRATAMIENTOS.**.

El objetivo del **"PROYECTO"** es la adquisición del equipo científico solicitado y aprobado por la Comisión de Evaluación.

SEGUNDA. CANALIZACIÓN DE RECURSOS

El **"CONACYT"** con cargo a su presupuesto, y con sujeción a lo establecido en el presente Convenio, canaliza al **"SUJETO DE APOYO"** la cantidad total de **$6,859,974.00 (SEIS MILLONES OCHOCIENTOS CINCUENTA Y NUEVE MIL NOVECIENTOS SETENTA Y CUATRO PESOS 00/100 MN)**.

El **"SUJETO DE APOYO"** deberá presentar previo a la entrega de recursos, el comprobante fiscal digital, debidamente requisitado, especificando con toda claridad el concepto del importe por el total de la ministración.

Únicamente se podrá adquirir el equipo que haya sido requerido en la solicitud presentada o autorizado por el **"CONACYT"**.

El "SUJETO DE APOYO" podrá acreditar el ejercicio de los recursos ministrados por el "CONACYT" mediante la exhibición de las órdenes de compra de equipos fechadas hasta antes del 31 de diciembre de 2014.

En caso de que el **"SUJETO DE APOYO"** no ejerza la totalidad de los recursos asignados al **"PROYECTO"** deberá efectuar su devolución al **"CONACYT"**, a más tardar el **12 de enero de 2015**, para su reintegro a la

Tesorería de la Federación.

TERCERA. ANEXOS

Los Anexos que forman parte integral del presente Convenio se componen por lo siguiente:

1. El **Anexo Uno** contiene el Desglose Financiero del **"PROYECTO"**.
2. El **Anexo Dos** contiene los objetivos, metas, actividades, entregables y plazos con los que se aprobó el **"PROYECTO"**.

Los Anexos sólo podrán ser modificados si para ello concurre la voluntad de las partes, mediante la suscripción de un Convenio Modificatorio.

CUARTA. OBLIGACIONES DEL "CONACYT"

a)Canalizar al **"SUJETO DE APOYO"**, los recursos económicos en una sola exhibición, a que hace referencia la Cláusula Segunda de este instrumento, en un término no mayor a 30 (treinta) días naturales, contados a partir de la fecha en que el **"SUJETO DE APOYO"** haya entregado la documentación que para tales efectos le requiera el **"CONACYT"**.

b)Vigilar por conducto de la Dirección de Investigación Científica Básica adscrita a la Dirección Adjunta de Desarrollo Científico, la debida aplicación y adecuado aprovechamiento de los recursos económicos, efectivamente canalizados al **"SUJETO DE APOYO"**, conforme al contenido en los **Anexos Uno** y **Dos**.

c)El **"CONACYT"**, a través de los medios que considere pertinentes, podrá en cualquier momento realizar auditorías y/o practicar visitas de supervisión, con el propósito de constatar el grado de avance en el desarrollo de los trabajos y la correcta aplicación de los recursos canalizados al **"SUJETO DE APOYO"**.

QUINTA. OBLIGACIONES DEL "SUJETO DE APOYO"

a)El **"SUJETO DE APOYO"** se obliga a entregar en un término no mayor a 30 (treinta) días naturales, contados a partir de la suscripción del presente instrumento jurídico, la documentación que le requiera el **"CONACYT"** para poder llevar a cabo la canalización de los recursos.

b)El **"SUJETO DE APOYO"** se obliga a destinar bajo su más estricta responsabilidad los recursos económicos ministrados por el **"CONACYT"**, exclusivamente a la realización del **"PROYECTO"** de conformidad con lo dispuesto en el presente Convenio y los Anexos que forman parte integral del mismo.

c)El **"SUJETO DE APOYO"** se obliga a desarrollar el **"PROYECTO"** conforme a lo contenido en los **Anexos Uno** y **Dos**, mismos que forman parte integral del presente Convenio.

d)El **"SUJETO DE APOYO"** queda expresamente obligado a proporcionar las facilidades necesarias para permitir el acceso a sus instalaciones, así como para mostrar la información técnica y financiera que le sea solicitada por el **"CONACYT"**.

e)El **"SUJETO DE APOYO"** deberá de guardar toda aquella información técnica-financiera que se genere y que estime relevante para realizar futuras evaluaciones sobre el **"PROYECTO"**, durante un periodo de 5 (cinco) años posteriores a la conclusión de la terminación del mismo.

f)El **"SUJETO DE APOYO"** deberá abrir un sistema de registro contable de los movimientos financieros relativos al **"PROYECTO"**, así como contar con un expediente específico para la documentación del mismo.

g)El **"SUJETO DE APOYO"** se obliga a proporcionar la información relacionada con el equipo científico y/o tecnológico adquirido para el desarrollo del **"PROYECTO"**, en la forma que le sea solicitado por el **"CONACYT"** con el propósito de integrarlo a su sistema de información sobre infraestructura científica.

h)El **"SUJETO DE APOYO"** se obliga a informar de manera inmediata al Área de Quejas y Responsabilidades del Órgano Interno de Control en el **"CONACYT"**, en el caso de que algún servidor público del **"CONACYT"**, por si, o por interpósita persona solicite o reciba indebidamente para sí o para otro, dinero o cualquier otra dádiva, o acepte una promesa, para hacer o dejar de hacer actos o acciones relacionadas con el cumplimiento del presente instrumento jurídico.

i)Rendir los informes a que hace referencia la Cláusula Sexta de este Convenio.

SEXTA. INFORMES

Al término del **"PROYECTO"**, el **"SUJETO DE APOYO"** deberá presentar los Informes Financiero y Técnico, de conformidad con lo siguiente:

1. Informe Financiero acorde al Desglose Financiero establecido en el **Anexo Uno** del **"PROYECTO"**, en un plazo no mayor a 30 (treinta) días naturales, contados a partir de la conclusión del mismo, el cual deberá estar auditado preferentemente por un despacho de Auditoría acreditado ante la Secretaría de la Función Pública, en el que se deberá incluir la solicitud expresa para la emisión de la Constancia de Conclusión Técnica y Financiera, considerando el debido de cumplimiento del **"PROYECTO"** y que los recursos canalizados fueron única y exclusivamente para su desarrollo.
2. Informe Técnico conforme a las actividades establecidas en el **Anexo Dos** del **"PROYECTO"**, en un plazo no mayor a 30 (treinta) días naturales contados a partir de la conclusión del mismo.

Los Informes deberán mencionar los entregables comprometidos, así como la información relacionada con la aplicación de los recursos canalizados al **"PROYECTO"**.

El Informe Financiero deberá considerar la rendición de cuentas del monto total del apoyo otorgado, incluyendo los reembolsos realizados de los recursos no ejercidos.

De proceder los Informes Financiero y Técnico, el **"CONACYT"** por conducto de la Dirección Adjunta de Desarrollo Científico, emitirá la Constancia de Conclusión Técnica y Financiera del **"PROYECTO"**.

El **"CONACYT"** se reserva el derecho de solicitar un informe acerca del impacto del equipo adquirido en la realización de proyectos de investigación y de tesis de grado, hasta un 1 (un) año posterior al cierre del **"PROYECTO"**.

SÉPTIMA. ÁREAS DE COORDINACIÓN

El **"CONACYT"** a través de la Dirección de Investigación Científica Básica adscrita a la Dirección Adjunta de Desarrollo Científico, llevará a cabo el seguimiento administrativo y financiero del uso de los recursos, así como el seguimiento técnico y evaluación de los resultados del **"PROYECTO"**.

El **"SUJETO DE APOYO"** designa al (la) DR. ROGELIO ENRIQUE HERNANDEZ PANDO, como Responsable Técnico del **"PROYECTO"**, quien será el enlace con la Dirección de Investigación Científica Básica adscrita a la Dirección Adjunta de Desarrollo Científico del **"CONACYT"** para los asuntos técnicos,

teniendo como obligación principal la ejecución del **"PROYECTO"**, del cumplimiento de sus objetivos y metas, así como de la generación de los productos entregables, y en general supervisar el fiel cumplimiento del presente Convenio.

En caso de ausencia temporal mayor a 30 (treinta) días naturales o definitiva del Responsable Técnico, el **"SUJETO DE APOYO"** deberá designar al sustituto, notificando de ello a la Dirección de Investigación Científica Básica adscrita a la Dirección Adjunta de Desarrollo Científico del **"CONACYT"**, en un plazo que no excederá de 15 (quince) días naturales posteriores a que éste se ausente.

El **"SUJETO DE APOYO"** designa al (a) LIC. MARTHA ARREDONDO URZUA, como Responsable Administrativo del **"PROYECTO"**, quien auxiliará al Responsable Técnico en su función de enlace con la Dirección de Investigación Científica Básica adscrita a la Dirección Adjunta de Desarrollo Científico, que tendrá la responsabilidad del control administrativo y contable, la correcta aplicación y comprobación de los recursos canalizados por el **"CONACYT"**, así como la elaboración de los informes financieros y administrativos requeridos por el **"CONACYT"**.

En caso de ausencia temporal mayor a 30 (treinta) días naturales o definitiva del Responsable Administrativo, el **"SUJETO DE APOYO"** deberá designar al sustituto, notificando de ello a la Dirección de Investigación Científica Básica adscrita a la Dirección Adjunta de Desarrollo Científico, en un plazo que no excederá de 15 (quince) días naturales posteriores a que éste se ausente.

OCTAVA. CUENTA BANCARIA

El **"SUJETO DE APOYO"** deberá disponer de una cuenta bancaria exclusiva para la canalización de los recursos asignados al desarrollo del **"PROYECTO"**, dicha cuenta estará a nombre del **"SUJETO DE APOYO"** y será operada mancomunadamente por el Responsable Técnico y el Responsable Administrativo a que se refiere la Cláusula anterior, por lo que será necesario que la misma se encuentre acreditada ante el **"CONACYT"**, previo a la entrega de los recursos.

En caso de que el **"SUJETO DE APOYO"** maneje cuentas concentradoras, deberá asignar una cuenta específica para el **"PROYECTO"** notificando de ello al **"CONACYT"** a través de Dirección de Investigación Científica Básica adscrita a la Dirección Adjunta de Desarrollo Científico, a fin de que se acredite la misma.

El **"CONACYT"** realizará la transferencia de manera electrónica, siendo obligación del Responsable Administrativo del **"PROYECTO"** cumplir con todos los requisitos administrativos y contables derivados del presente Convenio.

Por lo tanto, el Responsable Administrativo deberá de estar en permanente contacto con el personal del **"CONACYT"** para aclarar oportunamente cualquier duda, satisfacer sus requerimientos y conocer la forma en la cual debe de llevar el registro y contabilidad de sus operaciones.

Los recursos asignados al **"PROYECTO"** deberán permanecer en la cuenta específica del mismo, por lo que no podrán transferirse a otras cuentas que no estén relacionadas con el objeto del **"PROYECTO"**.

Los recursos asignados para la realización del **"PROYECTO"** no formarán parte del patrimonio del **"SUJETO DE APOYO"**, ni de su presupuesto.

NOVENA. DERECHOS DE PROPIEDAD INDUSTRIAL Y/O AUTOR

Las partes convienen en que los Derechos de Propiedad Industrial y/o los Derechos de Autor que se generen como resultado del desarrollo del **"PROYECTO"**, serán propiedad de la persona física o moral, a quien conforme a Derecho le correspondan, en el entendido de que el **"CONACYT"** no tendrá interés jurídico sobre

esos derechos.

En las publicaciones o presentaciones en eventos que se realicen, derivadas o relacionados con el resultado del **"PROYECTO"**, el **"SUJETO DE APOYO"** deberá dar, invariablemente, el crédito correspondiente al **"CONACYT"**, agregando la leyenda: **"Proyecto apoyado por el CONACYT"**.

DÉCIMA. INFORMACIÓN RESERVADA

Las partes se comprometen a tratar como reservada toda la información generada a través del **"PROYECTO"** en ejecución, así como la intercambiada o acordada con motivo del presente instrumento y la necesaria para el desarrollo del **"PROYECTO"**, excepto aquélla que deba considerarse pública en términos de lo dispuesto en la Ley Federal de Transparencia y Acceso a la Información Pública Gubernamental, su Reglamento y demás disposiciones jurídicas aplicables.

DÉCIMA PRIMERA. ACCESO A LA INFORMACIÓN

El **"SUJETO DE APOYO"** se compromete a proporcionar la información del **"PROYECTO"** que pudiera ser solicitada por la Dirección de Investigación Científica Básica adscrita a la Dirección Adjunta de Desarrollo Científico, para ser entregada al **Sistema Integrado de Información sobre Investigación Científica y Tecnológica (SIICYT)** que opera el **"CONACYT"**. Dicha información será publicada en su página de Internet, dando con ello cumplimiento a las disposiciones de la Ley Federal de Transparencia y Acceso a la Información Pública Gubernamental.

DÉCIMA SEGUNDA. TERMINACIÓN ANTICIPADA

Las partes podrán dar por terminado de manera anticipada el presente Convenio, cuando existan circunstancias que impidan continuar con el desarrollo del **"PROYECTO"**, previa notificación que por escrito realice cualquiera de ellas, con una antelación no mayor a 30 (treinta) días naturales.

DÉCIMA TERCERA. CASO FORTUITO Y/O FUERZA MAYOR

Para efectos de este Convenio se entenderá por caso fortuito y fuerza mayor, a los sucesos de la naturaleza o de hechos del hombre que, siendo extraños al **"SUJETO DE APOYO"**, lo afectan impidiéndole temporal o definitivamente el cumplimiento parcial o total de sus obligaciones.

DÉCIMA CUARTA. RESPONSABILIDAD CIVIL

Queda expresamente pactado que las partes no tendrán responsabilidad civil por los daños y perjuicios que pudieran causarse como consecuencia de caso fortuito o fuerza mayor, particularmente por el paro de labores académicas o administrativas, en la inteligencia de que una vez superados estos eventos, se reanudarán las actividades en la forma y términos que dictaminen las partes.

DÉCIMA QUINTA. RESCISIÓN

El **"CONACYT"** podrá rescindir el presente Convenio al **"SUJETO DE APOYO"**, sin necesidad de declaración judicial previa ni de dar aviso por escrito, cuando éste incurra en alguno de los supuestos de incumplimiento que de manera enunciativa más no limitativa, a continuación se señalan:

a)Aplique los recursos canalizados por el **"CONACYT"** con finalidades distintas a la realización directa del **"PROYECTO"**.

b)No brinde las facilidades de acceso a la información, o a las instalaciones donde se administra y desarrolla el **"PROYECTO"**.

c)Por identificación de desviaciones no reportadas, por parte de los Responsables Técnico y/o Administrativo.

d)No compruebe la debida aplicación de los recursos canalizados para el **"PROYECTO"** cuando le sea expresamente requerido por el **"CONACYT"**.

e)Proporcione información o documentación falsa.

f)Retirar los recursos de la cuenta específica del **"PROYECTO"** para transferirlos a otras cuentas no relacionadas con el objeto del mismo.

g)Incurra en algún otro incumplimiento a este Convenio y a sus Anexos.

Cuando el **"CONACYT"** ejercite el derecho contenido en la presente Cláusula, el **"SUJETO DE APOYO"** reembolsará la totalidad de los recursos que le fueron canalizados en un plazo no mayor de 30 (treinta) días naturales, contados a partir del requerimiento escrito que se le formule para tales efectos, con independencia de que se haga acreedor a la sanción a que se refiere la Cláusula siguiente.

DÉCIMA SEXTA. CANCELACIÓN DEL RENIECYT

En los casos en que el incumplimiento por parte del **"SUJETO DE APOYO"** a las obligaciones que asume por virtud del presente instrumento legal, que impida continuar con el desarrollo del **"PROYECTO"**, y que haya sido omiso a los requerimientos de la Dirección de Investigación Científica Básica adscrita a la Dirección Adjunta de Desarrollo Científico, solicitará a la Dirección Adjunta de Asuntos Jurídicos que a través de la Dirección del **RENIECYT**, se convoque a la Comisión Interna de Evaluación a efecto de conocer y resolver lo conducente respecto a la procedencia de cancelación del **RENIECYT**, conforme a lo dispuesto en el artículo 52 de las Bases de Organización y Funcionamiento del Registro Nacional de Instituciones y Empresas Científicas y Tecnológicas.

DÉCIMA SÉPTIMA. DEVOLUCIÓN DE LOS RECURSOS

El **"SUJETO DE APOYO"** en cualquier supuesto que implique la devolución de los recursos económicos canalizados al **"PROYECTO"**, ya sea el **remanente** de lo no ejercido o la **totalidad** de los mismos, tendrá un término no mayor a 30 (treinta) días naturales contados a partir la conclusión del mismo, o del requerimiento que por escrito le realice la Dirección de Investigación Científica Básica adscrita a la Dirección Adjunta de Desarrollo Científico, para efectuar dicho reintegro, entregando copia de la ficha de depósito o de la transferencia electrónica al Área de Coordinación del **"CONACYT"**.

La devolución de los recursos económicos asignados al **"PROYECTO"** no deberá exceder del día **12 de enero de 2015**.

DÉCIMA OCTAVA. RELACIÓN LABORAL

El **"CONACYT"** no establecerá ninguna relación de carácter laboral con el personal que el **"SUJETO DE APOYO"** llegase a ocupar para la realización del **"PROYECTO"**, en consecuencia, las partes acuerdan que el personal designado, contratado o comisionado para la realización del **"PROYECTO"**, estará bajo la dependencia directa del **"SUJETO DE APOYO"**; y por lo tanto, en ningún momento se considerará al **"CONACYT"** como patrón solidario o sustituto, ni tampoco al **"SUJETO DE APOYO"** como intermediario, por lo que el **"CONACYT"** no asume ninguna responsabilidad que pudiera presentarse en materia de trabajo y seguridad social, por virtud del presente Convenio.

DÉCIMA NOVENA. PREVISIONES ÉTICAS, ECOLÓGICAS Y DE SEGURIDAD

El **"SUJETO DE APOYO"** se obliga a cumplir y hacer cumplir durante el desarrollo del **"PROYECTO"** y hasta su conclusión la legislación aplicable especialmente en materia ecológica, de equidad de género, de protección a la bioseguridad y la biodiversidad, así como a respetar las convenciones y protocolos en materia ética aplicada a la investigación, la legislación aplicable y la normatividad institucional en materia de seguridad.

VIGÉSIMA. ACTUALIZACIÓN DE DATOS EN EL RENIECYT

El **"SUJETO DE APOYO"** tendrá la obligación de informar a la Dirección del **RENIECYT** adscrita a la Dirección Adjunta de Asuntos Jurídicos, entre otros cambios los de su situación económica, cambio de domicilio legal, razón o denominación social o representante legal. Asimismo, el **"SUJETO DE APOYO"** se obliga a mantener actualizada su inscripción e información en el **RENIECYT**.

VIGÉSIMA PRIMERA. VIGENCIA

El presente Convenio tendrá una vigencia de **12 (doce) meses**, contados a partir de la fecha de la ministración, entendiéndose como formalizado al momento en que se cuente con la firma de todas y cada una de las partes que intervienen en el mismo.

Las obligaciones a cargo del **"SUJETO DE APOYO"**, relacionadas con la fiscalización de los recursos empleados para el financiamiento del **"PROYECTO"**, continúan incluso después de que el **"CONACYT"** emita la Constancia de Conclusión Técnica y Financiera.

VIGÉSIMA SEGUNDA. CONSENTIMIENTO ELECTRÓNICO

En términos del artículo 1803, fracción I del Código Civil Federal, las partes acuerdan que es su voluntad aceptar íntegramente el contenido obligacional de este Convenio a través de su suscripción mediante el Sistema de "People Soft", por lo que reconocen que dicho medio constituye el consentimiento expreso del presente acuerdo de voluntades.

VIGÉSIMA TERCERA. ASUNTOS NO PREVISTOS

Los asuntos relacionados con el objeto de este Convenio y que no queden expresamente previstos en sus

Cláusulas, ni en sus Anexos, serán interpretados y resueltos de común acuerdo por las partes, apelando a su buena fe y consecución de mismos propósitos, haciendo constar sus decisiones por escrito.

VIGÉSIMA CUARTA. AUSENCIA DE VICIOS DE VOLUNTAD

Las partes manifiestan que en la celebración del presente Convenio no ha mediado circunstancia alguna que induzca a error, dolo, mala fe u otra circunstancia que afecte o vicie la plena voluntad con que celebran el presente instrumento, por lo que el mismo es válido para todos los efectos legales conducentes.

VIGÉSIMA QUINTA. DENOMINACIÓN DE LAS CLÁUSULAS

Las partes están de acuerdo en que las denominaciones utilizadas en las Cláusulas del presente Convenio, son únicamente para efectos de referencia, por lo que no limitan de manera alguna el contenido y alcance de las mismas, debiendo en todos los casos atender a lo pactado en las mismas.

VIGÉSIMA SEXTA. JURISDICCIÓN

Para la solución a toda controversia que se pudiera suscitar con motivo de la interpretación, ejecución y cumplimiento del presente Convenio y sus Anexos, y que no se resuelva de común acuerdo por las partes, éstas se someterán a las Leyes Federales vigentes y Tribunales Federales competentes de la Ciudad de México, Distrito Federal, renunciando desde ahora a cualquier otro fuero que les pudiera corresponder en razón de sus respectivos domicilios presentes o futuros.

PREVIA LECTURA Y CON PLENO CONOCIMIENTO DE SU CONTENIDO, LAS PARTES EXPRESAN SU CONSENTIMIENTO ELECTRÓNICO AL PRESENTE INSTRUMENTO QUE A CONTINUACIÓN SE INSERTA PARA CADA UNA DE ELLAS.

POR EL "CONACYT"	POR EL "SUJETO DE APOYO"
DRA. JULIA TAGÜEÑA PARGA DIRECTORA ADJUNTA DE DESARROLLO CIENTÍFICO	DR. DAVID KERSHENOBICH STALNIKOWITZ REPRESENTANTE LEGAL
DR. LUIS HUMBERTO FABILA CASTILLO DIRECTOR DE INVESTIGACIÓN CIENTÍFICA BÁSICA	DR. ROGELIO ENRIQUE HERNANDEZ PANDO RESPONSABLE TÉCNICO
	LIC. MARTHA ARREDONDO URZUA RESPONSABLE ADMINISTRATIVO

LAS FIRMAS QUE APARECEN EN ESTA HOJA SE REFIEREN AL CONVENIO DE ASIGNACIÓN DE RECURSOS CELEBRADO ENTRE EL CONSEJO NACIONAL DE CIENCIA Y TECNOLOGÍA, EL "CONACYT" Y EL/LA INSTITUTO NACIONAL DE CIENCIAS MEDICAS Y NUTRICION SALVADOR ZUBIRAN, EL "SUJETO DE APOYO".----------CONSTE.----------

---

Anexo 1: Desglose Financiero

Total de etapas: $6859974

Etapa: 001

Tipo de Recurso	Categoria del recurso	Subcategoria del recurso	Descripción de Subcategoría	Importe del recurso
FONDO	GINVE	402	Equipo de laboratorio	6859974

Total de etapa: $6859974

Anexo 2: Cronograma de actividades por etapa

Etapa #	Descripción De La Etapa	Descripción De La Meta	Actividades	Productos	Fecha inicial DD-MM-AAAA	Fecha de termino DD-MM-AAAA	Fecha informe avance y final DD-MM-AAAA
001	NO APLICA	NO APLICA	NO APLICA	NO APLICA	02/05/2014	01/05/2015	01/05/2015

Este contrato tiene como última Fecha de Firma	

MÉXICO
PRESIDENCIA DE LA REPÚBLICA

CONACYT
Consejo Nacional de Ciencia y Tecnología

Información indispensable para la solicitud de
Apoyo al Fortalecimiento y Desarrollo de la Infraestructura Científica y Tecnológica
Convocatoria 2014

Es indispensable adjuntar este documento a su solicitud.
Sin este documento su solicitud no será válida.
Este documento no deberá exceder los 2MB de tamaño.

Imprimir formulario

Guardar

Número de solicitud: 000000000229779

Modalidad: Apoyo Especial

Título de la solicitud

Infraestructura de apoyo a proyectos relacionados con la evaluación morfológica ultraestructural de los efectos patogénicos de agentes infecciosos, químicos y nutricionales y sus posibles tratamientos.

Institución

Instituto Nacional de Ciencias Medicas y Nutricion "Salvador Zubirán"

Unidad académica y departamento o equivalente

Sección de Patologia Experimental, Departamento de Patología

Otras unidades académicas o instituciones que intervienen en la propuesta (en su caso)

1. División de Nutrición, Departamento de Fisiología de la Nutrición, Instituto Nacional de Ciencias Médicas y Nutrición "Salvador Zubirán"
2. Facultad de Química. Universidad Nacional Autónoma de México..

Miembros del grupo de investigación o cuerpo académico, indicando su línea de investigación y nivel de SNI.

1. Dr. Rogelio Hernández Pando (sección de Patología Experimental, Instituto Nacional de Ciencias Médicas y Nutrición)
Patología Experimental. SNI Nivel III
2. Dr. José Pedraza Chaverri (Facultad de Química UNAM).
Bioquímica Toxicología. SNI Nivel III
3. Dr. Armando Tovar Palacio (Fisiología de la Nutrición, Instituto Nacional de Ciencias Médicas y Nutrición).
Biología Molecular de la Nutrición. SNI Nivel III

Líneas de investigación Institucionales en las que se va a utilizar el o los equipos a adquirir.

1. Inmunopatología de la tuberculosis pulmonar experimental
2. Desarrollo y prueba de inmunoterapia para la tuberculosis
3. Desarrollo y prueba de nuevas vacunas para la tuberculosis
4.- Biología molecular de la nutrición

Indicar, en su caso, a otros grupos de investigación o cuerpos académicos que utilizarían el equipo solicitado, ya sea de diferentes instituciones o diferentes unidades académicas de la misma institución.

El equipo solicitado podrá ser utilizado y aprovechado por diferentes investigadores y grupos de investigación del Instituto Nacional de Ciencias Médicas y Nutrición Salvador Zubirán, particularmente los involucrados en las líneas de investigación de Patología Experimental, Fisiología de la Nutrición, Nefrología y a través de proyectos colaborativos con otras instituciones como el CINVESTAV Departamento de Genética y de la Unidad de Investigación Biomédica del IMSS en Zacatecas. Es importante mencionar que el equipo será también de utilidad en el trabajo diagnóstico de los pacientes atendidos en el Instituto Nacional de Ciencias Medicas y Nutrición, particularmente del servicio de Nefrología.

Productos de investigación que aporten evidencias de la colaboración entre los miembros del Grupo de investigación o Cuerpos académicos (publicaciones, tesis, etc.) no menos de tres y no más de diez.

1.García-Niño WR, Tapia E, Zazueta C, Zatarain-Barrón ZL, Hernández-Pando R, Vega-García CC and Pedraza Chaverri J. Curcumin pretreatment prevents potassium dichromate-induced hepatotoxicity, oxidative stress, decreased respiratory complex I activity and membrane permeability transition pore opening. Evidence-Based Complementary and Alternative Medicine. 2013;2013:424692. doi: 10.1155/2013/424692.
2.- Zúñiga-Toalá A; Zatarain-Barrón AL; Hernández-Pando R; Negrete-Guzmán M; HuertaYepez S; Torres I; Pinzón E; Tapia E; Pedraza-Chaverri J. Nordihydroguaiaretic acid induces Nrf2 nuclear translocation in vivo and attenuates renal damage and apoptosis in the ischemia and reperfusion model. Phytomedicine 2013 Jul 15;20(10):775-9. doi: 10.1016/j.phymed.2013.03.020.
3.- Negrette-Guzmán M, Huerta-Yepez S, Medina-Campos O, Zatarain-Barrón L, Hernández Pando R, Torres I, Tapia E and Pedraza-Chaverri J. Sulforaphane attenuates gentamicin-induced nephrotoxicity: role of mitochondrial protection. Evidence-Based Complementary and Alternative Medicine vol. 2013, Article ID 135314, 17 pages, 2013. doi:10.1155/2013/135314.
4.- Tapia E, Zataraín-Barrón L, Hernández-Pando R, Zarco-Márquez G, Molina-Jijón E, Cristóbal-García M, Santamaría J, Pedraza-Chaverri J. Therapeutic effect of curcumin against renal injury and oxidant stress in 5/6 nephrectomized rats. Phytomedicine 2013; 20: 359-366.
5.- Zúñiga-Toalá A, Tapia E, Zazueta C, Correa F, Zataraín-Barrón ZL, Hernández-Pando R, Zarco-Márquez G, Medina-Campos O, Pedraza-Chaverri J. Nordihydroguaiaretic acid pretreatment prevents ischemia and reperfusion induced renal injury, oxidant stress and mitochondrial alterations. Medicinal Plant Research 2012; 6 (15): 2938-2947.
6.- Cano-Ramírez D, Torres-Vargas CE, Guerrero-Castillo S, Uribe-Carvajal S, Hernández-Pando R, Pedraza-Chaverri J. Orozco-Ibarra M. Effect of glycolysis inhibition on mithocondrial function in rat. Journal of Biochemical and Molecular Toxicology 2012; 26 (5): 206-11.
7.- González-Granillo M, Steffensen KR, Granados O, Torres N, Korach-André M, Ortiz V, Aguilar-Salinas C, Jakobsson T,

Breve descripción de los beneficios académico-científicos que se obtendrían por la adquisición del equipo.

Desde hace 30 años se adquirió para el Departamento de Patología del Instituto Nacional de la Nutrición un microscopio electrónico Carl Zeiss M-10, el cual ha dado un enorme servicio en el área de investigación específicamente en proyectos de Patología Experimental y colaborativamente con diversas lineas de investigación del mismo Instituto y de otras instituciones nacionales y extranjeras. Ademas el mismo equipo ha contribuido enormemente en el diagnostico de diversas enfermedades neoplásicas, metabólicas y sobre todo renales. Después de 3 décadas de servicio intenso, dicho microscopio es absolutamente obsoleto, de hecho se siguen utilizando rollos y placas fotográficas que actualmente ya no existen en el mercado y lo que se tiene en nuestro almacén esta a punto de agotarse con lo cual ya no se podrán obtener fotografías para ilustrar artículos de investigación y tampoco para los diagnósticos de los pacientes, material gráfico que también es utilizado para las sesiones anatomoclínicas que son de gran importancia para la formación de médicos especialistas. Se ha investigado sobre la renovación o actualización de este microscopio tratando de adaptar sistemas de adquisición de imagen con cámara y computadora modernas pero el costo es muy elevado y la garantía de que funcione es limitada, mas aun, diversos componentes básicos de este microscopio como bombas de vació ya no se producen y actualmente resulta imposible conseguirlos en el mercado nacional y extranjero, por lo que la eventual descompostura de alguno de estos componentes implicaría la total incapacidad de este equipo para seguir funcionando.

Por lo tanto se solicita la adquisición de un nuevo microscopio electrónico que permitirá continuar con el estudio ultraestructural de proyectos de investigación diversos, sobre todo en el área de las enfermedades infecciosas, metabólicas y por agentes tóxicos, aspectos en los que los proponentes han tenido una actividad colaborativa intensa y muy productiva; la adquisión de dicho equipo contribuirá también en la formación no solo de estudiantes de maestría y doctorado en diversos posgrados en investigacion biomedica si no ademas de especialistas médicos.

El microscopio electrónico ha tenido y sigue teniendo un lugar importante en la investigación experimental y el uso de técnicas especiales como la inmunoelectronmicroscopia contribuyen enriqueciendo substancialmente los resultados experimentales obtenidos con técnicas inmunológicas, bioquímicas o de biología molecular, integrando así aspectos morfológicos con moleculares. El resto del equipamiento como lo son ultramicrotomos y sistema de inclusión ya se tienen y la experiencia en el uso de este equipo por el grupo solicitante es muy sólida, de manera que el equipo solicitado sera fundamentalmente para substituir al ya existente y así poder continuar con una productiva actividad de investigación y de servicio asistencial para una de las instituciones académicas de mayor trayectoria y prestigio de nuestro país.

Descripción de la infraestructura científico-tecnológica con la que se cuenta y que tenga relación directa con el equipo solicitado.

La sección de Patología Experimental del Departamento de Patología del Instituto Nacional de Ciencias Médicas y Nutrición ocupa casi todo el segundo piso del Departamento de Patología. Físicamente esta sección tiene 3 oficinas para investigadores, dos cubículos para estudiantes, y un laboratorio amplio que tiene un equipo de inmunohistoquímica automatizada, microtomo semiautomático, una área para técnicas de biología molecular en donde hay un termociclador para tiempo real, dos termocicladores convencionales, estufa de hibridación, baños térmicos para procedimientos de hibridación in-situ y de PCR in situ, centrifugas, microcentrífugas, dos equipos de análisis de imagen para geles y laminillas histológicas y un equipo de microdisección con rayos laser. Existe una área de cultivo celular que tiene dos campanas de flujo laminar, una para cultivo celular y otra para cultivo de bacterias dotada con seis incubadoras. Se cuenta con equipo de cromatografía, espectrofotómetro, varios refrigeradores, cinco ultracongeladores, un fotomicroscopio, microscopio de fluorescencia, un citómetro de flujo.
En el área de microscopía electrónica se cuenta con 2 cubículos con un ultramicortomo y con mesas antivibratorias cada uno, una estufa de polimerización para bloques de resina, cortadora de cuchillas para elaborar cuchillas de cristal, una cuchilla de diamante, un microscopio electrónico de transmisión Carl Zeiss M-10 y dos ultramicrotomos.
En la sección de Patología Experimental laboran un investigador titular, tres asociados, dos técnicos y actualmente hay 5 estudiantes de doctorado y 5 estudiantes de maestría. El Bioterio del Instituto Nacional de Ciencias Médicas y Nutrición es un edificio de 3 pisos, en el segundo piso se albergan a los animales de experimentación para mantener a los animales en las mejores condiciones, esta área esta dotada de un sistema de control estricto de temperatura ambiental, humedad, limpieza constante del aire y de los ciclos de luz y obscuridad. En este piso existe una area grande para la sección de Patología Experimental, con dos campanas de seguridad biológica nivel 3, numerosos microaisladores, una centrífuga, un ultracongelador, una autoclave y un sistema de microaisladores dotado con un

Listado de los programas de posgrado que se beneficiarán con la instalación del equipo solicitado, indicando su nivel en el Programa Nacional de Posgrados de Calidad.

1.- Maestria y Doctorado en Ciencias Bioquimicas, Facultad de Quimica UNAM
2.- Doctorado en Investigación Biomédica Básica, Facultad de Medicina UNAM.
3.- Maestria y Doctorado en Inmunología, Escuela Nacional de Ciencias Biológicas, IPN.
4.- Maestria y Doctorado en Biologia Experimental, UAM.
4.- Residencias medicas en Patologia y Nefrologia, Fac de Medicina, UNAM

Impacto del equipo a adquirir en el desarrollo institucional, estatal o regional, o de redes de investigación.

El equipo solicitado permitirá continuar con el trabajo de investigación de varios años de la Sección de Patologia Experimental del Departamento de Patologia del Instituto Nacional de la Nutrición, el cual ha sido muy productivo y se ha fortalecido y ampliado con colaboraciones con grupos de investigación consolidados intrainstitucionales, como el del Dr Tovar, y extrainstitucionales como el del Dr Pedraza, colaboraciones que ha sido muy productivas en términos de publicaciones en revistas internacionales y en estudiantes de posgrado graduados. El grupo proponente de la presente solicitud tiene también proyectos de colaboración con otros grupos de investigación de importantes centros academicos locales, del interior del pais e incluso con Universidades e Institutos del extranjero, con los que se podrán continuar y ampliar diversos proyectos con el uso de la microscopia electrónica convencional y técnicas especiales como lo son análisis morfometricos y de inmunolocalizacion subcelular en las cuales el grupo solicitante es experto, este impacto del estudio con microscopia electronica en la actividad de investigacion para el desarrollo institucional, regional e incluso internacional es patente en publicaciones recientes en revistas internacionales con alto factor de impacto como las realizadas con grupos de investigacion locales como el CINVESTAV (European Journal of Cancer Prevention 2013 Nov;22(6):577-84) o el INER (European Journal of Immunology 2012, 16(6): 880-889.), o del interior del pais como el IMSS Zacatecas (International Journal of Antimicrobial Agents. 2013: 41: 143-148) y Universidades extranjeras como la de British Columbia Canada.(PlosOne 2013; 8(3): e59119. doi: 10.1371/journal.pone.0059119. Epub 2013 Mar 21).

MÉXICO
PRESIDENCIA DE LA REPUBLICA

CONACYT
Consejo Nacional de Ciencia y Tecnología

Información indispensable para la solicitud de
Apoyo al Fortalecimiento y Desarrollo de la Infraestructura Científica y Tecnológica
Convocatoria 2014

Es indispensable adjuntar este documento a su solicitud.
Sin este documento su solicitud no será válida.
Este documento no deberá exceder los 2MB de tamaño.

Imprimir formulario

Guardar

Número de solicitud 000000000229779

Modalidad Apoyo Especial

Título de la solicitud

Infraestructura de apoyo a proyectos relacionados con la evaluación morfológica ultraestructural de los efectos patogénicos de agentes infecciosos, químicos y nutricionales y sus posibles tratamientos.

Institución

Instituto Nacional de Ciencias Medicas y Nutricion "Salvador Zubirán"

Unidad académica y departamento o equivalente

Sección de Patologia Experimental, Departamento de Patología

Otras unidades académicas o instituciones que intervienen en la propuesta (en su caso)

1. División de Nutrición, Departamento de Fisiología de la Nutrición, Instituto Nacional de Ciencias Médicas y Nutrición "Salvador Zubirán"
2. Facultad de Química. Universidad Nacional Autónoma de México..

Miembros del grupo de investigación o cuerpo académico, indicando su línea de investigación y nivel de SNI.

1. Dr. Rogelio Hernández Pando (sección de Patología Experimental, Instituto Nacional de Ciencias Médicas y Nutrición)
Patología Experimental. SNI Nivel III
2. Dr. José Pedraza Chaverri (Facultad de Química UNAM).
Bioquímica Toxicología. SNI Nivel III
3. Dr. Armando Tovar Palacio (Fisiología de la Nutrición, Instituto Nacional de Ciencias Médicas y Nutrición).
Biología Molecular de la Nutrición. SNI Nivel III

Líneas de investigación Institucionales en las que se va a utilizar el o los equipos a adquirir.

1. Inmunopatología de la tuberculosis pulmonar experimental
2. Desarrollo y prueba de inmunoterapia para la tuberculosis
3. Desarrollo y prueba de nuevas vacunas para la tuberculosis
4.- Biología molecular de la nutrición

Indicar, en su caso, a otros grupos de investigación o cuerpos académicos que utilizarían el equipo solicitado, ya sea de diferentes instituciones o diferentes unidades académicas de la misma institución.

El equipo solicitado podrá ser utilizado y aprovechado por diferentes investigadores y grupos de investigación del Instituto Nacional de Ciencias Médicas y Nutrición Salvador Zubirán, particularmente los involucrados en las líneas de investigación de Patología Experimental, Fisiología de la Nutrición, Nefrología y a través de proyectos colaborativos con otras instituciones como el CINVESTAV Departamento de Genética y de la Unidad de Investigación Biomédica del IMSS en Zacatecas. Es importante mencionar que el equipo será también de utilidad en el trabajo diagnóstico de los pacientes atendidos en el Instituto Nacional de Ciencias Medicas y Nutrición, particularmente del servicio de Nefrología.

Productos de investigación que aporten evidencias de la colaboración entre los miembros del Grupo de investigación o Cuerpos académicos (publicaciones, tesis, etc.) no menos de tres y no más de diez.

1.García-Niño WR, Tapia E, Zazueta C, Zatarain-Barrón ZL, Hernández-Pando R, Vega-García CC and Pedraza Chaverri J. Curcumin pretreatment prevents potassium dichromate-induced hepatotoxicity, oxidative stress, decreased respiratory complex I activity and membrane permeability transition pore opening. Evidence-Based Complementary and Alternative Medicine. 2013;2013:424692. doi: 10.1155/2013/424692.
2.- Zúñiga-Toalá A; Zatarain-Barrón AL; Hernández-Pando R; Negrete-Guzmán M; HuertaYepez S; Torres I; Pinzón E; Tapia E; Pedraza-Chaverri J. Nordihydroguaiaretic acid induces Nrf2 nuclear translocation in vivo and attenuates renal damage and apoptosis in the ischemia and reperfusion model. Phytomedicine 2013 Jul 15;20(10):775-9. doi: 10.1016/j.phymed.2013.03.020.
3.- Negrette-Guzmán M, Huerta-Yepez S, Medina-Campos O, Zatarain-Barrón L, Hernández Pando R, Torres I, Tapia E and Pedraza-Chaverri J. Sulforaphane attenuates gentamicin-induced nephrotoxicity: role of mitochondrial protection. Evidence-Based Complementary and Alternative Medicine vol. 2013, Article ID 135314, 17 pages, 2013. doi:10.1155/2013/135314.
4.- Tapia E, Zataraín-Barrón L, Hernández-Pando R, Zarco-Márquez G, Molina-Jijón E, Cristóbal-García M, Santamaría J, Pedraza-Chaverri J. Therapeutic effect of curcumin against renal injury and oxidant stress in 5/6 nephrectomized rats. Phytomedicine 2013; 20: 359-366.
5.- Zúñiga-Toalá A, Tapia E, Zazueta C, Correa F, Zataraín-Barrón ZL, Hernández-Pando R, Zarco-Márquez G, Medina-Campos O, Pedraza-Chaverri J. Nordihydroguaiaretic acid pretreatment prevents ischemia and reperfusion induced renal injury, oxidant stress and mitochondrial alterations. Medicinal Plant Research 2012; 6 (15): 2938-2947.
6.- Cano-Ramírez D, Torres-Vargas CE, Guerrero-Castillo S, Uribe-Carvajal S, Hernández-Pando R, Pedraza-Chaverri J. Orozco-Ibarra M. Effect of glycolysis inhibition on mithocondrial function in rat. Journal of Biochemical and Molecular Toxicology 2012; 26 (5): 206-11.
7.- González-Granillo M, Steffensen KR, Granados O, Torres N, Korach-André M, Ortíz V, Aguilar-Salinas C, Jakobsson T,

Breve descripción de los beneficios académico-científicos que se obtendrían por la adquisición del equipo.

Desde hace 30 años se adquirió para el Departamento de Patología del Instituto Nacional de la Nutrición un microscopio electrónico Carl Zeiss M-10, el cual ha dado un enorme servicio en el área de investigación específicamente en proyectos de Patología Experimental y colaborativamente con diversas lineas de investigación del mismo Instituto y de otras instituciones nacionales y extranjeras. Ademas el mismo equipo ha contribuido enormemente en el diagnostico de diversas enfermedades neoplásicas, metabólicas y sobre todo renales. Después de 3 décadas de servicio intenso, dicho microscopio es absolutamente obsoleto, de hecho se siguen utilizando rollos y placas fotográficas que actualmente ya no existen en el mercado y lo que se tiene en nuestro almacén esta a punto de agotarse con lo cual ya no se podrán obtener fotografías para ilustrar artículos de investigación y tampoco para los diagnósticos de los pacientes, material gráfico que también es utilizado para las sesiones anatomoclínicas que son de gran importancia para la formación de médicos especialistas. Se ha investigado sobre la renovación o actualización de este microscopio tratando de adaptar sistemas de adquisición de imagen con cámara y computadora modernas pero el costo es muy elevado y la garantía de que funcione es limitada, mas aun, diversos componentes básicos de este microscopio como bombas de vació ya no se producen y actualmente resulta imposible conseguirlos en el mercado nacional y extranjero, por lo que la eventual descompostura de alguno de estos componentes implicaría la total incapacidad de este equipo para seguir funcionando.
Por lo tanto se solicita la adquisición de un nuevo microscopio electrónico que permitirá continuar con el estudio ultraestructural de proyectos de investigación diversos, sobre todo en el área de las enfermedades infecciosas, metabólicas y por agentes tóxicos, aspectos en los que los proponentes han tenido una actividad colaborativa intensa y muy productiva; la adquisión de dicho equipo contribuirá también en la formación no solo de estudiantes de maestría y doctorado en diversos posgrados en investigacion biomedica si no ademas de especialistas médicos.
El microscopio electrónico ha tenido y sigue teniendo un lugar importante en la investigación experimental y el uso de técnicas especiales como la inmunoelectronmicroscopia contribuyen enriqueciendo substancialmente los resultados experimentales obtenidos con técnicas inmunológicas, bioquímicas o de biología molecular, integrando así aspectos morfológicos con moleculares. El resto del equipamiento como lo son ultramicrotomos y sistema de inclusión ya se tienen y la experiencia en el uso de este equipo por el grupo solicitante es muy sólida, de manera que el equipo solicitado sera fundamentalmente para substituir al ya existente y así poder continuar con una productiva actividad de investigación y de servicio asistencial para una de las instituciones académicas de mayor trayectoria y prestigio de nuestro país.

Descripción de la infraestructura científico-tecnológica con la que se cuenta y que tenga relación directa con el equipo solicitado.

La sección de Patología Experimental del Departamento de Patología del Instituto Nacional de Ciencias Médicas y Nutrición ocupa casi todo el segundo piso del Departamento de Patología. Físicamente esta sección tiene 3 oficinas para investigadores, dos cubículos para estudiantes, y un laboratorio amplio que tiene un equipo de inmunohistoquímica automatizada, microtomo semiautomático, una área para técnicas de biología molecular en donde hay un termociclador para tiempo real, dos termocicladores convencionales, estufa de hibridación, baños térmicos para procedimientos de hibridación in-situ y de PCR in situ, centrifugas, microcentrífugas, dos equipos de análisis de imagen para geles y laminillas histológicas y un equipo de microdisección con rayos laser. Existe una área de cultivo celular que tiene dos campanas de flujo laminar, una para cultivo celular y otra para cultivo de bacterias dotada con seis incubadoras. Se cuenta con equipo de cromatografía, espectrofotómetro, varios refrigeradores, cinco ultracongeladores, un fotomicroscopio, microscopio de fluorescencia, un citómetro de flujo.
En el área de microscopía electrónica se cuenta con 2 cubículos con un ultramicortomo y con mesas antivibratorias cada uno, una estufa de polimerización para bloques de resina, cortadora de cuchillas para elaborar cuchillas de cristal, una cuchilla de diamante, un microscopio electrónico de transmisión Carl Zeiss M-10 y dos ultramicrotomos.
En la sección de Patología Experimental laboran un investigador titular, tres asociados, dos técnicos y actualmente hay 5 estudiantes de doctorado y 5 estudiantes de maestría. El Bioterio del Instituto Nacional de Ciencias Médicas y Nutrición es un edificio de 3 pisos, en el segundo piso se albergan a los animales de experimentación para mantener a los animales en las mejores condiciones, esta área esta dotada de un sistema de control estricto de temperatura ambiental, humedad, limpieza constante del aire y de los ciclos de luz y obscuridad. En este piso existe una area grande para la sección de Patología Experimental, con dos campanas de seguridad biológica nivel 3, numerosos microaisladores, una centrifuga, un ultracongelador, una autoclave y un sistema de microaisladores dotado con un

Listado de los programas de posgrado que se beneficiarán con la instalación del equipo solicitado, indicando su nivel en el Programa Nacional de Posgrados de Calidad.

1.- Maestria y Doctorado en Ciencias Bioquimicas, Facultad de Quimica UNAM
2.- Doctorado en Investigación Biomédica Básica, Facultad de Medicina UNAM.
3.- Maestría y Doctorado en Inmunología, Escuela Nacional de Ciencias Biológicas, IPN.
4.- Maestria y Doctorado en Biologia Experimental, UAM.
4.- Residencias medicas en Patologia y Nefrologia, Fac de Medicina, UNAM

Impacto del equipo a adquirir en el desarrollo institucional, estatal o regional, o de redes de investigación.

El equipo solicitado permitirá continuar con el trabajo de investigación de varios años de la Sección de Patologia Experimental del Departamento de Patologia del Instituto Nacional de la Nutrición, el cual ha sido muy productivo y se ha fortalecido y ampliado con colaboraciones con grupos de investigación consolidados intrainstitucionales, como el del Dr Tovar, y extrainstitucionales como el del Dr Pedraza, colaboraciones que ha sido muy productivas en términos de publicaciones en revistas internacionales y en estudiantes de posgrado graduados. El grupo proponente de la presente solicitud tiene también proyectos de colaboración con otros grupos de investigación de importantes centros academicos locales, del interior del pais e incluso con Universidades e Institutos del extranjero, con los que se podrán continuar y ampliar diversos proyectos con el uso de la microscopia electrónica convencional y técnicas especiales como lo son análisis morfometricos y de inmunolocalizacion subcelular en las cuales el grupo solicitante es experto, este impacto del estudio con microscopia electronica en la actividad de investigacion para el desarrollo institucional, regional e incluso internacional es patente en publicaciones recientes en revistas internacionales con alto factor de impacto como las realizadas con grupos de investigacion locales como el CINVESTAV (European Journal of Cancer Prevention 2013 Nov;22(6):577-84) o el INER (European Journal of Immunology 2012, 16(6): 880-889.), o del interior del pais como el IMSS Zacatecas (International Journal of Antimicrobial Agents. 2013: 41: 143-148) y Universidades extranjeras como la de British Columbia Canada.(PlosOne 2013; 8(3): e59119. doi: 10.1371/journal.pone.0059119. Epub 2013 Mar 21).